Buoyant Aerobot Design and Simulation Study
BADS

I. Van Dosselaer

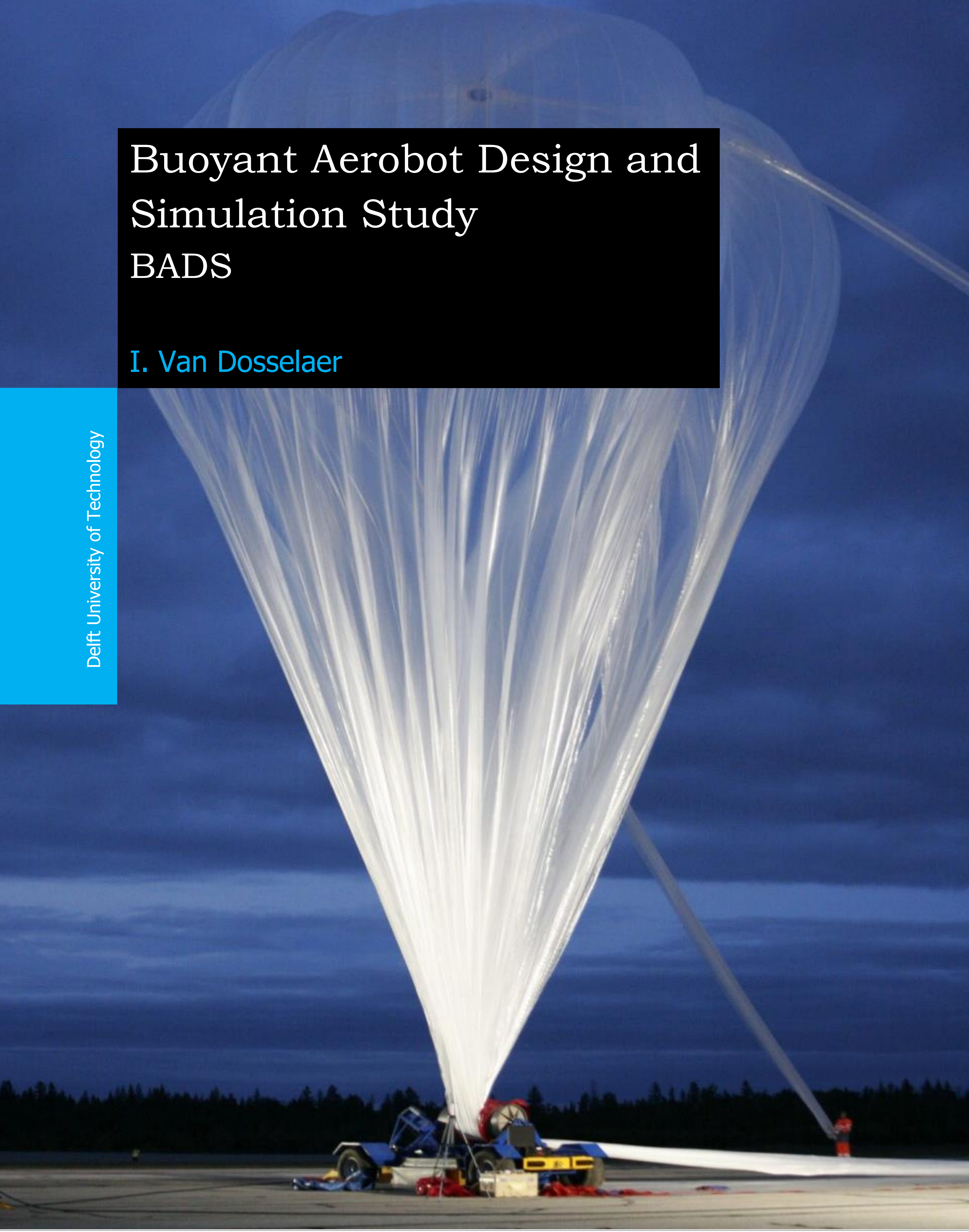

Delft University of Technology

TU Delft Delft University of Technology

Thesis Space Engineering:
AE5-006

Buoyant Aerobot Design and Simulation Study

BADS

By

I. Van Dosselaer

in partial fulfilment of the requirements for the degree of

Master of Science
in Aerospace Engineering

at the Delft University of Technology,
to be defended publicly on September 10th, 2014

Supervisor:	Ir. B.T.C. Zandbergen
Thesis committee:	Prof. dr. M. Menenti
	Ir. B.T.C. Zandbergen
	Ir. D. Steenhuizen

This thesis is confidential and cannot be made public until September 11th, 2014.

TU Delft Delft University of Technology

Acknowledgements

Foremost I want to thank my parents who gave me the opportunity to study Aerospace Engineering at the Delft University of Technology. Without their daily support and their relentless patience I wouldn't have been able to accomplish what I have realized so far.

Next I would want to thank my supervisor Barry Zandbergen for his continuous advice, guidance and knowledge. His enthusiasm and problem solving skills encouraged me when program crashes, mathematical problems and lack of information were giving me motivational issues. Also his remarkable amount of patience should be credited!

The following people were also very supportive. Let me start by saying thanks to hobbyist balloon builders *Henri Raaymakers*, *Herman* and *Yorick Bogaert*, *Bob Berden* of Ballooning.be and *Koen Audenaert* of Cameroon Ballooning for helping me with the basics on design and flight of miniature hot air and gas balloons. Thanks to *Susan Roche* and *Richard Anderson Jr.* from Lamcotec Coating Technologies for sending me a sample of balloon fabric for testing. Thanks to DUT students *Lily Ha* and *Andani Osuman* for discussing aerobot literature, balloon basics and robotics respectively.

I also want to thank a number of people and organizations who were invaluable in the process of acquiring information on the aerobot topic and in helping me out with technical issues; *Imke de Pater* from DUT on atmospheric models of Mars, *Geert Brouwer* of DUT on material characteristics, *Hannes Griebel* from the Institute of Spaceflight Technology in Munich on Archimedes, *Viktor Kerzhanovich* from the Jet Propulsion Laboratory on reproducing aerobot data, *Thomas Benson* from NASA on atmospheric models of Earth and Mars, *Nobuyuki Yajima* and *Izutsu Naoki* from JAXA on Scientific Ballooning, *Darrell Strobel* from Johns Hopkins University on an atmospheric model of Titan, and both *KMI* in Belgium and *KNMI* in The Netherlands on balloon and atmospheric issues.

Special thanks to *Rodger Farley* from NASA/Goddard Space Flight Center on helping me with simulating a balloon's flight behavior in general, introducing me to NASA's simulation Balloon Ascent program and assisting me with balloon bobbing, balloon thermal behavior, atmospheric and shape modeling.

Finally I want to thank all my friends for their continuous support. In particular I want to thank my friends Jennifer and Lieuwe who I was able to rely on when I needed a place to sleep near the university.

Abstract

Aerobots, and more specifically buoyant aerobots, are not that common in space or planetary exploration. There is however a small community of scientists and engineers who are exploring these technologies. “Aerial vehicles used in planetary exploration bridge the scale and resolution measurement gaps between orbiters, which have global perspective with limited spatial resolution, and landers which have local perspective with high spatial resolution, thus complementing and extending orbital and landed measurements.” This indicates that an aerobot can provide a substantial scientific return far beyond the alternatives like an orbiter, lander or surface rover.
Here on Earth buoyant aerobot technology is flown daily by meteorological institutes. A buoyant aerobot is nothing else than a type of balloon filled with a buoyant gas lighter than air. For the simple release of an atmospheric balloon however, a certain expertise is required.

Researching atmospheric balloons lead to the exploration of these balloons, airships and alike for planetary missions. Understanding the behavior of a scientific balloon here on Earth definitely increases the insight of balloon behavior on another planet.
Organizations across the world have been working on vertical flight simulation programs to estimate the balloon’s time of ascend and floating altitude. Over the years improvements were made and extensive programs were developed which included; planetary atmospheric models, 3D trajectory planning, buoyant gas selection, balloon envelope materials selection, propelled flights, etc.

This thesis presents the Buoyant Aerobot Design and Simulation tool BADS. The tool has been modeled as much as possible towards the current professional aerobot flight simulation programs. The program makes use of Matlab coding for the aerobot design and trajectory simulation and includes the following databases and parameters to specify the aerobot’s design and flight; 4 atmospheric models (Earth, Mars, Venus and Titan), 4 balloon shapes (Sphere, Oblate Pumpkin, Prolate, Prolate Airship), 4 balloon pressure types (Zero-Pressure, Super-Pressure, Over-Pressurized Zero-Pressure, Montgolfier), 15 envelope materials, 71 envelope coatings.

The validation of the tool has been achieved through thorough testing and comparison against existing flight simulation tools and specific aerobot design data. A sensitivity study proved that the assumptions made in BADS are similar to those in other programs and that any discrepancy effect, if present, can be minimized.

Table of Contents

List of Abbreviations

Abbreviation	Meaning	1st Page
AAB	Amateurs Atmospheric Balloon	25
ACHAB	Analysis Code for High-Altitude Balloons	103
ALTIME	Predecessor of SINBAD (see SINBAD)	123
AMSAT	The Radio Amateur Satellite Corporation	23
Ar	Argon	45
ARC	Ames Research Center	18
Archimedes	Aerial reconnaissance Robot Carrying High-resolution Imaging, a Magnetometer Experiment and Direct Environmental Sensors	24
AU	Astronomical unit	VII
AUVSI	Association for Unmanned Vehicle Systems International	XXV
B.C.	Before Christ	6
BADS	Buoyant Aerobot Design and Simulation tool	4
BEAM	Biology, Electronics, Aesthetics, and Mechanics robot games	XXV
C&DH	Command and data handling	XVIII
CH_4	Methane	45
CNES	Centre National d'études Spatiales	1
CO	Carbon Monoxide	45
CO_2	Carbon Dioxide	45
COTS	Commercial off the Shelf	19
CvHTC	Convective Heat Transfer Coefficients	65
DALR	Dry Adiabatic Lapse Rate	141
DLR	Deutsches Zentrum für Luft- und Raumfahrt’	24
ELV	Elevation Angle	67
EVAL	Ethylene-Vinyl-Alcohol	15
FMI	Finnish Meteorological Institute	24
FSC	Frisian Solar Challenge	160
GPS	Global Positioning System	13
GSFC	Goddard Space Flight Center	13
GUI	Graphical User Interface	123
H_2	Hydrogen	45
HASI	Huygens Atmospheric Structure Instrument	43
He	Helium	61
HTA	Heavier-than-air	5
IARC	International Aerial Robotics Competition	160
ICAO	International Civil Aviation Organization	36
IKI	Russian Space Research Institute	23
IMU	Inertial Measurement Unit	20
IR	Infra-red	10
IRIS	Infrared Spectrometer	43
ISA	International Standard Atmosphere	37
ISIS	Institute of Space and Astronautical Science	2
ISR	International Submarine Races	160

JAXA	Japan Aerospace Exploration Agency	1
JPL	Jet Propulsion Laboratory	1
LDB	Long Duration Balloon	2
LDBV	Long Duration Balloon Vehicle	10
LLDPE	Linear Low Density Polyethylene	14
LMA	Lockheed Martin Aeronautics	18
LTA	Lighter-than-air	5
MABS	Mars Aerobot/Balloon System	18
MSP	Mars Surveyor Program	19
N_2	Nitrogen	45
NA	None Available	76
NASA	National Aeronautics and Space Administration	1
NH_3	Ammonia	61
NOAA	National Oceanic and Atmospheric Administration	36
NRC	National Research Council	5
ODE	Ordinary Differential Equations	89
OZP	Over-Pressurized Zero-Pressure	9
PBO	Polybenzobisoxazole	8
Ref.	Reference	27
ROLIS	Rosetta Lander Imaging System	24
RPM	Rotations Per Minute	54
RPS	Radioisotope Power Supply	21
RSS	Radio Science Subsystem	43
RTG's	Radio-isotope Thermo-electric Generator	10
SALR	Saturated Adiabatic Lapse Rate	141
SDL	Space Dynamics Laboratory	18
SINBAD	Scientific Balloon Analysis Model	2
SP	Super-Pressure	8
THERMTRAJ	Thermal Properties and Trajectory of Balloons	2
TT&C	Telemetry tracking and command	XVIII
U.S	United States	5
UAV's	Unmanned Aerial Vehicle	2
ULDB	Ultra Long Duration Balloon	2
UVS	Ultraviolet Spectrometer	43
VTOL	Vertical Take-Off and Landing	5
WFF	Wallops Flight Facility	2
WSC	World Solar Challenge	160
ZP	Zero-Pressure	6

List of Symbols

Symbol	Meaning	Unit	1st Page
Δp	Overpressure	[Pa]	9
Δt	Timespan	[s]	47
$\sum F_y$, $\sum F_x$, $\sum F_z$	Sum of Forces	[N]	47
$\sum m_{component}$	Sum of Masses	[kg]	47
μ	Dynamic viscosity	[Pa s]	51
a, a_x, a_y, a_z	Acceleration	[m/s^2]	47
$A_{balloon}$, A_{cross}, A_y, A_{yz} A_{xz} A_{xy}	Surface Area	[m^2]	48
a_s	Albedo	[]	64
C	Sutherland Constant	[K]	52
C_D	Drag Coefficient	[/]	50
CF	Cloud Fraction	[%]	69
$CF_{airmass}$	Correction Factor Air-mass	[/]	66
C_L	Lift Coefficient	[/]	53
c_p, c_v, c_e	Specific Heat Capacity	[J kg^{-1}K^{-1}]	61
C_T	Thrust Coefficient	[/]	54
$C_{virtual}$	Added Mass Coefficient	[/]	49
d	Length/Thickness	[m]	58
d_b	Balloon Diameter	[m]	65
D_{total}, D, D_x, D_y, D_z,	Drag Force	[N]	46
e	Eccentricity	[/]	57
E	Endurance	[s]	29
f	Fineness Ratio	[/]	53
F_{bs}	Shape Factor	[/]	64
$F_{buoyant}$	Buoyancy Force	[N]	6
F_{Drag}	Drag Force	[N]	50
G	Gravitational Constant	[m^{3}kg^{-1}s^{-2}]	45
g, g_{planet}	Gravitational Acceleration	[m/s^2]	6
GI	Gross Inflation	[N]	46
Gr	Grashof Number	[/]	65
h	Geometric Altitude	[m]	37
h_{ae}, h_{ge}	Convective Heat Transfer Coefficient	[Wm^{-2}K^{-1}]	65
I	Irradiance	[W/m^2]	68
k_f	Construction Factor	[/]	107
KM_{spb}, KM_{zpb}	Bobbing Frequency	[s^{-2}]	115
l	Characteristic Length	[m]	51
L	Lift	[N]	46
Ls	Solar longitude	[°]	VII
M	Molar mass	[kg/mol]	9
m, m_{gas}, m_{gross}, $m_{balloon}$, $m_{payload}$	Mass	[kg]	9
MA	Mean Anomaly	[°]	67
Nu	Nusselt number	[/]	65
P	Power	[W]	29

p, p_{atm}, p_{gas}	Pressure	[Pa]	9
Pr	Prandtl Number	[/]	65
q	Heat Flows	[W/m^2]	68
Q	Heat Load	[W]	64
$Q_{discharge}$	Discharge Rate	[m^3/s]	62
r	Reflectivity	[/]	65
R	Radius	[m]	45
Ra	Rayleigh Number	[/]	75
R_{AU}	Astronomical Radius	[AU]	67
R_c	Universal Gas Constant	[$J\ K^{-1}mol^{-1}$]	9
Re	Reynolds number	[/]	51
R_g, R_a	Specific Gas Constants	[$J\ kg^{-1}K^{-1}$]	115
R_z	Sum of Forces in z-direction	[N]	49
S	Travelled Distance	[m]	90
t, t_1, t_2	Time	[s]	47
T, T_{atm}, T_{gas}	Temperature	[K]	9
TA	True Anomaly	[°]	67
T_x, T_y, T_z	Thrust in x, y, z directions	[N]	46
V, V_1, V_2, V_{wind}, ΔV, ΔV_A	Speed	[m/s]	47
Vol, $Vol_{balloon}$	Volume	[m^3]	6
W	Weight	[N]	48
x, y, z	Coordinate System	[m]	46
α	Angular Eccentricity	[°]	57
α	Absorptance	[/]	64
β	Volumetric Expansion Coefficient	[K^{-1}]	75
γ	Heat Capacity Ratio	[/]	72
ε	Emittance	[/]	64
η	Efficiency	[%]	54
Θ_{planet}	Planetary Rotation Speed	[°/s]	81
κ	Thermal Conductivity	[$Wm^{-1}K^{-1}$]	65
λ	Permeability Coefficient	[m^2]	62
ρ, ρ_g, ρ_a	Gas Density	[kg/m^3]	6
$\rho_{envelope}$	Envelope Density	[kg/m^2]	48
σ	Stress	[N/m]	58
σ_s	Stefan Boltzmann Constant	[$Wm^{-2}K^{-4}$]	64
τ	Transmissivity	[/]	65
φ	Ballast Rate	[kg/min]	95

List of Figures

List of Tables

List of Equations

1. Introduction

The challenge and expense of space travel only allows a select number of people the opportunity to experience it. Space exploration by means of some kind of machine is much more practical. Unmanned missions are able to explore the solar system in ways that humans can't.

Machines are ideal for space research because they can be designed and built specifically for the mission at hand. They are able to withstand the hostile conditions of space and are able to survive a long mission life. Equipped with scientific instruments, robotic spacecraft are able to safely research planets and space and radio back scientific data to researchers on Earth.

This chapter will introduce the role of aerobots in unmanned planetary exploration and the use of flight simulation programs to test the aerobot designs. Next the mission objective of this thesis will be defined. How the objective will be attained is explained through the thesis approach.

1.1. Unmanned Planetary Exploration

Satellites, rovers, landers and probes are the best known machines from today's unmanned space exploration. Depending on the goal of the exploration mission one or the other will be used or in conjunction with each other.

For planets with atmospheres of any substance however, there is an alternative: the aerobot, or aerial robot. Flying above obstructions and carried by the winds an aerobot could inspect large regions of a planet in situ and therefore in great detail. An area wherein other unmanned machines fail to deliver data.

H.S. Wright and J.S. Levine [a.4][1], V.V. Kerzhanovich and J.A. Cutts [a.5], are experts on aerobots at the National Aeronautics and Space Administration (NASA) and the Jet Propulsion Laboratory (JPL) respectively. All state the following; "Aerial vehicles used in planetary exploration bridge the scale and resolution measurement gaps between satellites, which have global perspective with limited spatial resolution, and rovers which have local perspective with high spatial resolution." Planetary aerial vehicles can also survey scientifically interesting terrain that is inaccessible or hazardous to landers. This indicates that an aerobot can provide a substantial scientific return far beyond the alternatives like a satellite, lander or surface rover.

Buoyant aerobots make use of a buoyant gas to create the required lift to be able to float. They exist as a subgroup of aerobots within the aircraft group and can be used for scientific research on Earth and any other planet with an atmosphere, in which Venus, Mars and Titan are prime candidates [a.4]. "There is a global interest in buoyant aerobots because it became evident that this kind of approach to scientific research for near-space applications is both successful and cost-effective [t.4]."

Research on buoyant aerobots originates from the meteorological and stratospheric balloons for atmospheric research on Earth. NASA, the Centre National d'études Spatiales (CNES) and the Japan Aerospace Exploration Agency (JAXA) have been key players in this field. "CNES has built up its balloon activities in the last 40 years and today its balloon program ranks second only to the United States [i.41]." The agency has earned worldwide recognition for its expertise in the design,

[1] References are presented between square brackets []. They are subdivided in; webpages [i.], articles [a.], datasheets [d.], theses [t.], books [b.]

construction, launch and operation of lighter-than-air vehicles. CNES was for instance the first agency to introduce the pumpkin shape for super-pressure balloons [a.15].

NASA's research on scientific ballooning is controlled by the NASA Balloon Program Office. One of their main facilities is NASA's, Wallops Flight Facility (WFF) [i.42]. NASA's balloon program has led to the development of the Long Duration Balloon (LDB), which is a zero-pressure balloon able to fly multiple days near the Earth's poles [a.16]. Further research on stronger balloon materials also led to the development of the Ultra Long Duration Balloon (ULDB), which is a pumpkin shaped super-pressure balloon able to fly continuously for a few months [a.16].

JAXA has been researching balloon technology since the seventies through their Institute of Space and Astronautical Science (ISIS). "The research is focused on thin-film high-altitude balloons for higher altitude flights and on super-pressure balloons for longer duration flights [i.43]". The goal however is to use this technology in a future planetary flight.

While a lot of research has been done on balloons and blimps for planetary and atmospheric applications, test models and actual planetary missions remain limited.

The problem to date is the reluctance to use fragile buoyant aerobots in space missions above sturdier applications like rovers, satellites or unmanned aerial vehicles (UAV's), even though the advantages and potential of buoyant aerobots are known. Reluctance is not the only problem there is however. Due to the fact that planetary environments are not easily reproduced and conditions are hardly the same on Earth, testing new designs is difficult at best. Real time results can however be simulated to some degree.

NASA has been working on an in-house flight simulation package, named Balloon Ascent [a.22], to support buoyant aerobot design and simulation. They have been developing software packages like THERMTRAJ [a.37] and the Scientific Balloon Analysis Model (SINBAD) [a.36] to improve simulation results on high-altitude balloons. About 30 years have passed since and all improvements have led to the current program, Balloon Ascent [a.22]. The research on these programs has also led to a working testbed [i.7] to correlate the simulation results. Organizations, universities, students, companies, all have tried to produce smaller programs for specific missions and concepts. However, currently no simulation programs exist that design, simulate and compare buoyant aerobots on different planetary environments, for different aerobot types, shapes, buoyant gases and so on, NASA's program excluded.

1.2. Mission Objective

Writing a simulation program for a type of robot which is in itself not common to the scientific world let alone to the public eye, is quite a challenge. NASA is still improving their program after 30 years of work.

Primarily the idea is to produce a helpful design and flight simulation tool for buoyant aerobots in a number of planetary atmospheres. The program should be able to design a buoyant aerobot, which would include a mass breakdown, volume restrictions, material properties and atmospheric influences. Further the program should simulate the buoyant behavior of the design in an atmospheric flight and represent flight performance. The program input and selection parameters should be as comprehensive as possible but in the end the program should also be very user-friendly. Secondly the output results should be verified with known mission data or similar simulation programs. Next the usefulness of such a program in the interplanetary community should be demonstrated.

1.3. Approach

The aerobot is defined and characterized by 4 main requirements from literature in chapter 2. Buoyant aerobots are chosen as the topic of research in this thesis and therefore the different buoyant types are described in detail. Aerobot value like, coverage and spatial resolution, hovering and maneuvering, high payload mass and long mission life are discussed to proof the advantages of aerobots beyond any other unmanned machine.

Chapter 3 studies the existing buoyant aerobots, some concepts and existing and upcoming missions. The lessons learned and technology used, are addressed in this chapter. With the information from literature, a trade-off between the different aerial platforms is made. The results verify the excellent potential of buoyant aerobots.

A general representation for a buoyant aerobot is selected from all reoccurring components in aerobot technology. This set-up is used throughout chapter 4 for modeling the buoyant aerobot simulation program. Chapter 4 presents a number of atmospheric models from Earth, Mars, Venus and Titan. The models are no exact measurement of the planet's atmosphere. They do represent the atmosphere as good as possible with current data and only for general conditions.

The chapter continues with the general equations of motion and aerodynamic properties of a buoyant aerobot. Next the design parameters of buoyant aerobots will be addressed; type of buoyant gases, balloon shapes, envelope material and permeability, balloon pressure and skin tension, mass and volume.

Chapter 5 will present the mathematical program for the buoyant aerobot design and flight simulation. The models and equations of chapter 4 form the foundation of the programming code. The mathematical method used is basic Euler. While other mathematical methods tend to make simulation programs generally more efficient and faster, the amount of options included in the program make other mathematical methods unstable after some time. The many design options to choose from will include; 4 planetary atmospheric models, 6 buoyant gases, 15 balloon fabrics, 71 coatings, 4 available balloon shapes, propelled and non-propelled options and a thermal model. A flowchart represents the entire program and will be explained in detail, with input and output parameters shown for each programming block.

Chapter 6 will be the testing and validation process of the simulation program. Simulation results will be discussed and compared to results from literature data sets, and small specific missions and concept models for verification. Program efficiency and the comprehensiveness of the program is compared to other programs to show the benefits and drawbacks of the simulation package.

When inconsistencies in parameters or models have been found it should be explored in what way these affect the simulation program, and more importantly the results of the program. Also the effect on the simulation of each assumption made should be further explored. Chapter 7 will subject the inconsistencies and the assumptions made to a sensitivity analysis.

The next step in the approach is the actual use of the program in a mission and aerobot design. Chapter 8 will discuss the possibilities of a buoyant aerobot design and simulation program for the scientific community. A program as this would be most interesting to student aerobot projects and to scientific planetary ballooning missions. Students will be able to use the program to estimate the design restrictions on a meteorological balloon or aerobot competition. Further they can use the flight path simulation for insight in the flight behavior of their balloon, and estimate the landing site of their payload.

A buoyant aerobot design and simulation (BADS) program used in planetary ballooning will be helpful in analyzing the design and flight limitations on other planets. The program will present the advantages and limitations of an aerobot design in simulated planetary environments through material, gas and shape selection, volume restrictions, balloon pressure types, etc. Analyzing the results will offer the user a preferred design option for planetary flight.

The last phase remaining in this thesis is the conclusions and recommendations chapter. Chapter 9 will describe the lessons learnt, and conclude with the current potential of the program. Recommendations on any work yet to be done will be formulated to further improve and expand the simulation program.

2. Aerial Robots – Aerobots

Aerial robots or aerobots are often categorized as rotorcraft. There is however a larger gamma of platforms that can be regarded as aerobots. This chapter deals with defining the aerobot, differentiating it from general aircraft and characterizing the different categories within the aerobot cluster. Additionally the value of aerobots for planetary missions will be addressed. Their ability to hover, accessing impassable terrain and loading a large amount of payload are just a few reasons why aerobots should be considered as a valuable space mission concept.

2.1. Defining Aerobots

According to literature; "An aerobot is an aerial robot, usually used in the context of an unmanned space probe or unmanned aerial vehicle; Most aerobot concepts are based on aerostats, primarily balloons, but occasionally airships [i.5]."

From this simple definition the only real constraint on what an aerobot is or isn't, is the fact that it is an unmanned aircraft. The National Research Council (NRC) in the United States (U.S) defines the aerobot as; "A balloon with one or more of the following characteristics is termed an aerobot" [b.1]:

I. "Autonomous position, altitude and velocity determination without ground intervention"
II. "Altitude control capability"
III. "Ability to execute a designated flight path in a planetary atmosphere using altitude change and global wind patterns"
IV. "Landing capability at designated surface sites"

These characteristics separate the aerobot somewhat from a standard aircraft and are therefore useful in defining an aerobot and its requirements. The definition however limits itself to balloons and neglects any other concept that can be used for aerobots. An aerobot will therefore be defined from here on as '*An aerial vehicle with one or more of the characteristics I to IV*.'

The available aerobot concepts or platforms for which requirements I to IV can hold are best divided into two main categories;

- Lighter-than-air (LTA) platforms
- Heavier-than-air (HTA) platforms

2.1.1. Heavier-than-Air

Heavier-than-air concepts make use of either aerodynamic lift or propelled lift or a combination of both. Concepts in this category include;

- Fixed wing concepts: Unmanned Aerial Vehicles (UAV) , gliders
- Moving wing concepts: Rotorcraft, Vertical Take-Off and Landing (VTOL) concepts

Li [t.1] made an initial study on HTA aerobot concepts for planetary exploration, describing both benefits and drawbacks. This thesis will focus more on LTA concepts, the reader is redirected to Li's work for further reading about HTA concepts.

2.1.2. Lighter-than-Air

Lighter-than-air platforms make use of buoyancy to stay afloat. LTA aerobots are therefore buoyant aerobots. The principle of buoyancy was discovered by Archimedes in the third century B.C. Archimedes principle states "an object submerged in a fluid experiences an upward force that is equal to the weight of the same volume of fluid [b.6]". How this applies to buoyant balloons is further explained by Abe et al [b.5]. The principle behind it however is that an upward force is created simply by the fact that the gas inside the balloon is lighter than the gaseous state of the surrounding atmosphere. The buoyant force for any LTA vehicle can be described from the Archimedes equation [b.3]:

$$F_{buoyant} = \rho_{atm} \cdot Vol_{balloon} \cdot g_{planet}$$

Equation 1: Archimedes Buoyancy Force

'$F_{buoyant}$' is the buoyant force, 'ρ_{atm}' is the atmospheric density, 'Vol' represents the balloon volume and 'g' the gravitational acceleration of the planet. Buoyant aerobots most common examples are balloons, aerostats and airships. Balloons fly free and uncontrolled, while airships are controlled with rudders and/or propellers and aerostats are blimps which are connected with a cable to the ground.

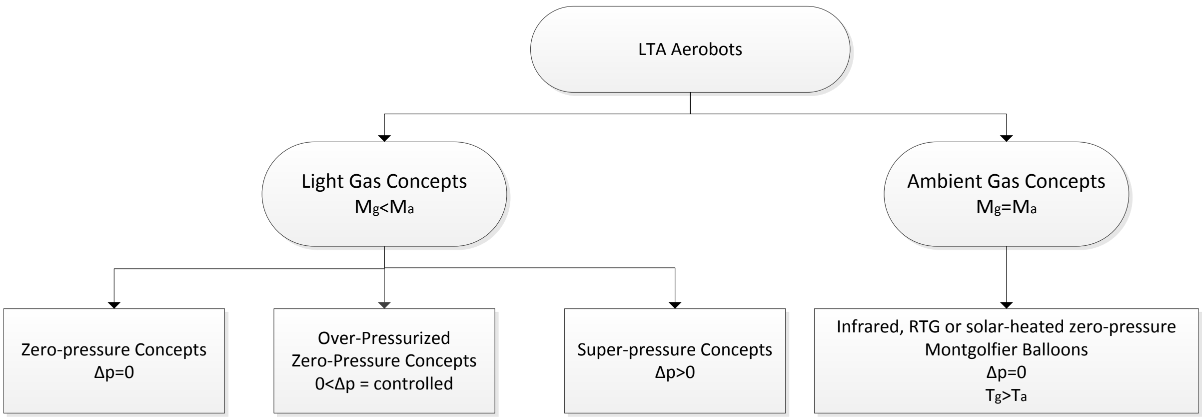

Figure 1: Modified 'Classification Scheme of LTA Aerobots' from Ball et al [b.3]

Buoyant aerobots can be further categorized through the state in which the buoyant gas inside the envelope is in. Figure 1 presents a modified division of LTA aerobots based on that of Ball et al [b.3]. The light gas concepts are based on the use of buoyant gases for which the molar mass M is lighter than that of the atmospheric surroundings. Within this group three additional concepts exist. They depend on the state of the pressure differential Δp between the gas pressure and the atmosphere pressure. The ambient gas concept makes use of the same ambient air inside and outside the balloon. The produced lift can only be controlled by the temperature T inside the balloon. Each concept of Figure 1 will be discussed in detail in the following sections.

2.1.2.1. Zero-Pressure Concept

"Zero-pressure (ZP) balloons are so termed as the internal-external pressure differential is zero at the balloon base. [b.5]" The pressure inside a balloon isn't uniform from base to apex though. Due to the fact that the buoyant gas is lighter than the surrounding atmosphere it will rise to the top of the balloon and will deliver the buoyant force. One can imagine that at the top more buoyant gas is gathered than at the base, which gives a higher gas density at that location and presumably also a higher gas pressure. While pressure distribution inside the balloon is outside the scope of this thesis, the above statement is supported by the results of a study on material stresses for 'Partially Inflated Shapes of Stratospheric Balloon Structures' by Deng and Pellegrino [a.40]. When the balloon is only partially inflated and acts like a ZP balloon, the material stresses are highest at the top of the balloon as seen in Figure 2(a).

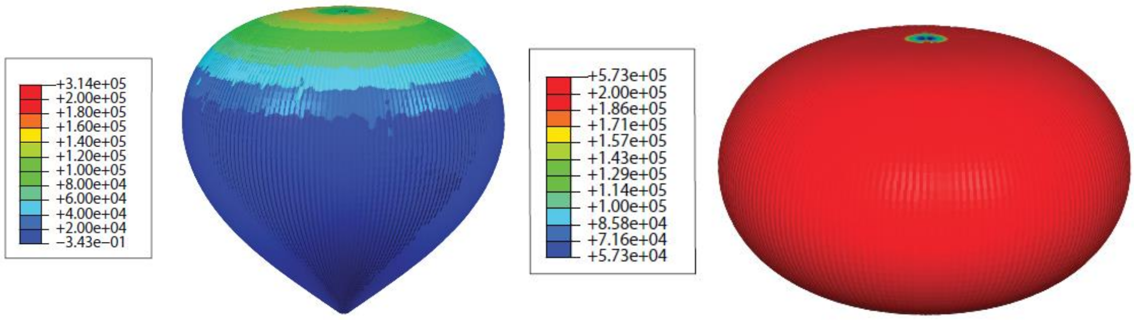

Figure 2: Envelope Hoop Stress for (a) Zero-Pressure and (b) Super-Pressure [a.40]

From here on whenever the pressure differential of a ZP balloon is discussed in this thesis it will be assumed to be the value at the base for simplicity, neglecting the pressure distribution across the balloon.

"A zero-pressure balloon has a vent to the atmosphere at the bottom, such as the one in Figure 4. The balloon is filled only partially on the ground, as shown in Figure 3. As the balloon rises, the gas bubble expands to fill out the balloon from the top downward [i.25]." At float altitude the gas inside the envelope has completely filled the balloon up to its maximum design volume. Since the volume of the balloon ceases to increase, no additional air will be displaced and no further rise in altitude will occur except due to the upward momentum of the balloon system [t.4]. Momentum can cause the balloon to overshoot the design altitude too much, which causes excessive gas venting due to volume restriction. This creates a drop in gas density and buoyancy. When too much gas is expelled the aerobot will start to descend, and it will be unable to stop this descent. "If the temperature difference between atmosphere and lifting gas is ignored, zero-pressure balloons will have an automatic stabilization point when they ascend, but they will not have a stabilization point when they descend [b.5]."

Temperature for zero-pressure balloons however can't be ignored that simply. Especially balloons with a transparent or a black coated envelope are subjected to high temperature differences between lifting gas and atmosphere. Zero-pressure balloons are especially sensitive for the 'sunset effect'. When the sun sets the balloon ceases to absorb radiation from the sun, as a result the temperature of the buoyant gas drops and the buoyancy drops as a result of that. This causes the balloon to descend. If the mission life should take several days, some ballast material, such as sand, can be dropped to maintain altitude. During the next day however, the gas will heat and expand again, but since the system is now lighter, it will ascend higher and dump some more gas. And so on until the supply of ballast is used up. Eventually, it will hit the ground, but this may take several days [i.25].

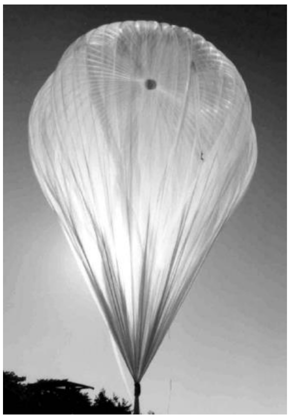

Figure 3: Partially inflated balloon [b.5]

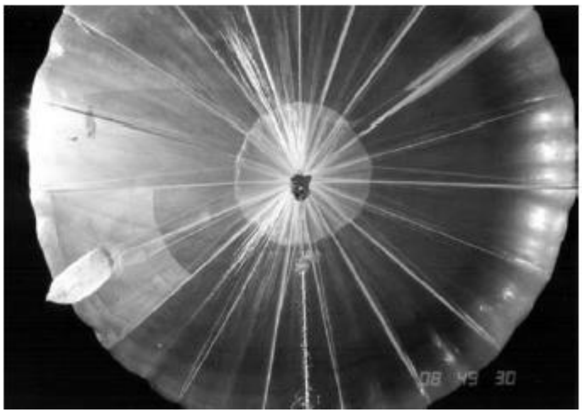

Figure 4: Venting Duct below the balloon [b.5]

2.1.2.2. Super-Pressure Concept

In a super-pressure (SP) balloon, the pressure of the buoyant gas inside the balloon exceeds the ambient pressure in an almost uniform manner, shown in Figure 2(b). The balloon envelope is filled completely on ground and has a fixed volume once it reaches its design altitude and builds up pressure. Therefore and unlike zero-pressure balloons, super-pressure balloons don't make use of a venting duct. However two exceptions are made;

- safety valves that operate automatically to release unexpected high pressures [b.5]
- exhaust valves that are opened and closed by remote operation from a ground base to control the buoyancy [b.5]

When using the latter, the super-pressure balloon becomes more and more an Over-pressurized Zero-pressure balloon, which is discussed in the next subchapter.

In order to stop the ascend of a super-pressure balloon the expansion of the free-lift portion of the gas must be constrained by the envelope. According to Abe et al [b.5], when the diurnal change in the lifting gas temperature is considered, and the pressure difference between lifting gas and atmosphere including the free-lift portion, the pressure differential is about 20% of the atmospheric pressure at flight altitudes. The diurnal cycle or diurnal temperature is the change in temperature during one full rotation of the Earth.

Super-pressure balloons are used for long duration flights and come at the cost of, strong and heavier materials and more demanding balloon designs. Materials often used are [b.3]; polyester, Kapton, nylon, Polybenzobisoxazole (PBO) films, composites. Even so, these balloon films can't always carry the loads for super-pressure balloons. Therefore super-pressure balloons often make use of high-strength reinforcing fibers, also called load tapes, or tendons. This technology increases the envelope's resistance to pressure. "Tendons take most of the super-pressure load, significantly relieving requirements on the balloon's envelope material and allowing the use of weaker films instead of stronger ones" [b.3].

The early balloons were often spherical by nature. When super-pressure balloons were investigated for long duration flights, the spherical balloon shape was initially explored with polyester films like Mylar as the balloon material [a.15]. The size of the spherical balloon turned out to be limited though, with a maximum volume of only 7000m^3. The French Space Agency CNES was the first to propose a pumpkin shaped balloon. "The idea is to relax the stress of the film by reducing the circumferential stress through the use of strong load tapes attached from apex to nadir [a.15]."

Figure 5: Super-pressure pumpkin balloon [b.5]

For super-pressure balloons the super-pressure Δp can be written as a function of gas mass m_{gas}, universal gas constant R_c, gas temperature T_{gas}, molar gas mass M_{gas}, balloon volume Vol and the atmospheric pressure p_{atm} [b.3];

$$\Delta p = \frac{m_{gas} \cdot R_c \cdot T_{gas}}{M_{gas} \cdot Vol} - p_{atm}$$

Equation 2: Super-Pressure

Δp increases with the temperature T_{gas} of the buoyant gas and balloon performance is therefore driven by environmental and balloon envelope properties. "In contrast to a zero-pressure balloon, a super-pressure balloon is stable in both the ascending and descending directions. Since it is not necessary to drop ballast to maintain altitude; long-duration flights become possible. [b.5]" This can be explained due to its constant volume. If the balloon ascends above its defined altitude, air density decreases resulting in a buoyancy drop. Conversely it the altitude decreases the buoyancy increases for a constant volume and the balloon would rise again creating a stable float around the design altitude. If for any reason however the temperature drop would be too big overnight, super-pressure would disappear and the super-pressure balloon would act like a zero-pressure, continuing its descend.

2.1.2.3. Over-Pressurized Zero-Pressure Concept

Within the light gas balloon category zero-pressure and super-pressure balloons are the two main categories. In 1994 a third type of light gas balloon, investigated by Simpson [a.14], was added. "Showing the feasibility of employing some super-pressure with current NASA approved polyethylene films and standard zero-pressure designs the Over-pressurized Zero-Pressure (OZP) balloon originated [a.14]." OZP balloons lack the ducts that normal zero-pressure balloons have. Instead they make use of a valve that will vent gas on command. Venting is required during float condition to limit excessive pressures in the polyethylene structure of the balloon. Close pressure control is applied to the OZP to limit the pressure.

OZP's have significant performance advantages over their zero-pressure brethren, according to Simpson [a.14], especially on mission lifetime and altitude controllability. "Although more gas is retained at float by an OZP balloon than a zero-pressure one, gas still must be vented to maintain safe operating pressure.

The OZP development project became later known as the Long Duration Balloon Vehicle (LDBV) project, which is discussed in detail in section 3.1.1. The project showed the performance gains and structural limits of the OZP concept through analysis and test flights. The inherently large resource risk involved with LDB campaigns dictates that a simple system with a high degree of operational reliability is desirable. [a.14]" One slight disadvantage for OZP systems is the typical delay to return to a stable ascend after venting. For large OZP systems this takes about ten minutes.

While OZP's are not an official part of the LTA aerobot concept schematic by Ball et al [b.3] in Figure 1, it combines some characteristics of both zero-pressure and super-pressure balloons to distinguish it from both other categories.

2.1.2.4. Ambient Pressure Concept

Ambient balloons use the air of the atmosphere as the buoyant gas, which means that both the molar mass and pressure of the gas and the atmosphere are the same. "The buoyancy of ambient gas balloons is created by heating of the gas and depends on an excess temperature ΔT [b.3]";

$$T_{gas} = T_{atm} + \Delta T$$

Equation 3: Temperature Difference Gas-Atmosphere

When the gas inside the balloon is heating up, the gas density shall attain a lower value than the atmosphere surrounding the balloon. The gas inside the balloon expands due to the increased temperature and is either expelled when the volume is restricted or able to expand when the balloon volume continues to grow. Both methods will preserve a zero-pressure level at the base of the balloon. An example of such a concept is a Montgolfier balloon. The Montgolfier is a hot air balloon which is filled with heated ambient gas. The first hot air balloon was flown by the Montgolfier brothers in 1783. Montgolfier balloons receive their heat from the sun, infrared (IR) radiation or Radio-isotope Thermo-electric Generator (RTG's). These techniques can be used on Earth, Mars and Saturn's moon Titan.

The Jet Propulsion Laboratory (JPL) and NASA have been testing this type of balloon and came to the conclusion that it would be possible to use a Montgolfier balloon as a "faster, better and cheaper landing system for payloads [a.17]" on the above mentioned planets. Further information on Montgolfier balloons is given in the JPL and NASA case study in section 3.1.2.

2.2. Aerobot Value

"Aerial vehicles used in planetary exploration bridge the scale and resolution measurement gaps between orbiters, which have global perspective with limited spatial resolution, and landers which have local perspective with high spatial resolution, thus complementing and extending orbital and landed measurements. Planetary aerial vehicles can also survey scientifically interesting terrain that is inaccessible or hazardous to landed missions [a.4]." This indicates that an aerobot can provide a substantial scientific return far beyond the alternatives like an orbiter, lander or surface rover. This subchapter will discuss the potential of an aerobot and shall address coverage, payload mass and maneuvering to indicate this.

2.2.1. Coverage and Spatial Resolution

"Autonomous aerial vehicles enable a new class of science and exploration through their unique near-surface perspective and regional-scale coverage capability. Orbital and other remote sensing measurement techniques provide global coverage but at the cost of resolution. Surface measurements provide high resolution and the ground facts needed to calibrate remotely sensed measurements, but they come at the expense of coverage and regional perspective. Aerial vehicles can increase the overall efficiency of the exploration of the solar system since they cover regional-scale areas at high resolution [a.4]." The aerial vehicles mentioned here include aerobots and are therefore a valuable platform for scientific planetary missions that require regional-scale research and high resolution with high mobility in a region.

2.2.2. Science Payloads

From a study done by NASA, it seems that aerial platforms are an efficient means of delivering science payloads when compared to other platforms used for planetary science. Figure 6(a) and (b) [a.4] illustrate the science payload dry and gross mass fraction respectively of various interplanetary missions. All three aerial missions, Titan (balloon discussed in section 3.1.5), Ares (plane) and Vega (balloon discussed in section 3.1.6), score very high in the payload mass fraction graph.

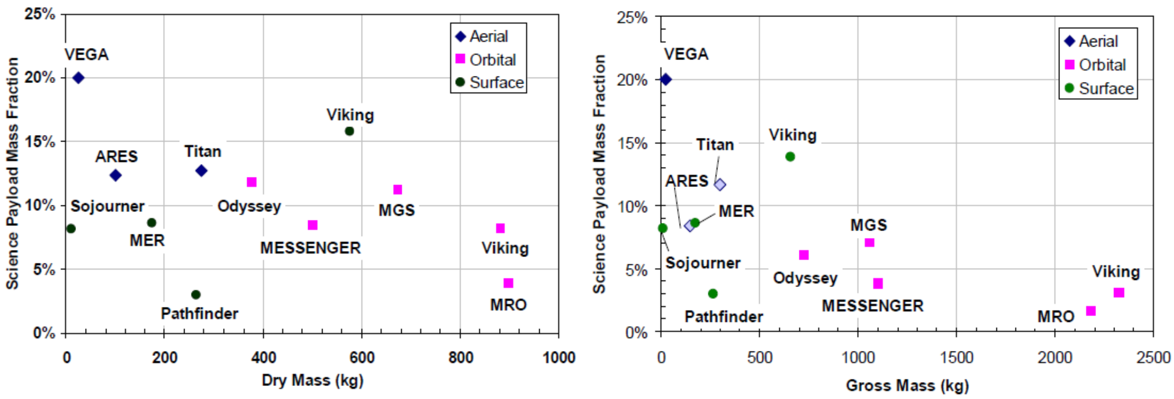

Figure 6: (a) Dry Mass and (b) Gross Mass Compared to Payload Mass [a.4]

"Extended mission life is a key concern for orbital platforms. As a result, significant attention is paid to the propellant quantity and its use throughout the mission. Rovers have a significant amount of their mass attributed to the drive and suspension systems. Landers have a similar longevity concern as orbiters, as well as the need for safely reaching the surface. Aerial platforms are no different in that they must attribute some of their mass to the system for remaining aloft as well as maintaining the desired control and orientation. One unique feature of the airplane is that an increase in science payload mass can be accommodated by removing propellant [a.4].” Most missions shown in Figure 6 are landers, rovers, satellites or models for airplanes under research. One existing mission points out though, namely ‘Vega’. This mission has a very low gross and dry mass compared to the other examples, and has a very high payload percentage onboard. It happens to be the only buoyant aerobot in this study, next to the Titan mission, with a balloon as a flying component. More importantly it is currently the only aerobot flown on another planet. From this study it should be stated that aerobots can be a very efficient means for scientific payload and in particular for atmospheric science packages and payload delivery such as small probes [t.1].

2.2.3. Hovering and Maneuvering

An aerobot can be designed to hover over one particular spot. This is something a UAV, plane or satellite can’t do. Planes and satellite can fly in the same vicinity of a spot but can’t hover over the same spot for a period of time. This might be useful in refueling the aerobot while hovering or landing near the refueling station. Similar a hovering aerobot can be used to drop-off probes at very specific spots or pick-up payload, currently something only a rover is able to do and only if the terrain allows it.

When designed small enough and capable of maneuvering, an aerobot might be able to fly where probes, satellite and rovers can’t reach. Caves and canyons for instance are impenetrable for rovers, and hard to see from the air by UAV, satellite or plane.

3. Learning from Past, Current and Future Aerobot Missions

Scientific balloons, of which stratospheric balloons are the best known, are buoyant aerobots used for atmospheric research on Earth. Scientific balloons are very large flexible structures that are designed to carry payloads to the upper layers of the atmosphere. There is a global interest in scientific ballooning because it became evident that this kind of approach to scientific research for near-space applications is both successful and cost-effective [t.4].

Section 3.1 will explore a number of concepts for planetary buoyant aerobots. Some of them like the LDB and ULDB show that stratospheric ballooning has been, and still is, a solid base for planetary buoyant aerobot research. Other concepts like the Tropical balloon, the Titan aerobot and the JPL Testbed make use of an airship and use propellers for a controlled propelled flight. The explored concepts will give a better understanding of the available technology on current buoyant aerobots.

Section 3.2 will summarize the obtained features of each concept discussed in section 3.1. Specifically a mass budget for each concept is acquired and the differences in aerobot design are addressed. These include; the type of balloon shape, the type of buoyant gas used, the range in flight altitude etc. Further a number of general lessons in aerobot design are formulated.

Based on the lessons learnt plus the advantages and disadvantages of each example discussed, extra general characteristics for buoyant platforms were listed. These characteristics, together with those from the aerobot definition in section 2.1, will serve as general requirements for buoyant aerobots and are used in a trade-off between different buoyant platforms in section 3.3. The trade-off is done to demonstrate the effectiveness of each type of buoyant platform compared to others.

3.1. Buoyant Aerobot Example Study

In this subchapter a number of buoyant aerobot concepts from past, present and future will be discussed. The goal of this study is to explore the available technology on current buoyant aerobots. The advantages and disadvantages of each concept discussed in this study will be used in the upcoming sections for further analysis on aerobot design.

3.1.1. Ultra and Long Duration Balloons

The Long Duration Balloon (LDB), and next the Ultra Long Duration Balloon (ULDB), are both scientific ballooning development programs of NASA. Management of the programs is held by Goddard Space Flight Center (GSFC) at the Wallops Flight Facility (WFF) [a.19].

NASA’s long duration balloon development effort began in 1988. “The objective was to provide a near global long duration balloon flight capability for both polar and non-polar scientific applications on Earth [a.19].” The LDBV project was basically established to develop an advanced generation of balloon vehicles with extended flight capability. It was soon recognized that long duration observations were indispensable for performing precise scientific observations. The two main problems to overcome to achieve such long duration flights however are; balloon drift and ballasting [a.15].

Balloon drift from a telemetry point of view was solved by the Global Positioning System (GPS) and using prepared recovery areas on Earth. “A balloon loses about 10% of its lift during the day to night excursion. [a.15]” This loss in lift has to be corrected by dropping an equivalent amount of ballast if the predefined altitude has to be maintained. As this is the most serious problem for long duration flights, a lot of attention to this problem was spent. Solutions to avoid ballast were: super-pressure, Montgolfier, and flying around the Polar Regions on Earth during periods of no sunset.

3.1.1.1. Long Duration Balloon

The LDB program makes use of zero-pressure balloons flying near the Polar Regions on Earth. While zero-pressure balloons need ballasting to stay afloat during night, due to the diurnal effect, the LDB makes use of certain regions on Earth, such as the Polar Regions, that have a long day to night ratio. This lowers the need for ballasting and increases the endurance of the balloon. “In principle ballasting is not even needed for Polar flights. [a.15]” At this stage this makes the Polar flights the most efficient long duration system.

In 2003 the program made use of 5 standard conventional zero-pressure balloons ranging in volume from 300000 to 1130000m^3 [a.20]. A new endurance record of 31 days and 20.3hrs was established in 2002. The zero-pressure balloon had a volume of 835000m^3.

The material used for those balloons is a polyethylene film. “Polyethylene film has a superior character as a balloon film, specifically its low brittleness temperature [a.15].” Polyester, Nylon and other plastic materials have also been investigated. “These have normally higher ultimate strength but their ultimate elongation is not large enough [a.15].” Zero-pressure balloons make use of their capability of volume expansion and as such Polyethylene film makes a good material for such balloons. In the 1980’s however balloon failure rates increased by the demand of increasing the size of balloons and the weights of payloads. NASA spent many efforts to improve the situation. Around the same time a new Linear Low Density Polyethylene (LLDPE) became available. It works well at low temperature. The films have brittleness temperatures nearly to -100°C. “The success rate of balloons increased again to almost 100% and the problem seemed to be solved as far as zero-pressure balloons were concerned [a.15].”

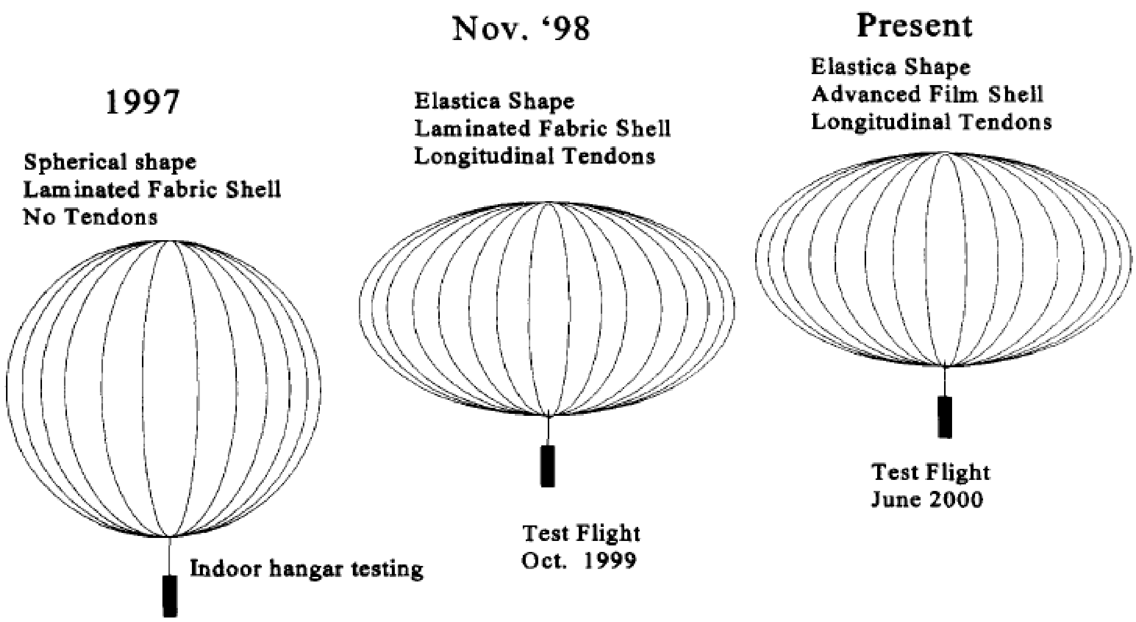

Figure 7: Evolution of the Ultra Long Duration Balloon [a.16]

3.1.1.2. Ultra Long Duration Balloon

"The ULDB project is focused on offering an extended duration platform at a constant density altitude. [a.20]" The ULDB program makes use of the pumpkin shaped super-pressure balloon for this. As mentioned before CNES was the first to propose the pumpkin shaped balloon instead of the spherical shaped balloon. It would lower the stress of the film in the circumferential direction through the use of strong load tapes. The equator sections for a pumpkin shaped balloon do exhibit the largest amount of stretching under the pressure loads, and if any permanent deformation occurs, this would be the area to exhibit this [a.21].

The development of the ULDB was an evolutionary process, illustrated in Figure 7. "The original concept was a spherical shell with a very strong coated fabric. The next step in the design was to keep the coated fabric but change the shape to an elastica shape, or pumpkin shape, and transfer the loads to longitudinal tendons along the seams. [a.16]"

Materials such as polyester, biaxial oriented-Nylon, Ethylene-Vinyl-Alcohol (EVAL) and a combination of these films were widely investigated for use in super-pressure balloons [a.15]. The current ULDB design is the elastica shape with an advanced multi-layer polyethylene shell.

"The first flight test of a 53000m^3 ULDB prototype was conducted from Fort Sumner New Mexico in October 1999. As the balloon ascended one of the tendons became detached from the surface of the balloon and rolled on an adjacent tendon [a.16]." This started a chain reaction that finally caused a displacement of twenty tendons and the shell material rupturing. The flaw in the material was discovered and a next test flight on June 4th, 2000 was flown with a multi-layer polyethylene shell and a 68000m^3 volume. This test flight was a complete success.

On February 4th, 2005 a 176000m^3 pumpkin design balloon was successfully launched. It ascended to, and reached, float altitude and started to pressurize [a.21]. As it reached float it experienced a failure in the closing seal of the balloon. The balloon only deployed fully in the upper section. The post flight investigation showed a surface oxidation of material from long-term plant light exposure that created a bad seal. Another test flight on June 12th, 2006, with a similar balloon showed an undesired S cleft formation, or deformity, shown in Figure 8. The balloon didn't fully deploy, and even a super-pressure of about 256Pa, which was 10% above maximum design pressure, didn't remove the S cleft. Even though despite the undesired shape the balloon operated perfectly; the balloon reached a stable float altitude and the ascend rates and initial pressurization were regulated as planned [a.21].

Figure 8: S-Cleft in Pumpkin [a.21]

Figure 9: Fully Deployed Pumpkin [a.21]

A detailed analysis on stable, but deformed, super-pressure balloons can be found from Deng [t.5]. After post test flight investigations, described by Cathey [a.21], a solution was found to avoid the S cleft. Each balloon has an excess of material, by removing some of the gores it was possible to lower the excess balloon material. Removing gores was done by trussing the balloon in a number of locations through stitching adjacent seals together. During deployment of this adapted balloon no cleft appeared. The balloon didn't deploy completely at first, but with a small overpressure this problem was solved too. With another method of inflation it was eventually completely deployed without problems.

In spring 2008 another test flight took place. With a volume of 56700m^3, a diameter of 54.47m, and a height of 33.36m during float, the balloon carried a suspended load of 295kg. The main goal of this test flight was full deployment of the balloon. "There was one un-deployed area in the balloon as it reached float. This feature looked similar to a smaller version of the malformed features seen before on test models and flight balloons [a.21]." When the balloon pressurized the feature slowly disappeared and the balloon fully deployed. The maximum differential pressure measured during this flight was over 360Pa, which represented 1.8 times the design level.

3.1.2. Planetary Montgolfier Balloons

Montgolfier balloons make use of the temperature difference between the heated ambient atmospheric gas inside the balloon and the air outside to be able to float. "NASA recently became involved in stratospheric testing of a solar-heated Montgolfier for mission applications. The primary focus of NASA's Jet Propulsion Laboratory (JPL) has been on high-altitude deployment of Montgolfier's to simulate atmospheric descent and deployment of a balloon in the thin atmosphere of Mars. [a.18]"

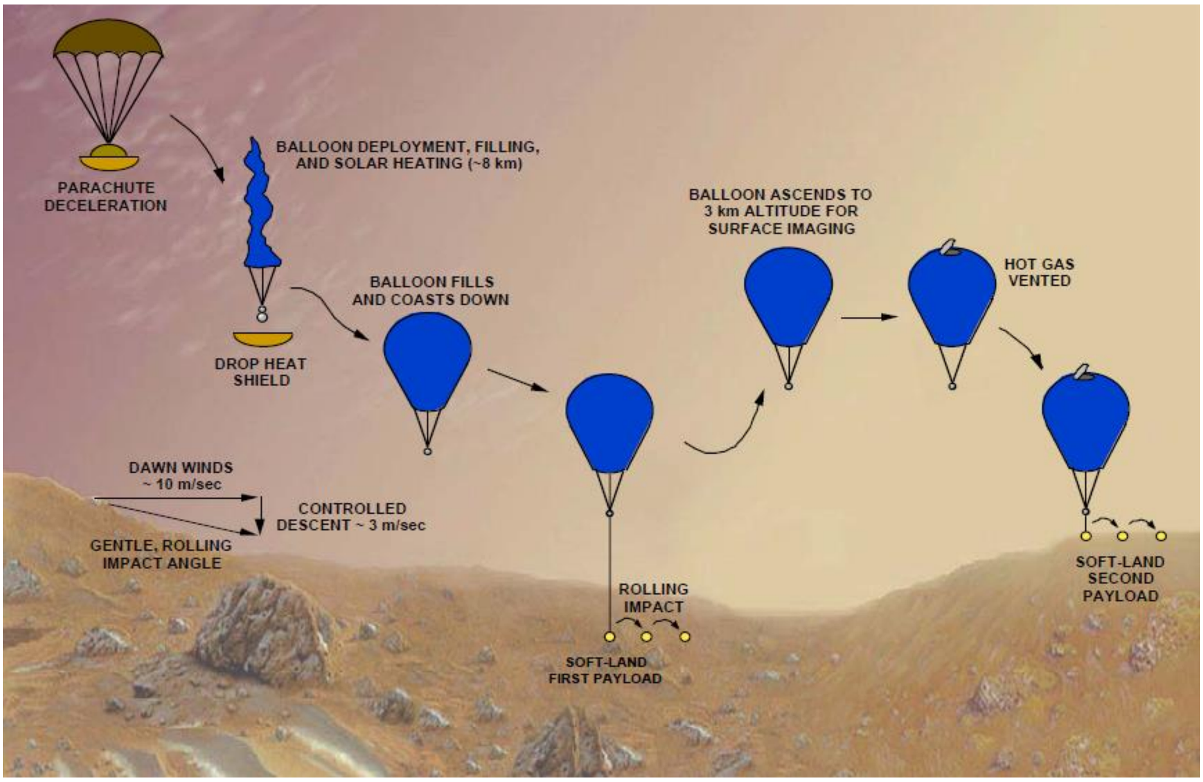

Figure 10: Solar Montgolfier Mission [a.18]

In the past the known Mars missions to explore the planet and its atmosphere included rovers and satellites. The option of sending a super-pressure balloon for a constant floating altitude was also available. A fourth possible concept now is the solar Montgolfier which appears quite viable for controlled landings at selected Martian surface locations. According to JPL the balloon could soft-land payload packages and be able to continue its path into the atmosphere [a.17]. Its atmospheric entry, mission and soft-landings are illustrated in Figure 10 and provided by JPL.

The soft-landings would be possible through the use of the heated air inside the balloon and the use of a radio controlled lightweight top air vent to control the ascend and descent rate. It would be possible to fly a 2kg gondola on Mars with a balloon mass of only 4.4kg [a.17]. Tests already confirmed the capability of actual landings and re-ascends of solar-hot-air balloons. The advantages beyond other Mars landing systems are [a.17];

- The use of 'simple' solar Montgolfier balloons can eliminate the need for heavy expensive retro-rocket landing systems
- Comparison with a double parachute system shows that the parachute becomes unstable below 20m/s descend velocity; whereas the Montgolfier approach is fully stable down to 0m/s. Low descent rates are therefore possible. It is also three times less massive.
- Montgolfier's can re-ascend and fly onwards for a long time when in constant daylight.

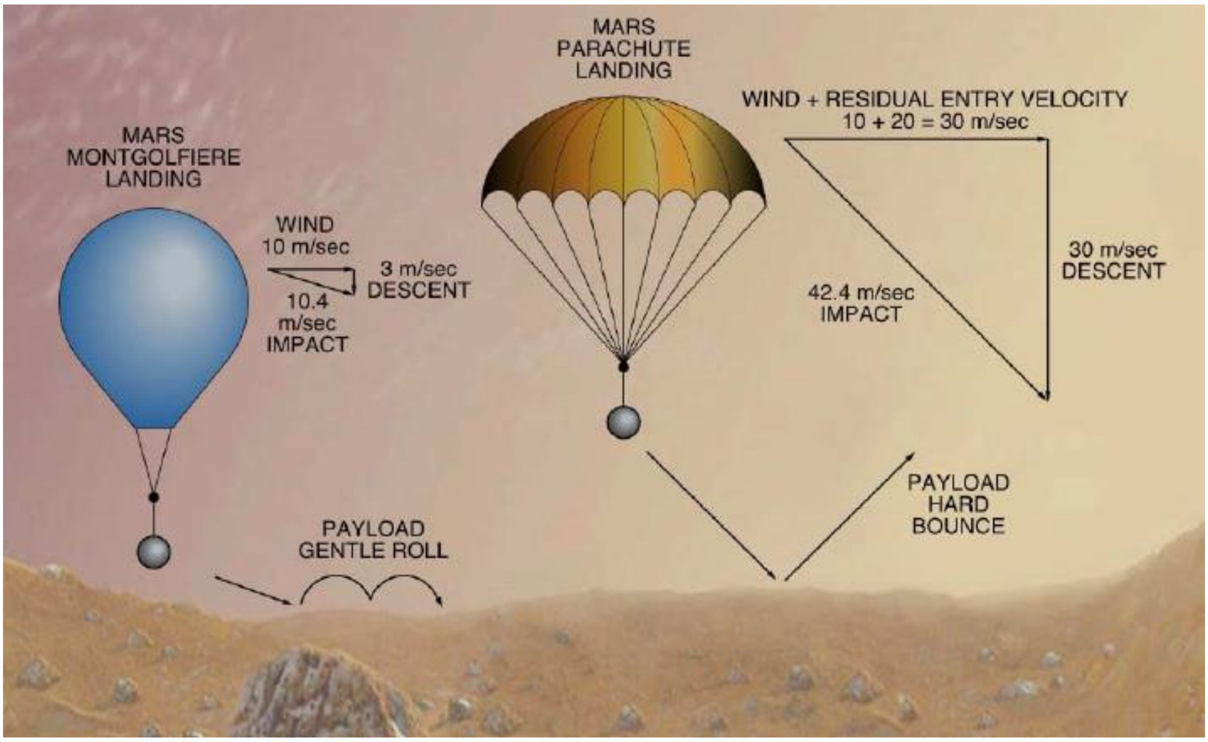

Figure 11: Montgolfier Landing Versus Parachute Landing [a.18]

After initial parachute deceleration and deployment of the Montgolfier balloon, the balloon attains significant buoyancy within two minutes, which slows the downward velocity to about 5-10m/s [a.17]. Buoyancy only increases and in the end lowers descent rate to a controlled 3m/s. Figure 11, provided by JPL, compares the payload impact between Montgolfier soft-landing and parachute landing. A lot of the vertical energy can be converted to rolling energy. The horizontal component however can't be damped out. The total impact velocity is therefore higher for a parachute than for a Montgolfier. 90% of the impact energy of the Montgolfier can be damped out into rolling energy, were only about 50% can be damped out for a parachute landing.

Montgolfier's were almost always fabricated from 12µm Mylar and Polyethylene since the 1970's. The French always deployed the Montgolfier's from ground; it is only since 1997 that JPL started with deployments in the stratosphere to get conditions similar to the Martian atmosphere. This however also meant higher stresses on the Polyethylene envelope fabric.
Three out of four test deployments in the stratosphere with 8m and 15m diameter Polyethylene Montgolfier's were successful. Two larger balloons with a diameter of 20m were unsuccessful [a.18]. Post analysis showed that the balloons weren't strong enough to withstand the deployment stresses. As Montgolfier's make use of sunlight to heat the air inside, a black colored plastic is being used for higher efficiency. An estimation of two Montgolfier designs from 1999 [a.17] is presented in Table 1;

Table 1: Montgolfier Envelope Mass Budgets [a.17]

Envelope Density [g/m^2]	**Gondola Mass [kg]**	**Balloon Diameter [m]**	**Balloon Mass [kg]**
9	2	12.46	4.39
13	2	15.05	9.25
9	10	17.96	9.12
13	10	19.97	16.29
Assumptions	Pressure at 3km = 0.00457bar Atmospheric Temperature = 200K Solar Absorptivity = 0.6, Emissivity = 0.03 Solar Flux = 500W/m^2		

3.1.3. Mars Aerobot/Balloon System (MABS)

"In late 1995, a study was initiated by JPL of a 2001 Mars Aerobot/Balloon System (MABS). Mission participants included NASA, Goddard Space Flight Center, WFF, Lockheed Martin Aeronautics (LMA), CNES's Toulouse Space Center, NASA Ames Research Center (ARC), and Space Dynamics Laboratory (SDL) plus numerous industrial partners [a.1]."

Table 2: MABS Baseline Design [a.1]

Volume	10500	[m^3]	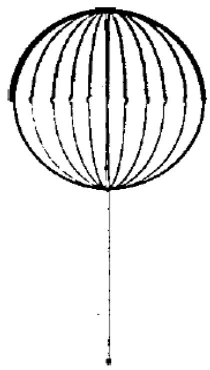
Diameter	27	[m]	
Balloon Mass	85	[kg]	
Payload Mass	15	[kg]	
Float Altitude	6.8	[km]	
Daytime Δp	240	[Pa]	
Night Δp	20	[Pa]	
Balloon Material	3.5pm Mylar, 55Denier Kevlar, 6µm SF-272	[/]	
Envelope Density	20	[g/m^2]	
Envelope Strength	2800	[N/m]	
Coatings	Top is aluminized, bottom is white	[/]	

The study scope included definition and identification of mission concept technical issues, including; science instruments, gondola, balloon system design, entry vehicle and cruise spacecraft design, and launch vehicle performance considerations. Key constraints on the mission study were a 2001 Mars launch opportunity, a Delta launch vehicle, maximum use of the Mars Surveyor Program (MSP) cruise and entry systems, the use of Mars Global Surveyor and MSP orbiter to relay communications and a 90 day mission duration. “Key assumptions of the study included a gondola mass of the order of 10kg including science instruments, “constant” density altitude, a super-pressure balloon design without landing capability and a cruise altitude of 5-8km [a.1].” The study effort concluded that the MABS mission is feasible, based on conservative environmental and technical readiness, provided that early and significant NASA investment in balloon system technology is initiated.

In the end the design by JPL, shown in Table 2, included a 10500m^3 balloon filled with helium or hydrogen, while the material of the balloon would be a composite of Mylar and Kevlar. The balloon would carry a gondola of 10-20kg. The flight system was spin stabilized in cruise and used sun sensors and redundant star cameras for attitude reference. The super-pressure Δp was expected to be 240Pa during daytime. When the sun sets and the temperature drops, the super-pressure was expected to drop to a value of only 20Pa. To know the impact of the Martian atmosphere and environment on the balloon a model for both was used to help with the design of the aerobot. A thorough trade and risk assessment was done before selecting key components from Commercial off the Shelf (COTS) products and custom components.

3.1.4. JPL Aerobot Testbed

Another design of JPL is the Aerobot Testbed. It is an autonomous airship as can be seen in Figure 12 and Figure 13. The testbed is currently testing the following technologies [i.7]:

- "Vehicle safing" to ensure the safety and integrity of the aerobot over the full duration of the mission, including extended communication blackouts.
- Accurate and robust autonomous flight control, including deployment/lift-off, long traverses, hovering/station-keeping, and touch-and-go surface sampling.
- Spatial mapping and self-localization for extended geographical surveys.
- Advanced perceptual hazard and target recognition, tracking and servoing, allowing the aerobot to detect and avoid atmospheric and topographic hazards, and also to identify, home in on, and keep station over predefined science targets or terrain features.

Figure 12: JPL Aerobot Testbed [i.7]

Figure 13: JPL Aerobot Testbed in Flight [i.7]

The airship specifications are as follows [i.7]:

- Length of 11m
- Diameter of 2.5m
- Total volume of $34m^3$
- Two 2.3kW, $23cm^3$ fuel engines
- Double-catenary gondola suspension
- Control surfaces in an "X" configuration
- Maximum speed of 13m/s

Additionally, the airship is able to carry;

- 12kg of payload through static lift
- 16kg of payload through dynamic lift

Static lift is the lift force the airship is capable to deliver through buoyancy. While the dynamic lift is the extra lift created through the engines. By controlling the direction of the engines, a vertical thrust component can be created for extra lift. This force can increase the airship's attainable payload mass.

"The avionics and communication systems are installed in the gondola. The aerobot avionics system is built around a dual-stack computer architecture. One of the stacks is used for navigation and flight control, while the other is dedicated to image processing. Wireless serial modems provide data/control telemetry links between the aerobot and the ground station, and additional video transmitters on the aerobot provide downlinks of video imagery to the ground station. The human backup pilot can always reassert "pilot override" control over the aerobot. " [i.7]

Available navigation sensors consist of; an inertial measurement unit (IMU) which measures angular rates and linear accelerations, a compass/inclinometer giving yaw, roll and pitch angles, a laser altimeter to measure relative altitude, a barometric altimeter for the absolute altitude against a reference point, and a global positioning system (GPS) for an absolute 3D position. "The vision sensors include two down-looking navigation cameras, one providing a 360° x 180° view, while the other has a narrower field of view. [i.7]"

3.1.5. Titan Balloon

The Titan balloon is a proposed design for a propeller-driven, buoyant vehicle that resembles terrestrial airships. However, the extremely cold Titan environment requires the use of cryogenic materials of construction and careful thermal design for protection of temperature-sensitive payload elements. Multiple candidate balloon materials have been identified based on extensive laboratory testing at 77K. The most promising materials to date are laminates comprised of polyester fabrics and/or films with areal densities in the range of 40-100g/m^2.

The aerobot hull is a streamlined ellipsoid 14m in length with a maximum diameter of 3m, illustrated in Figure 14 and provided by JPL. The enclosed volume of $60m^3$ is sufficient to float a mass of 234kg at a maximum altitude of 8km at Titan. Forward and aft ballonets are located inside the hull to enable the aerobot to descend to the surface while preserving a fully inflated streamlined shape. Ballonets are airbags inside the envelope filled with atmospheric air. As the air inside the ballonet has a higher density than the buoyant gas, they are able to inflate and deflate to maintain the external shape of the airship during ascend and descend. Altitude changes are effected primarily through thrust vectoring of the twin main propellers, with pressure modulated buoyancy change via the ballonets available as a slower backup option.

A total of 100W of electrical power is provided to the vehicle by a radioisotope power supply (RPS). Up to half of this power is available to the propulsion system to generate a top flight speed in the range of 1-2m/s. This speed is expected to be greater than the near surface winds at Titan, enabling the aerobot to fly to and hover over targets of interest. A preliminary science payload has been devised for the aerobot to give it the capability for aerial imaging of the surface, atmospheric observations and sampling, and surface sample acquisition and analysis. Targeting, hovering, surface sample acquisition and vehicle health monitoring and automatic saving actions will all require significant on-board autonomy due to the over two hour round trip light time between Titan and Earth. Autonomy architecture and a core set of perception, reasoning and control technologies are under development using the free-flying JPL testbed, just mentioned before, having approximately the same size as the proposed Titan aerobot. Data volume from the Titan science mission is expected to be in the order of 100-300Mbit per day, transmitted either direct to Earth through an 0.8m high gain antenna or via an orbiter relay using an omni-directional antenna on the aerobot" [a.2]. The schematic and technological details of this Titan aerobot can be found below [a.2].

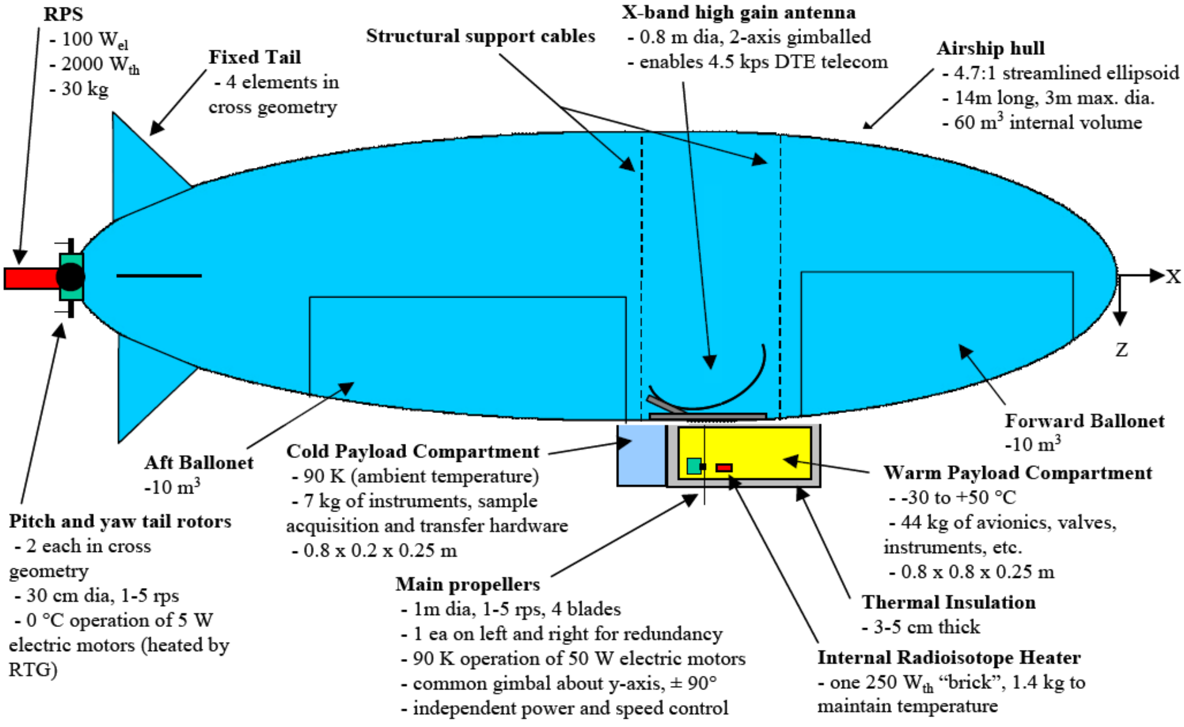

Figure 14: JPL's Titan Aerobot [a.2]

3.1.6. The Vega Missions

Vega was a redesigned Russian-French cooperation mission that flew two balloons into the Venusian atmosphere. The two aerobots, named Vega-1 and Vega-2, were designed to float at about 54km [a.8] from the surface, in the most active layer of the Venusian cloud system. The instrument pack had enough battery power for sixty hours of operation and measured temperature, pressure, vertical wind speed and aerosol density.

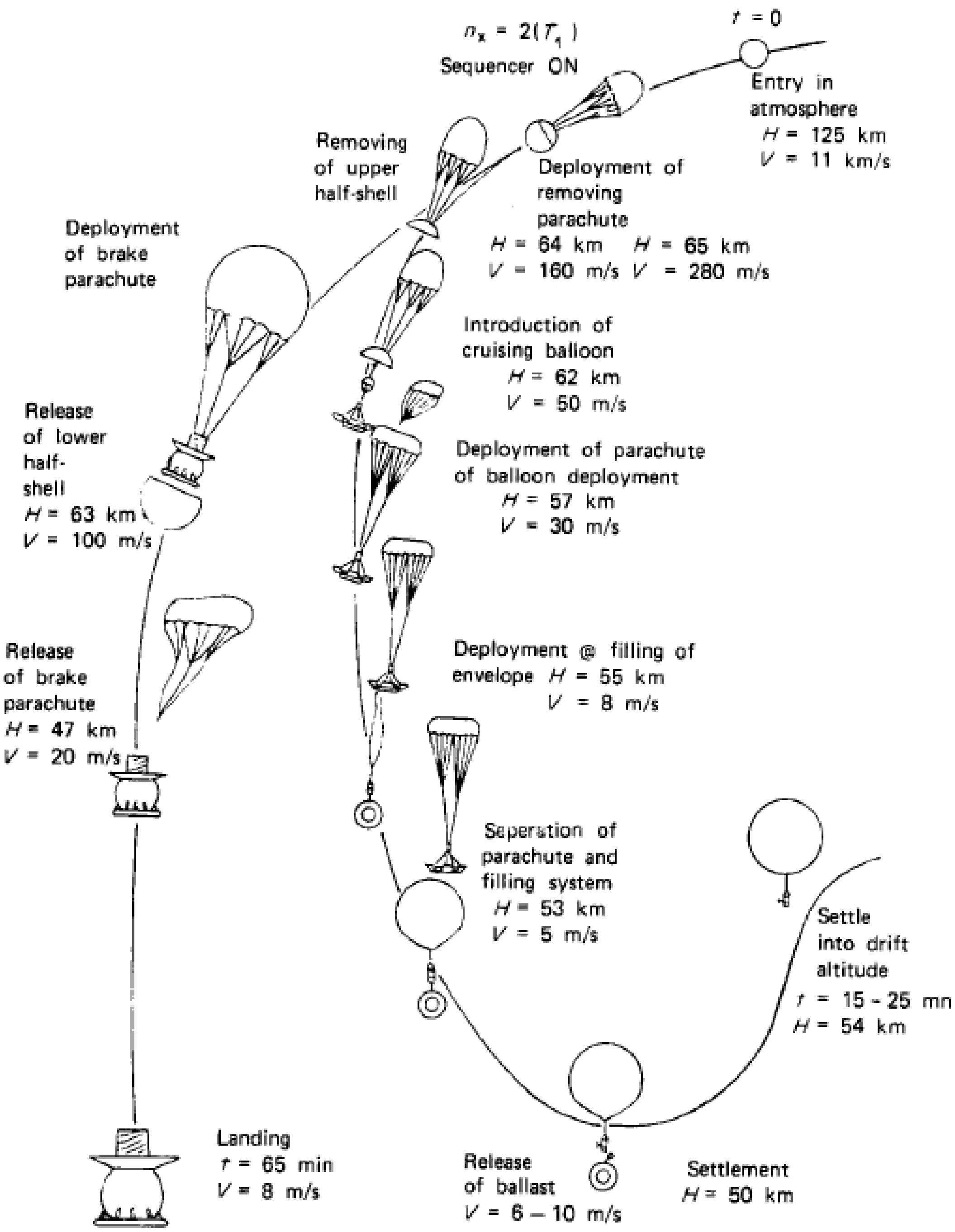

Figure 15: Vega Balloon and Lander Deployment Sequence [a.8]

Figure 15, provided by the Russian Space Research Institute (IKI), represents the landing and deployment sequence of the Vega module. The aerobot module was disconnected and deployed from the lander module in the atmosphere at an altitude of 64km. The balloons were spherical super-pressure types with a diameter of 3.54m and filled with helium at an altitude of 53km. A gondola assembly weighing 6.87kg [a.8] and 1.3m long was connected to the balloon envelope by a tether 13m long [i.9]. Total mass of the entire assembly was 21kg [a.8].

The balloons were dropped onto the planet's dark side and deployed at an altitude of about 50km. They then floated a few kilometers upward to their equilibrium altitude of 54km. At this altitude, pressure and temperature conditions of Venus are similar to those of Earth, though the planet's winds move at hurricane velocity and the carbon dioxide atmosphere is laced with sulfuric acid, along with smaller concentrations of hydrochloric and hydrofluoric acid [i.10].

So far, these two balloons are to only buoyant aerobots flown on another planet. Despite their promising results no successors were ever used in any other planetary missions.

3.1.7. Archimedes

The Mars Society of Germany has proposed Archimedes: a short duration, low cost Mars balloon project, that would be launched as a piggy-back payload on the amateur's satellite (AMSAT) orbiter AMSAT P5-A. "Archimedes is a small advanced interplanetary space mission which deploys a balloon in the atmosphere of planet Mars. This mission concept provides science capabilities complementary to orbiter and parachute descent missions [a.6]."

Aerobots offer great benefits but also give technical problems with deployment. "If they are filled under a parachute there is a vertical slipstream. If they are filled on the surface, the terrain may be unsuitable and there may be surface wind. [a.11]" "Ascending from the surface of Mars with a balloon or a sounding rocket is difficult at best, because relatively high wind speeds prevent the deployment of large delicate balloon hulls or airplane wings without considerable mechanical effort [a.10]." "A high altitude mission might also descent from space, provided it can be built to decelerate at a sufficiently high altitude to make scientific gains desirable. No conventional hypersonic aeroshell and parachute system will slow down sufficiently to allow deployment far enough above the surface, as its mass to drag ratio or "ballistic coefficient" is much too high [a.10]."

In the end the designers chose for deployment in space by means of a ballute, its drag slowing down the aerobot, to slowly sink to its operational altitude. A 'ballute', or balloon parachute, "is a concept that has been under active development for the past seven years by the Mars Society of Germany and the University of the Federal Armed Forces of Germany in Munich [a.11]." "Today, the term "ballute" is used for any inflatable device intended to raise an object's aerodynamic drag, no matter the shape or intended purpose [a.10]."

This way, the Archimedes mission will demonstrate the technology for inflatable atmospheric drag devices on Mars. This means it will provide valuable data even if later phases of the mission fail. The nominal duration of the mission is 10 sols, or Martian days.

Figure 16: Archimedes

Figure 17: Vega Balloon

The payload onboard resembles the name of the project, namely: ‘Aerial reconnaissance Robot Carrying High-resolution Imaging, a Magnetometer Experiment and Direct Environmental Sensors’ (Archimedes) [a.10]. The first payload is a camera, provided by the ‘Deutsches Zentrum für Luft- und Raumfahrt’ (DLR) in Germany; which will be based on the Rosetta Lander Imaging System (ROLIS) camera of the Rosetta space probe. It will be able to achieve a resolution of up to 20cm per pixel at a 7km distance from the surface. While this resolution is not really stunning, it will be able to take images from an oblique, 45 degree perspective.

The second payload is a magnetometer, provided by the Technical University of Braunschweig. Measurements of the Martian residual crustal magnetic field were last made by the Mars Global Surveyor spacecraft during the aero-breaking phase of the mission, in an altitude range between 100km and 200km. Archimedes would be able to make more local measurements. The combination of a high resolution camera and a magnetometer makes it possible to correlate magnetism and geological features. It would also be the first magnetic measurement below the ionosphere. It could also be compared to magnetic field measurements onboard the orbiter at the same time.

The third payload consists of a set of atmospheric sensors with a thermometer, barometer and hygrometer, by the Finnish Meteorological Institute (FMI). “It will help in the understanding of the atmospheric dynamics and structure of the atmosphere [i.8].” Included in the sensor package is also an accelerometer that records six degrees of freedom and is delivered by the Institute of Computer Sciences of the Technical University of Iasi, Romania. “It will help to understand the behavior of the vehicle during its entry and subsequent descend through the sound barrier. [i.8]”

3.1.8. Amateurs Atmospheric Balloon (AAB)

Colleges and universities across the world do a lot of atmospheric experiments. These experiments are sent up into the atmosphere by means of a meteorological balloon. These balloons bring a payload of about 1kg up in the air. The size of the balloon is about 4.85m^3. In the 1kg payload package the main components are: one camera, batteries, GPS and a flight computer [i.6].

Table 3: AAB's Detailed Mass Budget

Item	Mass [g]
7.4V Battery	92.14
3.7V Battery	92.14
9V Battery	49.61
Camera	148.83
Transistors (2)	14.175
Cutdown Relay	14.175
Power Plugs	28.35
Radio Relay	21.26
Radio	34.43
Optoisolator	14.175
Flight Computer	77.96
Parachute	163.01
Ice Chest	92.14
Cell GPS	63.79
Extras	92.99
Total Mass	**999.175**

Figure 18: Student Atmospheric Aerobot

As such, the balloon has no propulsion system and there is no control over flight direction. Further it acts like a zero-pressure balloon until it explodes when reaching its maximum attainable volume. Therefore one extra subsystem includes a cut down system with parachute to recover the payload. In Table 3 a detailed mass budget break-down of the main payload components can be found. These type of aerobots are uncontrolled but might be adapted with a propulsion system and are therefore open to further investigation as an aerobot platform.

3.1.9. Tropical Balloon

In 2002, G. E. Dorrington of the department of Engineering of the Queen Mary, University of London was approached by a wildlife film company that wished to obtain cinematographic images above the forest near the Roraima range in northern Amazonia. "The essential user requirement was to carry a 90kg cinematographer with a 15kg camera within about 5m of the canopy. The camera platform had to be stable, and capable of hovering within a radius of error of about 5m for about 20 minutes."[a.3] Research and calculations showed that an airship would be the most suitable and stable platform for such a mission.

The final layout for the airship is shown in Figure 19. “It consists of a 9.7m diameter near-spherical helium balloon and a fabric tail-cone, unsealed and hence air-filled, with a semi-apex angle of 30° attached to the balloon at 18 points on a pitch circle diameter of 7m. A smaller fabric bow-cone was also attached at 12 points to the front of the balloon on a pitch circle diameter of 4m. The resulting hull had a length of about 14.9m with a fineness ratio of about 1.54. The fineness ratio is the ratio of the length of the balloon to its diameter or width. The total hull volume was estimated to be 524.5m^3, so that the total inertial mass (including helium gas and trapped air) was about 600kg. One of the principal advantages of the spheroid-cone form was that the nominally-spherical balloon could be easily subcontracted.” [a.3]

The mass of the balloon and all the rigging lines was about 86kg. The bow-cone and tail-cone were made in-house using lightweight spinnaker-type sailcloth. Both cones were held in tension by 50.8mm diameter aluminum alloy tubes fore and aft of the balloon. The aft tube was also used to support the vertical, swept-leading edge fin made from the same sailcloth stretched between two 25mm diameter carbon fiber tubes 3m in length. The entire mass of the rear cone and fin was about 12kg.

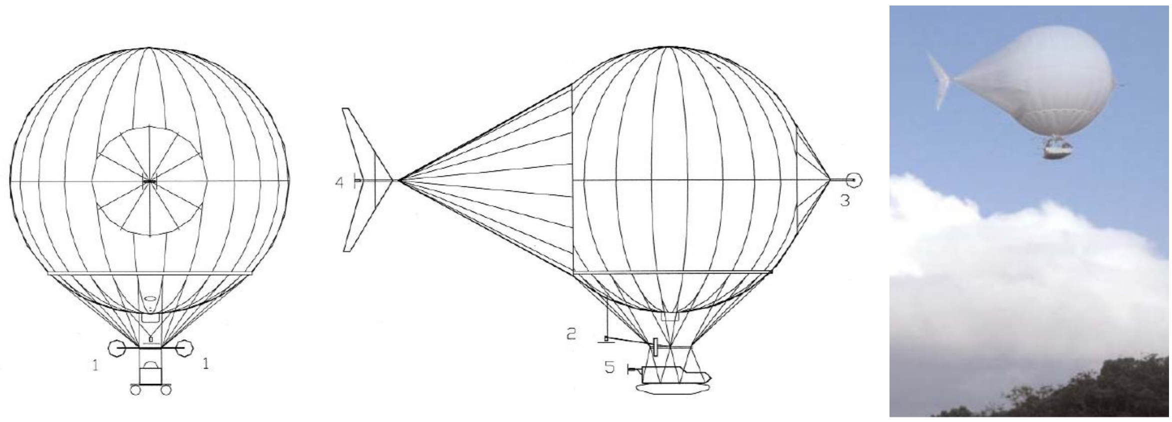

Figure 19: Tropical Balloon; (a) Lay-Out and (b) In-Flight Picture [a.3]

Altitude control was done by dropping ballast, or venting helium. Since the airship was not fitted with a ballonet, venting helium was undesirable though. It resulted in balloon sagginess as well as increasing costs. Next to helium venting, there was also quite a big amount of helium lost due to leakage through the envelope’s fabric.

The end design is quite interesting. The hull is different from the previous mentioned aerobots, which has a lot to do with drag. The design of the tropical balloon can be explained by the following engineering rule: “The major axis length of the hull should be more than three times its maximum diameter, in order to minimize the drag coefficient C_D and thereby maximize airspeed for a given engine power output. Also most non-rigid airship hulls have traditionally adopted ‘streamlined’ quasi-ellipsoidal forms with fineness ratios of about 3-6” [a.3] To avoid difficult and costly balloon shapes, standard COTS spherical balloons can be adapted with extra surfaces to implement the above rule and reduce drag significantly.

3.2. Overview Aerobot Example Study

This section will summarize the relevant aerobot information obtained from the aerobot concepts above. More precisely a mass breakdown of each of the discussed concepts will be of interest. The amount of payload that each concept can carry and the preferred design/float altitude will be important for future designs.

Next the most common similarities and characteristics of each aerobot will be summarized. These shall be required to define the main components of a general aerobot build-up in chapter 4. To conclude, the lessons learnt from aerobot literature will be listed.

3.2.1. Aerobot Concepts Mass Breakdown

Table 4 summarizes the obtained mass breakdown for the above examples. While there is a huge difference in payload mass between the buoyant aerobot examples it is clear that each concept has a high payload mass fraction.

Table 4: Mass Breakdown of Aerobot Concepts

Concept	Payload/Platform [kg]	Envelope [kg]	Propulsion [kg]	Power [kg]	Gas [kg]	Total [kg]	Ref.
LDB	400-2500		/				[a.16]
ULDB	3600		/				[a.16]
Montgolfier	2-10	4.4-9.12	/				[a.17]
MABS	27	45-85	25	21-40			[a.1]
JPL Testbed	12-16		8	43.3			[i.7]
Titan Balloon	52.4	24			16.7	234	[a.2]
Vega Balloon	6.87	10.5	/	2.6		21	[a.8]
Archimedes	18.3	15.1	/	0.01		34	[a.10]
AAB	1		/				[i.6]
Tropical Balloon	105	98	/			449	[a.3]

3.2.2. Aerobot Concepts Characteristics

A number of distinctive observations where made from each concept. Table 5 summarizes values for a number of characteristics from the discussed buoyant concepts.

Balloon volume is closely related to flight altitude, atmospheric density and total mass. The Titan balloon only requires 60m^3 in the dense atmosphere of Titan, while Archimedes requires 1437m^3 in the much less dense atmosphere of Mars.

The type of buoyant gas used is mostly helium, followed by hydrogen. These are of course the two lightest gases available, and give the highest buoyant force, which will give a higher total payload mass. In retrospect any buoyant gas will do, as long as it is lighter than the surrounding atmospheric gas composition. Some balloon categories tend to be better suited for low altitude use than others. While others can be used for much more accurate altitude accuracy. Similar observations in endurance can be made. It all depends in the end on mission characteristics from which aerobot parameters follow.

Table 5: Aerobots Concept and Mission Characteristics

	Balloon Volume [m^3]	Type of Gas [/]	Flight Altitude [m or km]	Altitude Accuracy [m]	Endurance [time]	Propelled Speed [m/s]	C_D [/]
LDB	300000-1130000	Helium	37km	low	1day-4weeks	/	
ULDB	53000-176000	Helium	>30km	100m	100days	/	
Montgolfier		Ambient	0-3km	<1m	50hrs-#days	/	
Tropical Balloon	524.5	Helium	50-100m	5m	20min	2	0.42±0.08
Titan Balloon	60	Hydrogen	8km		6-12 months	1-2	0.02-0.03
JPL Testbed	34		<500m		60min	<12.2	
MABS	10500	Hydrogen Helium	6.8km	100m	90days	/	
AAB	4.85	Helium	0-39.6km	/	2.5hr	/	
Vega	22.84	Helium	54km		60hrs	/	
Archimedes	1437	Helium	2-7km		6-20hrs	/	

All variances aside four main groups exist among the discussed aerobot examples in chapter 3.1, namely; ZP balloons, SP balloons, airships and Montgolfiers. From the available data in Table 4 and Table 5 some general observations can be clustered for each group. They are summarized in Table 6.
Almost all zero-pressure concepts for instance seem to be large in volume, fly at high altitudes and are very inaccurate in maintaining the design altitude. They do seem to be able to handle a high amount of payload though. Airships and SP concepts tend to have more altitude accuracy and are therefore quite stable at low and high altitudes. The general data on Montgolfiers is somewhat incomplete as only one concept was discussed and the results therefore only depend on that one concept. From it however, it could be stated that the altitude accuracy of such a concept is high. Lacking in any other data, all other characteristics on this ambient concept seem very limited.
Based on these results an aerobot designer can choose the preferred aerobot group for each specific mission. If the mission requirements include a high altitude accuracy and endurance, SP balloons and airships are preferred. When altitude accuracy isn't one of the key parameters but highest payload mass is, ZP balloon concepts are ideal.

Table 6: General Aerobot Observations

	Montgolfier	ZP	SP	Airship
General Buoyant Gas	Ambient	Helium	Helium	Helium
General Altitude	Low	High	Low to High	Low to High
General Volume	/	Large	Moderate	Moderate
Altitude Accuracy	High	Low	High	High
General Endurance	Low	Moderate	Very High	High
General Payload	Low	Moderate to High	Moderate	Moderate

3.2.3. General Aerobot Lessons

From the literature examples discussed above some general design rules and facts on aerobot flight behavior can now be summarized. An initial fact on flight behavior is the fact that balloons are easily influenced by wind and wind gusts. Countermeasures are required if controllability is a mission issue! Wind sensors can be used to directly notify propulsion systems to react to gusts and changing wind speeds, but even so reaction will not be instantaneous for huge balloons. The larger volume and surface makes them especially more susceptible to wind-induced control problems during near-earth flight operations.

Balloons not only are severely influenced by wind, they also tend to be less accurate on maintaining specific altitudes. Use of ballonets for maintaining shape during descent and rising can help. Also a downward thrusting propeller is one way of maintaining altitude. Volume and pressure control which both define the available buoyancy in a balloon, are two useful methods for altitude control.

A major conventional design rule in airship design, according to Dorrington [a.3], is; 'The major axis length of the hull should be more than three times its maximum diameter, in order to minimize the drag coefficient C_D and thereby maximize airspeed for a given engine power output.' Also most non-rigid airship hulls have traditionally adopted 'streamlined' quasi-ellipsoidal forms with fineness ratios of about 3-6. Further, spheres can be adapted with extra surfaces to adopt the above design rule and reduce drag significantly, while creating difficult shapes from COTS products becomes easier.

Next, balloon fabric and the type of buoyant gas will play an important role in mission life. Low buoyancy gas leakage rates are required for long mission lifetimes and thus envelope fabric with a low permeability will have to be used.

3.3. Buoyant Aerobot Platform Trade-Off

With only the specifics from the NRC's definition on aerobots to work with, and the literature concepts showing the potential of aerobots, a trade-off on different aerobot platforms will be done to verify the right choice of buoyant aerobot platform for planetary missions.

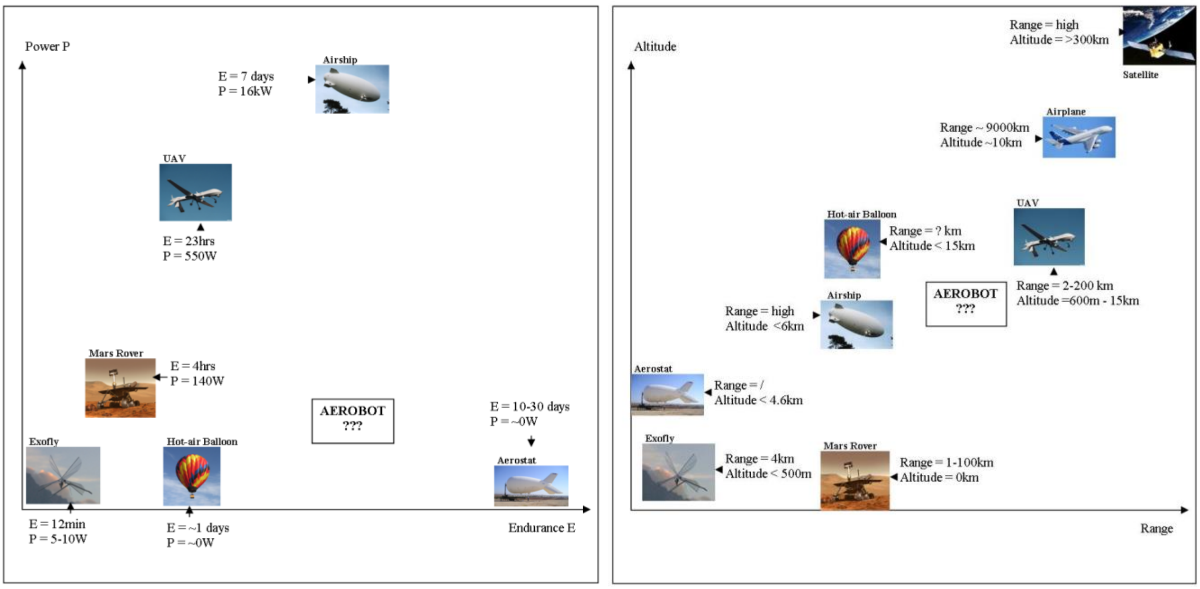

Figure 20: Assumed Characteristics for a Buoyant Aerobot Compared to COTS Concepts

The advantages and disadvantages of these platforms will also be compared to rovers, aircraft, satellites and micro-systems, but only for informatory purposes. Almost all these platforms will be discarded from the trade-off due to several obvious reasons;

- Rover; isn't able to fly and thus not accomplishing requirements; R2 (altitude control), R3 (executing predefined flight path), R4 (landing capability)
- Aircraft; high mass and size and human-dependence, not able to accomplish R4
- Satellites; not able to accomplish requirements R2, R3, R4

Figure 20 graphically represents the relation between power, endurance, range and altitude of a number of buoyant aerobots and other platforms. The position of each platform in the graph is based on the knowledge obtained in the previous sections, information obtained from the internet and scientific articles. One buoyant platform in there has not yet been discussed in this thesis; the aerostat. The aerostat is simply an airship which lacks the range of a real airship because it is connected with a cable to ground. Two other platforms in Figure 20 which are not yet discussed are the micro-system Exofly [a.9] and a standard UAV. They have not been included in the literature study of section 3.1 as the choice was made early on in this thesis that the focus would be on buoyant aerobots and not on heavier-than-air vehicles. The two HTA aerobots mentioned will however be used as a reference against the buoyant types. More information on the Exofly is found in article [a.9]. For details about UAV's the reader is directed to the world wide web.

The key aerobot design parameters shown in Table 7 will be used to assess the aerial platforms with a corresponding importance weights for each parameter. The key design parameters are based on the information obtained from buoyant aerobots throughout the literature study of section 3.1. Table 7 therefore only presents a limited amount of trade-off parameters, but are to the writers opinion the parameters that will reflect a buoyant aerobot's design most. Nevertheless one can imagine that other trade-offs based on specific mission needs, or based on a higher amount of parameters, can change the value of the importance weights and in the end might even change the outcome of the trade-off. This trade-off shall define the best option for a buoyant platform for a general buoyant flight. Any discrepancy that might occur with other trade-offs is likely do to mission specific factors.

Table 7: Weighing Trade-Off Parameters

Key Design Parameter	Trade-off Weight
Total Platform Mass	5
Payload Capability	4
Maximum Required Power	4
Flight Endurance	5
Altitude Range	2
Maneuverability/Controllability	3
Cost	1

Weights have been set from 1 to 5, with 5 being the parameter with the highest importance. Total mass is a very important factor. Volume and shape of the balloon directly follow from it. Planetary missions also have mass restrictions from the launcher. Therefore mass should be as low as possible for any planetary mission.

Size and mass in combination with the loss in buoyant gas will also give the endurance of the aerobot. A higher endurance also gives a bigger area that will be covered during the mission. Great coverage, due to high endurance, and high resolution are two advantages aerobots have over rovers and satellites as stated in section 2.2.1. Mass and endurance characterize the aerobot mission and are therefore given the highest importance, namely a value of 5.

Payload mass is very important for any mission. It will depend on the size of the balloon and the available platform space and more importantly the remaining lift force when all essential systems are onboard. A high value would be desirable, so an importance value of 4 was given. Mass will drive the design at this stage, closely followed by endurance and a desire for a low required power value. Low power values can extend the lifetime and lower the mass of any aerial platform.

The third most important parameter for an aerobot will be maneuverability and controllability, in general. Maneuverability and controllability for the aerobot's aerial platform benefits a science mission. Especially altitude control from requirements R2 and R4 increase the need for a high controllability.

Altitude range is mostly mission related and therefore given an importance value of 2. The need for a high altitude range in which the aerobot can work in is however of interest for a combined high altitude science mission and the ability to land.

Lowest importance value will be given to the low cost criteria. Cost is a very uncertain criteria at this moment and very dependent on the materials and components used and the mission flown, as such its lower importance.

Each aerial platform is graded with a set of compliance weights between 1 and 6, for which 6 is given to the platform with the highest compliance with respect to the importance parameter. This means;

- Total platform mass will have a weight of 6 for a low mass, while payload capability will have a weight of 6 when a lot of payload is onboard.
- Compliance for maximum required power requires a low amount of power for highest score.
- Flight endurance will have a weight of 6 when long flight duration is possible. A large altitude range will be required to ensure a compliance factor of 6.
- A high maneuverability and controllability is required for a compliance of factor 6.
- A low cost is required for a compliance factor of 6.

From Figure 20 a number of compliance values can be set. Other are assumed from current existing aerial platforms. Further down in Table 8 the importance weights have been repeated and are taken into account to calculate the end result of the trade-off. From the end results, the buoyant vehicles (balloon, airship, aerostat) seem to have an advantage over aircraft based on aerodynamic lift (UAV) and micro systems (Exofly).

While micro systems, such as Exofly [a.9], offer a very low mass they do have a lot of limitations with respect to payload and endurance. While offering a very low mass and low power usage, which benefits space missions, it's not the best platform for an aerobot mission where payload is quite important too. Such systems can however be used as payload/probes on an aerobot for example.

UAV's and aircraft have the disadvantage that they are quite heavy and use a lot of power. Both are related as most mass and power goes to the propulsion system, to generate lift and controllability, which keeps the platform afloat.

Table 8: Aerial Platform Trade-Off Results

Aerial Platform	Total Platform Mass	Payload Capability	Max. Req. Power	Flight Endurance	Altitude Range	Maneuver/ Control	Cost	/
Balloon	5	6	6	4	4	1	5	
Airship	4	5	5	5	4	4	4	
Aerostat	4	5	6	5	2	1	5	
UAV	3	2	4	4	4	4	3	
Exofly	6	1	6	1	1	3	6	
Aircraft	1	6	1	4	3	4	1	
Satellite	1	3	2	6	6	1	1	
Rover	2	2	3	0	0	1	2	
Weight	**5**	**4**	**4**	**5**	**2**	**3**	**1**	
Aerial Platform	**Total Platform Mass**	**Payload Capability**	**Max. Req. Power**	**Flight Endurance**	**Altitude Range**	**Maneuver/ Control**	**Cost**	**Result**
Balloon	25	24	24	20	8	3	5	**109**
Airship	20	20	20	25	8	12	4	**109**
Aerostat	20	20	24	25	4	3	5	**101**
UAV	15	8	16	20	8	12	3	**82**
Exofly	30	4	24	5	2	9	6	**80**
Aircraft	5	24	4	20	6	12	1	**72**
Satellite	5	12	8	30	12	3	1	**71**
Rover	10	8	12	0	0	3	2	**35**

This last aspect isn't the case for a buoyant platform, which carries its own mass by a buoyant gas, which benefits the amount of payload that can be stored onboard and the total mass. Buoyant platforms offer a wide range of altitude possibilities as well as flight range. While a propelled airplane or a micro-system, need thrust/power to create lift, the buoyant platforms will only need power for controllability but at a much lower level than robotic systems. Balloons have no controllability and maneuverability capabilities, which is basically the only flaw for this platform.
The airship however ends up with the same trade-off score as the balloon. Due to an included propulsion system the airship has a lower payload mass and a higher total mass. Also cost is slightly higher and required power is higher too. The main advantage over a balloon is its controllability and maneuverability and a slightly higher endurance. These two parameters boost any negative effect of the other airship's parameters within the trade-off, explaining the same end result as the balloon. Due to its better controllability and maneuverability however the airship, or any other propelled buoyant platform, comes out as the best result for an aerobot platform.

This result was confirmed from a similar trade-off done by Li [t.1]. In a study for a combined aerobot and rover system on Mars, an extensive trade-off was done between the following aerobot platforms;

- Balloons
- Airship

- Gliders
- Aircraft
- Rotorcraft
- Vertical Take-Off and Landing (VTOL) aircraft

The trade-off criteria on which the end result was based and the importance weights were;

Table 9: Trade-Off Parameters and Weightings by Li [t.1]

Key Design Parameter	Trade-off Weight
Vehicle mass and size	9
Payload Capability	9
Maneuverability/Controllability	8
Mobility/Terrain Coverage	7
Flight Endurance	7
Degree of Surface Interaction	6
Adverse Weather Capability	4
Complexity/Reliability	3

A resemblance of the importance parameters exist between the trade-off of Li [t.1] and the one above. The extra parameters give a higher degree of detail to the trade-off, especially from a scientific point of view. Terrain coverage and mobility together with the degree of surface interaction will definitely help in choosing the right platform for the right mission. In the end, the airship came out as the best result.

Why choose a new trade-off above the trade-off done by Li and still end up with a similar result?

- Li's trade-off was based on a specific Mars aerobot-rover mission and included a degree of surface interaction and an adverse weather capability in the design parameters. Both were deemed interesting, but not necessary for a general trade-off on LTA platforms.
- The balloon was discarded from the trade-off results due to an important mission requirement of controllability; if not, the result for a balloon would also have been high, but lower than that of an airship.
- The trade-off included a high number of HTA vehicles which were not the focus of this thesis. The results obtained from Li already concluded that LTA platforms ranked higher than HTA platforms.
- Due to the above, the writer was more interested in the best LTA platform but also willing to compare these results with a few special HTA concepts and discarded options for reference.
- The difference in importance weight value, lays with the number of key design parameters. As fewer design parameters were chosen than in Li's trade-off, there was no need for a higher weight value than 5.

A trade-off offering more trade parameters and other importance factors, which are mission dependent, will change the outcome of the trade-off eventually. Even though, the buoyant vehicles seem to have significant advantages over their aerodynamic lift counterparts. Both trade-offs did confirm this result. The most useful aerial platform for an aerobot is therefore quite clear; a buoyant platform! Therefore buoyant platforms, either powered or unpowered, will be further investigated and used in mission designs from here on.

4. Design Methods and Subsystem Modeling

Two groups of aerobots, which are mission dependent, were found in the examples of chapter 3; Those that continuously use their payload and send data automatically to a ground station, and those that need their payload recovered for analysis. An aerobot of the first group consists of five main components from Figure 21:

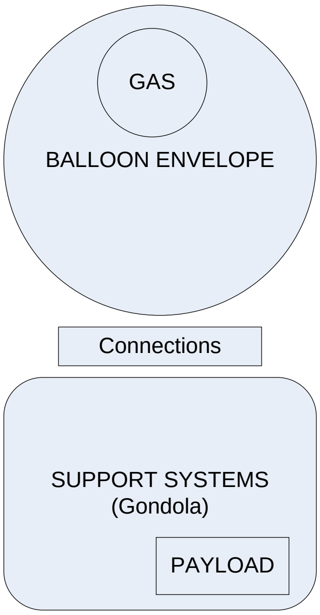

Figure 21: Aerobot Build-Up: General

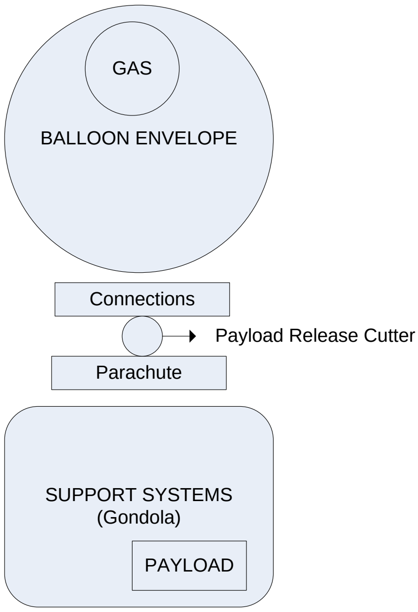

Figure 22: Aerobot Build-up: Recovery

An aerobot system for an Earth-based-aerobot for which payload has to be recovered consists out of the same components but also includes a parachute and a cut-down system between gondola and balloon. This is shown in Figure 22. When the gondola is cut-down from the balloon it will fall back to Earth while the balloon will go its own way or explodes. The gondola will however be of no use if it gets damaged, so that's why a parachute will lower the platform at a low descent speed back to Earth.

Sections 5.6 and 8.3.1 will address the parachute feature again, but for now the decision is made that balloon build-up will be according to Figure 21 during this thesis. The aerobot should use other means to a controlled payload landing without parachute systems, such as balloon volume control, if this is required.

Section 4.1 will discuss a number of atmospheric models found for Earth, Mars, Venus and Titan. From these models one will be chosen for each planet or moon to be used in the simulation program of chapter 5. Next in section 4.2 a dynamical model for aerobot flight is proposed, followed by an analysis on balloon design in section 4.3 and a discussion on thermal models in section 4.4. The balloon design is subdivided by; balloon shape, envelope materials, envelope fabric permeability and gas discharge rate, balloon pressure and skin tension, and buoyant gas selection.

4.1. Atmosphere Models

This section will primarily describe and compare the atmospheric models used and examined for the simulation program of chapter 5. One of the advantages of the program will be the number of available planetary atmospheres. Four standard planetary atmospheres are modeled, namely; Earth, Mars, Venus and Titan. A standard atmosphere is a hypothetical vertical distribution of atmospheric properties which, by international agreement, is roughly a representation of year-round, mid-latitude conditions. It should be recognized that actual day-to-day conditions may vary considerably from this standard. These standard models are effective for behavioral analysis of a buoyant aerobot in a specific atmosphere, but not accurate enough for day-to-day simulations or findings. Therefore there are also several different standard models which include; a standard or average day, a hot day, a cold day, and a tropical day. The models are updated every few years to include the latest atmospheric data.

Each model reproduces the atmosphere temperature, pressure and air density. These are all parameters which influence a buoyant aerobot's flight behavior and therefore have to be examined. This section will always depict the temperature profiles of the explored atmospheres and models to show the similarities and differences of the atmospheric models to the standard conditions. Both pressure and density are modelled in the same way but are not depicted graphically.

Something to point out is the fact that; the atmospheric models below are all modeled for dry air on an average day. No water vapor or moisture of any other kind is being considered in these standard atmosphere models unless otherwise stated. The effect moisture has on the atmosphere models shall be discussed briefly in a sensitivity study in chapter 7. The simulation program of chapter 5 will include the chosen and preferred standard atmosphere models of the current chapter though.

The section ends with an introduction to the planetary environments of Earth, Venus, Mars and Titan. This will include the composition of the atmospheres and the gravitational acceleration at each planet. Two parameters that will influence the buoyant aerobot's flight and design.

4.1.1. Earth's Atmosphere Models

Earth's atmosphere is the most studied atmosphere in the solar system. Simply because it is in our immediate vicinity and therefore the easiest to investigate. A number of standard atmosphere models and data tables exist which are efficient for simulation purposes. Very useful are Schlatter's [a.23] atmospheric composition article and NASA's public atmospheric model [i.31].

According to Thomas Benson, propulsion engineer at NASA, the NASA model in Table 10 [i.31] was developed by the International Civil Aviation Organization (ICAO) in 1964, approved by NASA, and published by the National Oceanic and Atmospheric Administration (NOAA) after some revisions to the upper atmosphere in 1976. “The model was developed from atmospheric measurements that were averaged and curve fit to produce the given equations. The model assumes that the pressure and temperature change only with altitude. [i.31]” The model in Table 10 is only a model for educational purposes, but presents the air pressure ‘p’, air temperature ‘T’, and air density ‘ρ’ with respect to the geometric height ‘h’, which is the altitude above the Earth’s surface. Since publication, there have been improvements to the upper atmosphere but these are not incorporated into the model, according to Benson. Therefore the user is advised not to trust the results of the equations from the upper stratosphere beyond 30km.

Table 10: ICAO Atmospheric Model for Earth

Altitude	Temperature, Pressure and Density
h > 25000m	$T = -131.21 + 0.00299 \cdot h$ **Equation 4: Earth’s Atmospheric Temperature above 25km** $p = 2.488 \cdot \left[\frac{T + 273.1}{216.6}\right]^{-11.388}$ **Equation 5: Earth’s Atmospheric Pressure above 25km**
11000m < h < 25000m	$T = -56.46$ $p = 22.65 \cdot e^{(1.73 - 0.000157 \cdot h)}$ **Equation 6: Earth’s Atmospheric Pressure between 11km and 25km**
h < 11000m	$T = 15.04 - 0.00649 \cdot h$ **Equation 7: Earth’s Atmospheric Temperature below 11km** $p = 101.29 \cdot \left[\frac{T + 273.1}{288.08}\right]^{5.256}$ **Equation 8: Earth’s Atmospheric Pressure below 11km**
All altitudes	$\rho = \frac{p}{(0.2869 \cdot (T + 273.1))}$ **Equation 9: Earth’s Atmospheric Density**

Schlatter describes three standard atmosphere models.

- Standard atmosphere ICAO, 1993
- The International Standard Atmosphere (ISA)
- The U.S. Standard Atmosphere, 1976

According to Schlatter; “The U.S. Standard Atmosphere 1976 is identical to the ICAO Standard Atmosphere up to 32 km and to the International Standard Atmosphere up to 50 km. [a.23]” Figure 24 does contradict this statement a bit. The first statement about ICAO only holds for the first 20km, due to the NASA model keeping the isothermal relation for an extra 5km and not taking into account any temperature relation beyond 25km. This might be due to ‘outdated’ data. The second statement about ISA is more accurate, however the available ISA data [i.33] only goes up to 30km and therefore no accurate results can be shown above 30km with the interpolation method.

The simulation program in chapter 5 has to give an impression of Earth’s atmosphere. Even standard atmosphere models are simplified versions of the actual atmosphere under general assumed conditions. The US Standard Atmosphere of 1976 in Figure 23, provided by Schlatter, and simulated

in Figure 24, correspond very well. As the 1976 model resembles the other models for the lower atmosphere, takes into account the isothermal regions and is widespread over the altitude range it is therefore a more optimum choice as an atmospheric model for Earth in the simulation program.
It should be mentioned again that these models present a standard average day which is a representation of year-round, mid-latitude conditions. This means that actual day-to-day conditions may vary considerably from this standard. As far as a daily analysis is considered the accuracy of the atmospheric model will vary with the weather conditions for any specific day. The atmospheric model should rather be used for general flight behavioral analysis of a buoyant aerobot than for actual specific day-to-day results. Chapter 6.2 shall further discuss the impact, of the atmospheric discrepancies in the model, on the aerobot design.

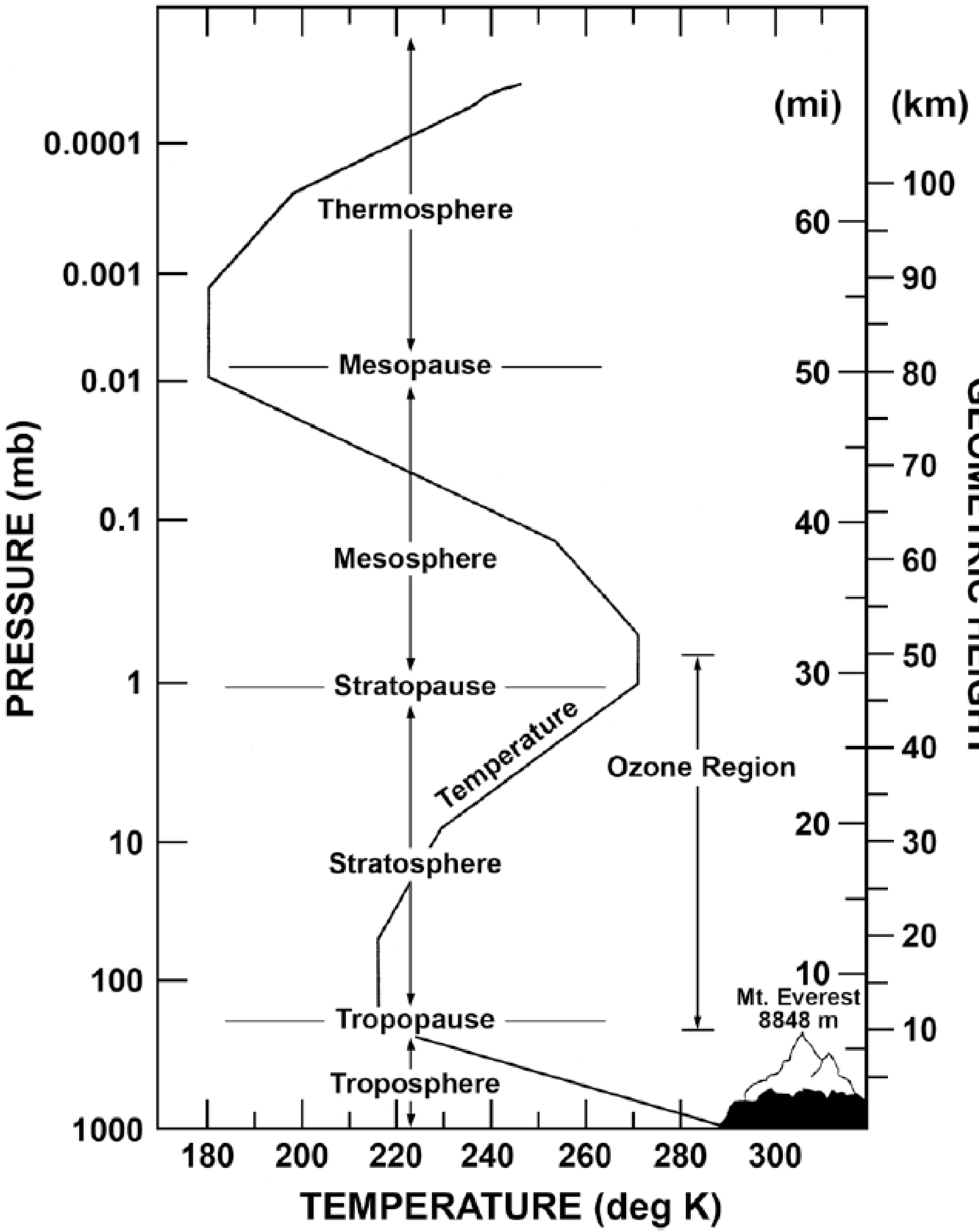

Figure 23: US Standard Atmosphere, 1976 Model [a.23]

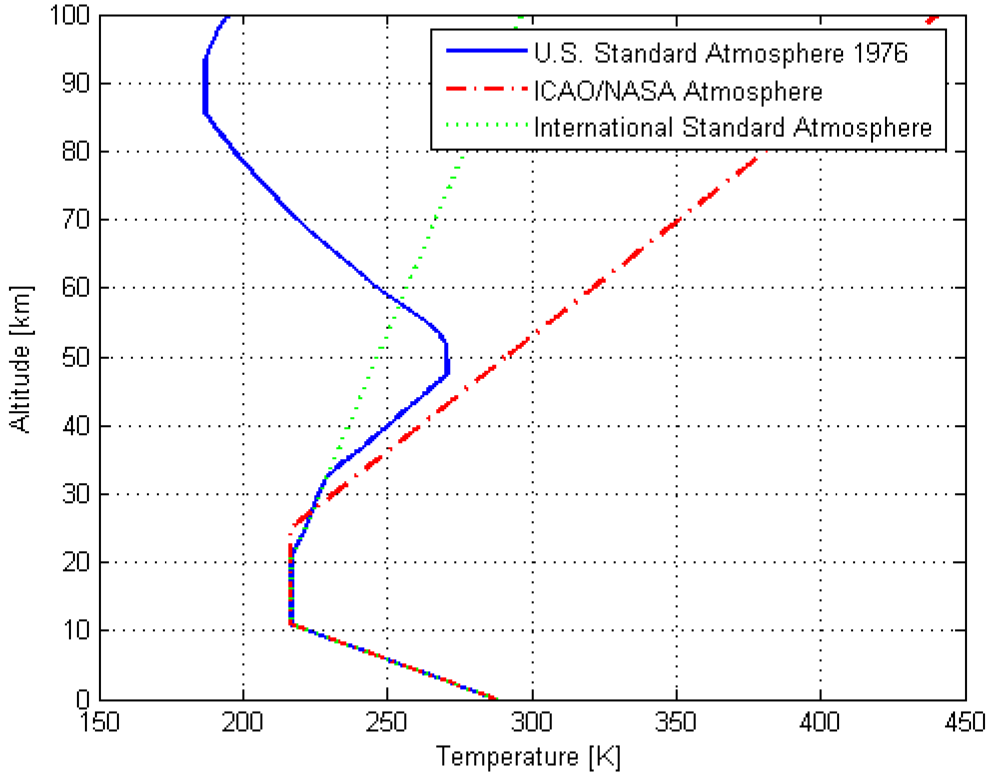

Figure 24: Earth's Simulated Atmosphere Models

4.1.2. Mars' Atmosphere Models

Mars is the second planet where atmospheric research peaked due to the many Mars missions that have visited the planet. A good amount of data [i.34, i.35] is therefore available on local atmospheric conditions at different latitudes and altitudes. Mars planetary environment is quite different from Earth's. Appendix B presents the planet's atmosphere and climate in detail. Compared to Earth, Mars has; a very thin atmosphere, huge dust storms, strong winds or gusts and much lower temperatures.

Table 11: Mars NASA Student Atmosphere Model [i.32]

Altitude	Mars' Atmospheric Model
h > 7000m	$T = -23.4 - 0.00222 \cdot h$ **Equation 10: Mars' Atmospheric Temperature above 7km** $p = 0.699 \cdot e^{-0.00009 \cdot h}$ **Equation 11: Mars' Atmospheric Pressure above 7km**
h < 7000m	$T = -31 - 0.000998 \cdot h$ **Equation 12: Mars' Atmospheric Temperature below 7km** $p = 0.699 \cdot e^{-0.00009 \cdot h}$ **Equation 13: Mars' Atmospheric Pressure below 7km**
All altitudes	$\rho = \dfrac{p}{(0.1921 \cdot (T + 273.1))}$ **Equation 14: Mars' Atmospheric Density**

A general atmospheric model is less accurate but handier for simulation purposes. Initially a model was used from NASA [i.32], shown in Table 11. According to Thomas Benson, this model was actually created by some students that shadowed him for a couple of weeks. They used publicly available data from one of the Mars orbiting satellites, graphed it and curve fitted it. Pressure ‘p’ and density ‘ρ’ are related to the geometric altitude ‘h’ and temperature ‘T’ respectively and are found from Equation 11, Equation 13 and Equation 14.

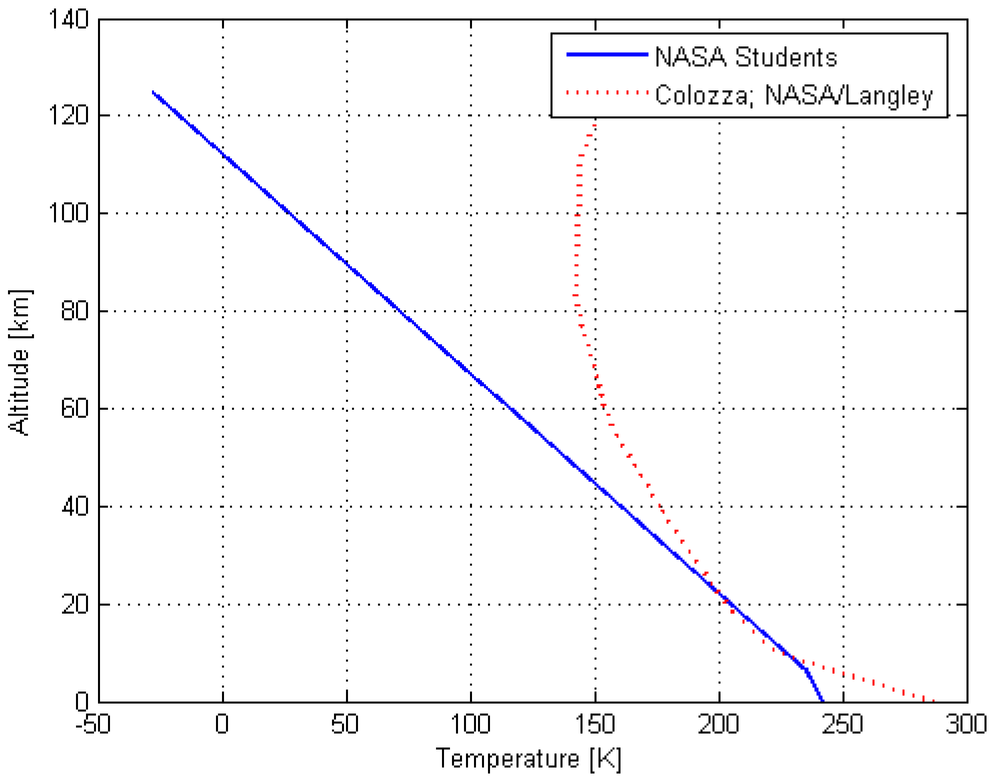

Figure 25: Mars Simulated Atmosphere Models

Pursuits for a better general atmospheric model of Mars lead to listed data of the Martian atmosphere from Colozza [a.26]. In his final report, for a Solid State Aircraft, prepared for the NASA Institute for Advanced Concepts, he describes multiple atmosphere models for Earth, Mars, Venus and Titan. The Martian standard atmosphere model is used by NASA-Langley and lists per kilometer; temperature, pressure and density values from ground up to 125km. By interpolating this data it is possible to find the intermediate values.

Both the Colloza-NASA model and the student-NASA model are simulated in Figure 25. The student’s model loses its accuracy around 20km. The Colloza-NASA model however starts at a higher ground temperature. The most likely reason for this is that the student model makes use of the specific day temperature and Colozza makes use of standard average temperature. Nonetheless, the Colozza or NASA-Langley general atmospheric model corresponds way better with the general Martian atmosphere model of Figure 26. It is also useful for a larger range of altitudes and has been improved over the years, compared to the student model which is 10 years old. The Colloza-NASA/Langley model is therefore used for simulating the Martian atmosphere.

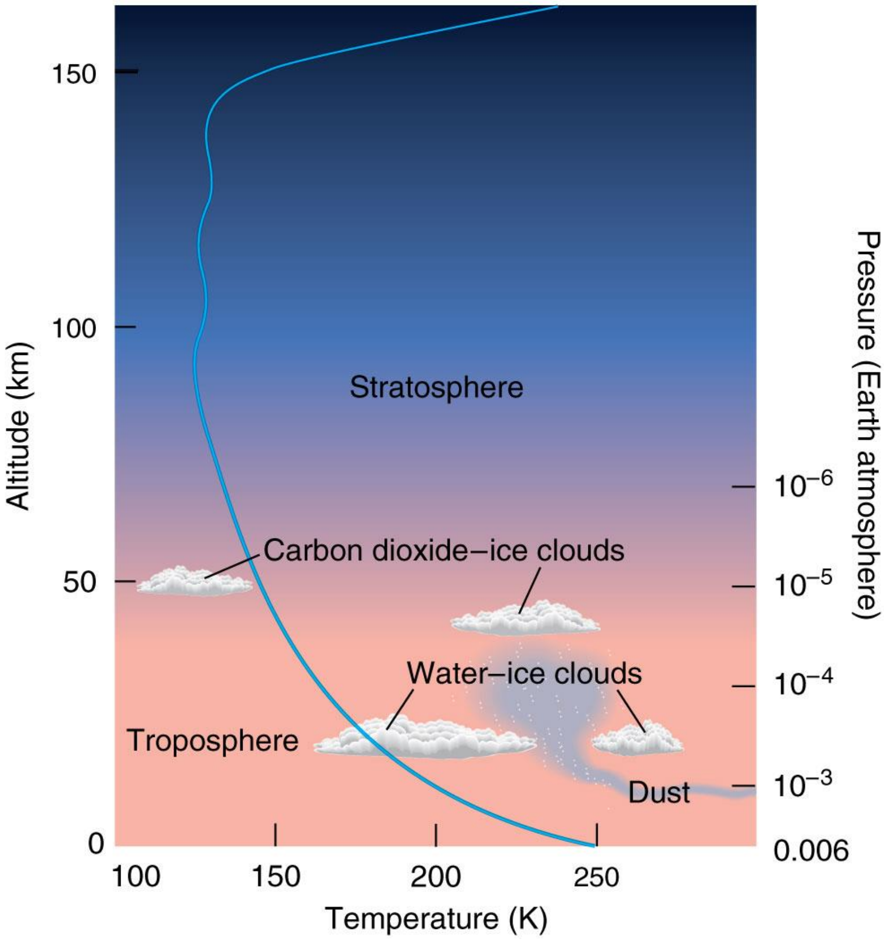

Figure 26: Standard Martian Atmosphere Model [i.36]

4.1.3. Venus' Atmosphere Models

Venus is a planet with a very opaque atmosphere. From Earth it's impossible to look through the clouds on to the surface. This planet however has been the location where the only buoyant aerobot mission to date has taken place; namely Vega. Results from Vega, landers and from orbiting satellites, have made it possible to model the Venusian atmosphere. Though the models mostly date from the 1970's and 80's. The following atmospheric models were found;

- 'Kerzhanovich, 1985 [a.24]' goes up to 70km,
- 'Hunten D.M. et al, 1983 [a.25]' has data up to 100km,
- 'Veneras 5+6, 1970 [a.27]' ends at 300km
- 'Kerzhanovich, 2000 [a.26]' gives data up to 100km.

All models make use of listed data for temperature, density and pressure. The simulated models will use cubic interpolation for the points in-between. No equations were found because of the fact that most data is in situ measured data from missions like the Venera probes and the Vega balloons. Figure 27, provided by the University of Oregon [i.44], gives an impression of the standard Venusian atmosphere, to which the simulated models can be compared to.

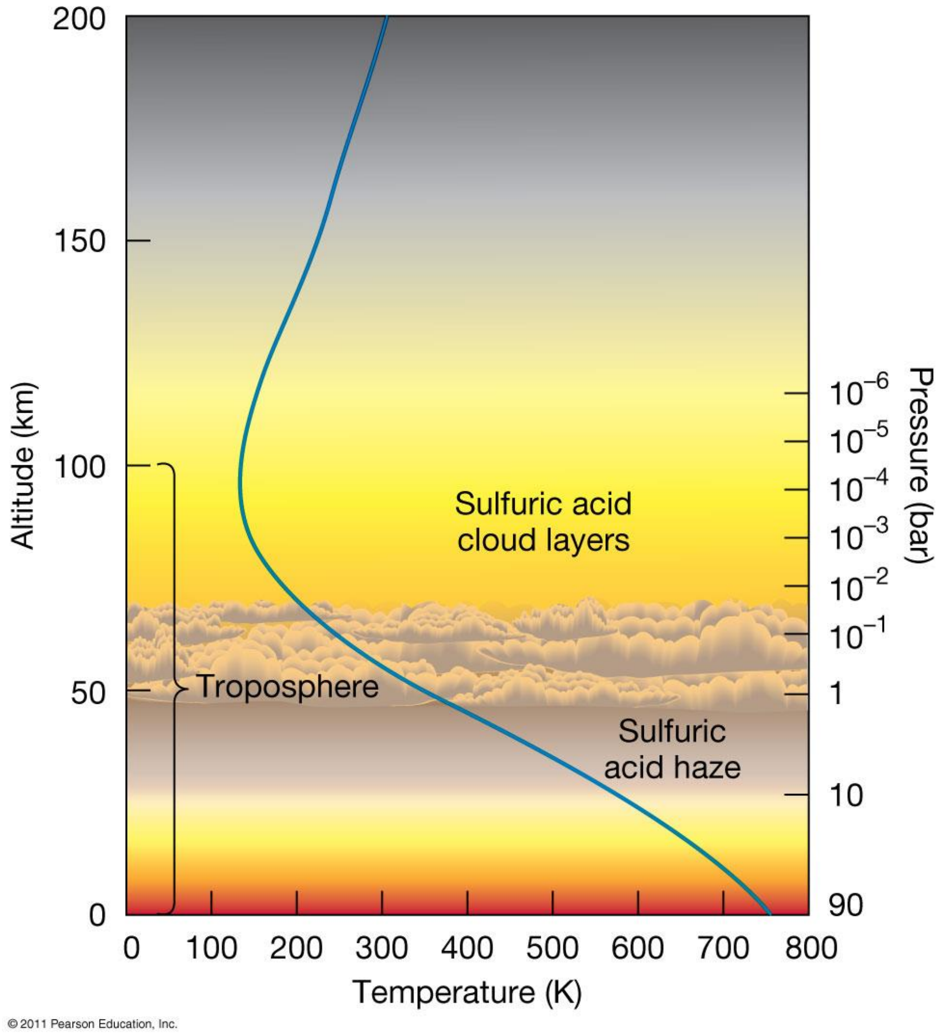

Figure 27: Venus Atmosphere [i.44]

Figure 28 compares each temperature profile of the before mentioned Venusian models with respect to altitude. The horizontal lines at lower altitudes from the Kerzhanovich profiles follow from a lack of data above 70 and 100km. Veneras 5+6 of 1970 moves up linear with all other models, it just has a temperature offset which is understandable because it is based on momentary data of those missions. All models develop in a very similar manner. For a higher altitude range one could use the Veneras model. When doing so the user should keep in mind that this model is based on transient data. For behavioral analysis of a buoyant aerobot however this model will be able to present temperature, pressure and density from 0km to 300km (not shown in Figure 28 though).

As a standard atmosphere model however one should probably use Kerzhanovich improved model of 2000. This model’s temperature, pressure and density range is limited to 100km, but the temperature profile corresponds more to the general Venusian atmosphere in Figure 27 than for example the Veneras missions do. This is also the most up to date model of the afore mentioned models. This means that, compared to the Kerzhanovich 2000 model, all other models are outdated due to the fact that Kerzhanovich 2000 includes the obtained data of Venusian atmospheric research between the seventies and the year 2000. In general though the standard atmospheres are good enough for the behavioral analysis of a buoyant aerobot.

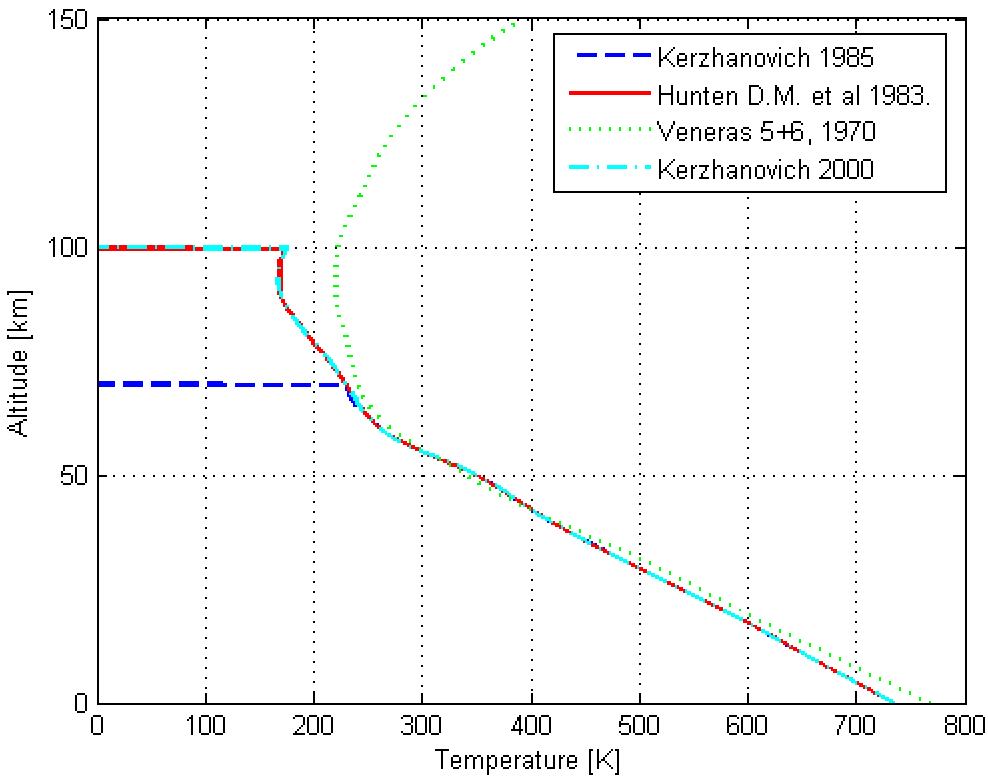

Figure 28: Comparison of Atmospheric models of Venus

4.1.4. Titan's Atmosphere Model

Titan is the biggest moon from Saturn. From all the previous planets this moon is the most difficult to get in situ information on. Not only the huge distance from Earth, but also the very dense atmosphere plays a role in this.

The report of Yelle and Strobel et al [a.28] covered engineering models for Titan's atmospheric structure used in the design and analysis of the Huygens Probe and its mission. Their atmospheric models were based on observations made by the Voyager 1 Radio Science Subsystem (RSS), Infrared Spectrometer (IRIS) and Ultraviolet Spectrometer (UVS). The recommended model of 'Yelle and Strobel et al' provides an adequate fit to all three data sets. The data table of the model was however not digital available and almost unreadable on paper.

Contacting the writers resulted in receiving an engineering model [d.1] of Titan's atmosphere based on the Huygens Probe HASI (Huygens Atmospheric Structure Instrument) data set. Not only is this model brand new compared to the one found in Yelle and Strobel et al [a.28] but the in situ measurements of HASI are definitely more accurate than those from the flyby of Voyager. The model is however based on specific time in situ data.

The HASI Titan data model is the most extensive one from all previous discussed atmospheric models as it gives listed data for temperature, pressure, density and a couple of other parameters up to 1380km. The model will be implemented in the simulation program and is only adapted for interpolation to find the intermediate values, other than that it remains the same. For illustrative purposes the atmospheric temperature profile of the HASI model, provided by Strobel [d.1], is plotted in Figure 29.

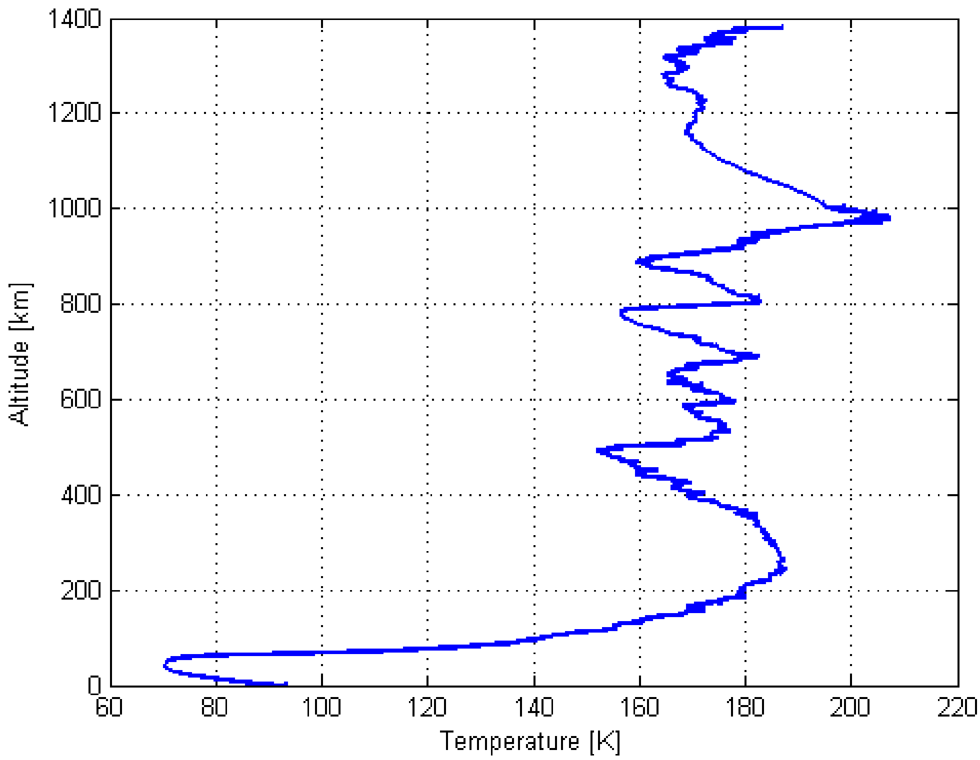

Figure 29: Atmospheric HASI Model of Titan [d.1]

4.1.5. Planetary Environments

Each planet or moon in our solar system has its specific characteristics which makes them unique. The surface of each planet is different, although some similarities exist. Of Earth there is however only one of a kind. No other planet in our solar system has oceans of water. Venus, Mars and Titan have a similar rocky surface according to the obtained data over the years. From the Cassini-Huygens mission scientists learnt that next to the rocky surface there are also lakes on Titan and that they are probably composed of liquid methane.

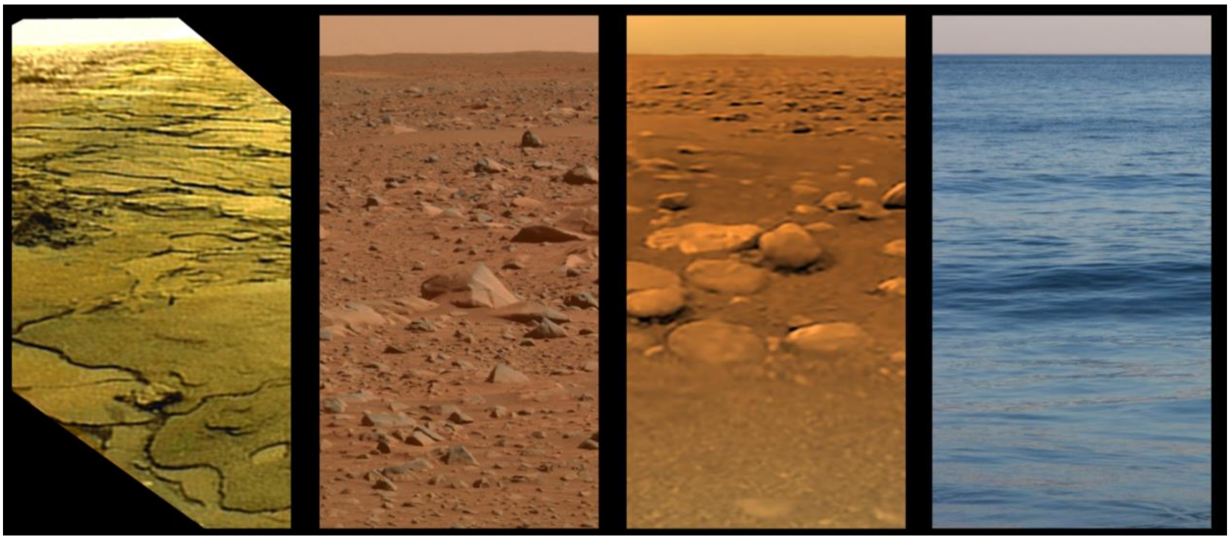

Figure 30: Planetary Surfaces of Venus, Mars, Titan and Earth [i.47]

Each planet or moon also has a different atmosphere composition. The atmosphere composition will influence the flight behavior of a buoyant aerobot. The aerobot relies on the difference in atmospheric density and buoyant gas density for buoyant lift. The higher the density difference the higher the lift and therefore the ascend speed. Table 12 presents the composition of each atmosphere.

Table 12: Atmosphere Composition of Earth, Mars, Venus and Titan

	CO_2 [%]	N_2 [%]	O_2 [%]	H_2 [%]	Ar [%]	CO [%]	CH_4 [%]	Ref.
Venus	96.5	3.5						[i.3]
Mars	95.32	2.7	0.13		1.6	0.08		[i.2]
Titan		98.4		0.1-0.2			1.4	[i.46]
Earth	78.08		20.95					[i.1]

Section 4.3.4 will further elaborate on the gas and atmospheric properties. For Mars, Venus and Titan however, it is assumed that atmospheric thermal and chemical properties will behave according to the prime gas present in the atmosphere. The atmosphere for Venus and Mars will therefore only be composed of CO_2, while that of Titan will be composed of N_2. The composition of Earth's atmosphere will be maintained throughout the calculations as thermal and chemical data is available on this composition.

As each planet or moon differs in size and composition also the gravitational acceleration is different. Gravity changes with altitude, which generally means that the gravity drops when moving further away from the planet. The gravitational acceleration 'g', at any planet, is written as;

$$g = \frac{G \cdot m_{planet}}{\left(R_{planet} + h\right)^2}$$

Equation 15: Gravitational Acceleration [i.48]

Wherein G represents the gravitational constant of 6.67384 x $10^{-11}m^3kg^{-1}s^{-2}$, m_{planet} is the mass of the planet, R_{planet} is the radius of the planet and 'h' is the geometric altitude measured from the surface. Often the gravitational acceleration g is assumed constant throughout calculations though. Therefore it is assumed from here on that g is constant with altitude and that the effect on the flight of a buoyant aerobot will be minimal. Chapter 7 will explore the effect of this assumption further.
The values of the gravitational acceleration for Earth, Mars, Venus and Titan, which will be used throughout the remainder of this thesis, are set to be the gravity values at ground/sea level from here on, and are presented in Table 13.

Table 13: Surface Gravity for Earth, Mars, Venus and Titan

	Gravitational Acceleration [m/s^2]	Ref.
Earth	9.80	[i.1]
Mars	3.71	[i.2]
Venus	8.87	[i.3]
Titan	1.35	[i.46]

4.2. Dynamical Model

A buoyant aerobot with a balloon as the main component is influenced by wind, drag, thrust, lift and weight. These forces are inherently influenced by the atmospheric conditions discussed in the previous subchapter. The equations of motion for a buoyant aerobot will be described below and all parameters influencing flight will be discussed. Focus lays on vertical motion as the buoyant force acts in this direction.

Before the equations of motion can be described, a general coordinate system needs to be defined. All aerobot motion will take place in a x, y, z coordinate system, as shown in Figure 31. Positive z direction defines the rise of the aerobot. The horizontal movement is described through x-y coordinates. The definition of this coordinate system will be maintained throughout this thesis.

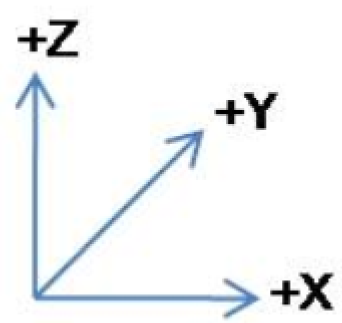

Figure 31: Coordinate System x, y, z

4.2.1. Forces on the Aerobot

The basic aerodynamic forces on a buoyant aerobot are the same to those on any other aerial vehicle, with the exception of buoyancy, namely; drag D, lift L, thrust T and weight W. All forces are illustrated in Figure 32, which is provided by Palumbo [t.4] but modified with a thrust force. Drag and thrust will be discussed in detail in sections 4.2.2 and 4.2.5 respectively.

Archimedes principle, stated in Equation 1, gives the buoyant force. The total net buoyant force produced by the balloon is usually defined as the gross inflation GI, which is the lift force in vertical z-direction and is given by Equation 16 [t.4]. The weight of the gas mass m_{gas} is hereby subtracted from the buoyant force, creating an equation based on the atmospheric density ρ_a, the gas density ρ_g and balloon volume $Vol_{balloon}$. The atmospheric density will always be available through the atmosphere models from section 4.1, while balloon volume and buoyant gas density are calculated from the available buoyant gas mass.

$$GI = F_{buoyant} - m_{gas} \cdot g = g \cdot \left(\rho_a - \rho_g \right) \cdot Vol_{balloon}$$

Equation 16: Gross Inflation

In Figure 32 all aerodynamic forces and buoyancy on an aerobot are illustrated. This 2D representation in xz-plane holds also for the yz-plane, with similar forces acting on the aerobot. An extra lift-force can be generated by thrust in upward direction. Buoyancy and thrust are counteracted by drag induced by the aerobot's motion and by the aerobot's shape.

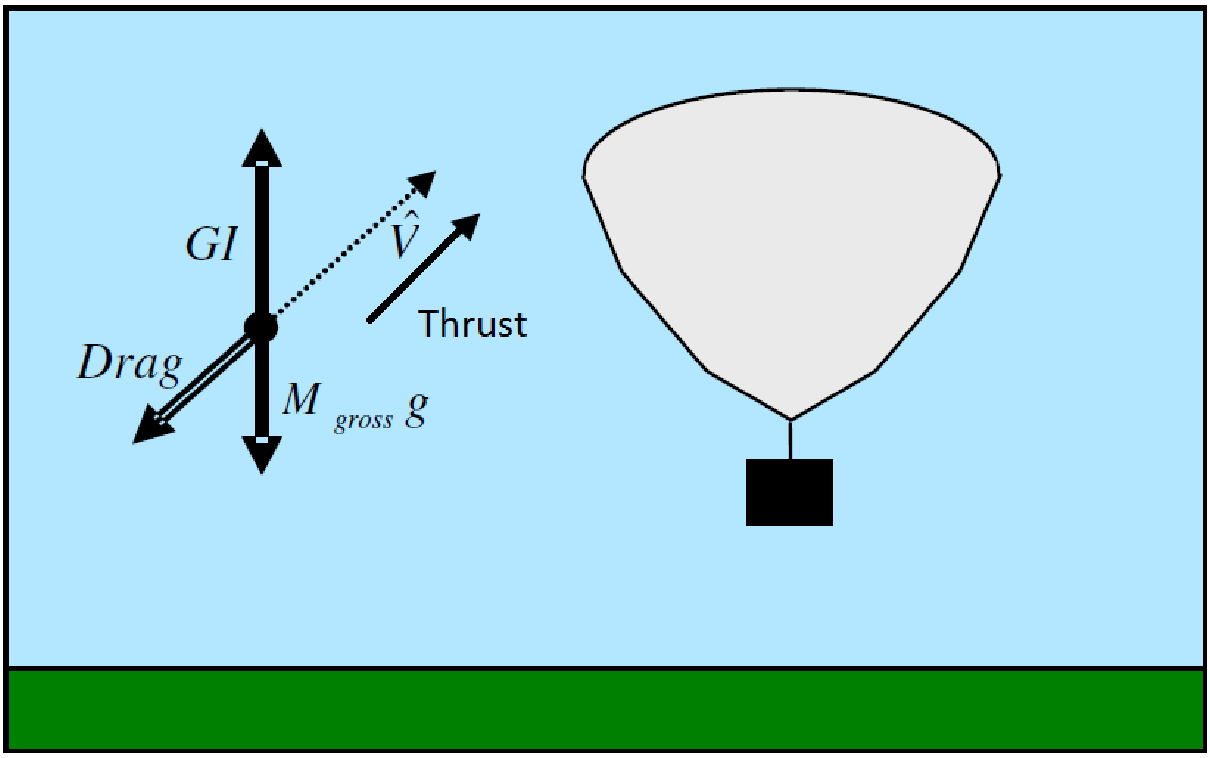

Figure 32: Forces on a Buoyant Aerobot [t.4]

From Figure 32 the equations of motion for an aerobot in flight are written with respect to the accelerations a_x, a_y and a_z and the total mass m_{tot}:

$$\sum F_x = m_{tot} \cdot a_x = m_{tot} \cdot \frac{dV_x}{dt} = T_x - D_x$$

Equation 17: Equilibrium of Forces in x-direction

$$\sum F_y = m_{tot} \cdot a_y = m_{tot} \cdot \frac{dV_y}{dt} = T_y - D_y$$

Equation 18: Equilibrium of Forces in y-direction

$$\sum F_z = m_{tot} \cdot a_z = m_{tot} \cdot \frac{dV_z}{dt} = GI + T_z - D_z - W$$

Equation 19: Equilibrium of Forces in z-direction

The total mass m_{tot} in the equations can be written as the sum of the balloon mass $m_{balloon}$, the mass of the buoyant gas m_{gas} and the payload mass $m_{payload}$. Often these symbols will be shortened to m_b, m_g, and m_p respectively. Further the sum of the balloon mass and the payload mass is defined as the gross mass, m_{gross}.

$$m_{tot} = m_{balloon} + m_{gas} + m_{payload}$$

$$m_{tot} = m_{gross} + m_{gas}$$

Equation 20: Total Mass

The payload mass is defined as the sum of all payload components and support systems. This includes the gondola, the scientific instruments, the connections between balloon and gondola and any extra ballast. Basically everything that the buoyant aerobot carries into the air, and is no part of the balloon or the buoyant gas, is seen as payload.

$$m_{payload} = \sum_{i} m_{component}$$

Equation 21: Payload Mass

The mass of the balloon envelope can be determined through the areal density of its envelope material $\rho_{envelope}$, which is expressed in [kg/m^2], and the balloon surface area $A_{balloon}$.

$$m_{balloon} = A_{balloon} \cdot \rho_{envelope}$$

Equation 22: Balloon Mass

The mass of the buoyant gas can be calculated by introducing the equation of state for an ideal gas into its mass equation. An ideal gas obeys the ideal gas law of Equation 23. Opposed to that, a real gas exhibits properties that cannot be explained entirely using the ideal gas law of Equation 23. “To understand the behavior of real gases, other properties such as compressibility effects, variable specific heat capacity, non-equilibrium thermodynamic effects, etc. need to be taken into account [i.50].”

For most applications, such a detailed analysis is unnecessary, and the ideal gas approximation can be used with reasonable accuracy. “Many gases such as nitrogen, oxygen, hydrogen, noble gases, and some heavier gases like carbon dioxide can be treated like ideal gases within reasonable tolerances. Generally, a gas behaves more like an ideal gas at higher temperature and lower pressure. The ideal gas model tends to fail at lower temperatures or higher pressures, when intermolecular forces and molecular size become important. It also fails for most heavy gases and for gases with strong intermolecular forces, notably water vapor [i.49].” Atmospheres which include water will not act like an ideal gas for instance.

$$p = \frac{\rho \cdot R_c \cdot T}{M}$$

Equation 23: Equation of State

$$m_{gas} = Vol_{balloon} \cdot \rho_{gas}$$
$$m_{gas} = Vol_{balloon} \cdot \frac{M_{gas} \cdot p_{gas}}{R_c \cdot T_{gas}}$$

Equation 24: Buoyant Gas Mass

Now that all masses have been defined the weight of the aerobot can be written as;

$$W = m_{gross} \cdot g$$

Equation 25: Aerobot Weight

Both Abe et al [b.5] and Farley [a.22] add a virtual component to the total mass. This virtual component is related to the mass-spring behavior of a buoyant aerobot. “Statically, the buoyancy force acting on the aerobot makes it appear less massive. In addition to the buoyancy effect, an added mass term must therefore be considered. In a physical sense, this added mass is the weight added to a system due to the fact that an accelerating or decelerating body, in unsteady motion, must move some volume of surrounding fluid with it as it moves. The added mass force opposes the motion [a.41]."

$$m_{virtual} = m_{tot} + C_{virtual} \cdot \rho_a \cdot Vol_{balloon}$$

Equation 26: Virtual Mass

Values for the virtual mass coefficient $C_{virtual}$ range between 0.25 and 0.5 [a.22]. The virtual coefficient depends on shape and size of the balloon but will be a fixed parameter in the Buoyant Aerobot Design and Simulation (BADS) tool in chapter 5, with a value of 0.37 [t.4]. The effect of this parameter will be discussed further during a sensitivity study in chapter 7.

Next the focus will be placed on the equation of motion in the vertical z-direction. The ascend rate of the balloon can be found from the equation of motion in z-direction. Note that from here on the equation of motion in the vertical direction will use the virtual mass. The lifting force that is available after loading the aerobot with its maximum weight W, and after subjecting the balloon to its drag force, is the remaining lift R_z.

$$R_z = m_{virtual} \cdot a_z = GI + T_z - D_z - W$$

Equation 27: Free Lift

The value of R_z provides the aerobot with an ascend or descend rate. If this value is high the aerobot will rise quickly while otherwise the aerobot will rise more steadily into the atmosphere. If R_z would be zero, the aerobot finds itself in a stable float which resembles hovering at a constant altitude.
The value of the ascend speed can be derived by rewriting the equation of motion in z-direction. The acceleration is a function of time and speed. Integrated, the ascend speed can be found as a function of time, virtual mass, free lift and initial speed.

$$R_z = m_{virtual} \cdot \frac{dV}{dt} = GI + T_z - D_z - W$$

$$R_z \cdot dt = m_{virtual} \cdot dV = (GI + T_z - D_z - W) \cdot dt$$

$$\int_{t_1}^{t_2} R_z \cdot dt = \int_{V_1}^{V_2} m_{virtual} \cdot dV = \int_{t_1}^{t_2} (GI + T_z - D_z - W) \cdot dt$$

$$R_z \cdot \Delta t = m_{virtual} \cdot \Delta V$$

$$\Delta V_A = \frac{R_z \cdot \Delta t}{m_{virtual}}$$

Equation 28: Ascend Speed Derivation

4.2.2. Drag Force

The standard drag force of a vehicle depends on a number of parameters [b.2]; cross-sectional area A_{cross}, total speed V, air density ρ and drag coefficient C_D.

$$F_{Drag} = 0.5 \cdot C_D \cdot \rho \cdot V^2 \cdot A_{cross}$$

Equation 29: Drag Force

Each component of the aerobot induces a certain amount of drag based on the cross-sectional area of the component. For a buoyant aerobot however the main component is its balloon. Compared to the size of the balloon all other components can be neglected and the aerobot can be seen as one big balloon. The assumption is therefore made that the main drag will come from the balloon, and any other components inducing drag will be ignored. The effect of this assumption will be explored further in chapter 7.

$$D_{aerobot} = D_{total} = D_{balloon}$$

Equation 30: Total Drag

The drag force components in x, y and z-direction can be written with respect to the relative velocity and the aerobot's cross area in the respective direction;

$$D_x = 0.5 \cdot C_D \cdot \rho \cdot \left(\frac{V_{rx}}{V_{re}} \right) \cdot V_{re}^2 \cdot A_{yz}$$

$$D_y = 0.5 \cdot C_D \cdot \rho \cdot \left(\frac{V_{ry}}{V_{re}} \right) \cdot V_{re}^2 \cdot A_{xz}$$

$$D_z = 0.5 \cdot C_D \cdot \rho \cdot \left(\frac{V_{rz}}{V_{re}} \right) \cdot V_{re}^2 \cdot A_{xy}$$

Equation 31: Drag Directional Components

With;

$$V_{rx} = V_{aerobot_x} - V_{wind_x} \qquad V_{ry} = V_{aerobot_y} - V_{wind_y} \qquad V_{rz} = V_{aerobot_z} - V_{wind_z}$$

$$V_{re} = \sqrt{V_{rx}^2 + V_{ry}^2 + V_{rz}^2}$$

Equation 32: Relative Velocity

In z-direction negative drag can occur when the aerobot's actual velocity is downward or in the negative z-direction. This actually will help the aerobot to slow down its descend and recover its flight altitude.

$$D_z = -0.5 \cdot C_D \cdot \rho \cdot \left(\frac{V_{rz}}{V_{re}} \right) \cdot V_{re}^2 \cdot A_{xy}$$

Equation 33: Negative Drag

4.2.3. Drag Coefficient

"The drag coefficient C_D, is not a constant but varies as a function of speed, flow direction, object position, object size, fluid density and fluid viscosity. Speed 'V', dynamic viscosity 'μ' and a characteristic length 'l' of the object are incorporated into a dimensionless quantity called the Reynolds number 'Re' [i.27]".

$$\mathrm{Re} = \frac{\rho \cdot V \cdot l}{\mu}$$

Equation 34: Reynolds Number

Drag coefficient C_D is thus a function of Reynolds number Re. In compressible flow, the speed of sound is relevant and C_D is also a function of Mach number.

For certain body shapes however the drag coefficient only depends on the Reynolds number Mach number, and the direction of the flow. For low Mach number, and therefore low speed, the drag coefficient is independent of Mach number. Also the variation with Reynolds number within a practical range of interest is usually small. So the drag coefficient in these occasions can often be treated as a constant.

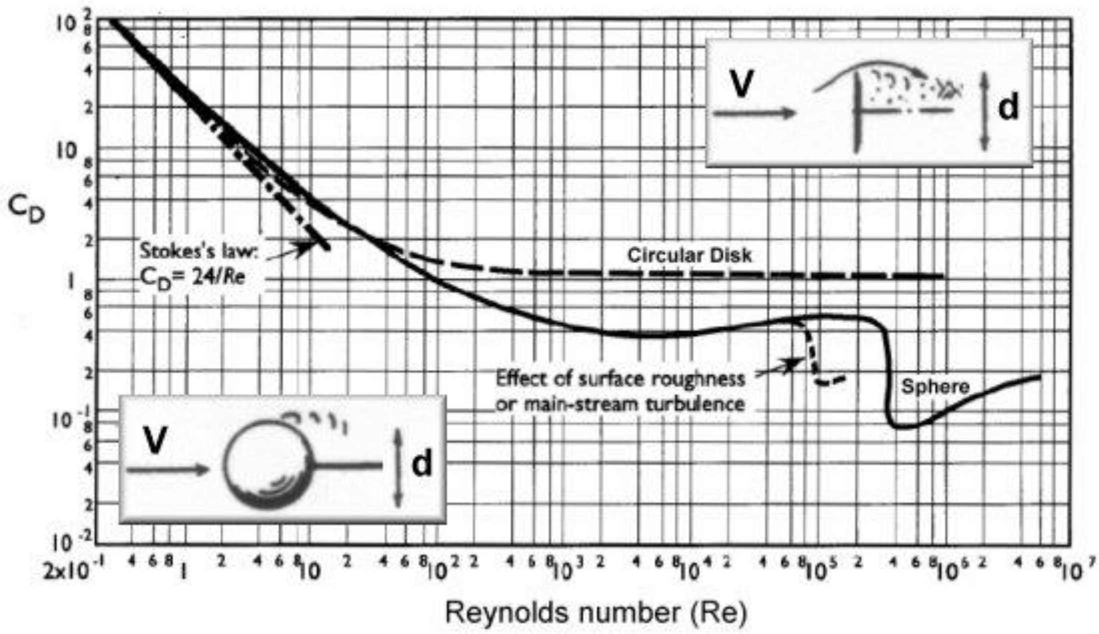

Figure 33: Drag Coefficient vs Reynolds Number [i.28]

Figure 33 [i.28] shows the relation between drag coefficient and the Reynolds number for a sphere. "At a low Reynolds number, the flow around the object does not convert to turbulent but remains laminar, even up to the point at which it separates from the surface of the object. At very low Reynolds numbers, without flow separation, the drag force D is proportional to speed V instead of V^2, for a sphere this is known as Stokes law. Reynolds number will be low for small objects, low velocities, and high viscosity fluids [i.27]." Stokes law at low Reynolds number gives a linear relation between Reynolds number and drag coefficient:

$$C_D = \frac{24}{Re}$$

Equation 35: Drag Coefficient for Stokes Law

In general, the drag coefficient is not an absolute constant for a given body shape, nor does a linear relation holds. A smooth sphere, for example, has a C_D that varies from high values for laminar flow to 0.47 for turbulent flow. Yet, these values can't be used to determine the drag coefficient of a balloon on another planet, due to the fact that the drag coefficient is dependent on the Reynolds number, which in turn depends on the atmospheric density. These parameters greatly influence the drag on an object.

Based on the information on ideal gases of section 4.2.1 it is assumed that all the buoyant gases in Table 14 and all atmospheres mentioned in section 4.1 will act like ideal gases. Therefore Sutherland's equation [i.29] can be used to derive the dynamic viscosity of an ideal gas as a function of temperature:

$$\mu = \mu_0 \cdot \frac{T_0 + C}{T + C} \cdot \left(\frac{T}{T_0} \right)^{\frac{3}{2}}$$

Equation 36: Sutherlands Equation

Dynamic viscosity μ is expressed in Pascal-seconds for an atmospheric input temperature T. The reference viscosity μ_0 holds for a reference temperature T_0. Temperatures are expressed in Kelvin. Furthermore the equation makes use of the Sutherland constant C, also expressed in Kelvin. The constant is defined for different gases in Table 14 [i.29] together with the reference temperature T_0. The constants are valid for temperatures between 0 and 555K with an error less than 10% due to pressure below 3.45MPa.

Table 14: Sutherland's Constant for Gases

Gas	C [K]	T_0 [K]	μ_0 [10^{-6} Pa s]
Air on Earth	120	291.15	18.27
Nitrogen	111	300.55	17.81
Oxygen	127	292.25	20.18
Carbon dioxide	240	293.15	14.8
Carbon monoxide	118	288.15	17.2
Hydrogen	72	293.85	8.76
Ammonia	370	293.15	9.82
Sulfur dioxide	416	293.65	12.54
Helium	79.4	273	19

For Earth's atmosphere exact numbers are available, other planets have a combination of gases in their atmosphere for which the viscosity can be determined from the constants in Table 14. If the viscosity of an atmosphere has to be calculated, the main constituent of the atmosphere will be chosen as a reference, which was pointed out in section 4.1.5.

The fact that shape, size, velocity, altitude and atmospheric density, seem to have their influence on the Reynolds number, which has its influence on the drag coefficient, made it difficult to find the drag coefficient at any time during flight for any shape in any environment.
Initially the choice was therefore made to keep the drag coefficient constant for specific shapes. Not accurate in flight, but rather accurate when hovering. From another rapport of Colozza [a.31] a functional equation, demonstrated in Equation 37, was found for the drag coefficient based on the fineness ratio 'f' of the aerobot. "The equation representing the fineness ratio is valid for fineness ratios up to 10 for a cylindrical shape with hemispherical end [a.31]". Although still a constant drag coefficient, this equation is at least based on the shape of the balloon.

$$C_D = 0.23175 - 0.15757 \cdot f + 0.04744 \cdot f^2 - 7.0412 \cdot 10^{-3} \cdot f^3 + 5.1534 \cdot 10^{-4} \cdot f^4 - 1.4835 \cdot 10^{-5} \cdot f^5$$

Equation 37: Constant Drag Coefficient with respect to Fineness Ratio

Chapter 6.3.2 will discuss what effect a, Reynolds based, variable drag coefficient has on the flight of a buoyant aerobot. Further research on this topic is recommended though.

4.2.4. Lift and Buoyancy

Lift forces can be calculated from the adapted Equation 29 in a similar manner, only making use of another coefficient, namely the lift coefficient C_L. For the cross-sectional area again use is made of the balloon's envelope, as this is the largest component and has the biggest effect on drag, thrust and lift.

$$L_x = 0.5 \cdot C_L \cdot \rho_{atm} \cdot V_{x_{Aerobot}}^2 \cdot A_{xz_{balloon}}$$

Equation 38: Lift in x-direction

$$L_y = 0.5 \cdot C_L \cdot \rho_{atm} \cdot V_{y_{Aerobot}}^2 \cdot A_{yz_{balloon}}$$

Equation 39: Lift in y-direction

$$L_z = 0.5 \cdot C_L \cdot \rho_{atm} \cdot V_{z_{Aerobot}}^2 \cdot A_{xy_{balloon}}$$

Equation 40: Lift in z-direction

Lift equations for a buoyant aerobot however can be simplified from the buoyant force. Assuming that no lift is generated through geometry, meaning C_L is set to zero, L_z is equal to the gross inflation GI, and L_x and L_y become zero. This assumption is supported by the fact that nowhere in literature any mention is made of geometric lift nor is it incorporated in the equations of motion by Ball et al, Abe et al [b.5] or Farley [a.22]. This results in the following simplified equation for lift:

$$L_z = g_{planet} \cdot \left(\frac{M_{atm} \cdot p_{atm}}{R \cdot T_{atm}} - \frac{M_{gas} \cdot p_{gas}}{R \cdot T_{gas}} \right) \cdot Vol_{balloon}$$

Equation 41: Lift Equals Buoyancy

4.2.5. Propulsion and Thrust

A buoyant aerobot without a propulsion system is an uncontrolled object. Even with a propulsion system it might be subjected to too much wind, gusts or storms on other planets to be a controllable aerobot, just because a balloon's behavior is very susceptible to these phenomena. Nevertheless it is wise to have a propulsion system onboard for some controllability.

A set of equations similar to that of drag and lift can be found for the thrust force of the aerobot. Thrust basically depends on the same parameters. However it makes use of a certain thrust coefficient that's related to propulsive efficiencies. For the cross-sectional area again use is made of only the balloon's envelope, as this is the largest component and has the biggest effect on the required thrust to overcome the drag.

$$T_{x_{req}} = 0.5 \cdot C_T \cdot \rho_{atm} \cdot V_x^2 \cdot A_{yz}$$

Equation 42: Thrust in x-direction

$$T_{y_{req}} = 0.5 \cdot C_T \cdot \rho_{atm} \cdot V_y^2 \cdot A_{xz}$$

Equation 43: Thrust in y-direction

$$T_{z_{req}} = 0.5 \cdot C_T \cdot \rho_{atm} \cdot V_z^2 \cdot A_{xy}$$

Equation 44: Thrust in z-direction

Thrust will be simulated in chapter 5 through the input of the preferred propelled speed. Therefore, an assumption is made about the type of propulsion from hereon. Based on the fact that a buoyant aerobot will fly at low speeds, no expensive and high power systems are required. The propulsion system investigated below will be an electric propeller driven system.

Colozza [a.32] provides an equation for the total amount of power P needed to produce the amount of thrust desired. The required power P by the power system is equal to the thrust T times the flight velocity V divided by the system efficiency η_t.

$$P = \frac{T_{req} \cdot V}{\eta_t}$$

Equation 45: Total Electric Power

According to Colozza the total efficiency for an electric propulsion system is given by;

$$\eta_t = \eta_e \cdot \eta_m \cdot \eta_g \cdot \eta_p$$

Equation 46: Total Propulsive Efficiency

The operational efficiencies, according to Colozza, are given in Table 15. These are based on the propeller set-up of Figure 34, provided by Colozza [a.33]. "The function of the gearbox in Figure 34 is to step down the shaft rotations per minute (RPM) from the motor speed to the desired propeller RPM [a.32]."

The efficiencies are representative approximations, which are subject to change, based on a more detailed system and component design. Nevertheless, for an initial approximation of the total power, they can be used.

Table 15: Propulsion System Efficiencies [a.33]

Component	Efficiency [%]	η
Control Electronics	0.98	η_e
Motor	0.90	η_m
Gearbox	0.85	η_g
Propeller	0.85	η_p
Total System Efficiency	0.637	η_t

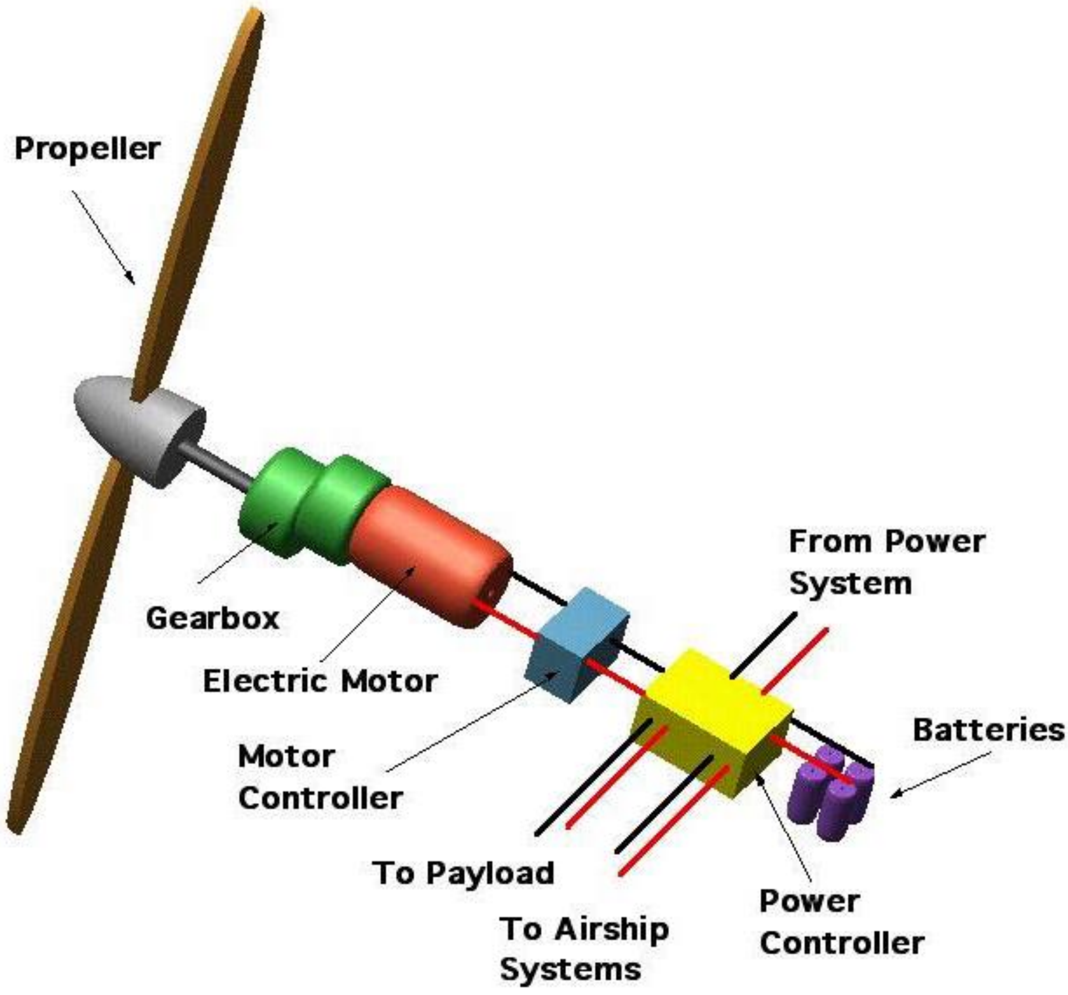

Figure 34: Basic Propeller System [a.33]

Colozza presents a more detailed analysis on propeller power in [a.31] and [a.33], iterating the propeller sizing for highest efficiency. These equations are beyond the range of this thesis though. In future the program user will have a chance to change the component's efficiencies in BADS and with this be able to investigate different types of propeller systems. Currently use will be made of the propulsion system efficiencies in Table 15, together with the preferred propelled speed to simulate powered flight.

4.3. Balloon Design

Balloon design plays an important role in the aerobot's way of operation. Volume and type of gas will decide the maximum amount of total mass that can be lifted, while shape plays a role in the aerodynamics and pressure distribution on the balloon. The topics discussed below all play a part in the programming of chapter 5, and point out the basics of each.

4.3.1. Balloon Shape and Volume

"An ellipsoid is a solid for which all plane sections through one axis are ellipses and through the other are ellipses or circles. If any two of the three axes of that ellipsoid are equal, the figure becomes a spheroid, an ellipsoid of revolution. If all three are equal, it becomes a sphere. [i.23]" Spheroids can be defined through their fineness ratio 'f', which is the ratio of the length of the balloon to its diameter or width. A sphere has a fineness ratio of 1. An oblate spheroid has a fineness ratio higher than 1 and looks a lot like a super-pressure pumpkin, discussed in section 2.1.2.2. It is illustrated in Figure 36. A prolate spheroid has a fineness ratio between 0 and 1 and represents the shape of a cigar, illustrated in Figure 37. Rotated around the y axis however it looks a lot like an airship flying in x-direction, as the one discussed in section 3.1.4 and illustrated in Figure 38. The characteristics of each of these shapes will be further analyzed as they represent every balloon shape discussed in chapter 3.

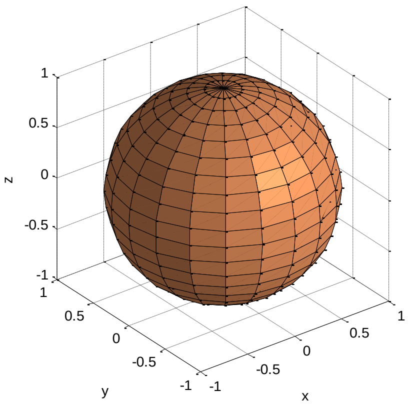

Figure 35: Sphere

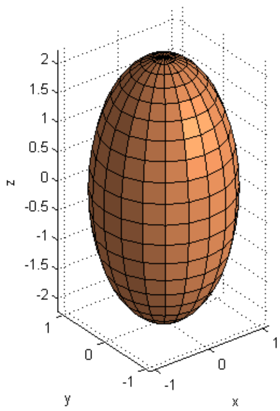

Figure 37: Prolate Spheroid

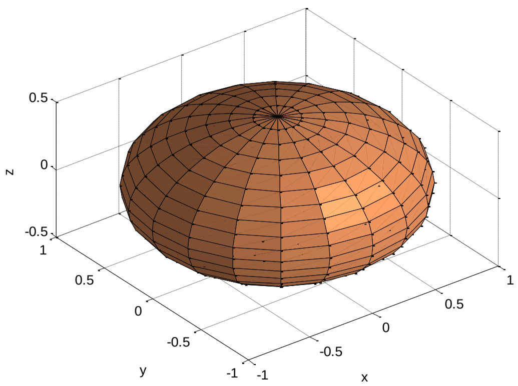

Figure 36: Oblate Spheroid

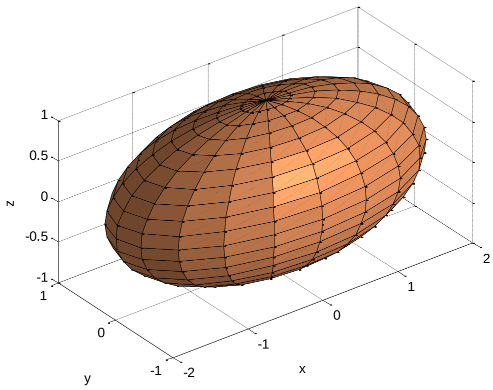

Figure 38: Airship Rotated Prolate Spheroid

The volume of an ellipsoid is calculated from Equation 47, where a, b and c are the major and minor axis lengths in x, y, z direction respectively and 'Vol' is the volume. This equation can be simplified for a sphere, where the axis lengths all have the same radius 'R', shown in Equation 48.

Table 16: Spheroid's Surface Area and Volume

$Vol_{ellipsoid} = \frac{4}{3} \cdot \pi \cdot a \cdot b \cdot c$ **Equation 47: Ellipsoid Volume**	$Vol_{sphere} = \frac{4}{3} \cdot \pi \cdot R^3$ **Equation 48: Sphere Volume**	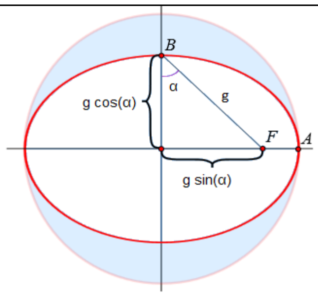
$A_{sphere} = 4 \cdot \pi \cdot R^2$ **Equation 49: Sphere Surface Area**		
$A_{prolate} = 2 \cdot \pi \cdot \left[a^2 + \left(c^2 \cdot \left(\frac{\alpha}{\tan(\alpha)} \right) \right) \right]$ **Equation 50: Prolate Surface Area**	$\alpha_{prolate} = \arccos\left(\frac{a}{c} \right)$ **Equation 51: Prolate Angular Eccentricity**	
$A_{oblate} = 2 \cdot \pi \cdot \left[a^2 + \left(\frac{c^2 \cdot \arctan h(\sin(\alpha))}{\sin(\alpha)} \right) \right]$ **Equation 52: Oblate Surface Area**	$\alpha_{oblate} = \arccos\left(\frac{c}{a} \right)$ **Equation 53: Oblate Angular Eccentricity**	

Surface areas for ellipsoid are calculated from incomplete elliptic integrals. For oblate and prolate spheroids, where a circular equator a=b is present, exact solutions can be found though, through Equation 50 and Equation 52 [i.51]. These equations give exact solutions for the surface areas if the angular eccentricity α is modified for each particular case. The sine of α is the eccentricity 'e'.
The cross-sectional areas of a sphere, oblate and prolate spheroid as well as the airship are listed in Table 17. Notice that most equations for the xz and the yz-plane remain the same except those of the airship. As this configuration is rotated 90° compared to the prolate spheroid, the cross-sections rotate as well, meaning $a \neq b$ but $c = b$.
The cross-sectional area is an important parameter for the flight performance of an aerobot. A bigger cross-sectional area shall for example result in a higher drag. The prolate spheroid configured as in Figure 37 has a high drag in x-direction but a low drag in z-direction, whereas the opposite holds for the airship of Figure 38.

Table 17: Cross-Sectional Areas of Spheroids

	A_{xy}	A_{xz}	A_{yz}
Sphere	$A_{xy} = \pi \cdot a^2$	$A_{xz} = \pi \cdot a^2$	$A_{yz} = \pi \cdot a^2$
Oblate Spheroid	$A_{xy} = \pi \cdot a^2$	$A_{xz} = \pi \cdot a \cdot c$	$A_{yz} = \pi \cdot a \cdot c$
Prolate Spheroid	$A_{xy} = \pi \cdot a^2$	$A_{xz} = \pi \cdot a \cdot c$	$A_{yz} = \pi \cdot a \cdot c$
Airship	$A_{xy} = \pi \cdot a \cdot c$	$A_{xz} = \pi \cdot a \cdot c$	$A_{yz} = \pi \cdot c^2$

4.3.2. Balloon Pressure and Skin Tension

Pascal's principle states: “Pressure exerted anywhere in a confined incompressible fluid is transmitted equally in all directions throughout the fluid such that the pressure ratio remains the same” [i.24].

Laplace’s law [i.24] describes the relation between the radius of the balloon, inside pressure and wall tension in Equation 54. “The larger the vessel radius, the larger the wall tension required to withstand a given internal fluid pressure.” This relation can be explained as follows: “If the upward part of the fluid pressure remains the same, then the downward component of the wall tension must remain the same. But if the curvature is less, then the total tension must be greater in order to get that same downward component of tension. [i.24]” For a given vessel radius and internal pressure, a spherical vessel will therefore have half the wall tension of a cylindrical vessel.

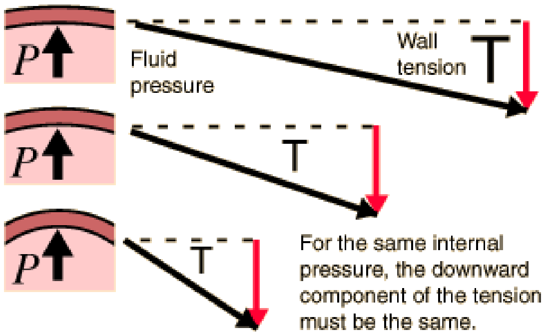

Figure 39: Skin Tension [i.24]

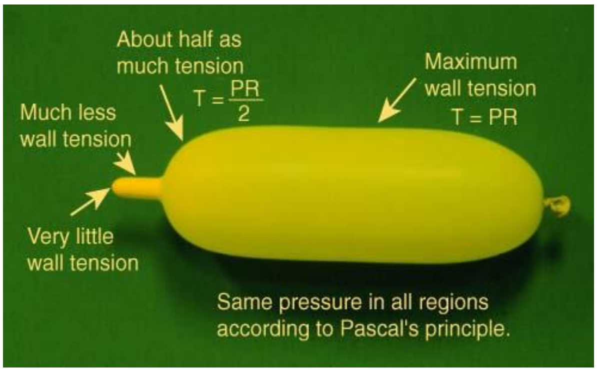

Figure 40: Locating highest Tension [i.24]

$$F_{Tension_{Cylinder}} = p \cdot R$$

$$F_{Tension_{Sphere}} = \frac{p \cdot R}{2}$$

Equation 54: Envelope Tension Force

Tension Force $F_{Tension}$ is calculated in N/m. More use is made however from skin pressure in N/m^2. The equations can be found from the stress relations for thin-walled pressure vessels and are simply versions of Equation 54 divided by the wall thickness ‘d’:

$$\sigma_{Sphere} = \frac{p \cdot R}{2 \cdot d}$$

$$\sigma_{Cylinder_\theta} = \frac{p \cdot R}{d}$$

$$\sigma_{Cylinder_{Long}} = \frac{p \cdot R}{2 \cdot d}$$

Equation 55: Envelope Tension

A balloon is basically a pressure vessel, so these equations are valid. σ_{Sphere} is the hoop stress for a sphere, $\sigma_{Cylinder_\theta}$ is the hoop stress for a cylinder and $\sigma_{Cylinder_{Long}}$ is the stress in longitudinal direction. When using a cylindrical shape the highest pressure should be taken into account, which is the pressure in the circumferential direction.

The above equations do not take into account any safety factors to account for uncertainties, calibration errors, unexpected loads, material degradation, etc. Safety factors make components overly strong and provide redundancy. In aerobot design however, as it is in aircraft design, including safety factors would mean adding extra weight to the design. This negatively influences design, performance and endurance.

The simulation tool of chapter 5, does not take into account skin tension at this time, nor does it take into account any safety factors. Future work should however include the direct bond between material strength, balloon gas pressure and balloon failure. Currently, some standard material properties from the balloon envelope manufacturers have been put into a material database, such as those illustrated in Table 18 and Table 19. This topic will be addressed next.

4.3.3. Balloon Envelope Materials and Coatings

The envelope fabric of a balloon has an influence on the total mass of the aerobot, the flight endurance and the thermal behavior. The thickness and density of the fabric are key parameters in reducing or increasing weight of the envelope. A wide range of materials and areal density exist. Some datasheets and samples of typical balloon materials were obtained from Lamcotec Inc. [d.2]. They use a number of urethane products with polyester and nylon for Earth-based balloons. Material properties are presented in Table 18.

Table 19 also presents a number of materials, specifically used for a Titan aerobot mission. When compared to the materials of Lamcotec, a wide variety between areal density is detected. This is just one example of mission and design parameters which can influence a basic aerobot design.

Table 18: Elasticity, Strength and Areal Density of Lamcotec Urethane Materials [d.2]

Envelope Material	Density	Elongation	Strength
	[g/m^2]	[%]	[N/m]
(PE/DC) #867 NATURAL, 30 DENIER NYLON RIPSTOP	119	21	9631.97
(M1/DL) #867 NATURAL, 30 DENIER NYLON RIPSTOP	170	21	9631.97
(PM/AP/KC) #109 WHITE, 70 DENIER NYLON TAFFETA	144	17	12258.88
(PM/AP/KC) #142 NATURAL, 70 DENIER NYLON RIPSTOP	144	33	14010.15
(PM/AP/KC) #841 NATURAL, 150 DENIER POLYESTER	181	17	19263.95
(DL) #870 NATURAL, 200 DENIER VECTRAN	248	8	70050.73
(PE/KC) #442 NATURAL, 210 DENIER NYLON RIPSTOP	229	25	33274.10
(M1/DL) #442 NATURAL, 210 DENIER NYLON RIPSTOP	281	21	35025.37
(M1/DL) #410 NATURAL, 210 DENIER NYLON HIGHCOUNT	356	25	50786.78
(M1/DL) #452 NATURAL, 210 x 315 DENIER NYLON PLAIN	322	33	47284.25
(DL) #887 NATURAL, 400 DENIER VECTRAN	288	8	115583.71
(M1/DL) #857 NATURAL, 500 DENIER POLYESTER	403	21	54289.32
(M10/DL) #857 NATURAL, 500 DENIER POLYESTER; CARBON BLACK COATED	383	21	54289.32
(M1/DL) #894 NATURAL, 1000 DENIER POLYESTER	505	25	57791.86

Earth's scientific balloons use latex or Mylar. Latex has the possibility to expand a lot, while Mylar is lighter than latex but lacks elasticity. Balloons with a fabric of no elasticity will reach their maximum volume at the design altitude and from there on gas pressure will increase inside the balloon or gas is vented to maintain a zero-pressure level. Balloons with an elastic material will increase in size even when the design altitude is reached. The gas pressure inside will remain zero as volume can expand, but material stresses will increase due to elongation. When the maximum elongation is reached and the fabric has reached its breaking strength the balloon will fail. The breaking strength can be found from the equations in section 4.3.2.

The atmosphere on Earth is less hostile compared to other planetary atmospheres in the solar system. Envelope fabrics however should be able to withstand the atmospheric conditions at those hostile planets too. The more sophisticated balloons used in space are therefore protected against radiation, temperature, sulfuric acids, sand storms, etc. and as such are suited for long mission durations and hostile environments. These types of materials are made of multilayered films, including; PBO, polyurethane coatings, polyester, Mylar, Kevlar, nylon. Table 19 shows some examples of improved balloon materials for a Titan aerobot.

Table 19: Titan Aerobot Envelope Fabrics [a.12]

Material	**Thickness [μm]**	**Areal Density [g/m^2]**
Mylar film	3.6	5.0
Mylar film	8.9	12.5
Mylar film	12.2	17.0
Kapton 30HN	7.6	11.9
Polyehtylene napthalate (PEN) film	3.0	5.9
Fiberglass/PTFE (Chemlam Ultra 1100)	107	190.0
Norlam 1.7 (70 denier polyester fabric + .5 mil Mylar film	89	78.0
Mylar bilaminate (2x3.6μm layers glued together)	8.9	12.3
Mylar hexalaminate (6x3.6μm layers glued together)	27.9	41.1
Polyester fabric (94x93 weave, 50 denier) plus Mylar hexalaminate	99.1	98.0
Nylon fabric (122x80 weave, 30 denier) plus Mylar hexalaminate	96.5	83.3

A thin polymeric or metallic layer other than the main material can be applied as a coating to reduce the gas leakage, which will be discussed in section 4.3.5. It can also be used for thermal control purposes, discussed in section 4.4. The thickness of the envelope should however be minimized, as it will add extra weight to the aerobot [a.13, p206], which could otherwise be utilized, for instance as payload. A very detailed study on solar absorptance and thermal emittance of numerous coatings can be found in [a.29], but will be explored later on.

4.3.4. Buoyant Gas Selection

The buoyant gas inside the balloon will give the aerobot the lift necessary to stay afloat. The type of gas is therefore important. The two most suitable lighter-than-air gases on Earth are Hydrogen and Helium, with Hydrogen being the lightest but also the most flammable. Helium on the other hand is an inert gas. In the examples in chapter 3, helium is the most used. There are however a number of other candidates when planetary atmospheres are taken into account. While helium and hydrogen stay the lightest and the most efficient, any gas lighter than the composition of the atmosphere can be used to let an aerobot float.

For ambient aerobots not even that requirement is essential as the local atmosphere is being used and heated to lift the aerobot. Abe et al present the buoyant gases that can be used on either Earth, Venus, Mars or Titan [b.5, p179]. The chemical properties of these gases are listed in Table 20 together with those of the atmospheres of the four celestial bodies. Only in the dense atmosphere of Venus all buoyant gases of Table 20 can be used to fly a buoyant aerobot. On Earth, Mars and Titan only hydrogen and helium are suitable.

Table 20: Buoyant Gas and Atmosphere Composition Characteristics [b.5], [b.8]

Gas/Atmosphere	Molar Mass [g/mol]	c_p [J/kgK]	c_v [J/kgK]
H_2	2.016	14310	10180
He	4.026	5230	3150
CH_4	16.04	2230	1690
CO_2	44.01	846	657
NH_3	17.031	2190	1660
N_2	28.0134	1039	743
Earth	28.97	1005	718
Venus	43.35	846	657
Mars	44.01	846	657
Titan	28.60	1039	743

The data in Table 20 will be used throughout the simulation program of chapter 5. The molar mass M is regularly used throughout the thesis when for instance the equation of state is used. c_p and c_v are the specific heat capacities and will be used during the thermal modelling in section 4.4. All data was reproduced from Abe et al [b.5] and D.R. Lide's 'CRC Handbook of Chemistry and Physics' [b.8]. Thermal conductivity has been reproduced for a wide temperature range, based on Lide's [b.8] information. As such, the simulation tool in chapter 5 is able to simulate a temperature dependent thermal conductivity instead of a constant value for each of the buoyant gases and atmospheres. When data on thermal conductivity, viscosity or specific heat capacity was not available for a specific atmosphere the main constituent gas was used as reference data. For Mars and Venus this is CO_2 and for Titan this is N_2.

4.3.5. Gas Discharge Rate and Envelope Permeability

Permeation is the amount of diffusion of a gas passing through a material in a certain time. When the gas is leaving an enclosed form it is called the leakage rate. The permeability of the envelope will therefore determine the time that a balloon is able to fly at a certain altitude. The leakage rate can be approximated using Darcy's law [i.37].

$$Q_{discharge} = -\frac{\lambda \cdot A_{balloon}}{\mu} \cdot \frac{(p_g - p_a)}{l}$$

Equation 56: Darcy's Law

'$Q_{discharge}$' is the discharge rate in [m^3/s], 'λ' is the fabric permeability coefficient in [m^2], 'A' the balloon envelope area in [m^2], p_g and p_a the pressure of gas and atmosphere respectively in [Pa], 'μ' is the buoyant gas viscosity in [Pa s] and 'l' is the thickness of the envelope material in [m].

Every parameter is quite straightforward in Darcy's law, except the permeability coefficient λ. Permeability is the degree of ability of a material to allow fluids or gases to pass through it. This means that permeability is influenced by the material properties and the composition of the buoyant gas passing through. Firstly, lighter gases like hydrogen and helium have smaller molecules and will pass easier through a material than for instance carbon dioxide. Secondly, gases of any kind will also pass through a material easier when the material has a larger porosity. Both relations are described by the permeability coefficient λ.

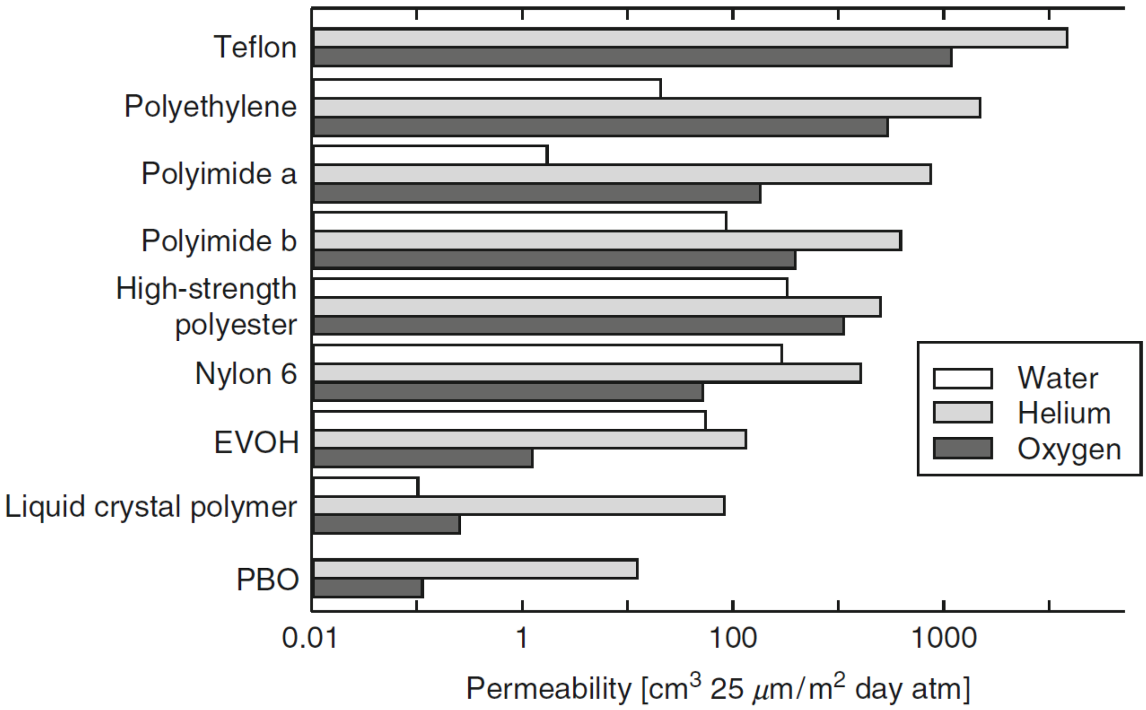

Figure 41: Comparison of the Gas Barrier Performances of Heat-Resistant Films [b.5]

While in Darcy's law λ is expressed in [m^2], it is mostly presented in a number of units selected by the manufacturers of the balloon fabric. Lamcotec [d.2], for instance, presents the permeability in terms of [$l/m^2/24hrs$]. Abe et al [b.5, p183] shows permeability coefficients in [cm^3 25µm/m^2 day atm.] for a number of materials tested under specific Earth atmosphere conditions, illustrated in Figure 41.

Ha [t.3, p47] converted the values from Figure 41 to the standard permeability coefficient λ in units of [m^2], shown in Table 21. This makes it easier in calculating the discharge rate Q from Darcy's law, which is a very useful parameter in finding the loss of buoyant gas mass. Unfortunately not all permeability coefficients of every envelope material are listed in Figure 41. Plus these coefficients only hold when used against helium. Any other permeability coefficient based on another gas has to be determined through testing.
The simulation tool of chapter 5 will use a constant permeability coefficient based on the values below. Chapter 7 shall further explore the effect that a permeability coefficient has on the aerobot flight.

Table 21: Permeability Coefficients of Heat-Resistant Films Against Helium [t.3]

Balloon Envelope Material	Permeability Coefficient
Teflon	$1.71 \cdot 10^{-17}$
Polyethylene	$7.16 \cdot 10^{-18}$
Polyimide a	$2.86 \cdot 10^{-18}$
Polyimide b	$2.29 \cdot 10^{-18}$
High-strength polyester	$2.00 \cdot 10^{-18}$
Nylon 6	$1.71 \cdot 10^{-18}$
Ethylene vinyl alcohol	$4.29 \cdot 10^{-19}$
Liquid crystal polymer	$2.86 \cdot 10^{-19}$
PBO	$1.43 \cdot 10^{-19}$

When λ is provided by the manufacturer in units of [m^2] Darcy's law is useful to analyze the buoyant gas loss over time. From it the following can be deduced [t.3, p45];

- The lower the permeability coefficient, the less the permeability
- The lower the viscosity the higher the leakage
- The larger the pressure differences between the gas inside the balloon and the atmosphere, the bigger the leakage
- The thicker the envelope material, the less permeability as the length through which the molecule has to travel increases
- The larger the relative area, with the same pressure difference, the larger the permeability

Some solutions to the permeability problem are; coatings, thicker materials, or impermeable materials, which would lower the discharge rate. All have an impact on the weight of the envelope but it is finding the balance between extra weight and mission endurance. One more solution is considering a different, less permeable, buoyant gas. This however will have an effect on the buoyancy, as heavier gases lower the amount of lift.

4.4. Thermal Models

It is important to model the thermal environment in which the aerobot moves. The vertical motion of the aerobot is influenced by the heat transfer to and from the buoyant gas and envelope. The gas temperature and density determine the buoyant force of the aerobot and any change in temperature or density influences its behavior. The balloon envelope plays an important role in the heat transfer mechanism, its radiation properties significantly influence the performance and the vertical flight of the balloon. Literature presents two thermal models; Farley's [a.22] extensive thermal model from the NASA's Balloon Ascent program and a general thermal model from Abe et al [b.5]. Each model has its advantages and drawbacks, when implemented in BADS. A number of limitations in both models, related to specific shapes and buoyant gas, requires a more general approach. Therefore a general modified thermal model is assembled, by selecting only the most useful equations of both models. This model includes all the advantages of both the initial models but also streamlines a number of equations, while others are discarded as they are yet too extensive for the simulation purposes of BADS.

4.4.1. Heat Transfer Model from Abe et al

Abe et al [b.5] present heat loads on a balloon's envelope and buoyant gas for an approximate spherical balloon with an effective-cross sectional area A_{cross} and an effective surface area A_e.

$$
\begin{aligned}
Q_e = \tilde{\alpha}_e \cdot I_0 \cdot \left(A_{cross} + F_{bs} \cdot a_s \cdot A_e\right) + \tilde{\varepsilon}_e \cdot \sigma_s \cdot A_e \cdot \left(F_{bs} \cdot T_s^4 - T_e^4\right) \\
+ \tilde{\varepsilon} \cdot \sigma_s \cdot A_e \cdot \left(T_g^4 - T_e^4\right) + h_{ge} \cdot A_e \cdot \left(T_g - T_e\right) + h_{ae} \cdot A_e \cdot \left(T_a - T_e\right)
\end{aligned}
$$

Equation 57: Heat Load on the Envelope

$$
\begin{aligned}
Q_g = \tilde{\alpha}_g \cdot I_0 \cdot \left(1 + a_s\right) \cdot A_e + \tilde{\varepsilon}_g \cdot \sigma_s \cdot A_e \cdot \left(F_{bs} \cdot T_s^4 - T_g^4\right) \\
+ \tilde{\varepsilon} \cdot \sigma_s \cdot A_e \cdot \left(T_e^4 - T_g^4\right) + h_{ge} \cdot A_e \cdot \left(T_e - T_g\right)
\end{aligned}
$$

Equation 58: Heat Load on the Buoyant Gas

I_0 is the solar constant, a_s is the reflectance of the ground surface or albedo. Both vary in time, location and altitude and are influenced by the presence of clouds. Variance in time includes the day and night cycle for these parameters.

$\tilde{\alpha}_e$ is the effective solar absorptivity and $\tilde{\varepsilon}_e$ is the effective infrared emissivity, of the envelope. $\tilde{\varepsilon}$ is the effective emissivity between the envelope and the buoyant gas. $\tilde{\alpha}_g$ is the effective solar absorptivity and $\tilde{\varepsilon}_g$ is the effective infrared emissivity of the buoyant gas.

T_s denotes the effective temperature of the ground surface viewed from the balloon, it varies with altitude and with diurnal time. No research is been done into the calculation of this parameter though. Chapter 7 will explore the effect of ground temperature, but further research is recommended. BADS currently keeps T_s fixed to the initial atmosphere temperature at ground.

σ_s is the Stephan-Boltzman constant and F_{bs} is the shape factor from the balloon to the planet. Shape factors for balloons are currently fixed in BADS. The shape factor for a sphere is being used as the standard, which is 0.5. Chapter 7 will investigate the effect of the shape factor further.

Next, the thermo-optical parameters are formulated. Considering the reflections of the balloon's interior, the effective solar absorptivity of the envelope and gas can be written as;

$$\tilde{\alpha}_e = \alpha_e \cdot \left(1 + \frac{\tau_e \cdot (1-\alpha_g)}{1 - r_e \cdot (1-\alpha_g)} \right)$$

Equation 59: Effective Solar Absorptivity of the Envelope

$$\tilde{\alpha}_g = \left(\frac{\alpha_g \cdot \tau_e}{1 - r_e \cdot (1-\alpha_g)} \right)$$

Equation 60: Effective Solar Absorptivity for Gas

The effective emissivity of the envelope, the gas and emissivity between them are written as;

$$\tilde{\varepsilon} = \frac{\varepsilon_e \cdot \varepsilon_g}{1 - r_{ei} \cdot (1-\varepsilon_g)}$$

Equation 61: Effective IR Emissivity Envelope-Gas

$$\tilde{\varepsilon}_e = \varepsilon_e \cdot \left(1 + \frac{\tau_{ei} \cdot (1-\varepsilon_g)}{1 - r_{ei} \cdot (1-\varepsilon_g)} \right)$$

Equation 62: Effective Emissivity of the Envelope

$$\tilde{\varepsilon}_g = \frac{\varepsilon_g \cdot \tau_{ei}}{1 - r_{ei} \cdot (1-\varepsilon_g)}$$

Equation 63: Effective Emissivity for the Gas

In these equations τ_e and τ_{ei} are the solar transmissivity and the infrared transmissivity of the envelope respectively. r_{ei} is the infrared reflectivity of the envelope, α_e is the solar absorptivity of the envelope, α_{ei} is the infrared absorptivity of the envelope, ε_e is the infrared emissivity of the envelope, α_g is the solar absorptivity of the lifting gas and finally ε_g is the infrared emissivity of the buoyant gas.

The last parameters required in Equation 57 and Equation 58 are the convective heat transfer coefficients (CvHTC) h_{ge} and h_{ae};

$$h_{ge} = \frac{Nu_g \cdot \kappa_g}{d_b}$$

Equation 64: CvHTC Gas-Envelope

$$h_{ae} = \frac{Nu_a \cdot \kappa_a}{d_b}$$

Equation 65: CvHTC Atmosphere-Envelope

The thermal conductivities κ_a and κ_g, balloon diameter d_b and the Nusselt numbers 'Nu' of both the atmosphere and buoyant gas are used for calculating the convective heat transfer coefficients h_{ge} and h_{ae} respectively.
The Nusselt number 'Nu' is the ratio of convective to conductive heat transfer across the boundary, which in this case is the balloon envelope. According to Izutsu Naoki, co-writer of Abe et al [b.5], the Nusselt number for a sphere is basically related to Prandtl and Grashof numbers, Pr and Gr respectively. "Nusselt can be calculated for different gases by their definitions, although most Nusselt expressions are approximate results by experiments or numerical computations, so a lot of equations exist. The expressions in our book are just one set of such results."
The expressions listed in Abe et al, are indeed limited to a spherical balloon. The simulation program in chapter 5 will incorporate 4 balloon shapes. Therefore the Nusselt equation of Abe et al is too

limited for general simulation purposes, but for a sphere the equations can be used. The Nusselt number will be further addressed in 4.4.3.

Abe et al [b.5] describe, with the above information and equations, the heat flow into the envelope and gas as follows through Equation 66 and Equation 67. In these equations, m_e is the envelope mass, g is the gravitational acceleration, c_e is the specific heat capacity of the envelope, M_a and M_g are the molar masses of air and gas, T_a and T_g are the temperatures of air and gas while the specific heat capacity of the buoyant gas is c_{p_g} . The last term in Equation 67 represents the ascend speed in z-direction in which 'z' is the altitude, changing with time 't'.

$$\frac{dT_e}{dt} = \frac{Q_e}{c_e \cdot m_e}$$

Equation 66: Heat Flow in/out the Balloon Envelope

$$\frac{dT_g}{dt} = \frac{Q_g}{c_{p_g} \cdot m_g} - \frac{g \cdot M_a \cdot m_g \cdot T_g}{c_{p_g} \cdot T_a \cdot M_g} \cdot \frac{dz_b}{dt}$$

Equation 67: Heat Flow in/out the Buoyant Gas

The Abe et al [b.5] thermal model makes use of general conditions, but includes a broad thermo-optical section. While cloud influence, day and night cycle and other atmospheric disturbances are mentioned, no equations are available in the model to compensate for these effects. There are however possibilities to include these effects by varying for instance the solar constant, albedo and ground temperature in equation Equation 57 and Equation 58. These options will be further investigated in section 4.4.3.

4.4.2. NASA's Balloon Ascent Thermal Model

The NASA Balloon Ascent program presented by Farley [a.22] is the famous in-house program which NASA uses for their planetary aerobot simulations. Farley describes the program very brief in [a.22]. Approximated geometric properties for zero-pressure spherical balloons are discussed briefly, as well as the flight motion, but the thermal model used is fully explained. Therefore a lot of the equations can be used.

Farley starts with calculating the transmissivity of the atmosphere, a factor that was neglected by Abe et al [b.5]. The transmissivity of the atmosphere follows from Beer's Law format of exponential decay. The law states that there is a logarithmic dependence between the product of transmissivity of light through an atmosphere, the attenuation coefficient and the distance the light travels through the atmosphere. The attenuation coefficient symbolizes how easily the atmosphere can be penetrated by a beam of light. A large attenuation coefficient means that the beam is quickly attenuated as it passes through the medium, and a small attenuation coefficient means that the medium is relatively transparent to the beam. Light can be either absorbed or scattered if it's not transmitted.

The constants in Equation 68, describing the air mass, were derived experimentally for a clear atmosphere, by Farley. A correction factor $CF_{airmass}$ was factored into the air mass ratio to account for fog, smoke or a different planet's atmosphere. The correction factor can be seen as a type of

attenuation coefficient from Beer's law. The values for the correction factor however should be derived experimentally, and are currently not available.
The Air Mass ratio where the sun shines through is calculated from the surface pressure p_0. Further it makes use of the solar elevation angle (ELV), which can be found through calculating date, time and location on the planet of interest. Further information on the subject can be found in the calculations of Palumbo [t.4] as this was outside the scope of the thesis.

$$AirMass = CF_{airmass} \cdot \left(\frac{p_a}{p_0} \right) \cdot \left[\sqrt{1229 + \left(614 \cdot \sin\left(ELV\right)\right)^2} - 614 \cdot \sin\left(ELV\right) \right]$$

Equation 68: Air Mass

During twilight and night Air Mass can be rewritten by setting ELV = 0 [t.4].

$$AirMass = CF_{airmass} \cdot \left(\frac{p_a}{p_0} \right) \cdot \left[\sqrt{1229} \right]$$

From the Air Mass ratio the transmissivity of a solar beam through the atmosphere can be found;

$$\tau_a = 0.5 \cdot \left(e^{-0.65 \cdot AirMass} + e^{-0.95 \cdot AirMass} \right)$$

Equation 69: Atmospheric Transmissivity

This equation shows that the transmissivity at the top of the atmosphere will have a value of 1 as no air mass has to be penetrated. Transmissivity will only become poorer when the light beam travels to ground. This is due to the fact that atmosphere density and path length are related to the transmissivity.

4.4.2.1. Solar Environment

To generalize the solar environment for any planet, orbital eccentricity e, and the mean radius R_{AU} must be known. These values are summarized for Earth, Venus, Mars and Titan below;

Table 22: Planetary Orbit Data

Planet/Moon	Astronomical Radius R_{AU} [AU]	Eccentricity e [/]	[Ref.]
Venus	0.723	0.0068	[i.3]
Earth	1	0.016708	[i.1]
Mars	1.52368	0.093400	[i.2]
Titan	9.54	0.0288	[i.38], [i.30]

According to Farley one can approximate the true anomaly (TA) as being reasonably close to the value of the much easier calculated mean anomaly (MA).

$$TA \approx MA = 2 \cdot \pi \cdot \frac{Day_{number}}{DaysPerYear}$$

Equation 70: Mean Anomaly

DaysPerYear is simply the total number of days in a year for the considered planet while according to Palumbo the Day_{number} is the amount of days of the balloon in flight counting from perihelion, which occurs on January 2nd for Earth. If a more accurate solution is preferred one can use the true anomaly equation from Palumbo [t.4] for small orbital eccentricities;

$$TA \approx MA + 2 \cdot e \cdot \sin(MA) + \frac{5}{4} \cdot e^2 \cdot \sin(2 \cdot MA)$$

Equation 71: True Anomaly by Palumbo [t.4]

Solar irradiance flux can then be found by;

$$I_{sun} = \frac{1358}{R_{AU}^2} \cdot \left[1 + 0.5 \cdot \left(\left\{ \frac{1+e}{1-e} \right\} - 1 \right) \cdot \cos(TA) \right]$$

Equation 72: Solar Irradiance Flux

The direct solar irradiance is equal to the product of the irradiance value above the atmosphere and the atmospheric transmittance;

$$I_{sun_h} = I_{sun} \cdot \tau_a$$

Equation 73: Solar Irradiance at Flight Altitude

4.4.2.2. Infrared Environment and Albedo

Next Farley assumes that the same coefficients in the above equations also apply for the following equations for the infra-red. Just as the direct solar power is attenuated for atmosphere thickness, also the cloud infra-red (IR) and the ground IR have to pass through an amount of atmosphere before reaching the balloon. The heat flow from ground surface is written as;

$$q_{IRground} = \varepsilon_{ground} \cdot \sigma_s \cdot T_{ground}^4$$

Equation 74: Infra-Red from Ground

As with visible light the ground infra-red is also attenuated by;

$$\tau_{a_{IR}} = 1.716 - 0.5 \cdot \left(e^{-0.65 \cdot \frac{p_a}{p_0}} + e^{-0.95 \cdot \frac{p_a}{p_0}} \right)$$

Equation 75: Atmosphere IR Transmittance

The actual heat flow from ground IR felt by the aerobot at its flight altitude is;

$$q_{IRground_h} = q_{IRground} \cdot \tau_{a_{IR}}$$

Equation 76: Ground IR at Flight Altitude

When a beam of sunlight enters the atmosphere under an angle, I_{sun} is attenuated on its transmissivity. “Since the solar angle is not directly overhead, the beam of light is smeared out over a larger surface area. Balloon Ascent uses the effect of the solar elevation angle to achieve the instantaneous time varying albedo flux. [a.22]” The albedo flux at the top of the atmosphere follows from;

$$q_{albedo} = a_s \cdot I_{sun} \cdot \sin(ELV)$$

Equation 77: Albedo Heat Flux

4.4.2.3. Cloud Modification

Farley also includes a cloud modification to the thermal model which works with a cloud fraction CF, which is defined as the fraction of sky obscured by clouds. The method is used to find the actual received IR radiation, albedo, and solar flux. It’s an interesting addition to any thermal model. Clouds temper the solar rays when the balloon is under the cloud level and have an influence on the amount of solar heat which is getting in and out the balloon. If the flight altitude is below the cloud layer, the direct solar flux modified for clouds reads;

$$q_{sun} = I_{sun_h} \cdot (1 - CF)$$

Equation 78: Solar Flux below Clouds

If the flight altitude is above the cloud layer the direct solar flux is;

$$q_{sun} = I_{sun_h}$$

The planet’s infrared is attenuated when the aerobot is above the cloud layer, due to obscuration. When the aerobot is below the cloud layer there is no effect due to cloud albedo. Cloud albedo however will only be counted when the aerobot is above the cloud layer [a.22]. The planetary diffuse infrared radiation modified for an aerobot below the cloud layer is;

$$q_{IRplanet} = q_{IRground_h} + CF \cdot q_{IRcloud_h}$$

Equation 79: IR Radiation Below Cloud Layer

Planetary diffuse radiation above the cloud layer;

$$q_{IRplanet} = q_{IRground_h} \cdot (1 - CF) + CF \cdot q_{IRcloud_h}$$

Equation 80: IR Radiation Above Cloud Layer

Planetary albedo is attenuated once when the aerobot is below the cloud level, and twice when the aerobot is above the cloud level. The albedo below a cloud layer is written as;

$$a_s = a_{s_{ground}} \cdot (1 - CF)$$

Equation 81: Albedo Below Cloud Layer

Albedo above the cloud layer, where $a_{s_{ground}}$ is attenuated twice and $a_{s_{cloud}}$ once, is given as;

$$a_s = a_{s_{ground}} \cdot (1 - CF)^2 + a_{s_{cloud}} \cdot CF$$

Equation 82: Albedo Above Cloud Layer

4.4.2.4. Envelope Optical Properties

The envelope optical properties, absorptance α, emittance ε, reflectivity r and transmissivity τ play an important role in heating and cooling the buoyant gas inside the balloon. "These coefficients are usually wavelength dependent. In addition, while ε strictly depends on the surface material or coating of the balloon, absorptivity, transmissivity and reflectivity, depend on both the kind of balloon material and the kind of irradiance [t.4]." r, α and τ are related through;

$$r = 1 - \alpha - \tau$$

Equation 83: Reflectivity

The balloon envelope is not only affected by the planetary environment at the outside, but also by the inner environment and the multiple reflections inside the balloon's envelope. The multiple reflections inside raise the effective interior absorptivity. Therefore Farley makes use of an effective reflectivity r_{eff};

$$r_{eff} = r + r^2 + r^3 + r^4 + r^5 + \ldots$$

Equation 84: Effective Reflectivity

Rewritten by Palumbo [t.4];

$$1 + r_{eff} = \frac{1}{1 - r}$$

Another factor to keep in mind is the View Factor. It is the ratio of balloon surface area that 'sees' the planet surface, divided by the total exposed balloon surface area.

$$ViewFactor = \frac{1 - \cos\left(HalfCone_{angle}\right)}{2}$$

Equation 85: View Factor

Where the Half-cone-angle is a function of flight altitude h;

$$HalfCone_{angle} = \sin^{-1}\left(\frac{R_{planet}}{R_{planet} + h}\right)$$

Equation 86: Half-Cone Angle

From Kirchoff's law of radiation heat transfer, at any specific wavelength the absorptivity is equal to the emissivity while in thermal equilibrium. While Farley's analysis holds for transient conditions, Kirchoff's law is still followed. So in this analysis, $\alpha_{IR} = \varepsilon$.

4.4.2.5. Radiant Heat Loads

After the extensive work above, the thermal model finally touches the subject of heat loads. The above equations and parameters all lead to the various absorbed heat loads which are summed below;

$$Q_{sun} = \alpha \cdot A_{projected} \cdot q_{sun} \cdot \left[1 + \tau \cdot \left(1 + r_{eff}\right)\right]$$

Equation 87: Absorbed Heat of Direct Sunlight

$$Q_{albedo} = \alpha \cdot A_{surf} \cdot q_{albedo} \cdot Viewfactor \cdot \left[1 + \tau \cdot \left(1 + r_{eff}\right)\right]$$

Equation 88: Absorbed Albedo Heat

In the equations above the absorptance α, and transmissivity τ are thermo-optical properties of the balloon's envelope.

$$Q_{IR_{planet}} = \alpha_{IR} \cdot A_{surf} \cdot q_{IR_{planet}} \cdot ViewFactor \cdot \left[1 + \tau_{IR} \cdot \left(1 + r_{eff}\right)\right]$$

Equation 89: Absorbed Heat of Planetary IR

$$Q_{IR_{sky}} = \alpha_{IR} \cdot A_{surf} \cdot q_{IR_{sky}} \cdot \left(1 - ViewFactor\right) \cdot \left[1 + \tau_{IR} \cdot \left(1 + r_{eff}\right)\right]$$

Equation 90: Absorbed IR from the Sky

$$Q_{IR_e} = \sigma \cdot \varepsilon \cdot \alpha_{IR} \cdot A_{surf} \cdot T_e^4 \cdot \left(1 + r_{eff}\right)$$

Equation 91: Absorbed IR from inside the Envelope

$$Q_{IR_{out}} = \alpha \cdot \varepsilon \cdot 2 \cdot A_{surf} \cdot T_e^4$$

Equation 92: Emitted IR Energy of Envelope

4.4.2.6. Convective Heat Loads

On a balloon two types of convection can be distinguished; forced and free convection. Inside the balloon only free convection can take place, as no forced air is circling around. Farley [a.22], describes this through the internal convection heat transfer coefficient for a sphere, in Equation 93.

$$h_{\text{int}} = 0.13 \cdot \kappa_g \cdot \left(\frac{\rho_g^2 \cdot g \cdot \left|T_e - T_g\right| \cdot \Pr_g}{T_g \cdot \mu_a^2}\right)^{1/3}$$

Equation 93: Free Internal Convection Coefficient

At the exterior of the balloon both free and forced convection takes place. In the end Farley uses the greater value of the two, to calculate the external convection. During the ascend of a balloon, forced convection mainly depends on the vertical velocity of the relative movement of air and not so much on differentially warm buoyant air. Therefore Equation 95 is a function of the Reynolds number 'Re'.

$$h_{ext_{free}} = \frac{Nu_a \cdot \kappa_a}{d_b}$$

Equation 94: Free External CvHTC

$$h_{ext_{forced}} = \frac{\kappa_a}{d_b} \cdot \left(2 + 0.41 \cdot \mathrm{Re}^{0.55}\right)$$

Equation 95: Forced External CvHTC

The Nusselt number Nu in Equation 94, formulated in [a.22], and Equation 93 are unfortunately limited to spheres. Further the Prandtl and the Grashof numbers, Pr and Gr respectively, are only defined for helium in [a.22]. These equations are not general enough for BADS which would support 4 planetary atmospheres, 4 different shapes and 6 different gases. In section 4.4.3 convection will therefore be addressed more generally. Next, the heat convection is calculated by Farley;

$$Q_{conv_{ext}} = h_{conv_{ext}} \cdot A_{eff} \cdot \left(T_a - T_e\right)$$

Equation 96: External Heat Convection

$$Q_{conv_{\mathrm{int}}} = h_{conv_{\mathrm{int}}} \cdot A_{eff} \cdot \left(T_e - T_g\right)$$

Equation 97: Internal Heat Convection

4.4.2.7. Temperature Differential Equations

The vertical motion of balloon systems depends highly on the heat transfer to and from the buoyant gas, because the gas temperature and gas density are related to the lift of the aerobot. Taking into account the rate of change of temperature of both gas and envelope will therefore be required in the equations of motion.

The rate of change in temperature of the lifting gas is formulated on the adiabatic expansion response modified with the internal convection interaction with the envelope, presented in Equation 98. Whether from mass loss or purely a change of volume, or a combination of both, the gas will respond according to adiabatic expansion if the heat input $Q_{conv_{\mathrm{int}}}$ is zero.

$$\frac{dT_g}{dt} = \frac{Q_{conv_{\mathrm{int}}}}{c_v \cdot m_g} + \left(\gamma - 1\right) \cdot \frac{T_g}{\rho_g} \cdot \frac{d\rho_g}{dt}$$

Equation 98: Gas Temperature Differential

For the buoyant gas; m_g is the gas mass, γ is the heat capacity ratio, c_v is the specific heat capacity at constant volume, T_g is temperature and ρ_g is density. According to Farley, this can be rewritten expressed in terms of mass 'm_g' and volume 'Vol' change derivatives;

$$\frac{dT_g}{dt} = \frac{Q_{conv_{\mathrm{int}}}}{c_v \cdot m_g} + \left(\gamma - 1\right) \cdot T_g \cdot \left(\frac{dm_g}{dt} \cdot \frac{1}{m_g} - \frac{dVol}{dt} \cdot \frac{1}{Vol} \right)$$

Further, the rate of change in envelope temperature is derived from the simple transient-energy balance equation;

$$\frac{dT_e}{dt} = \frac{\left(Q_{sun} + Q_{albedo} + Q_{IR_{planet}} + Q_{IR_{sky}} + Q_{IR_{sky}} + Q_{conv_{ext}} - Q_{conv_{int}} + Q_{IR_{out}}\right)}{c_e \cdot m_e}$$

Equation 99: Envelope Temperature Differential

Which is the sum of the heat loads Q divided by the envelope's mass m_e and the specific heat of the envelope material c_e.

4.4.3. Modified Thermal Simulation Model

The detailed thermal model of Farley [a.22] is too extensive to implement in BADS at this stage without further knowledge on the subject. At the same time its equations are too restricted on boundary conditions of shape, buoyant gas and planetary atmosphere. Similar restrictions exist for the model of Abe et al. However, this model is a general, compact and user friendly thermal model.
From the models of Abe et al and Farley the equations will be modified, implemented or discarded for a modified thermal model suitable for any planetary atmosphere, and the types of balloon configurations discussed before.

4.4.3.1. Discarded Thermal/Geometric Parameters from Balloon Ascent

Some parameters, equations and subparts of Balloon Ascent will be discarded due to unknown parameters, limitations in buoyant gas and balloon shape, and being too extensive for simulation purposes. These are;

- ELV calculations by Palumbo [t.4]
- Approximated balloon surfaces; A_{surf}, $A_{projected}$, $A_{effective}$ and A_{top} [a.22]
- Prandtl, Grashof, Nusselt numbers limited to helium and spherical balloons
- Convection coefficients, viscosity, conductivity, limited to helium and spherical balloons

The elevation angle is based on Julian date, hour angle, sidereal time. These parameters are used on Earth, and are no standard on any other planet. Discarding the ELV calculation would mean the Air Mass can't be calculated and next the transmissivity of the atmosphere. In future, ELV will therefore be an input parameter with respect to a specific flight time in the simulation. It will indicate the approximate ELV seen from horizon, and will then be uniformly changed through time, with respect to the flight time given and the time left to sunset to simulate the diurnal time.

Farley calculated some approximate geometric properties for ZP natural shaped and SP pumpkin shaped balloons. The thermal model is based on these surfaces for calculating the illuminated projected area of the balloon. The calculated balloon surfaces A_{surf}, $A_{projected}$, $A_{effective}$ and A_{top} are however limited to the above mentioned shapes. Therefore another approach for BADS is chosen to represent these surfaces in the simulation program.
A_{surf} in Balloon Ascent represents the balloon surface when deployed. In early flight however the envelope will not be fully deployed, an excess of envelope surface will be present. Farley includes

this by calculating the excess amount of surface A_{surf1} and combined with A_{surf} an effective visible surface area $A_{effective}$ arises. The simulation program will simplify this by presenting A_{surf} only and discarding $A_{effective}$. A_{surf} will be found from the balloon's design equations in Table 16, by recalculating the surface area step by step during flight, when volume increases. Farley defines A_{top} as 1/4th of the surface area of a sphere. $A_{projected}$ is the illuminated projected area of a balloon which varies with the solar elevation angle. For a spherical shape $A_{top} = A_{projected}$. For simplicity and generalization for different balloon shapes, it is assumed that $A_{top} = A_{projected}$ for all balloon shapes and that A_{top} is actually the top halve of the balloon shape, or $A_{surf}/2$, unaffected by solar elevation angle.

The predetermined equations for Nusselt, Grashof and Prandtl based on spherical shapes and helium gas will not be used for general purpose. They are not suitable when simulating different balloon shapes and using different buoyant gases. Similar rational holds for the convection coefficients, viscosity and conductivity used in Farley's thermal model.

As no in-depth flight results were available on neither Farley's thermal model or Abe et al's model, it is difficult to test and check the effectiveness of these models. Chapter 8 however, will demonstrate what the effect of a change in thermo-optical parameters will do to the simulated results of BADS. Further, chapter 7 will also explore the change of T_{ground} and shape factor F_{bs}. In this way both studies will contribute in analyzing the influence of the above mentioned thermal models and their effectiveness.

4.4.3.2. Useful Thermal Parameters

Farley's equations that are effective for any type of atmosphere and balloon shape are summed below;

- True anomaly; Equation 71
- Solar flux; Equation 72, Equation 73
- View factor; Equation 85
- Half-cone-angle; Equation 86
- Cloud Modification; Equation 78 to Equation 82
- Differential equations; Equation 98, Equation 99

The above equations can be immediately implemented in the modified thermal model. The equations that are valid but need some small modifications or future work before implementation are;

- Air Mass: ELV predetermined input
- Heat Loads: with modified surface areas

The Air Mass equation will be used with a predetermined ELV. In future the ELV will be defined and calculated as explained in the section above, at this stage however the ELV will be a variable input in BADS. The heat load equation will remain the same, with the exception that the surface parameters A_{surf}, $A_{projected}$, $A_{effective}$ will be defined as explained in the previous section.

4.4.3.3. Basic Parameters

A number of equations in thermal modeling can be used for all balloon shapes at any planetary atmosphere. One of them is the Prandtl number. The dimensionless Prandtl number is the ratio of the kinematic viscosity to thermal diffusivity and is only dependent on the fluid and the fluid state.

$$\Pr_g = \frac{\mu_g \cdot c_{p_g}}{\kappa_g}$$

Equation 100: Gas Prandtl Number

$$\Pr_a = \frac{\mu_a \cdot c_{p_a}}{\kappa_a}$$

Equation 101: Atmosphere Prandtl Number

In which μ is the dynamic viscosity found from Sutherlands equation in Equation 36. c_p represents the specific heat capacity at constant pressure and κ is the thermal conductivity.

The dimensionless Grashof number approximates the ratio of the buoyancy and the viscous force acting on the buoyant gas. It is used to determine the boundary between natural and forced convection in Equation 105 and Equation 106. The Grashof number is expressed as;

$$Gr_g = d_b^3 \cdot \rho_g^2 \cdot g \cdot \beta_g \cdot \frac{\left(T_e - T_g\right)}{\mu_g^2}$$

Equation 102: Gas Grashof Number

$$Gr_a = d_b^3 \cdot \rho_a^2 \cdot g \cdot \beta_a \cdot \frac{\left(T_e - T_a\right)}{\mu_a^2}$$

Equation 103: Atmosphere Grashof Number

In which the volumetric expansion coefficient β, for ideal gases, can be written as;

$$\beta_g = \frac{1}{T_g}$$

$$\beta_a = \frac{1}{T_a}$$

4.4.3.4. Free Convection Modeling

As already stated, the Nusselt numbers required in the calculations of the convection coefficients are difficult to calculate and mostly experimentally obtained. It is therefore impossible to model a general Nusselt equation that would fit all shapes in any atmosphere or gas.

$$Nu^T = G \cdot \overline{C}_l \cdot Ra^{1/4}$$

$$Nu_l = \left[Nu_{cond}^n + \left(Nu^T\right)^n \right]^{1/n}$$

$$Nu_t = \overline{C}_t \cdot Ra^{1/3}$$

$$Nu = \left[Nu_l^m + Nu_t^m \right]^{1/m}$$

Equation 104:Free Convection Nusselt Correlation

From the Handbook of Heat Transfer [b.7], Nusselt correlations for free convection on 3D and axisymmetric flows for bodies of "small aspect ratio" were found. The bodies include a sphere and an oblate and prolate spheroid. For these bodies, the correlation equations are formulated in Equation 104 [b.7, p4.25].

Ra is the Rayleigh number, which is the product of the Grashof and the Prandtl number. The length scales on which the Nusselt number Nu and the Rayleigh number Ra are based, and the values of all constants, are provided in appendix C. The basis for these relations is discussed in Hassani and Hollands [a.30]. When data is listed as 'none available' (NA), it means that the correlation is based entirely on an approximate method. "Values of n = 1.07 recommended by Hassani and Hollands, and m = 10 are used for these cases. When data is available, the values of G have been adjusted to provide a best fit of the data. $\overline{C}_t$ was never adjusted, mainly because so few of the available data fall in the turbulent regime." The second table in appendix C provides references to all data used, as well as the range of Ra and Pr covered by the data. The Nusselt number in the Ra --> 0 limit is the conduction Nusselt number Nu_{COND}. The Rayleigh number range for which the Nusselt numbers where found, are limited. Despite this, it is the most useful data on free convection for multiple 3D bodies found to date.

The thermal model will use the free convection Nusselt correlations from Equation 104, combined with the constants of appendix C, to calculate the Nusselt number for free convection on a sphere, oblate or prolate spheroid. At intermediate Prandtl numbers and intermediate fineness ratios data is inter- and extrapolated to find the approximate Nusselt number. Primarily the obtained data should be used for a flow around the balloon. The same equation however will be assumed valid, for the buoyant gas inside the balloon, to be able to calculate the Nusselt number for the gas.
The thermal model will also include the equation already available from Farley and Abe et al, limited to spheres, for comparison.

4.4.3.5. Forced Convection Modeling

Forced convection only takes place outside the balloon and is therefore not of importance to the buoyant gas inside the balloon. Similar correlations as those of Hassani and Hollands [a.30] for the free convection model, would have been useful. Unfortunately, after contacting the writer of chapter 4 of the *Handbook of Heat Transfer* [b.7], no such correlations exist for forced convection. Experimental data does exist on a limited scale, but again only for specific circumstances and shapes. No forced convection model therefore is added to the modified thermal model, with the exception of the equation of Farley [a.22] for spheres. This means that the thermal model, if used, should only be activated when the aerobot flies in an environment where the following holds;

$$\text{Free Convection: } \frac{Gr}{\mathrm{Re}^2} >= 1$$

Equation 105: Free Convection Boundary

While forced convection will remain unexplored for now;

$$\text{Forced Convection: } \frac{Gr}{\mathrm{Re}^2} < 1$$

Equation 106: Forced Convection Boundary

4.4.3.6. *Optical Properties of Coatings, Envelope and Buoyant Gas*

The typical optical properties of the balloon envelope are absorptivity α, transmissivity τ, emissivity ε and reflectance r. These properties are determined by the fabric or coating manufacturers. For simulation purposes the assumption is made that any fabric will be coated for extra protection. The standard properties of fabric strength, density and elasticity will hold, but every optical property will be based on the properties of the coatings.

Main reason behind this assumption is the fact that a huge NASA database [a.29] on 'Solar Absorptance and Thermal Emittance' factors of numerous common spacecraft thermal-control coatings can be used.

The equations for optical properties from Abe et al are used for convenience and modified to the needs for simulation purposes. From Kirchoff's law $\alpha_{IR} = \varepsilon_{IR}$ holds and α_e and ε_{IR} are known from [a.29]. If infrared transmissivity is set to an input parameter the infrared reflectivity follows from a similar form of Equation 83 for the infrared.

$$r_{IR_e} = 1 - \alpha_{IR_e} - \tau_{IR_e}$$

Equation 107: Envelope Infrared Reflectivity

Next, also the transmissivity of the envelope/coating is given as an input parameter to calculate the reflectivity with the assumption that $\varepsilon = \varepsilon_{IR}$. When using Equation 59 to Equation 63 the effective values for absorptivity and emissivity can be calculated.

Similar approach holds for the optical properties of the buoyant gas. The optical properties of gases however are difficult to find in literature. If such results are required tests will have to be done. Therefore currently the assumption is made for BADS so that absorptivity, emissivity and transmissivity are set to 0, with the secondary option to simulate it as a user input parameter in the future.

4.4.4. Thermal Model Conclusions

From the above explained thermal models and parameters a set of equations will be transferred to the simulation program of chapter 5. None of the above mentioned thermal models will be incorporated as a unique and complete model though.

The heat balance equations and heat transfer equations for a balloon from Abe et al will be taken as the standard equations for all of the above models. These equations of Abe et al are very similar to those from Farley and can be expected to be complete.

Convection models and specifically Nusselt numbers are the one thing no thermal model ever agrees on when incorporating different shapes, envelope materials and buoyant gases. The user will therefore be able to select two types of Nusselt calibration methods for Nusselt numbers and convection coefficients. These are; Nusselt numbers of Abe et al and the equations of Hassani and Hollands [a.30].

5. Buoyant Aerobot Design and Simulation Program

The previous chapter described the modeling of the planetary atmospheres, the balloon designs, and the thermal models. These equations and models will now be used throughout a Matlab based simulation program for buoyant aerobot design and flight, named BADS. The chapter will present the program's input and output parameters, databases, set-up, assumptions and extra features.

5.1. Simulation Program Set-Up

The simulation tool was developed in the mathematical platform Matlab. The tool can analyze the performance of a balloon flight in multiple atmospheres, predict the 3D position of the aerobot, predict the geometrical variations in envelope surface and volume during flight along with envelope and lifting gas temperatures.

Figure 42 illustrates the set-up of BADS and shows how each module is interrelated. Each module has been assigned a color code which will be used throughout this chapter. The colors will indicate where each parameter is situated in the program's main level when the detailed charts per module are discussed.

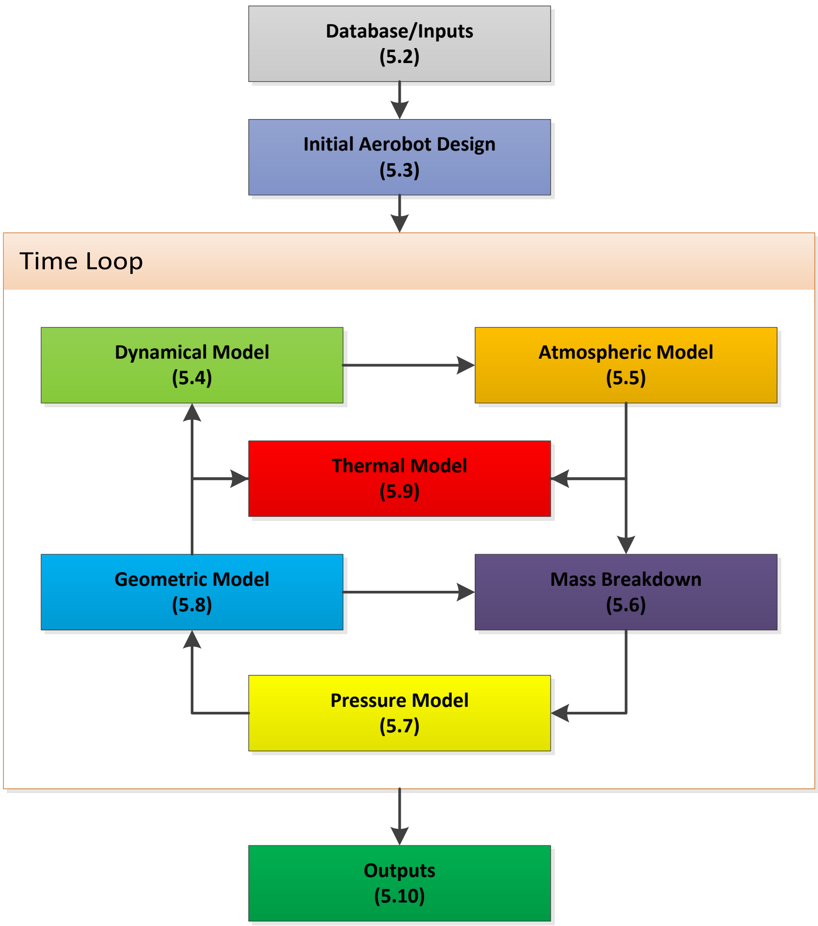

Figure 42: Simulation Program Main Level

The foundation of the program contains a primary database and a user input section that is used in support of the initial aerobot design. The database contains predetermined general planetary orbit and atmosphere data, different buoyant gases and balloon parameters such as material and coating information. This database is used to limit the user input somewhat, nevertheless the user input section is still filled with a lot of variables. The selected data and input information go into the initial aerobot design phase.

The data that follows from the aerobot design is then send through a time loop into six main models to analyze the aerobot's flight and show the impact the flight has on the aerobot and vice versa. The simulation results in a number of predetermined output parameters.

Table 23: Correlation Between Design Equations and Simulation Modules

Module	Section Chapter 4	Section Chapter 5
Initial Aerobot Design	4.2.1	5.3
Dynamical Model	4.2	5.4
Atmospheric Model	4.1	5.5
Mass Breakdown	4.2.1	5.6
Pressure Model	/	5.7
Geometric Model	4.3.1	5.8
Thermal Model	4.4	0

Each module will be described in detail in the coming sections, as indicated in Figure 42, but were already theoretically described in chapter 4. Where each set of equations will be used is summarized in Table 23.

5.2. Input Parameters and Databases

This section will list the predetermined input parameters and the variable parameters that the user is able to alter. In addition it will highlight the assumptions made throughout the simulation tool.

5.2.1. Parameter Database

The information currently in the database includes planetary data and typical balloon data. The data has been found in articles, on the internet and in books. The data is used as predetermined data of which the user can select the data suitable for the preferred design.

5.2.1.1. Planetary Data

The planetary data includes two main sets of parameters for Venus, Earth, Mars and Titan, namely the planet and atmosphere sets, illustrated in Table 24. Each parameter is shown per planet, followed by its unit, the reference of where the data was obtained and an equation number in which the parameter is used.

The planetary albedo is considered a constant throughout the simulation for each planet or moon. The same holds for the gravity of the planets, though gravity differs with altitude it is assumed to be a constant throughout the aerobot's flight, as mentioned in section 4.1.5. Specific heats of buoyant gases and atmospheres have been assumed constant, with the exception of those of Earth's atmosphere. A lack of data for different temperature ranges is the main cause for this assumption.

A constant value for diurnal temperature change was found from literature for every planet and moon. These values can differ with season and are only an approximation. They are assumed to be a good estimate to simulate the diurnal effect though. The planet's rotation speed, to be used in Equation 116 is a constant value as well as; the planet's length of year, length of day and orbit parameters.

Table 24: Planeteray Database

	Earth	Mars	Venus	Titan	Unit	Ref.	Equation
Planets							
Rotation Speed Θ	7.27E^{-05}	7.04E^{-05}	6.23E^{-07}	4.56E^{-06}	[rad/s]	[i.1,2,3,30]	Equation 116
Albedo a_s	0.367	0.17	0.67	0.22	[/]	[i.1,2,3,30]	Equation 77
Gravitational Acceleration g	9.80	3.71	8.87	1.35	[m/s^2]	[i.1,2,3,30]	Equation 15
Astronomical Unit	1	1.5236	0.723	9.54	[AU]	[i.1,2,3,30]	Equation 72
Orbit Eccentricity e	0.0167	0.0934	0.0068	0.0288	[/]	[i.1,2,3,30]	Equation 72
Length of year	365.26	686.98	224.68	10759	[days]	[i.1,2,3,30]	Equation 70
Length of day	24	24.6	2802	382.68	[hrs]	[i.1,2,3,30]	Equation 116
Diurnal Temperature ΔT	10	68	0	6	[K]	[i.1,2,3,30]	Equation 116
Atmospheres							
Specific Heat Capacity c_p	1005	846	846	1039	[J/kgK]	[b.5], [b.8]	Equation 100
Specific Heat Capacity c_v	718	657	657	743	[J/kgK]	[b.5], [b.8]	Equation 98
Molar Mass M	28.97	43.35	44.01	28.60	[g/mol]	[b.5], [b.8]	Equation 23
Sutherland's C	120	240	240	111	[K]	[i.29]	Equation 36
Sutherland's Ref. μ_0	18.27	14.8	14.8	17.81	[µPa s]	[i.29]	Equation 36
Sutherland's Ref. T_0	291.15	293.15	293.15	300.55	[K]	[i.29]	Equation 36

The atmosphere parameters in Table 24 differ with height or vary with atmospheric thermal and compositional changes. For simplicity the assumption is made though that these parameters stay constant during flight. One exception is made for the thermal conductivity, which is modeled for Earth and all buoyant gases in Table 25. The atmosphere parameters for Venus, Mars and Titan shall use reference values from their main atmospheric constituent, which are CO_2 and N_2 respectively.

Table 25: Thermal Conductivity of Buoyant Gases [b.8, p6-175]

T [K]	H_2 [W/m K]	He [W/m K]	CH_4 [W/m K]	CO_2 [W/m K]	NH_3 [W/m K]	N_2 [W/m K]	Earth's Air [W/m K]
100	68.2E^{-3}	74.7E^{-3}	10.4E^{-3}	3.35E^{-3}	9.08E^{-3}	9.4E^{-3}	9.4E^{-3}
200	132.8E^{-3}	118.3E^{-3}	21.8E^{-3}	9.6E^{-3}	16.11E^{-3}	18.3E^{-3}	18.4E^{-3}
300	186.6E^{-3}	155.7E^{-3}	34.4E^{-3}	16.8E^{-3}	16.8E^{-3}	26.0E^{-3}	26.2E^{-3}
400	230.9E^{-3}	189.6E^{-3}	50.0E^{-3}	25.2E^{-3}	37.2E^{-3}	32.8E^{-3}	33.3E^{-3}
500	270.9E^{-3}	221.4E^{-3}	68.4E^{-3}	33.5E^{-3}	53.1E^{-3}	39.0E^{-3}	39.7E^{-3}
600	309.1E^{-3}	251.6E^{-3}	88.6E^{-3}	41.6E^{-3}	68.6E^{-3}	44.8E^{-3}	45.7E^{-3}

Next to the parameters above, the planetary database includes the listed values for the atmospheric pressure, temperature and density varying with altitude. These values are based on the selected atmospheric models of chapter 4;

- Earth: US Standard Atmosphere, 1976, found from Schlatter [a.23]
- Venus: Kerzhanovich 2000, found from Colozza [a.26]
- Mars: Mars Standard Atmosphere, found from Colozza [a.26]
- Titan: HASI in-situ measurements, Yelle and Strobel et al [a.28] and [d.1]

5.2.1.2. Balloon and Buoyant Gas Data

For the 6 available buoyant gases (He, H_2, CH_4, CO_2, NH_3, N_2) discussed in chapter 4, the database contains the following parameters;

- Gas specific heat at constant pressure of Table 20
- Gas specific heat at constant volume of Table 20
- Gas thermal conductivity of Table 25
- Gas molar mass of Table 20
- Gas Sutherland's constant and reference viscosity and temperature of Table 14

The Sutherland constant, reference temperature and reference viscosity are constant values. These values have been mentioned before and are listed in Table 14. The specific heats and thermal conductivities change with temperature. The specific heats however are assumed to be constant for each gas. Data on these values were listed next to the molar mass of each buoyant gas in Table 20.
Data on thermal conductivity for the different gases is available from the Handbook of Chemistry and Physics [b.8, p6-175] and was already listed in Table 25. Some values were extrapolated however for lower temperature ranges. As was mentioned in section 4.1.5 currently no use is made for gas mixtures, either in buoyant gases or atmospheres, with the exception of Earth's atmosphere composition. Therefore Mars, Venus and Titan atmosphere properties are based on those of the main constituent gas in the atmosphere.

Next to the buoyant gas parameters, the database also contains a number of balloon envelope materials with their specific properties as well as the Nusselt shape constants;

- Nusselt Correlations [b.7]
- Lamcotec Envelope data [d.2]
- Thermo-Optical Coating Data [a.29]

From the Handbook of Heat Transfer [b.7] the Nusselt correlations for free convection on 3D and axisymmetric flows for bodies of "small aspect ratio", discussed in chapter 4, were obtained. The constants for Equation 104 are available for spheres, oblate and prolate spheroids and are listed in appendix C. Next, 14 different materials of Lamcotec [d.2] have been implemented into BADS. The properties of each material include; areal density, breaking strength and maximum elongation. The values of these parameters can be found in Table 18. One slot in this material matrix has been reserved for a user defined material input. The database ends with the solar absorptance and thermal emittance factors of 71 common thermal spacecraft coatings [a.29] which are listed in appendix D.

5.2.2. Input Data

The input data in the simulation tool can be divided into two data sets. The input that can be altered by the user and the predetermined input. The first group, the changeable parameters, are already set to default values into the program but can be altered by the user to specify the aerobot's design and mission. The second data set, the predetermined data, contains all parameters that are assumed or can't be improved, and additionally it contains the data from the available databases discussed above.

5.2.2.1. Preliminary Settings

The variable input parameters have some preliminary settings which the user is asked to evaluate at the start of the simulation. If these settings are not according to the user's wishes, than the user is able to change them. The preliminary settings are as follows;

Table 26: Preliminary Settings with Default Values

Parameter	**Default Value**	**Unit**
Initial Conditions at time t_0=0;		
▪ Initial Position	(x, y, z) = (0,0,0)	[m]
▪ Initial Flight Speed	(V_x, V_y, V_z) = (0,0,0)	[m/s]
▪ Initial/Constant Wind Speed	(Vw_x, Vw_y, Vw_z) = (0,0,0	[m/s]
Powered Flight		
▪ Propelled Speed	(Vp_x, Vp_y, Vp_z) = (0,0,0)	[m/s]
Basic Flight Set-Up		
▪ Design Flight Altitude	h = 5000	[m]
▪ Total Mass	m_t = 10	[kg]
Balloon Settings		
▪ Selected Shape	Sphere	
• Fineness Ratio	f=1	[/]
▪ C_D Selection	Constant	
• C_D Value	0.55	[/]
▪ Balloon Pressure type	Zero-Pressure	
• Parachute Descend	No	
▪ Free Lift Percentage	10	[%]
Ballast, Gas and Envelope Settings		
▪ Permeability	No	
▪ Ballast Drops	No	
• Manual		
- Ballast	0.2	[kg]
- Altitude %	60	[%]
• Automatic		
- Ballast	0	[kg]
- Rate	0	[kg/min]
- Time	0	[s]
▪ Buoyant Gas	Helium	
▪ Envelope Selection	Predetermined by User	
▪ Coating Selection	Brilliant Aluminum Paint	
Temperature Model	No Model	
Planetary Settings		
▪ Planet Selection	Earth	
▪ Day of Launch	1st of January	
▪ Diurnal Cycle	No	
▪ Cloud Fraction	No	[0-1]
Time Settings		
▪ Total Simulation Time	t = 2	[hrs]
▪ Time Step	Δt = 1	[s]

For the initial settings at t_0 the user can basically fill in any value within reason. Speeds above 5m/s are not preferred for instance. If a powered flight is selected, also the propelled speed can be initialized. The basic flight set-up contains the design altitude and the total mass, from which basically the entire mass budget is calculated.

Next the user will have to choose the balloon settings. The user can select three types of balloon shapes; sphere, oblate or prolate. The fineness ratio is limited from 0.1 up to 10 and needs to be specified for the oblate and prolate shapes. Default shape is the sphere with a fineness ratio of 1. There are also three types of pressure levels in a balloon of which the user can choose from; the zero-pressure, the super-pressure and the over-pressurized-zero-pressure. If a ZP or OZP is selected, the user will be asked if a parachute descend is required or not. Next two aerodynamic parameters can be specified, namely; the free lift and the drag coefficient.

Ballasting is another extensive feature which can be selected by the program user. There are three options available; no ballasting, manual or automatic ballasting. If ballasting is selected however it is recommended to keep the ballast drop rate low, even for huge balloons. A buoyant gas balloon is sensitive to any mass difference. The ascend speed will rise quickly. The sudden rise in ascend speed, if too high, also triggers an instability effect in the simulation.
Next the user can choose a buoyant gas from the six gases available; H_2, He, CH_4, CO_2, NH_3, N_2. If the user chooses a zero-pressure balloon with the right buoyant gas, namely the gas that corresponds to the composition of the atmosphere, a fourth type of balloon can be simulated, namely an ambient balloon, or Montgolfier. The default gas used in the simulation will be helium.
The envelope and coating selection has a big effect on envelope mass. Choose the right material from the database for the right mission. If not available, the input parameters for any type of material can be added in the program database.

Selecting a thermal model is possible; three models are available. However, forced convection is either neglected or only available for a sphere. The option to ignore the thermal influence is the standard input, it sets the temperature of gas and envelope equal to that of the atmosphere.

For planetary settings the standard planet is Earth and the aerobot launch date is 1st of January. Both can be modified by the user. Another option is the use of a diurnal cycle. This diurnal cycle is based simply on the planet's rotational speed to simulate a general decay in temperature over one day's time. It does not keep track of the solar elevation angle or any other positioning system at this time. It does however give an impression of what a daily temperature drop does to a buoyant aerobot's flight altitude over time.
The last planetary feature is the planet's cloud fraction. A cloud fraction, between 0 and 1, can be entered together with the altitude at which the clouds reside.

Finally, the total simulation time and the time step can be selected. Time steps should not be set larger than 1s or go below 0.1s. The mathematical method used in the simulation has an instability effect when time steps outside the proposed range are being used.

5.2.2.2. *Predetermined Input Data*

A number of parameters are assumed for simplicity or due to lack of data on the subject. The following parameters are assumed to be constant or fixed throughout the simulation;

Table 27: Predetermined Fixed Input Data

Parameter	Value	Unit	Ref.	Equation
Balloon Shape Factor	$F_{bs} = 0.5$	[/]	[b.5]	Equation 57
Thickness of Envelope Fabric	$d = 0.1$	[mm]	Assumption	Equation 55
Specific Heat of Envelope	$c_e = 1700$	[J/kgK]	Assumption	Equation 66
Parachute Drag Coefficient	$C_{Dparachute} = 1.75$	[/]	[i.4]	Equation 129
Added Mass Coefficient	$C_{virtual} = 0.37$	[/]	[t.4]	Equation 26
Thrust Coefficient	$C_T = 0.5$	[/]	Assumption	Equation 42
Permeability Factor	$\lambda = 2E^{-19}$	[m^2]	[t.3]	Equation 56
Electric Propulsion Efficiency	$\eta_t = 0.637$	[%]	[a.33]	Equation 46
Time of sun rise	$t_{sunup} = 8.00$	[hrs]	Assumption	Equation 116
Infrared Transmissivity Envelope/Coating	$\tau_{eIR} = 0$	[/]	Assumption	Equation 62
Transmissivity Envelope/Coating	$\tau_e = 0$	[/]	Assumption	Equation 59
Absorptivity of Buoyant Gas	$\alpha_g = 0$	[/]	Assumption	Equation 59
Emissivity of Buoyant Gas	$\varepsilon_g = 0$	[/]	Assumption	Equation 62

The shape factor is set to the value of a sphere, which is 0.5 [b.5]. The sun rise is set at 08.00hrs, which will start any diurnal cycle at that time. The specific heat of the envelope is set to 1700, and the thickness of all materials is set to 0.1mm, due to a lack of data on these subjects. Similar reasoning holds for the optical parameters such as transmissivity, absorptivity and emissivity. All parameters can be reprogrammed in the program's database if necessary.

The value for the parachute drag coefficient and added mass coefficient have been based on standard literature values. While the permeability factor is chosen, from Ha's [t.3] work on gas leakage rates, as a suitable factor to simulate the permeability through Darcy's law.

The electric propulsion efficiency is based on the work of Colozza [a.33], discussed in section 4.2.5. The possibilities of the propulsion system are limited in BADS and therefore the efficiencies and the thrust coefficient are only used as an approximation. In the future this subsystem will be more comprehensive and the correlated parameters changed to variable inputs.

As mentioned before a number of input parameters are not set as constants but are modeled to change with time, temperature or altitude. These are;

- Atmospheric viscosity for all planets and buoyant gases
- Atmospheric conductivity for all planets and buoyant gases
- Earth's atmospheric specific heats

These parameters are modeled to create a more accurate simulation of the environment, and because data was available. The lack of data, is the main reason behind parameter assumptions and fixing of values. Future improvements to the simulation tool may change this.

In the near future it will be possible for the program user to predetermine all available parameters in the input screen. Including the ones that are currently fixed.

5.3. Initial Simulated Aerobot Design

The initial aerobot design makes use of the input parameters given by the user, illustrated in grey in Figure 43. Main parameters to model the aerobot are its design altitude and the total weight. Sub-parameters used throughout the calculations are; envelope material, buoyant gas, fineness ratio, free lift percentage, etc. The initial aerobot design also makes use of two other models to calculate the design parameters. These are the atmospheric model and the geometric model, which are described in section 5.5 and 5.8 respectively.

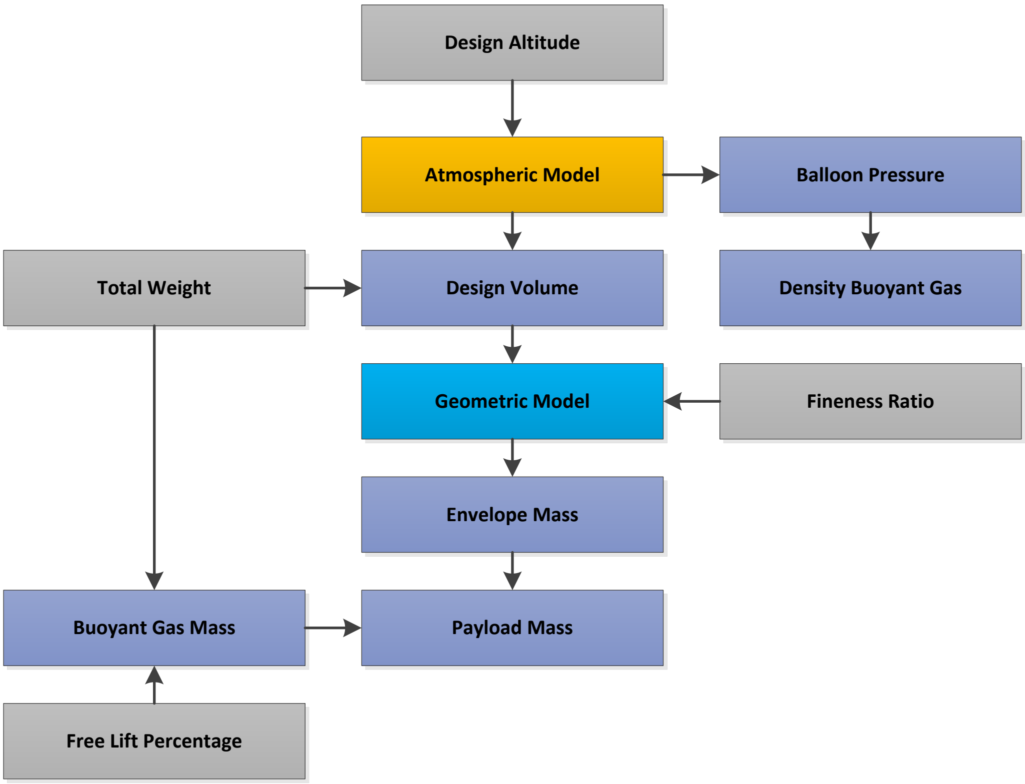

Figure 43: Initial Aerobot Design

The design calculations start from the design float altitude, which is defined by the user. The value is used in the atmosphere model to find the air pressure, temperature and density at the design altitude. The assumption is made, that when the balloon is in equilibrium and floating at its design altitude, the gas temperature inside the balloon, is equal to the outside atmosphere temperature. With this assumption only the balloon pressure has to be given to calculate the density of the buoyant gas. For a zero-pressure and the ambient balloon the gas pressure equals the atmospheric pressure. For a super-pressure and OZP the inside gas pressure equals the atmosphere pressure plus an over-pressure, which has to be predefined by the user. With the equation of state for an ideal gas, the gas density can then be calculated. The volume of the balloon at the design altitude is found from the equilibrium condition at that height. The ascend speed at float altitude is zero, which means lift equals weight in vertical direction. Setting Equation 25 equal to Equation 41 and rewriting it gives the design volume in Equation 108;

$$m_{gross} \cdot g_{planet} = g_{planet} \cdot \left(\frac{M_{atm} \cdot p_{atm}}{R_c \cdot T_{atm}} - \frac{M_{gas} \cdot p_{gas}}{R_c \cdot T_{gas}} \right) \cdot Vol_{balloon}$$

$$m_{gross} \cdot g_{planet} = g_{planet} \cdot \left(\rho_{atm} - \rho_{gas} \right) \cdot Vol_{balloon}$$

$$m_{tot} - m_{gas} = \rho_a \cdot Vol_{balloon} - m_{gas}$$

$$Vol_{balloon} = \frac{m_{tot}}{\rho_{atm}}$$

Equation 108: Balloon Design Volume

With the volume and the gas density at the float altitude known, the buoyant gas mass required to float at the design altitude can be found from Equation 24. The amount of gas mass required to lift-off from ground however requires an additional amount of gas. The initial gas mass is calculated from the design volume at a higher altitude than ground. This means that the gas mass is sufficient to let the balloon float in the atmosphere near the design altitude but not sufficient to lift-off from ground, due to a higher atmosphere density at ground. Therefore an extra percentage of buoyant gas is taken into account, which will create a free lift portion. The free lift is an input parameter which the user can choose, but is mostly around 10% for large balloons. To calculate the total gas mass with a free lift portion an equation from Palumbo [t.4] is used;

$$m_{gas_0} = \frac{m_{gross} \cdot \left(\frac{FreeLift}{100} + 1 \right)}{\frac{M_a}{M_g} - 1}$$

Equation 109: Buoyant Gas Mass w.r.t. Free Lift [t.4]

To use this equation in the initial simulated aerobot design it has to be rewritten in a form based on the total aerobot mass, which is the only input parameter in BADS from which every other mass is calculated from. This gives;

$$m_{gas_0} = \frac{m_{tot} \cdot \left(\frac{FreeLift}{100} + 1 \right)}{\left(\frac{M_a}{M_g} \right) + \left(\frac{FreeLift}{100} \right)}$$

Equation 110: Buoyant Gas Mass w.r.t. Free Lift and Total Mass

The next step in the mass budget is the calculation of the envelope mass. The maximum design volume and the fineness ratio are inputs in the geometric model to calculate the envelope surface through the equation of Table 16. The envelope mass is then determined from Equation 22 and the density of the envelope material. The payload mass is the mass that is left if all other sub-masses are subtracted from the total mass.

$$m_{pay} = m_{tot} - m_{envelope} - m_{gas_0}$$

Equation 111: Design Payload Mass

If no mass budget is left to actually take payload onboard, the buoyant gas can be changed into a lighter gas, or the envelope material should be changed to a lighter fabric. It can be an iterative process to find a correct balance between envelope mass, gas mass and payload mass.

5.4. Dynamic Simulation Model

The dynamical model is the most compartmented of the six core models. The reason behind it is the interrelation between the dynamic flight parameters and all other design and atmospheric parameters. The model computes the trajectory from the forces acting on the aerobot. Forces which are sensitive to all atmospheric and design parameters and therefore entwined into the dynamical model. The model continuously recalculates the flight parameters over time and exchanges them with the other program modules again and again.

In this subchapter the mathematical problems encountered during programming are addressed. Further the entire dynamical simulation model, illustrated in green in Figure 44, is described step by step. The atmospheric, thermal, pressure and geometrical models which are entwined in the dynamic model will be described separately in the next subchapters.

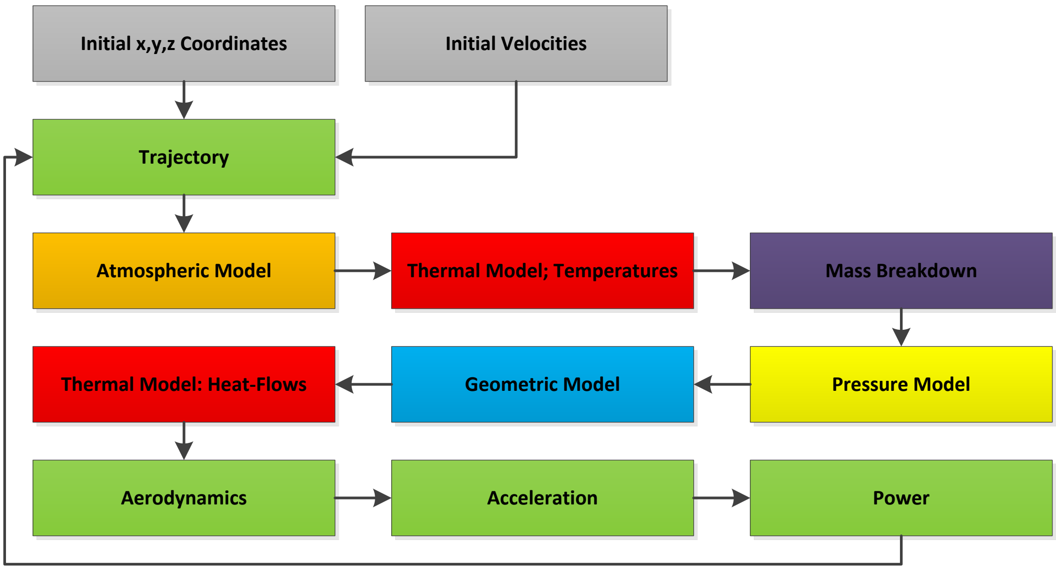

Figure 44: Dynamic Simulation Model

5.4.1. Mathematical Methods

The mathematical method used for the simulation is the Euler method. In mathematics and computational science, the Euler method is a first-order numerical procedure for solving ordinary differential equations (ODE) with a given initial value. It is the most basic explicit method for numerical integration of ordinary differential equations. The Euler method is a first-order method, which means that the error per step is proportional to the square of the step size, and the error at a given time is proportional to the step size [i.40].

Other methods like the midpoint method, Runge-Kutta method, Runge–Kutta–Fehlberg method and the Newton–Raphson method are known to be more accurate compared to the Euler method. Especially when the size of the time steps increases, these higher order methods have lower errors. The reason behind the choice of Euler above the other methods lies in the stability of the mathematical methods when used in the simulation tool.

Initially the mathematical method used in the simulation tool was Euler, but the time steps that had to be used were restricting the total simulation time and the accuracy was limited when larger time steps were used. The next methods that were used were the midpoint method and the Runge-Kutta method. A slight increase in time step size was achieved with these methods, but soon simulation results became unstable again. According to literature for some differential equations the standard methods such as the Euler method, explicit Runge–Kutta methods, or multistep methods exhibit instability in the solutions. “When integrating a differential equation numerically, one would expect the requisite step size to be relatively small in a region where the solution curve displays much variation and to be relatively large where the solution curve straightens out to approach a line with slope nearly zero. For some problems this is not the case. Sometimes the step size is forced down to an unacceptably small level in a region where the solution curve is very smooth [i.39].” The phenomenon being exhibited here is known as stiffness.

In mathematics, a stiff equation is a differential equation for which certain numerical methods for solving the equation are numerically unstable, unless the step size is taken to be extremely small. It has proven difficult to formulate a precise definition of stiffness, but the main idea is that the equation includes some terms that can lead to rapid variation in the solution [i.39]. This is indeed the case for a buoyant aerobot simulation tool in which initial ascend speeds can be high, and where sudden ballasting can induce inappropriate high peaks in velocity. Also thermal modeling of gas inside a balloon can create a high degree of variation and therefore instability.

There are methods that work well in stiff problems and others that don’t work at all. The fact that both types of mathematical methods were analyzed, and both turned to be unstable in the end, would conclude that the flight of a buoyant aerobot in a planetary atmosphere, is not a completely stiff problem, but neither is it a non-stiff problem. To tackle this problem the choice was made to simulate the buoyant aerobot’s flight with a simple Euler method again, while using a very small time step. It is not as efficient as any other method, but using a small enough time step at least keeps the simulation rather stable, which isn’t always the case for any other method. Neither Abe et al [b.5] or Farley [a.22] describe their mathematical method used to simulate a buoyant aerobot flight. No comparison on this end was therefore possible.

5.4.2. Simulated Trajectory

With the initial coordinates and the initial velocities as an input, the trajectory equations can be modeled with Euler. These equations calculate the travelled distance of the aerobot and the velocity at any time t. These parameters, especially the vertical component, will be required in the atmospheric model afterwards to recalculate the atmospheric parameters for each altitude measurement.

$$S_i = S_{i-1} + \Delta t \cdot V_{i-1} + 0.5 \cdot a_{i-1} \cdot \Delta t^2$$

Equation 112: Aerobot Distance Travelled

$$V_i = V_{i-1} - V_{w_{i-1}} + \Delta t \cdot a_{i-1}$$

Equation 113: Aerobot Velocity

'S' is the distance travelled at time t. 'V' is the aerobot 's relative velocity and V_w is the wind velocity at time t. 'a' is the acceleration at time t. Δt is the time frame, or time step, in which the displacement takes place. The trajectory equations stay the same for x, y and z-directions.

Some boundary settings have been added. For instance, if the aerobot descends to the ground and reaches sea level, or an altitude of 0m, the velocity components in all three directions are set to 0. As if the aerobot would come to a complete stop. If for some reason the simulation tool would calculate altitudes below zero, the altitude will be set to zero automatically. The simulation tool at this moment does not keep into account the planet's topography such as valleys below sea level.

5.4.3. Simulated Gas Composition

The composition of the gas will be important at any moment in time. The gas density, pressure and temperature are key parameters for the balloon volume. In this module the gas pressure and gas density are recalculated per time step. For zero-pressure balloons the gas pressure always equals the atmospheric pressure. This holds until the maximum balloon volume is reached. At that time active venting will be required to keep the gas pressure equal to the atmospheric pressure.

Super-pressure and OZP balloons are treated different from zero-pressure balloons during simulation. Both are seen as zero-pressure balloons until the maximum balloon volume is reached. From then on pressure will start to build up and they start to act as over- or super-pressurized balloons. The over-pressure is calculated from the maximum design volume, the gas composition and the gas mass inside the balloon which is constant in an enclosed volume;

$$\Delta p = \frac{m_{gas} \cdot R_c \cdot T_{gas}}{M_{gas} \cdot Vol_{\max}} - p_a$$

Equation 114: Over-Pressure

The first term on the right side of the equation is the gas pressure. For all balloon pressure types the gas density follows from the equation of state in Equation 23.

5.4.4. Simulated Aerodynamics

The aerodynamics module contains the aerodynamic forces on the aerobot; lift, drag, thrust and weight. Also the variable drag coefficient, discussed in 6.3.2, is calculated here if not set constant by the user. These parameters are vital for the equations of motion. The required equations have been mentioned in chapter 4.2. The equations make use of the recalculated parameters of the modules above, such as; velocity, volume, atmospheric density, cross sectional areas and total mass.

5.4.5. Simulated Acceleration

The acceleration of the aerobot can be calculated from the equations of motion. From the remaining lift force in Equation 27 for the vertical motion, and from similar equations for the x and y directions, acceleration is defined as;

$$a_z = \frac{R_z}{m_{virtual}}$$

Equation 115: Aerobot Acceleration

The boundary conditions for the acceleration are similar to those of the velocity. When ground is reached the acceleration is set to zero, to simulate a crash or landing. Maximum acceleration for an unpowered descend is limited to the planet's gravitational acceleration.

5.4.6. Simulated Power Budget

The electric power budget currently only computes the total electric power required for a propeller thrust force with predetermined propulsion efficiencies. The power module uses the total efficiency of Table 15 as a reference. The power budget currently only calculates the required power to overcome total drag.

The program user is able to include a constant propelled speed when a powered simulation is selected at the start of the simulation. The propelled force will counteract the wind force if present and pursue a powered flight in a predetermined direction.

5.5. Atmospheric Simulation Model

The atmosphere models for Earth, Mars, Venus and Titan have been discussed in detail in chapter 4. As a reminder, the following models were included;

- Earth: US Standard Atmosphere, 1976, found from Schlatter [a.23]
- Venus: Kerzhanovich 2000, found from Colozza [a.26]
- Mars: Mars Standard Atmosphere, found from Colozza [a.26]
- Titan: HASI in-situ measurements, Yelle and Strobel et al [a.28] and [d.1]

From the planetary database scientific data on atmospheric pressure, temperature and density varying with altitude can be applied for simulating the atmospheric environment. As these values are listed for intermittent altitudes, data will have to be interpolated when the aerobot flies through the atmosphere. A cubic interpolation is used for this in Matlab.

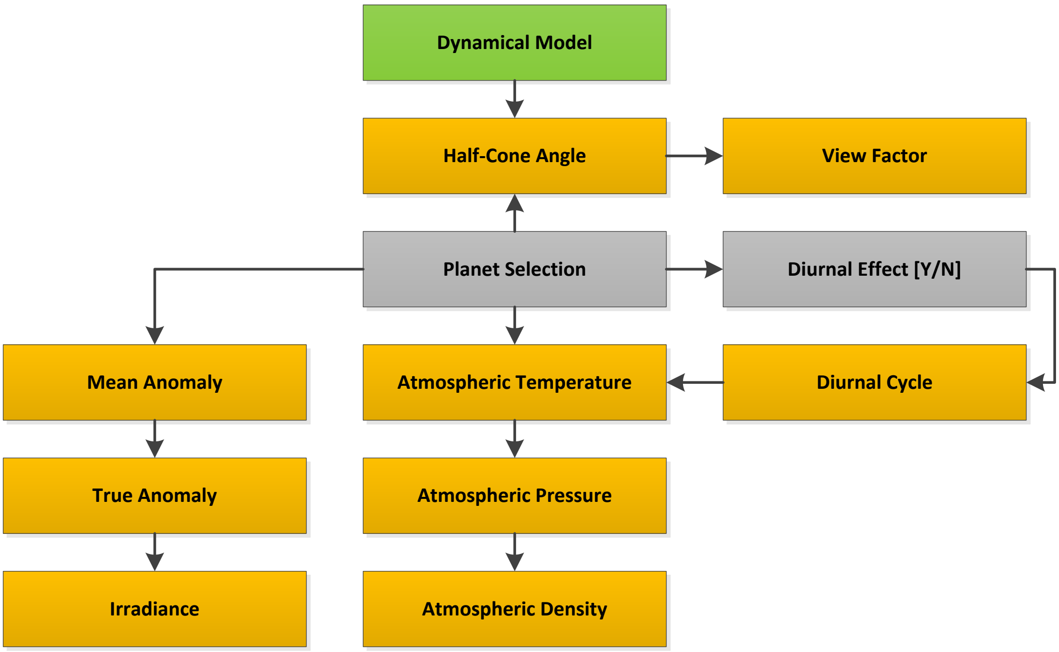

Figure 45: Atmospheric Simulation Model

When the use of a diurnal cycle is selected by the user, the following diurnal temperature is added to the atmospheric temperature.

$$T_{cycle} = \Delta T_{diurnal} \cdot \sin\left(\theta_{planet} \cdot \left(t - t_{sunrise} \cdot 3600\right)\right)$$

Equation 116: Diurnal Temperature

T_{cycle} represents the added temperature rise caused by the sunrise during the day. The maximum temperature rise is represented by $\Delta T_{diurnal}$ which is a specific constant for each planet or moon. Θ_{planet} is the rotation speed of the planet. Temperature rise starts at sunrise and is distributed up to a maximum during midday. Then temperature decreases again until sunrise. Total atmospheric temperature is;

$$T_{total} = T_a + T_{cycle}$$

Equation 117: Total Atmospheric Temperature

Atmospheric pressure and density will be influenced by the diurnal temperature effect. No equations however have been implemented to simulate the effect. The assumption is made that the effect will be minimal.

Irradiance in Equation 72 is modeled through calculation of the mean and true anomalies from Equation 70 and Equation 71 respectively. Both are based on planetary data such as eccentricity, planet's radius and length of day. This information is input from the planetary database. Also the view factor and the half-cone angle are computed from the database inputs and the aerobot's altitude from the dynamical model. The latter are however not being used at this moment, but are available to the user for further improvements to the simulation tool.

5.6. Simulated Mass Breakdown

The initial mass budget for the aerobot was calculated at the very beginning of the simulation. The variations in mass during the aerobot's operational life however do influence its operation. The main components that will be effected over time are the amount of buoyant gas and the payload mass.

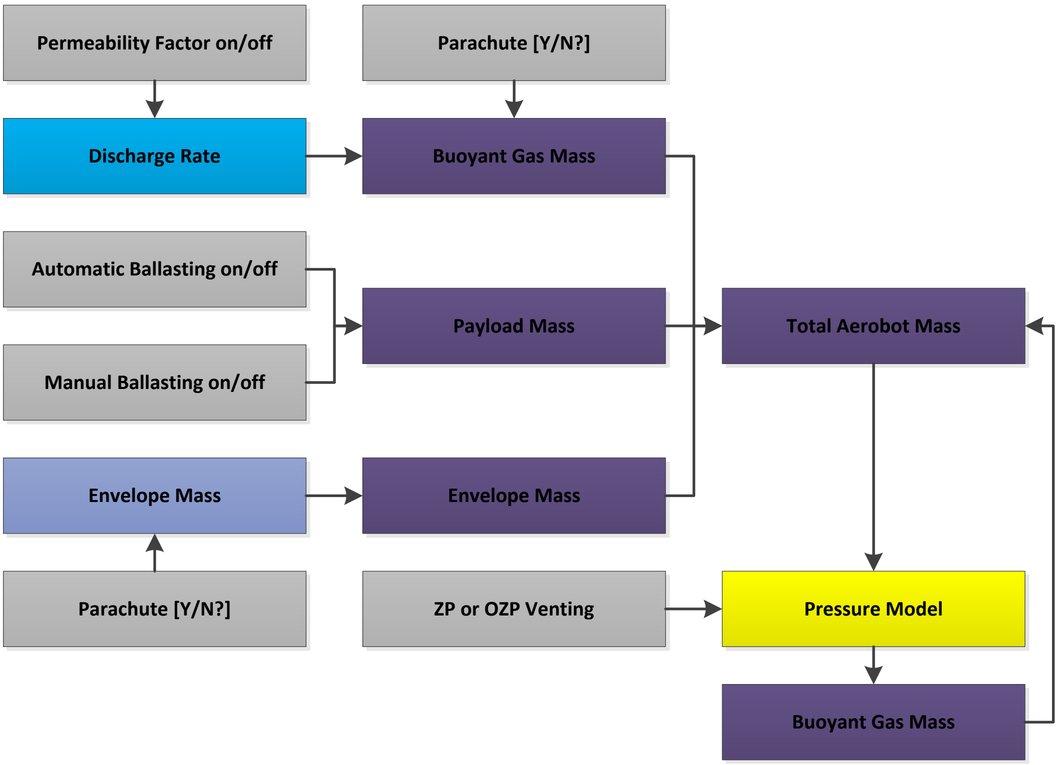

Figure 46: Simulated Mass Budget

The buoyant gas loses mass through permeability. This is simulated by the discharge rate from Darcy's law, in Equation 56, at which gas is leaving the envelope. This is a very small factor for short missions, but over time it can become an important parameter. Including permeability losses is an input variable which can be selected by the user. Combining Darcy's law with the gas density, the loss in buoyant gas per time step becomes;

$$m_{gas_t} = m_{gas_{t-1}} - Q_{discharge} \cdot \rho_{gas_{t-1}} \cdot \Delta t$$

Equation 118: Buoyant Gas Mass with Discharge

An additional way to dispose gas mass is by automatically or manually venting the gas. Via manual venting the program user discharges gas deliberately at specific time intervals to lower the ascend speed or altitude. Manual venting is not yet implemented into BADS though. Automatic venting occurs when the balloon's internal gas pressure increases as a result of volume restriction or temperature induced pressures. BADS will only include automatic venting for zero-pressure and OZP balloons. Super-pressure balloons have an enclosed volume and generally have no vents or valves through which gas can escape. In an OZP automatic venting occurs when the gas pressure is higher than the maximum valve pressure for which the OZP is designed for. For an OZP the user will be able to give a design over-pressure for which the valve has to open. For a zero-pressure the gas loss through the vent will be automatically activated when the gas pressure becomes higher than the atmospheric pressure. To simulate this behavior the gas mass is recomputed after the pressure calculation. This is done when the maximum design volume is reached or exceeded; only then the overpressure starts to buildup. Using the maximum design pressure, the exact amount of gas that should remain within the balloon envelope can be found;

$$m_{gas} = \frac{(p_a + \Delta p_{\max}) \cdot M_g \cdot Vol_{\max}}{R_c \cdot T_g}$$

Equation 119: Recalculated Gas Mass for Overpressure

One more parameter will influence the gas mass, and in this case also the envelope mass, namely a parachute descend. The user is able to select a parachute descend to simulate an envelope failure and soft payload return when the maximum volume is reached.

All buoyant gas mass will be lost when the envelope fails and the gas mass will be set to zero. Simulating the parachute in BADS will be done by taking the top-half of the maximum balloon volume as the reference area. In future, parachute specifics will be put into the program and better results will follow. The new mass-breakdown in free-fall will become;

$$m_{tot} = m_{pay} + \frac{m_{balloon}}{2} = m_{pay} + m_{parachute}$$

For a buoyant aerobot any loss in payload will be caused by ballasting, which is the intentional release of payload mass. In BADS payload is seen as the sum of the scientific payload and an amount of ballast that can be thrown overboard. Ballast can still be useful to the mission as it might be probes or small rovers, but it can also be added mass to prolong the lifetime of a zero-pressure balloon. The program user can select ballasting as manual, automatic or no ballasting. When automatic ballasting is chosen, the program will simulate a balloon flight which will automatically drop an amount of ballast, predefined by the user, when the balloon is descending and reaches a user defined altitude. This is repeated each time step, until the velocity returns to a positive value. For stability reasons the amount of ballast to be dropped each time should be kept as low as possible.

$$m_{pay_t} = m_{pay_{t-1}} - \% m_{pay_{t_x}}$$

Equation 120: Automatic Ballasting

When does the ballast needs to be dropped? When the aerobot is still rising the loss in weight will increase the ascend speed and the aerobot will overshoot its design altitude. When the aerobot is descending and ballast is dropped, the aerobot will slow down or stop descending. If enough ballast is dropped the aerobot might rise again to a new stable altitude. The latter is the new aerobot state the automatic ballasting command will try to acquire. It is up to the user however to estimate the correct altitude at which the ballast has to be dropped. If the chosen altitude is too low the aerobot will not have the time necessary to reacquire a positive ascend rate.

When manual ballasting is chosen, the user needs to input the amount of ballast to be dropped, the ballast rate φ at which the ballast has to be dropped, and the exact time at which ballasting needs to commence.

$$m_{pay_t} = m_{pay_{t-1}} - \frac{\varphi}{60} \cdot \Delta t$$

Equation 121: Manual Ballasting

The manual ballasting parameters are entered in the input screen as a matrix. An unlimited number of ballast drops can be entered, as long as there is enough payload mass to go around.

When no ballasting is selected, BADS will simulate an aerobot flight where height stabilization will not depend on ballasting. When the altitude starts to drop below the design altitude the aerobot shall stabilize on its own due to momentum and temperature variations or softly descend back to Earth.

5.7. Pressure Model

The pressure model computes pressure and overpressure levels throughout the simulated time loop. Three modules are available within the model, which correspond to the three types of balloons that the user is able to select.

When a zero-pressure balloon is chosen the assumption is made that the pressure difference between atmospheric and gas pressure remains zero at all time. The gas pressure at the base of the balloon is therefore always equal to the atmospheric pressure.
This assumption actually holds until the design volume is reached. Due to volume restriction, pressure starts to build up if no gas is vented. To be able to hold the zero-pressure level at the base of the balloon during simulation, the state of the balloon volume and the amount of gas mass need to be known at all times. Therefore, as illustrated in Figure 47, the balloon volume is recalculated at each time step through the geometric module, which is discussed in the next section. When the volume has reached its maximum dimension, the gas mass needs to be recalculated, as gas mass has to be vented to maintain a pressure difference of zero Pascal.

A super-pressure balloon acts like a zero-pressure balloon during ascend until the maximum attainable volume or design volume is reached. From then on the balloon will act as a super-pressure balloon by building up its overpressure. Simulating the ascend of a super-pressure balloon is similar to that of the zero-pressure balloon with the exception that no gas mass will be vented when the maximum volume is reached. The moment the design volume is reached the super-pressure is computed from the constant volume and density.

The OZP balloon acts like a zero-pressure balloon during ascend until the design volume is reached. From then on it will act like a super-pressure balloon. The only difference between the OZP and a super-pressure balloon is the maximum attainable overpressure. The OZP has a relief valve which will vent gas when the maximum valve pressure is reached. This means that the balloon volume, gas mass and over-pressure need to be controlled and recalculated each time step, as illustrated in Figure 47.

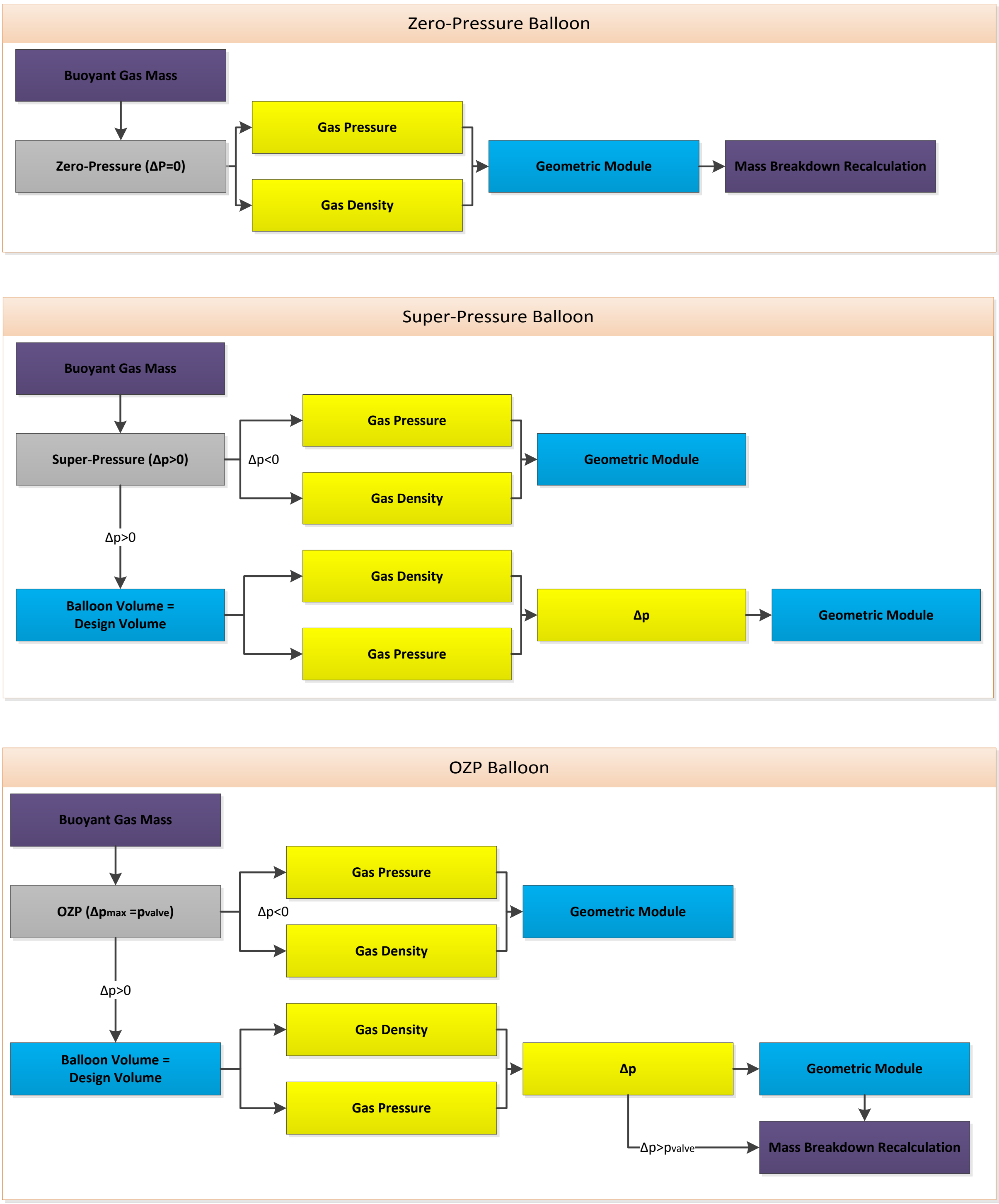

Figure 47: Simulated Pressure Model

5.8. Geometric Simulation Model

The geometric model focuses on the size and shape of the balloon. Throughout the aerobot's flight the balloon volume changes with altitude. Balloon volume is therefore calculated from the available gas mass and the gas density which is related to temperature and pressure;

$$Vol_{balloon} = m_g \cdot \frac{R_g \cdot T_g}{p_g}$$

Equation 122: Variable Balloon Volume

With the volume known and fineness ratio given by the user, the dimensions of the balloon can be calculated from Equation 47.

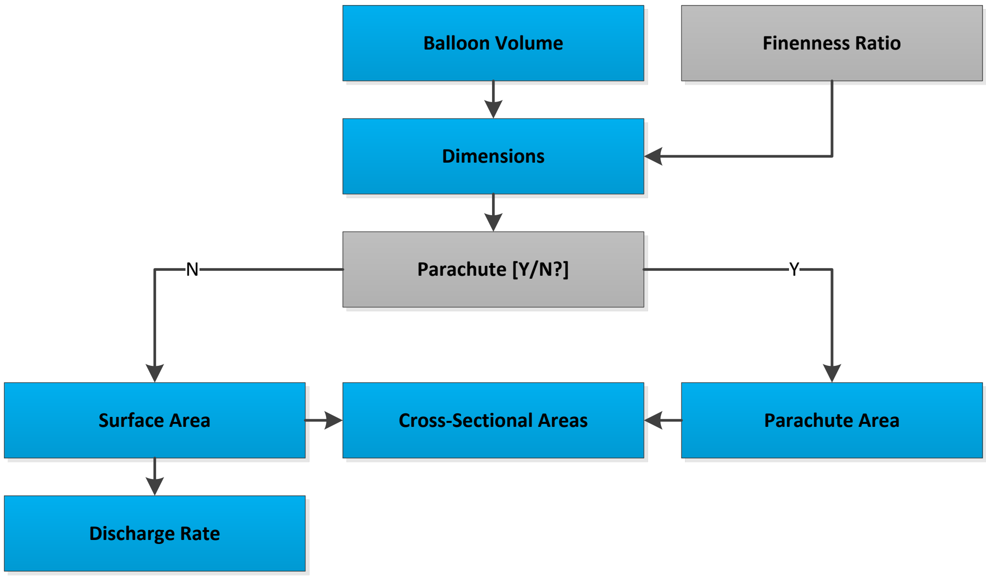

Figure 48: Geometric Simulation Model

As illustrated in Figure 48, the balloon's dimensions are implemented into the equations of Table 16 to calculate the surface area. Similarly, the cross-sectional areas for a sphere or ellipsoid are found from the equations in Table 17.

A special case in the geometric model is the addition of the parachute module. When maximum balloon volume is reached and the user has selected the parachute option, the parachute area will be calculated from the maximum volume. At this time BADS defines the parachute area to be the top halve of the balloon, halving the surface area and cross-sectional areas.

Finally, also the discharge rate is calculated here, as it is related to the total balloon surface area. The discharge rate will only be of use however, when permeability is selected by the user.

5.9. Thermal Simulation Model

The thermal simulation model has been divided into two main modules, illustrated in Figure 49. They have been separated because each module is required at a different phase in the simulation. They also require input from other models such as the geometric and the atmospheric models. The first thermal module to be implemented into the time loop is the temperature module. The module computes the temperatures of the envelope and the buoyant gas throughout the aerobot's flight process. The temperatures follow from the differential temperatures of Equation 66 and Equation 67. Integrated over time and rewritten for simulation purpose, the equations become;

$$T_{g_t} = T_{g_{t-1}} + \Delta t \cdot \left(\frac{Q_{g_{t-1}}}{c_{p_g} \cdot m_{g_{t-1}}} - \frac{g \cdot M_a \cdot T_{g_{t-1}} \cdot \Delta h}{c_{p_g} \cdot T_{a_{t-1}} \cdot M_g} \right)$$

Equation 123: Gas Temperature

$$T_{e_t} = T_{e_{t-1}} + \frac{Q_e}{c_{env} \cdot m_e} \cdot \Delta t$$

Equation 124: Envelope Temperature

Both equations make use of the specific heats of the buoyant gas and the envelope respectively. These parameters are found from the input database. Further the equations make use of the initial temperatures of gas, atmosphere, ground and the balloon, which are all set equal to the value of the atmosphere.

Subsequent, the viscosity is being calculated from Sutherlands equation in Equation 36 and the found temperature values of both gas and atmosphere. The thermal conductivity of both the planet's atmosphere and the buoyant gas in the balloon follows from listed data which differs with temperature. Cubic interpolation is being used to find the intermediate values, while similar extrapolation is used to find the values outside the range of reference data.

The second module in the thermal model computes the heat flows of the envelope and the buoyant gas. The dimensionless Prandtl and Grashof numbers are calculated first from Equation 100 up to Equation 103. Both Prandtl and Grashof use information obtained from the temperature module, such as viscosity, conductivity and temperature from gas and atmosphere. Grashof will also require the dimensions of the balloon.

From the Grashof and Prandtl numbers the Nusselt number can be found if a good correlation is available for the selected buoyant gas and balloon shape. As mentioned in chapter 4.4 this is based on experimental data which is available for free convection, but limited for forced convection.

If Nusselt number correlations are available the convective heat transfer coefficients can be calculated. If Nusselt numbers aren't available the user is best to ignore convection in the thermal model. From the Reynolds and Grashof numbers the boundary conditions on convection can be found, in Equation 105 and Equation 106, to proof if forced convection is present or not.

When the heat transfer coefficients are computed the heat flows of the envelope and buoyant gas can be found with the input of the optical properties of both gas and envelope fabric. The calculated parameters can also be modified for cloud interference through the equations of Farley [a.22]. The modifications are optional and are either selected or deselected by the user before simulation.

Figure 49: Thermal Simulation Model

Simulation stability drops with an increase in calculations and parameters. Likewise the stability drops with parameter values which rapidly change over time. The temperature model has both. The amount of parameters that are introduced in the thermal model is quite large and temperatures may differ quickly when an aerobot is rising fast, drops payload or discharges buoyant gas. This means that the temperature model will cause an accuracy loss over time. The effect of the instability on the results can be overcome by introducing a more stable mathematical method. This will be one of the recommendations on future work. A temporary solution to the instability problem will be lowering the time step size when the thermal models are used in the simulation, to obtain at least an average accuracy.

5.10. Output Data

Output data is presented in the form of graphical information and numerical data. All calculated parameters are saved numerical into a Microsoft Excel datasheet. The following data is standard graphical output data;

- Atmosphere and buoyant gas pressure alongside time
- Atmosphere and buoyant gas temperature alongside time
- Atmosphere and buoyant gas density alongside time
- Flight altitude alongside time
- Ascend speed alongside time
- Aerodynamic forces alongside time
- Envelope and gas heat flows alongside time
- Mass breakdown alongside time
- Balloon volume alongside time
- 3D Flight coordinates
- 3D Balloon shape

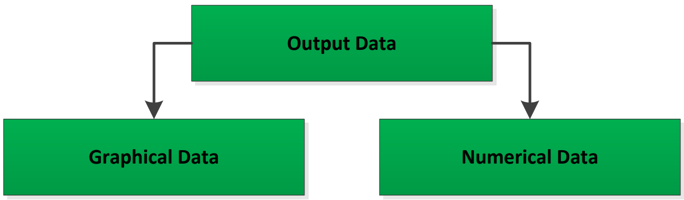

Figure 50: Output Data

Evaluating temperature, pressure and density of both the buoyant gas and the atmosphere over time, makes it easier to monitor the state of the buoyant gas. Both atmosphere and gas start at the same temperature and pressure, but evolve over time. It is this evolution which makes it worthwhile to graphically illustrate these parameters.

The dynamical model of BADS is programmed to simulate the flight trajectory of a buoyant aerobot. A graphical simulation of the aerobot's flight path is therefore one of the prime results of BADS. Two useful graphs are illustrated in the output data. The 3D flight coordinates represent the flight path from the launch site to either the crash site or the flight altitude. This representation of results is especially handy when a wind model or propelled flight is being included into the simulation. Buoyancy is however a force in vertical direction. To emphasize the flight results in this direction the aerobot's flight in vertical direction has been graphed against time. In conjunction with the ascend speed the program user can estimate how a real balloon flight would behave.

The aerodynamic forces and the mass breakdown have been plotted over time to show the effect a ballast drop or gas venting event has on the buoyancy force, drag force, etc. Likewise the aerodynamic forces and ascend speed can be compared to view the effect the forces have on the ascend speed.

When the temperature model is used, not only the change in the buoyant gas and envelope temperatures are valuable to the user, but also the heat flows in and out of the envelope and gas.

From the figures the highest heat flow can be detected. Further analysis might give the user a better insight in the thermo-optical limitations of the envelope material, or the type of coating he’s using.

Balloon volume has been graphically illustrated to give the user an idea on how the balloon geometrically behaves between launch and arriving at the design altitude. Likewise a 3D representation of the balloon is presented for visual reference.

While these figures are the ones preferred by the writer, other available data can always be plotted by the user at the end of the simulation. Examples of the discussed output data can be found in chapters 6 and 7, where mission results, program evaluation and sensitivity are discussed.

6. Testing and Validating of BADS

The simulation tool discussed in chapter 5 will require detailed testing and validation of each of the models separately and as a whole. Section 6.1 shall describe the debugging, testing and validation sequence used throughout the chapter.

Two main segments have to be tested in BADS; the aerobot design and the flight simulation. Section 6.2 shall describe the validation of the initial aerobot design in conjunction with the planetary environment. This is done through a JPL aerobot evaluation study for Earth, Mars, Venus and Titan.

Next the flight simulation validation will be explored. In section 6.3 a buoyant aerobot flight behavioral analysis is implemented; addressing specific topics that influence the general flight behavior and exploring the simulated results from these events.

The last two steps in the validation process are the numerical validation methods. The first method compares the results from BADS with those of other existing programs. Aerobot simulation programs are limited though and their code and data results are not always publicly available. Section 6.4 shall therefore compare BADS to Analysis Code for High-Altitude Balloons (ACHAB) [t.4] and SINBAD [a.36], through an evaluation study by Palumbo [t.4]. Further, BADS shall also be compared with the available data on Balloon Ascent [a.22]. By using similar input parameters, thus creating a comparable environment, specific simulated mission results are compared. The last method is comparing flight results of some programs above with real scientific flight data, measured in situ. The discrepancies in results between BADS, ACHAB and SINBAD, will be addressed and the performance of BADS will be discussed throughout this section.

6.1. Debugging, Testing and Validation Sequence

The BADS tool will undergo a series of general testing and debugging phases before any validation of the tool shall take place. The debugging, testing and validation sequence can be found below;

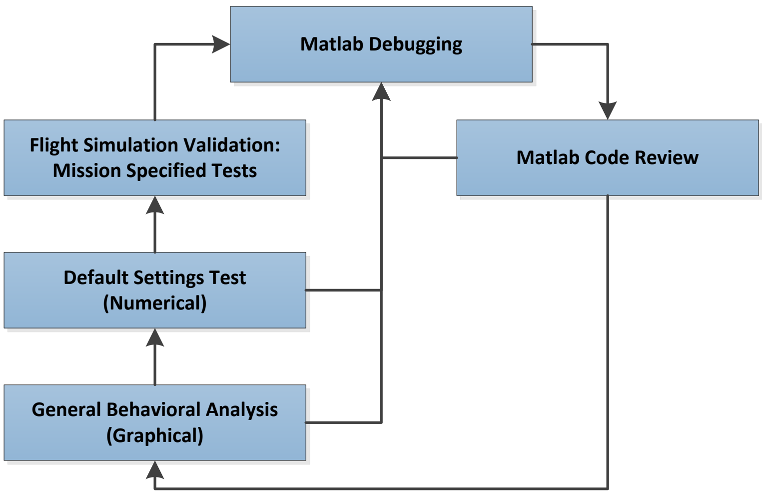

Figure 51: Testing and Debugging Sequence

Each step in this process is redone when an error is detected in the coding or in the behavior of the simulation. The first phase in the sequence is the Matlab debugging. The Matlab debugging is a code test in Matlab which is automatically done before each simulation run. This is a very basic test, as it only checks for basic coding mistakes; mainly command errors. Equation deviations or value imperfections are not being considered by the Matlab debugging. Therefore a second phase in the debugging requires a thorough code review. The code review requires the knowledge of all equations used and the basic understanding of buoyant aerobot flight. Each equation is checked and rechecked, input and database values are compared to the original data, and boundary conditions are assessed.

When the Matlab debugging and the Matlab code review have been dealt with, the simulation process will undergo the next series of testing and debugging phases. A general behavioral analysis will be done by evaluating the graphical output data. This graphical analysis will give the programmer a general idea of the behavior of the simulation and its many modules. For instance, do all modules interact accordingly through each simulated event?
Next the accuracy of the numerical output data will be analyzed by comparing the data in default settings against known simulated or in situ data. The best way to test the functionality and the accuracy of the code will be simulating in default settings after each modification or debugging attempt to see the impact each change made.
When all previous steps are taken into account, no obvious errors appear, and all modules seem to interact accordingly, the finale validation of the simulation tool will be completed by means of comparing real data of interplanetary missions with the simulated data.

6.2. Aerobot Initial Design and Atmospheric Validation

A JPL aerobot evaluation done by Ball et al [b.3][a.5] in 2007 is a great source of information. Ball et al compare the designs of standard buoyant aerobots for the atmospheres of Venus, Mars, Earth and Titan. The four atmospheres that have been incorporated into the simulation tool. The data will be used for the validation of the initial aerobot design module and the atmospheric module.

Table 28: Ball et al [b.3] Planetary Environment Evaluation

Parameter	Venus	Mars	Titan	Earth
Acceleration of gravity (Earth g)	0.9	0.37	0.14	1
Main atmospheric gas	CO_2	CO_2	N_2	N_2
Surface temperature (K)	735	230	92	290
Surface pressure (atm)	92	0.0067	1.4	1.0
Surface air density (kg m^{-3})	64	0.015	4.9	1.2
Solar flux at the upper atmosphere (W m^{-2})	3200	700	13	1300
Solar flux near the surface (W m^{-2})	5	700	~1	600
Altitude of tropopause (km)	~65	11	40	17
Pressure at tropopause (mbar)	97	2.7	200	90
Temperature at tropopause (K)	240	190	70	220
Diurnal temperature variations near the surface, $\Delta T/T$ (%)	<0.3	30–50	<1	<10
Winds at the tropopause (m s^{-1})	80–100	20–30	15	20–30
Winds in lower atmosphere (m s^{-1})	1–3	5–20	~1	5–20

Table 28 represents the planetary environments as used by Ball et al [b.3] in the aerobot design calculations. The environment influences the buoyant aerobot's design significantly; mainly the envelope's volume and total aerobot mass. The environment parameters are either set as fixed values in BADS, or calibrated from the selected atmospheric models. As such, the selected atmospheric models will cause some discrepancies in the design results compared to those of Ball et al. However this doesn't necessarily mean that the results are wrong. As mentioned in section 4.1, any standard atmospheric model is an averaged environment based on a representation of year-round, mid-latitude conditions, which in case of BADS is shown in Table 29.

Table 29: Simulation Tool Planetary Environment Evaluation

Parameter	**Venus**	**Mars**	**Titan**	**Earth**
Acceleration of gravity [g]	0.904	0.378	0.138	1
Main Atmospheric gas []	CO_2	CO_2	N_2	N_2
Surface Temperature [K]	768	287	93.5	288.15
Surface Pressure [atm]	97	0.0078	1.45	1
Surface Air Density [kg/m³]	63.1	0.0144	5.34	1.225
Solar Flux upper atmosphere [W/m²]	2615	645	15.4	1381
Altitude of Tropopause [km]	65	11	40	17
Pressure at Tropopause [mbar]	97.63	3.37	145.3	89.06
Temperature at Tropopause [K]	243.5	221	70.5	216.6
Diurnal temperature variations ΔT/T [%]	0	23.7	6.4	3.5

Comparing Table 28 and Table 29, the reader will see that atmospheric winds and solar flux near the surface have not been compared in the BADS environment. No standard wind profile has been incorporated yet in BADS and therefore no values have been included in Table 29. Similarly no solar flux variations with altitude have yet been included in BADS.

The main discrepancies between Table 28 and Table 29 can be found in the atmospheric temperature and pressure profiles. Other variances are found in the diurnal temperature variations which are related to the difference in temperature profile but also due to the way these values are calculated; the diurnal effect is calculated day by day during the planet's movement around the sun. All other planetary parameters however are quite similar to the ones used by Ball et al.

The planetary aerobot comparison done by Ball et al uses a standard payload mass of 10kg for each aerobot. Furthermore the envelope areal density is assumed to be ~20g/m² and all aerobots are shaped as spheres.
Initially the results from the simulation tool varied quite a bit from the results by Ball et al. Mainly the balloon mass for all planetary cases and every parameter from the '4km Earth' case. After contacting one of the writers, Viktor Kerzhanovich, the issue became clear; the 4km Earth case was a type error that had to be a 34km case. Also extra mass was added to the balloon mass by the following equation;

$$m_{envelope} = \rho_{envelope} \cdot A_{balloon} \cdot k_f + m_{fitting}$$

Equation 125: Envelope Mass with Added Fitting

Table 30: Planetary Aerobot Parameters Ball et al

Parameter	Venus, 1 km	Venus, 60 km	Mars, 5 km	Titan, 1 km	Earth, 1 km	Earth, 4 km
Atmospheric density, (kg m^{-3})	61.56	0.489	0.010	4.80	1.13	0.010
Temperature of atmosphere (°C)	454	−10	−51	−181	−2	−33
Payload mass (kg)	10	10	10	10	10	10
Balloon diameter (m)	0.72	3.70	20.65	1.73	2.83	21.41
Balloon volume (m^3)	0.2	26.5	4610	2.7	11.9	5140
Balloon mass (kg)	0.84	1.79	31.6	1.02	1.37	33.9
Mass of buoyant gas (He) (kg)	1.16	1.25	4.46	1.97	1.94	7.44
Total floating mass (kg)	12.0	13.0	46.1	13.0	13.4	51.4
Payload mass as percentage of floating mass (%)	83.4	76.5	21.6	77.1	75.2	19.5
Mass of entry vehicle (kg)	36	39	138	39	N/A	N/A

Table 31: Planetary Aerobot Designs from the Simulation Tool (a)

	Venus 1km	**Venus 1km *(Improved)***	**Venus 60km**	**Venus 60km *(Improved)***	**Mars 5km**	**Mars 5km *(Improved)***
Atmospheric Density [kg/m^3]	60.5	60.5	0.62	0.62	0.011	0.011
Atmospheric Temperature [°C]	486.3	486.29	-1.15	-1.15	-17.15	-17.15
Payload Mass [kg]	10.81	9.91	10.986	10.086	17.17	12.57
Balloon Diameter [m]	0.72	0.72	3.42	3.42	19.82	19.82
Balloon Volume [m^3]	0.2	0.2	20.97	20.97	4079.6	4079.6
Balloon Mass [kg]	0.033	0.93	0.735	1.63	24.69	29.3
Buoyant Gas Mass [kg]	1.156	1.156	1.278	1.278	4.23	4.23
Total Floating Mass [kg]	12	12	13	13	46.1	46.1
Payload Mass Percentage [%]	90.09	82.59	84.5	77.58	37.24	27.26

Table 32: Planetary Aerobot Designs from the Simulation Tool (b)

	Titan 1km	**Titan 1km *(Improved)***	**Earth 1km**	**Earth 1km *(Improved)***	**Earth 34km**	**Earth 34km *(Improved)***
Atmospheric Density [kg/m^3]	5.14	5.14	1.11	1.11	0.01	0.01
Atmospheric Temperature [°C]	-180.8	-180.8	8.5	8.5	-40.1	-40.1
Payload Mass [kg]	10.98	10.09	11.04	10.14	15.2	9.93
Balloon Diameter [m]	1.69	1.69	2.84	2.84	21.51	21.51
Balloon Volume [m^3]	2.52	2.52	12.05	12.05	5216.2	5216.2
Balloon Mass [kg]	0.18	1.079	0.51	1.4	29.09	34.35
Buoyant Gas Mass [kg]	1.84	1.84	1.85	1.85	7.11	7.11
Total Floating Mass [kg]	13	13	13.4	13.4	51.4	51.4
Payload Mass Percentage [%]	84.47	77.54	82.39	75.67	29.57	19.33

In BADS, the balloon mass is calculated from the envelope density $\rho_{envelope}$ and balloon surface area $A_{balloon}$. Ball et al makes use of an extra fitting of ~0.9kg and a construction factor k_f which is 1 for small balloons and 1.15 for large balloons.

Table 31 and Table 32 show the simulated results of Table 30 [a.5] for all planetary aerobots. The tables show standard and improved results, for which the latter makes use of Equation 125. The improved results are clearly closer to the results by Ball et al. One parameters isn't being compared however, namely the 'mass of the entry vehicle'. BADS only takes into account the 'buoyant aerobot', or the 'total floating mass' by Ball et al, in its design calculations. The mass of the entry vehicle by Ball et al includes a heat shield and any other component required for an atmosphere descend from space. Therefore this parameter has not been included in the comparison of Table 31 and Table 32.

The small inconsistencies between values still present after the improvements are most likely caused by the following;

- $m_{fitting}$ is approximately 0.9kg for all cases. Exact values can influence the envelope mass.
- $\rho_{envelope}$ is approximately 20g/m^2 for all cases. Exact values can influence the envelope mass.
- Atmospheric temperature influences the atmospheric and gas density, which influences the total buoyant volume required to stay afloat. The latter influences the envelope mass and the buoyant gas mass.
- Any discrepancy in envelope mass and buoyant gas mass will influence the remaining space for payload mass.

Table 33: Variance Percentage [%] of Improved Results compared to Ball et al

	Venus 1km	**Venus 60km**	**Mars 5km**	**Titan 1km**	**Earth 1km**	**Earth 34km**
Atmospheric Density	1,72	*26,79*	*10,00*	7,08	1,77	0
Atmospheric Temperature	7,11	*88,50*	*66,37*	0,11	*525*	*21,52*
Payload Mass	0,90	0,86	*25,70*	0,90	1,40	0,70
Balloon Diameter	0	7,57	4,02	2,31	0,35	0,47
Balloon Volume	0	*20,87*	*11,51*	6,67	1,26	1,48
Balloon Mass	*10,71*	8,94	7,28	5,78	2,19	1,33
Buoyant Gas Mass	0,34	2,24	5,16	6,60	4,64	4,44
Total Floating Mass	0	0	0	0	0	0
Payload Mass Percentage	0,81	1,08	5,66	0,44	0,47	0,17

Temperature changes have a certain impact on the atmosphere's density but especially the gas density changes rapidly. This means the required buoyant gas mass will change for that specific temperature range at the chosen design altitude. To show the impact of atmospheric differences on the design results, atmospheric temperature and density are set equal to those of Ball et al, and the above calculations are repeated. Results are displayed in Table 34.

The outcome is a considerably lower error percentage on almost all design parameters shown in Table 35. This means that the variance in atmospheric variables has the largest impact on any discrepancies in the calibrated parameters. The remaining error percentage is found with the buoyant gas mass parameter and the balloon mass. From the results one can suspect that the density of the balloon material is not exactly 20g/m^2 and therefore shows a difference in result. Also suspicion is high that the buoyant gas mass is increased with an extra amount, similar to the added mass of the balloon mass, most likely to sustain gas leakage during the aerobot mission. No confirmation however was obtained.

Table 34: Planetary Aerobot Design with Adapted Atmospheric Parameters

	Venus 1km	**Venus 60km**	**Mars 5km**	**Titan 1km**	**Earth 1km**	**Earth 34km**
Atmospheric Density [kg/m^3]	61.56	0.489	0.01	4.8	1.13	0.01
Atmospheric Temperature [°C]	454	-10	-51	-181	-2	-33
Payload Mass [kg]	9.98	10.05	10.13	10.09	10.15	10.27
Balloon Diameter [m]	0.72	3.7	20.65	1.73	2.83	21.41
Balloon Volume [m^3]	0.2	26.58	4610	2.71	11.86	5140
Balloon Mass [kg]	0.93	1.76	31.71	1.09	1.4	34.03
Buoyant Gas Mass [kg]	1.09	1.18	4.26	1.82	1.85	7.1
Total Floating Mass [kg]	12	13	46.1	13	13.4	51.4
Payload Mass Percentage [%]	83.13	77.35	21.98	77.64	75.71	19.98

Table 35: Error Percentage of Design with Adapted Atmospheric Parameters

	Venus 1km	**Venus 60km**	**Mars 5km**	**Titan 1km**	**Earth 1km**	**Earth 34km**
Atmospheric Density	0	0	0	0	0	0
Atmospheric Temperature	0	0	0	0	0	0
Payload Mass	0,20	0,50	*1,30*	0,90	1,50	2,70
Balloon Diameter	0	0	0	0	0	0
Balloon Volume	0	*0,30*	*0*	0,37	0,34	0
Balloon Mass	*10,71*	1,68	0,35	6,86	2,19	0,38
Buoyant Gas Mass	6,03	5,60	4,48	7,61	4,64	4,57
Total Floating Mass	0	0	0	0	0	0
Payload Mass Percentage	0,27	0,85	0,38	0,54	0,51	0,48

While the calculation method by Ball et al starts with a standard payload of 10kg and works its way up to all other parameters, BADS will calculate all parameters starting from the total floating mass. The distinction in calculation method explains the different payload masses compared to the exact total masses. All deviations in parameter value therefore influence the payload mass while otherwise it would have influenced the total mass.

However, the variance in payload mass percentage compared to Ball et al is limited and is most likely related to the inaccurate value of the envelope areal density. Kerzhanovich mentioned that the calculated values from Equation 125 would yield values close to those of Table 30 and not exact.

Concluding the above evaluation; The standard atmospheric models influence the data results of the initial buoyant aerobot design too much to make a thorough comparison between the BADS designs and those of Ball et al. However the standard atmosphere does present a lot of possibilities in flight behavior analysis, which will be discussed in 6.3.

When the atmospheric influences are being neglected the initial aerobot design shows its real potential. Small discrepancies in the range of 0 to 5% between actual values and BADS's simulated design values have been found, with one or two exceptional inconsistencies of 10%. Both, however, can be subscribed to the inaccurate input parameters and starting assumptions.

6.3. Flight Behavioral Analysis

The flight path of a buoyant aerobot is very susceptible to change in any planetary atmosphere. Wind, ballast, temperature, gas release are just a few examples of parameters that influence the aerobot's behavior during flight. This subchapter will isolate the aerobot's simulated behavior for the most common modifications during flight as a validation of that behavior. The flight modifications include; the calculation and effect of free lift, the influence of a constant versus a variable drag coefficient, the balloon bobbing effect at float, a buoyant gas discharge event, the influence of a ballast drop and a payload parachute descend. No thermal models are taken into account during this analysis, unless stated otherwise!

6.3.1. Free Lift

The standard behavior of a buoyant aerobot during flight without any other phenomena happening consists out of a steep or gentle rise towards a stable floating altitude. For a zero-pressure balloon this might often turn into a soft descend back to ground after reaching its design altitude, shown in Figure 52. The gradient of the ascend will be determined by three main features; the amount of free lift available, the temperature difference between gas and atmosphere, and finally the drag coefficient of the aerobot. The latter two will be addressed later on.

A large amount of free lift will launch the aerobot into a flight with high ascend speeds, which can cause excessive cooling of gas and envelope, which can even lead to 'envelope bursting' [t.4]. A too small amount of free lift however will end up in a float altitude well below the planned design altitude, due to a lack in lift and momentum.

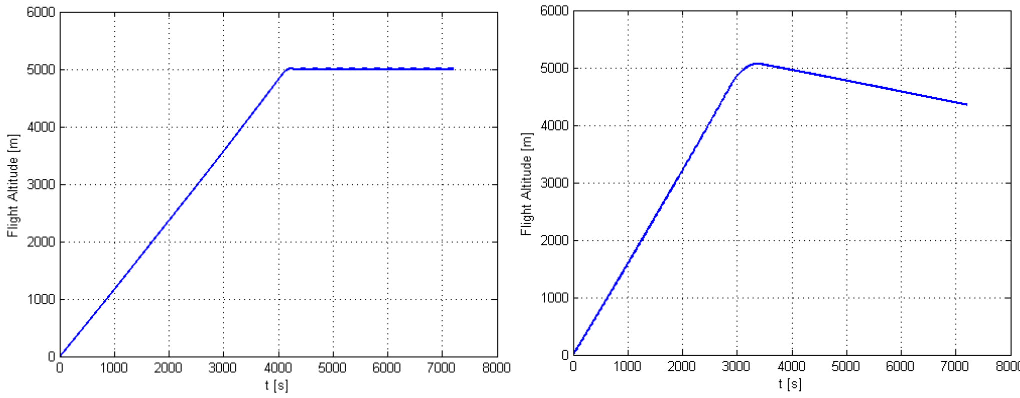

Figure 52: Standard Aerobot Flight; (a) Super-Pressure, (b) Zero-Pressure

Initially the mass budget calculations from chapter 4.2 are made for the planned design altitude. With the initial buoyant gas mass the aerobot will be able to float at the specific altitude as mentioned in section 5.6. The way up to the design altitude however often requires an extra boost by means of extra buoyant gas. Small aerobots are sometimes able to fly with the design gas mass, larger aerobots however do feel the effect of the lack in free lift and require 10-20% of free lift to lift off and reach the design altitude. The amount of free lift will influence the altitude overshoot due to extra momentum and sometimes it will change the actual floating altitude if the excessive amount of gas mass isn't released on time. This is illustrated in Figure 53, where a 200kg ZP aerobot's flight path is presented for a free lift percentage of 10% and 30% respectively. Free lift increases the ascend speed and increases the overshoot with about 250m.

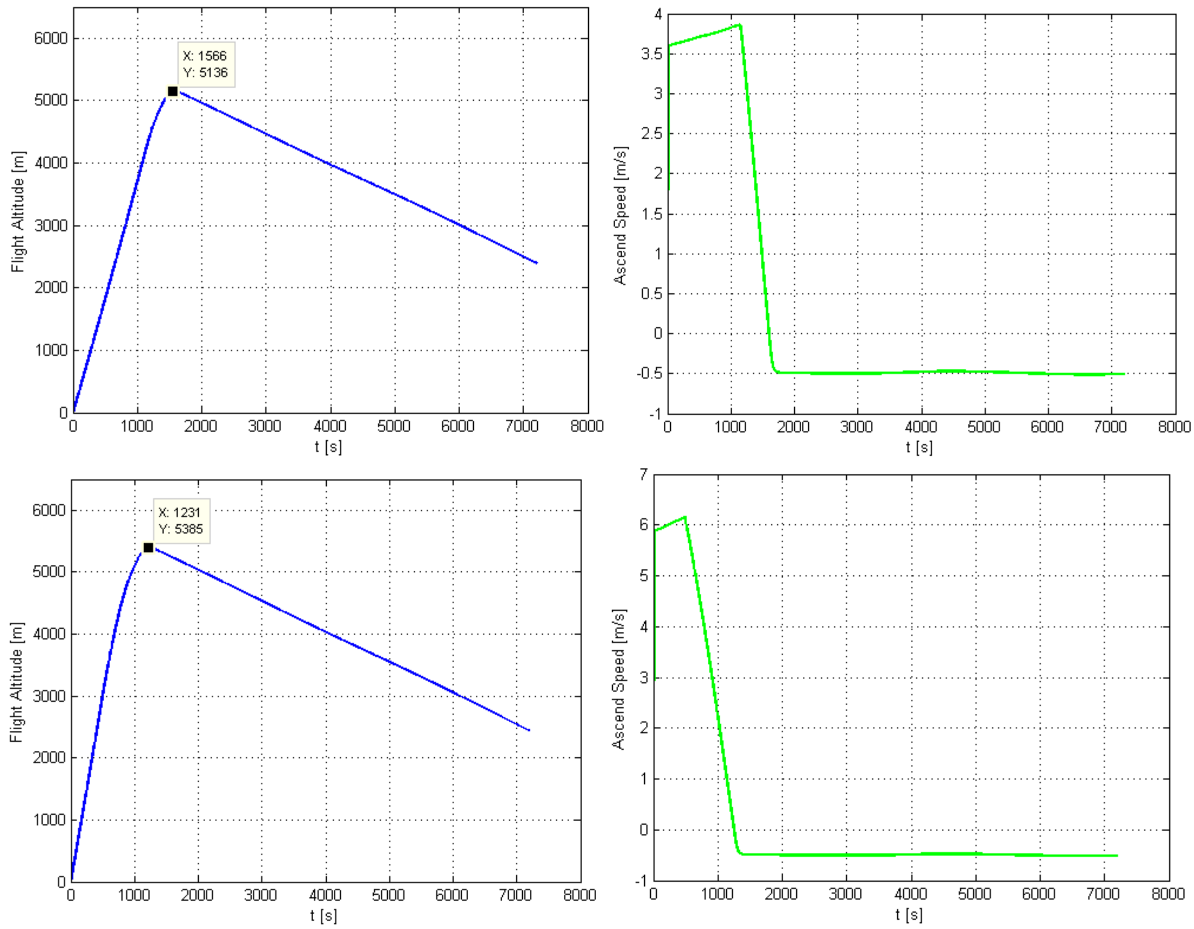

Figure 53: Free Lift Overshoot; (a)+(b) 10% Free Lift, (c)+(d) 30% Free Lift

Although this approach is useful for zero-pressure balloons it is tricky when used in super-pressure balloons. Super-pressure balloons will not encounter a too big overshoot, as they are a more stable system, but they will encounter a pressure problem. If extra gas mass is forced into the enclosed volume of the SP balloon, the balloon would develop a higher super-pressure at the design altitude.

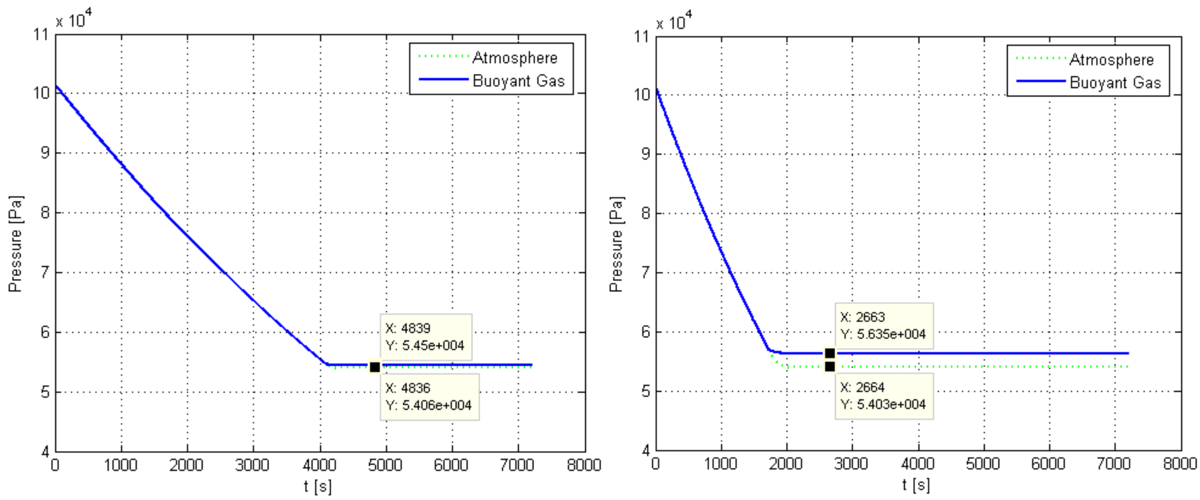

Figure 54: SP Pressure Increase; (a) 1% Free Lift, (b) 5% Free Lift

In Figure 54 the pressure difference, between atmosphere and buoyant gas, of a 200kg SP aerobot is displayed for a 1% and a 5% free lift case respectively. The SP aerobot is originally designed for a 100Pa super-pressure. A 1% free lift added to the super-pressure balloon will create a pressure difference of 440Pa at the design altitude. A 5% free lift added will create a pressure difference of 2320Pa. In this simulation no material restrictions are taken into account. If this had been the case however, the balloon envelope would have ruptured when the material couldn't handle the high pressures.

6.3.2. The influence of the Drag Coefficient on the Ascend Speed

During testing it was observed that the simulated ascend speed from BADS differed with the data from ACHAB by Palumbo [t.4]. At launch the difference was highest. This phenomena could be described to the influence of the drag coefficient on the ascend speed of the aerobot and therefore on the location of the aerobot in time.

Zero-pressure balloons experience a big change in volume and shape during flight. The simulation tool however only takes the first into account and maintains the type of shape during flight. The change in volume has its effect on drag through the change in cross-sectional area. Due to the change in size however also the drag coefficient of the aerobot changes. Up till now the drag coefficient was always simulated as a constant parameter. Even so, the large change in volume makes it worthwhile to make use of a variable drag coefficient, which will influence the ascend speed and in time will simulate a more precise location of the aerobot.

A good equation for a variable drag coefficient of a spheroid however is difficult to find. Most data on this subject comes from specific tests. Figure 33 provides an initial approach though; a variable drag coefficient based on the change in Reynolds number. According to Palumbo [t.4] the drag coefficient can't be exclusively dependent of the Reynolds number due to;

- Inconsistent shape of the balloon
- Shape deformability
- Dimensional reasoning

While the reasoning on this subject is accurate, the drag calculations in the simulation tool at this stage are not that evolved. Of the above arguments the program only takes into account the change in dimensions through the change in volume to simulate drag. Therefore an equation for a variable drag coefficient exclusively based on the Reynolds number should suffice as it would already add some more realism to the drag calculations, the drag coefficient and BADS in general.

A number of drag coefficient equations based on the Reynolds number were investigated. Most of them however lacked the accuracy to be used for a wide range of Reynolds numbers. The drag coefficient for a sphere in Figure 33, presented for a large range of Reynolds numbers, was reproduced by members of the Clarkson University in [a.34] and [a.35]. From these equations one specific set of equations was introduced in the simulation program, namely Equation 126. The main reason to select this equation above all others was the fact that it was modelled for the largest amount of Reynolds numbers. The set of equations reproduces the drag coefficient of a sphere for each region of Reynolds number.

For $\mathrm{Re} \le 0.01$	$C_d = \frac{9}{2} + \frac{24}{\mathrm{Re}}$
For $0.01 < \mathrm{Re} \le 20$	$C_d = \frac{24}{\mathrm{Re}} \cdot \left(1 + 0.1315 \cdot \mathrm{Re}^{0.82-0.05 \cdot w}\right)$
For $20 < \mathrm{Re} \le 260$	$C_d = \frac{24}{\mathrm{Re}} \cdot \left(1 + 0.1935 \cdot \mathrm{Re}^{0.6305}\right)$
For $260 < \mathrm{Re} \le 1.5 \cdot 10^3$	$\log_{10} C_d = 1.6435 - 1.1242 \cdot w + 0.1558 \cdot w^2$
For $1.5 \cdot 10^3 < \mathrm{Re} \le 1.2 \cdot 10^4$	$\log_{10} C_d = -2.4571 + 2.5558 \cdot w - 0.9295 \cdot w^2 + 0.1049 \cdot w^3$
For $1.2 \cdot 10^4 < \mathrm{Re} \le 4.4 \cdot 10^4$	$\log_{10} C_d = -1.9181 + 0.637 \cdot w - 0.0636 \cdot w^2$
For $4.4 \cdot 10^4 < \mathrm{Re} \le 3.38 \cdot 10^5$	$\log_{10} C_d = -4.339 + 1.5809 \cdot w - 0.1546 \cdot w^2$
For $3.38 \cdot 10^5 < \mathrm{Re} \le 4 \cdot 10^5$	$C_d = 29.78 - 5.3 \cdot w$
For $4 \cdot 10^5 < \mathrm{Re} \le 10^6$	$C_d = 0.1 \cdot w - 0.49$
For $\mathrm{Re} > 10^6$	$C_d = 0.19 - \frac{8 \cdot 10^4}{\mathrm{Re}}$

Equation 126: Variable Drag Coefficient for a Sphere [a.35]

Re is the Reynolds number and 'w' is;

$$w = \log_{10} \mathrm{Re}$$

The downside with this set of equations compared to a constant drag coefficient equation based on shape, is that it is limited to a sphere. While the drag on a spheroid is different than that on a sphere, the assumption is made that a spheroid will act similar to a sphere with respect to the Reynolds number. Based on research of Hoerner [b.4] and DeMoss [t.2] drag coefficients of oblate spheroids are generally lower than those of spheres. "Through all of the Reynolds numbers, the effect of the fineness ratio is the same, with higher fineness ratios generally producing lower drag coefficients [t.2]" No reference was found to assume the opposite holds for prolate spheroids, namely that fineness ratios smaller than 1 would produce higher drag coefficients than those of a sphere. The higher cross-sectional area in the xz-direction would assume so though. This can be related to the observations from Dorrington [a.3] who lowered the drag coefficient of a sphere by adding conical shapes fore and aft of the sphere, changing the fineness ratio and making it look like an airship.

The equation for a variable drag coefficient for spheroids will therefore be kept the same as that for a sphere. The C_D values for oblate spheroids and airships will be lowered, while those for prolate spheroids are increased. All are lowered or increased with a percentage based on the fineness ratio to represent the above mentioned effect.

Another downside for the Reynolds based C_D equations are the results of near zero Reynolds values. To avoid too high C_D values in that region, the maximum value for C_D can be set to 2, which holds for rotational symmetrical bodies according to F. Stern [i.26].

The user of the simulation program will be able to select either a constant drag coefficient based on the fineness ratio (Equation 37) or a variable drag coefficient based on the Reynolds number (Equation 126). The user should keep in mind that both methods are subject to improvement.

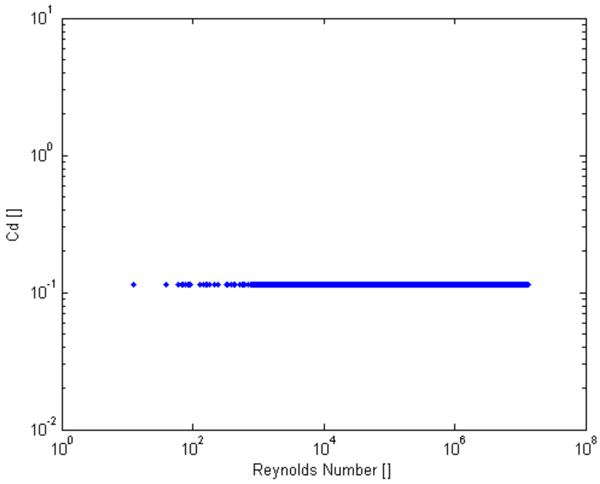

Figure 55: (a) Constant C_D, (b) Variable C_D vs Reynolds Number

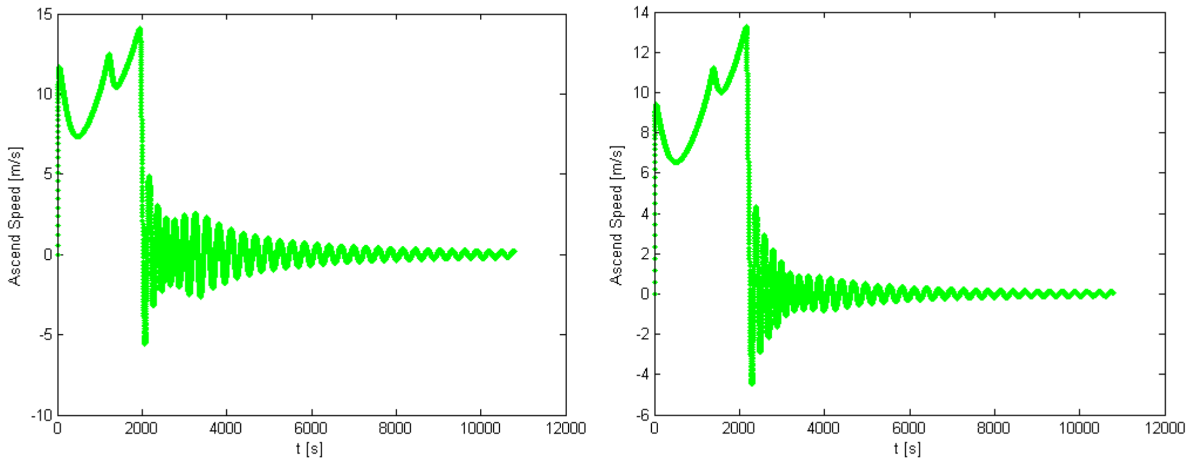

Figure 56: (a) Ascend Speed with Constant C_D, (b) Ascend Speed with Variable C_D

Figure 55 presents the simulated drag coefficient throughout a general zero-pressure flight against the Reynolds number. Figure (a) shows no relation towards the Reynolds number as it is a constant value. Figure (b) shows the variable drag coefficient as a function of Reynolds. Clearly this behavior agrees with the behavior of the drag coefficient of a sphere in Figure 33.

The effect both methods have on the overall flight of the aerobot is best shown through the ascend speed in Figure 56. The constant C_D, which is generally lower in value compared to the variable one, creates a higher ascend speed at launch compared to the variable C_D. Consequently, the aerobot with a lower C_D reaches its design altitude sooner than the aerobot with a variable drag coefficient. The aerobot with a higher C_D however stabilizes quicker, while the other aerobot continues to bob a little longer. An effect that will be discussed in the following section.

6.3.3. Floating and Balloon Bobbing

When simulating the aerobot's flight and nearing the design altitude, the aerobot will often overshoot the altitude due to momentum. The aerobot continues to move on around the design altitude as a sinus wave dampening out. Initially it was ascribed to the mathematical method used, and although step size does influence the amplitude of the overshoot, it never disappears when using a smaller step size. Personal correspondence with Rodger Farley [a.22] provided the following;

"Balloons can bob at float altitudes due to their inherent mass-on-a-spring behavior. Adiabatic expansion/compression is complicit in that if there is a perturbation in altitude, say upwards, there is an expansion and cooling of the gas which in turn contracts to reduce buoyancy. The balloon sinks, over travels the equilibrium point, and then compresses with an increase in temperature, increasing buoyancy.

The atmosphere as a body behaves similarly with so-called Vaisala-Brunt gravity waves, and when the wind blows over mountains the gravity waves can set up the perturbations necessary to disturb the balloon in the stratosphere. When the super temperatures are just right ($T_a = T_g$), vertical bobbing resonances can occur. Waves can occur in any medium in which the density decreases with height. If the restoring force is gravity, these waves are called gravity waves, sometimes referred to as buoyancy waves. The difference is that the density changes in the height direction and thus the magnitude of the wave changes with height. Vaisala-Brunt gravity wave oscillation periods vary with altitude and are in the order of 300 seconds at 30 km. This corresponds closely to zero pressure balloon bobbing frequencies."

When a balloon is at float, it is in a stable equilibrium much like a mass suspended on a spring. Disturbances such as first arrival to float or sunrise can start the balloon bobbing just as vibrating the suspended mass on a spring can do. The total mass in motion must be accounted for, which includes the gas mass and the amount of displaced air that gets dragged along, discussed in section 4.2.1.

For a simulated flight of a small aerobot of 10kg, a design altitude of 5km and keeping gas and atmosphere temperatures equal, this results in the bobbing phenomena of Figure 57 and Figure 58. The super-pressure balloon of Figure 57 will overshoot its altitude at first and then stabilize around the design altitude, leaving behind the distinct bobbing pattern in both the altitude and the ascend speed. As the ascend speed damps out to a value near zero, one can imagine that the altitude also returns to a stable value.

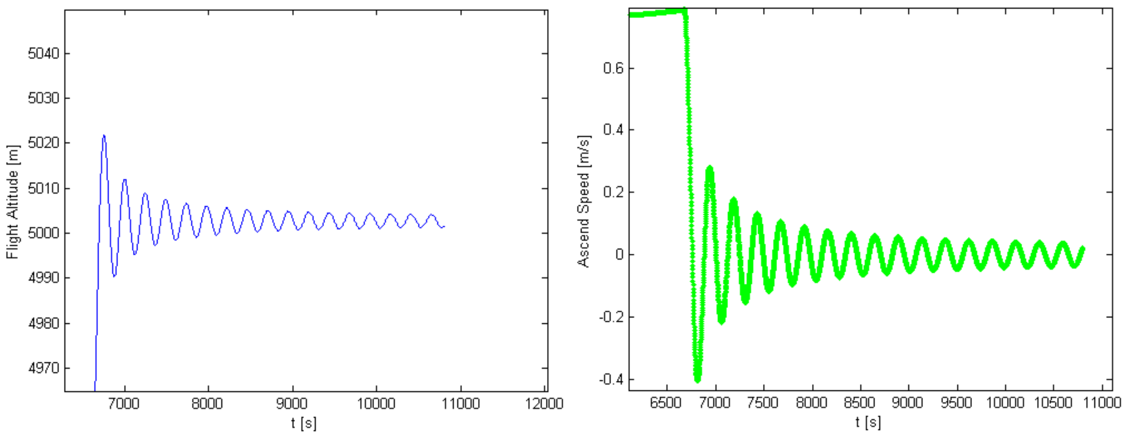

Figure 57: Super-Pressure Floating; (a) Flight Altitude, (b) Ascend Speed

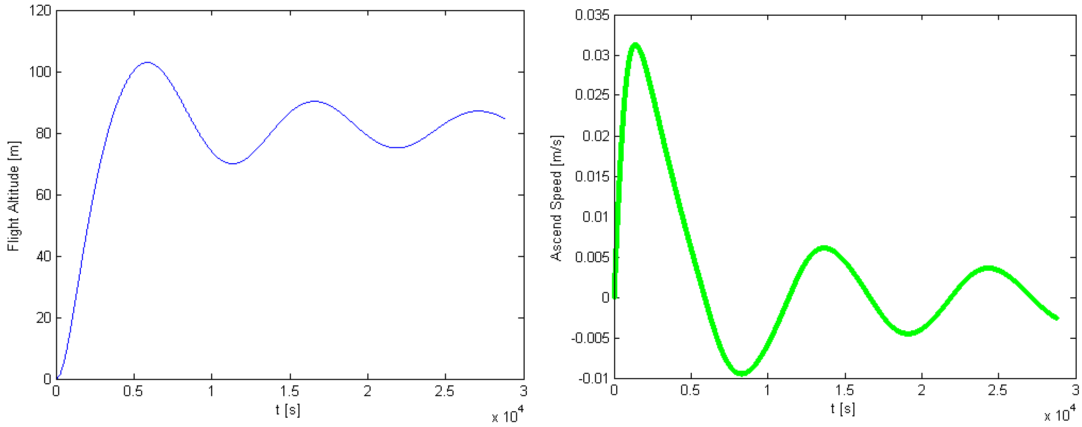

Figure 58: Zero-Pressure Floating; (a) Flight Altitude, (b) Ascend Speed

The same aerobot with a zero-pressure balloon tells a similar story with two exceptions; it's flight altitude and the oscillation period. The simulated aerobot has been given near-zero free lift and will therefore stabilize around an altitude which is below the design altitude. Zero-pressure balloons with free lift will create too much momentum and will overshoot their design altitude, release buoyant gas, and will never again stabilize around the design altitude or any other altitude. It will steadily fall back to earth due to a lack in lift. As discussed in section 2.1.2.1, when the temperature difference between atmosphere and lifting gas is ignored, a zero-pressure balloon will have an automatic stabilization point when it ascends, but it will not have a stabilization point when it descends. This is the reason why the balloon, which is lacking momentum or free lift, stabilizes around a lower altitude. Due to the altitude below its design altitude it will never release gas.

The zero-pressure balloon acts more slowly towards a stable altitude compared to a super-pressure balloon. This phenomena can be explained by the oscillation period of both. Although the float altitude differs in the examples above, the oscillation period can be deduced from the equations and graph obtained from the personal correspondence with Rodger Farley [a.22]. Figure 59 (a) shows a distinct difference in oscillation period between the super- and zero-pressure types for any given altitude.

For a zero-pressure balloon the bobbing period is calculated from;

$$KM_{zpb} = g \cdot \frac{\left[\dfrac{\left(\dfrac{dp_a}{dz}\right)}{R_g \cdot T_a \cdot \gamma_g}\right] \cdot \dfrac{\rho_a}{\rho_g} - \dfrac{d\rho_a}{dz}}{\rho_a \cdot (1 + C_{virtual})} \qquad Period_{adiabatic} = \frac{2 \cdot \pi}{\sqrt{KM_{zpb}}}$$

Equation 127: Zero-Pressure Bobbing Period

In which KM_{zpb} is the bobbing frequency of a zero-pressure balloon, $C_{virtual}$ is the virtual mass coefficient, ρ is the density, R_g is the specific gas constant, g is the gravitational acceleration, T is temperature, z is altitude, and γ is the heat capacity ratio.

For a super-pressure balloon the bobbing period is calculated from;

$$KM_{spb} = g \cdot \frac{-\left(\frac{d\rho_a}{dz}\right)}{\rho_a \cdot (1 + C_{virtual})} \qquad Period_{spb} = \frac{2 \cdot \pi}{\sqrt{KM_{spb}}}$$

Equation 128: Super-Pressure Bobbing Period

Using these equations the oscillation waves for zero- and super-pressure balloons were reproduced in Figure 59 (b). The type of atmosphere model however does influence the results, causing a non-linear result in the simulated reproduction.

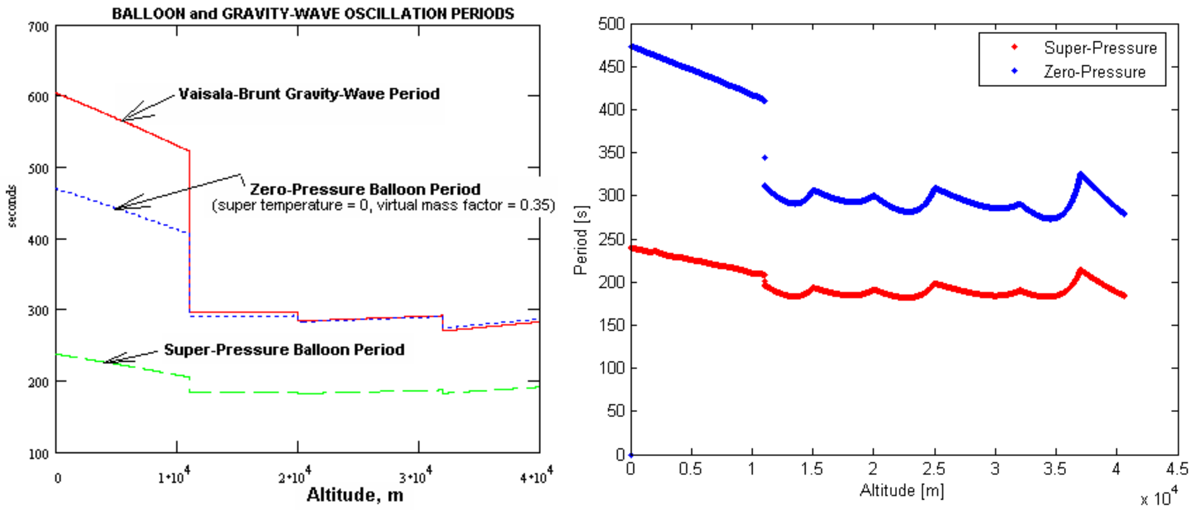

Figure 59: (a) Oscillation Periods by Rodger Farley, (b) Simulated Oscillation Periods

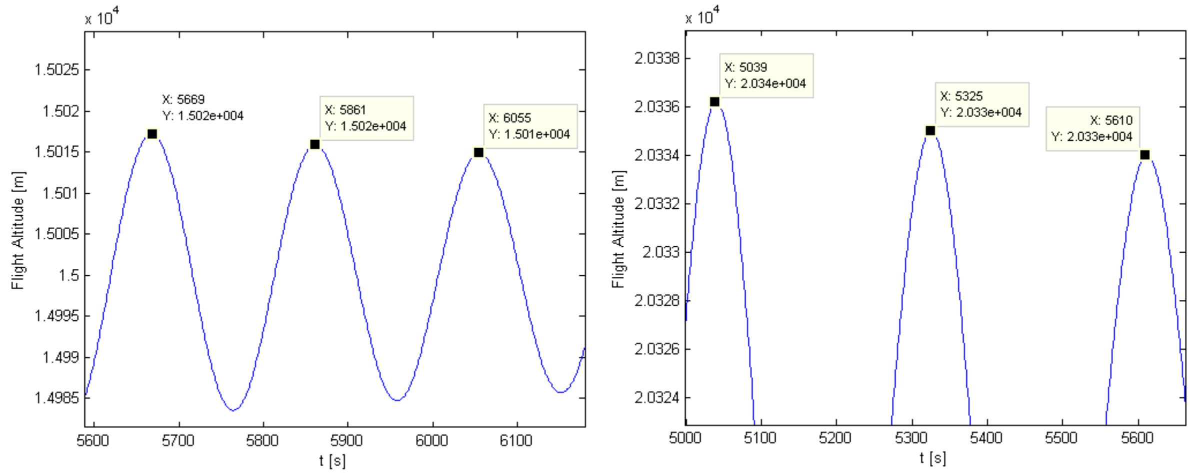

Figure 60: Oscillation Period; (a) SP at 15km, (b) ZP at 20km with temperature model

To test the effectiveness of BADS, the oscillation period of both super- and zero-pressure balloons was checked for a number of different altitudes. Zero-pressure balloons however are difficult to test for stable floating conditions, when no temperature model is included. Due to their momentum they always overshoot the design altitude and descend back to Earth after a gas discharge. When the gas temperature isn't set equal to the atmospheric temperature during flight the zero-pressure balloon however does stabilize due to the cooling of the gas which slows the balloon down. For a zero-pressure balloon with a design altitude of 20km, bobbing takes place at an oscillation period of about 300s. The super-pressure balloon shows a bobbing period of about 200s at a flight altitude of 15km. These results are similar to those presented in Figure 59.

6.3.4. Buoyant Gas Discharge

Of the three buoyant aerobot types in BADS, two can release buoyant gas through a duct, namely the zero-pressure and the over-pressurized-zero-pressure (OZP) aerobots. The zero-pressure balloon will release the gas as soon as the balloon reaches its maximum volume expansion to maintain a zero pressure level at the base. The OZP makes use of an overpressure valve, and will start to release the buoyant gas whenever the maximum overpressure on the valve is reached.

The zero-pressure balloon has to release gas to avoid an over-pressure and risk an envelope failure. By doing so it will affect the ascend speed, less gas means a lower lift force and therefore a lower ascend speed. Figure 61 represents a zero-pressure flight with an automatic gas release when the design altitude at 5000m is reached. Although the amount of gas released almost isn't noteworthy, the effect it has on the ascend speed and the steady drop in altitude is. The zero-pressure balloon 'with an overshoot of the design altitude and a gas release' will never return to its design altitude without a drop in ballast or an increase in buoyant gas.

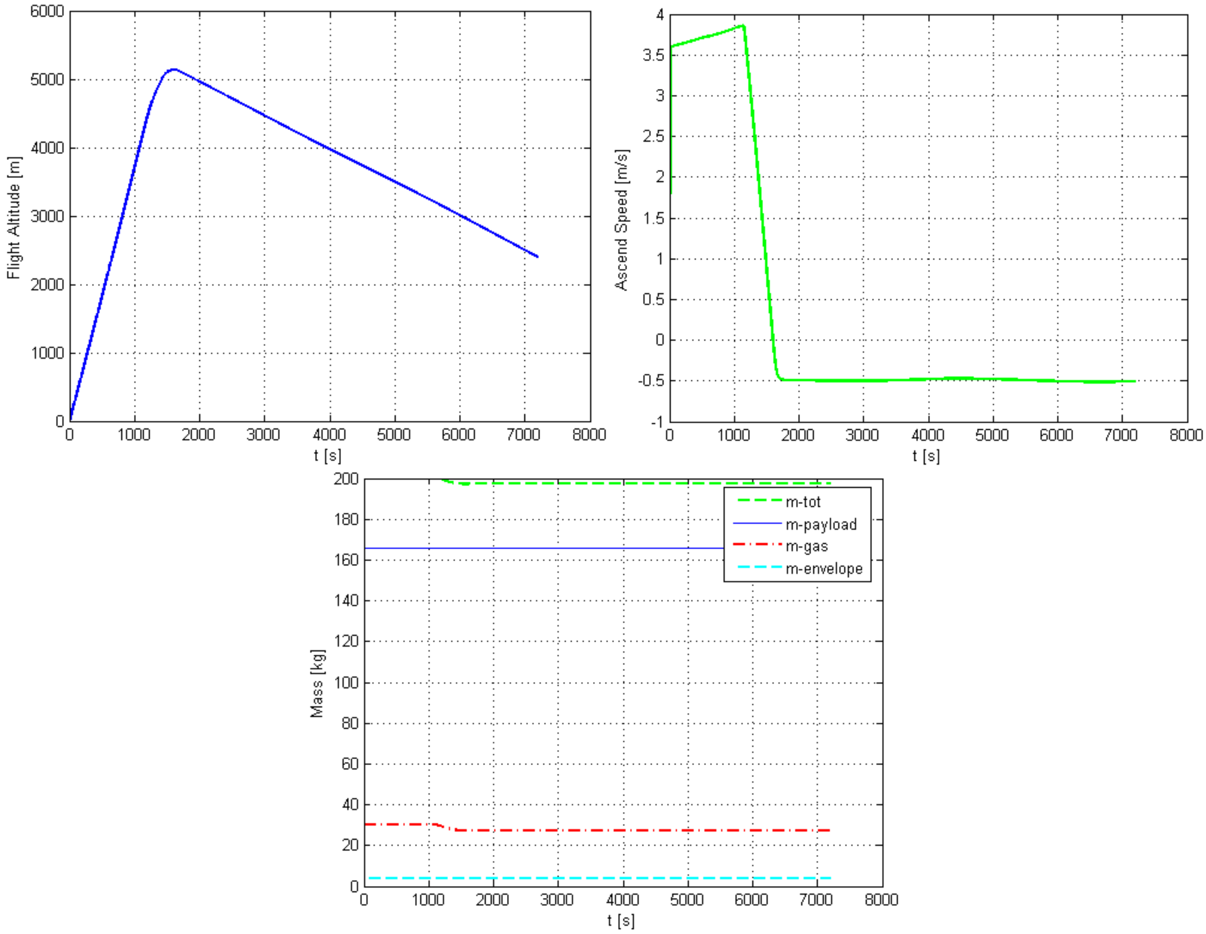

Figure 61: Zero-Pressure Gas Release; (a) Altitude, (b) Ascend Speed, (c) Mass

Figure 62 represents the same flight as before with an OZP aerobot. The OZP is a more stable type of aerobot with respect to the zero-pressure. It will build up a small amount of pressure before releasing the buoyant gas through a valve to avoid envelope rupture. Again the amount of buoyant gas discharged is not much, but it's enough to lower the ascend speed and to put the balloon to a standstill. The pressure in the balloon still reaches higher values than the atmosphere pressure at some times, but never high enough again to discharge more gas through the valve.

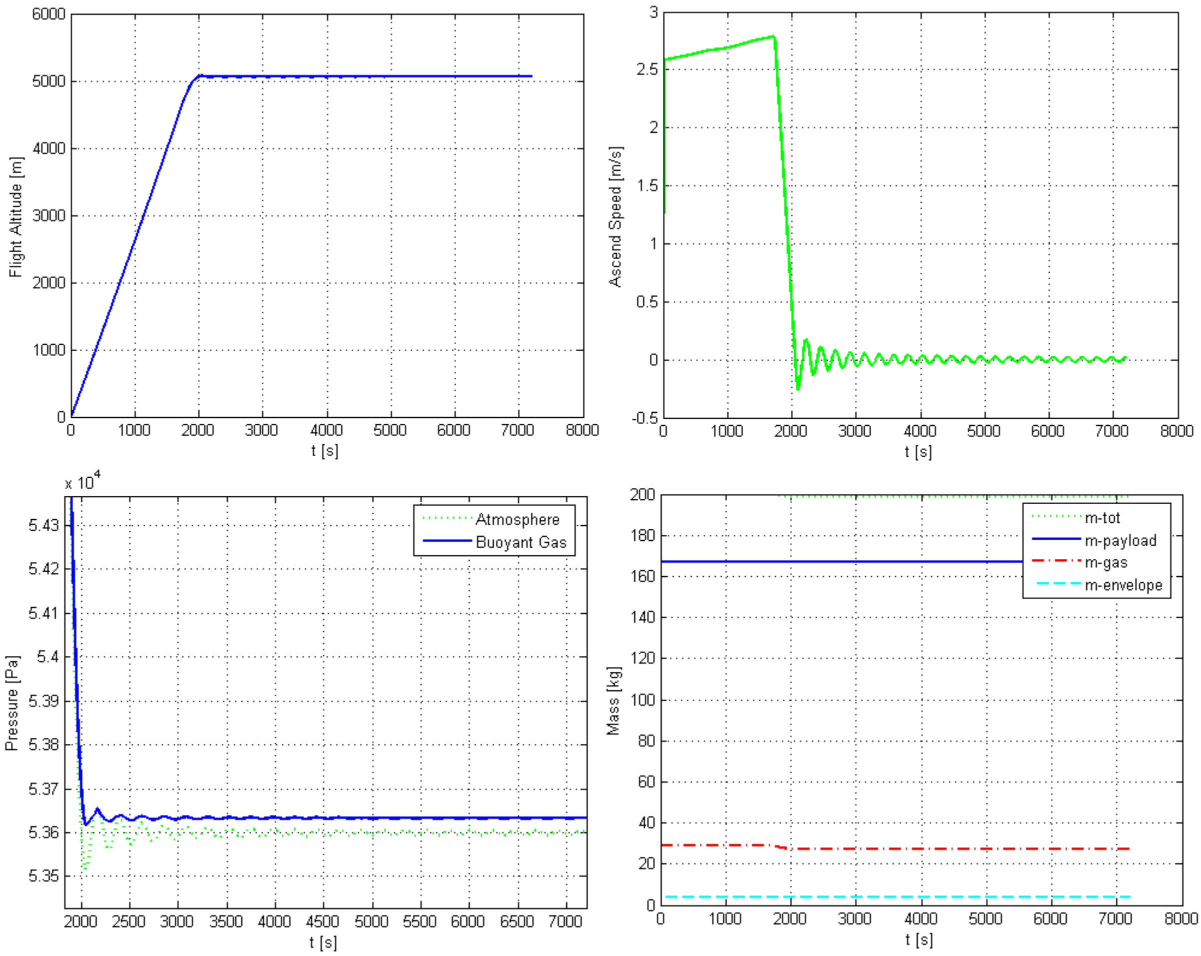

Figure 62: OZP Gas Release; (a) Altitude, (b) Speed, (c) Pressure, (d) Mass

6.3.5. Ballast Drop

An aerobot has a certain amount of payload onboard. In BADS, as mentioned in section 4.2.1, a portion of the payload is reserved for an amount of ballast that can be thrown overboard. The aerobot will behave in a typical way after a ballast drop. Due to the mass drop the buoyant lift force will increase, ascend speed will rise and drag will counteract. The flight altitude will go up until the ascend rate decreases again due to the drag and lack in buoyant lift at higher altitude.

Figure 63 shows the zero-pressure flight from before. When the aerobot is already in a descend after a small gas discharge, not visible but definitely present, a ballast drop takes place. The ascend speed rises immediately and in no time the aerobot crosses its design altitude. At that time the aerobot again discharges an amount of buoyant gas to limit the pressure inside the balloon. Soon after the

ascend speed drops back to its original speed. Again the aerobot goes in a downward direction and will go towards ground unless another ballast drop takes place.
A super-pressure balloon has a similar behavior with respect to the ascend speed. Each ballast drop presents a sudden rise in ascend speed. While a zero-pressure discharges buoyant gas, a super-pressure balloon doesn't. Therefore no loss in buoyant lift occurs and the balloon simply stabilizes itself around a new altitude, shown in Figure 64. This new design altitude however presents a higher pressure difference between the gas and the atmosphere. As long as the envelope fabric can handle this higher pressure difference the balloon is able to float at the higher altitude.

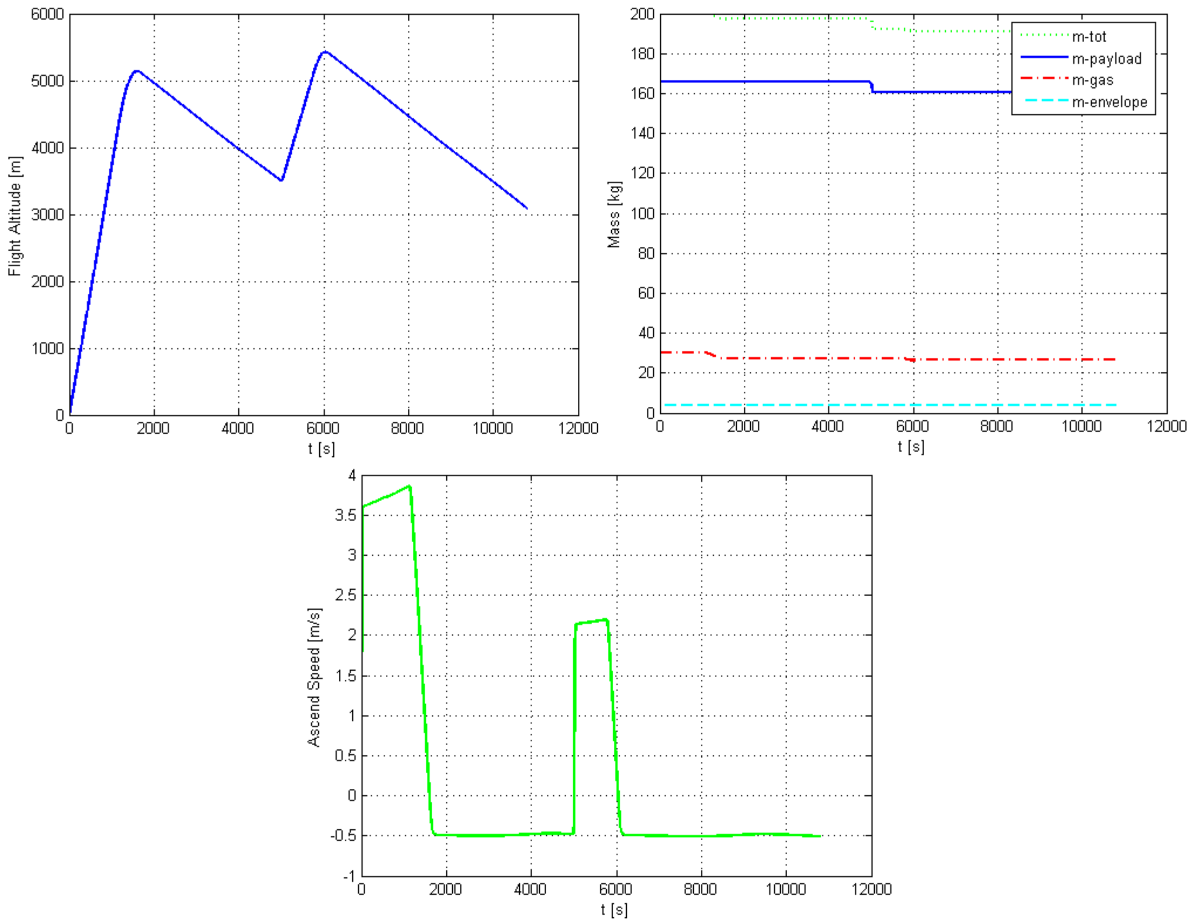

Figure 63: ZP Ballast Drop; (a) Altitude, (b) Mass, (c) Ascend Speed

The simulated behavior from ballast drops and the gas discharge in section 6.3.4 can be demonstrated through Figure 65 from Abe et al [b.5]. The figure illustrates the general behavior of a buoyant aerobot when subjected to gas venting and ballast drops. Near the initial design altitude the aerobot in Figure 65 is subjected to multiple small gas discharges to stop the ascend. Similar to the automatic venting for an OZP in BADS. This stops ascend and even starts a descend, verifying the statement that an aerobot that loses too much buoyant gas will commence its descend. A medium ballast drop however prevents this, and the aerobot starts to rise again. This behavior is similar to that of the SP in Figure 64. The aerobot will continue its rise and finally stabilizes around a new altitude.

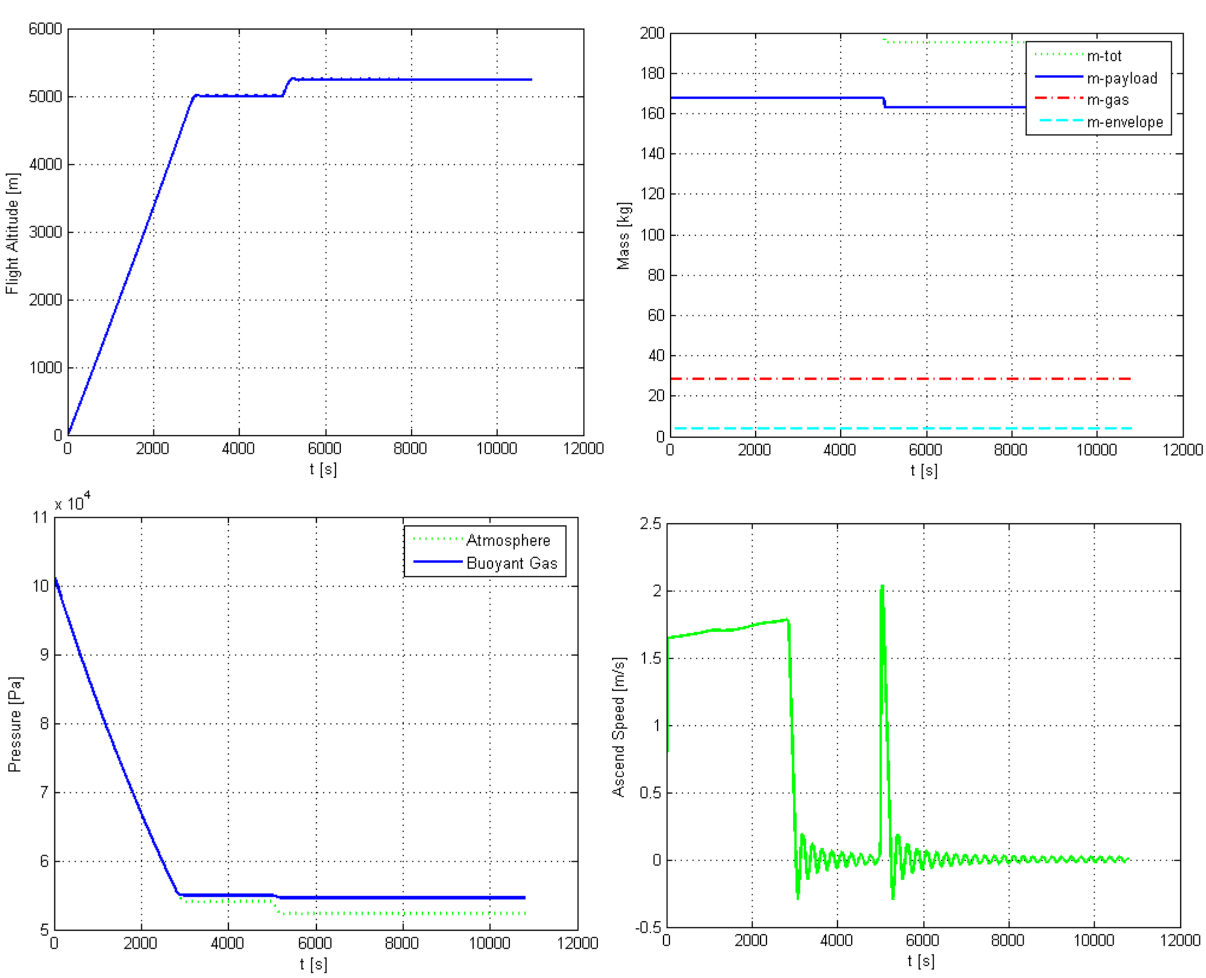

Figure 64: SP Ballast Drop; (a) Altitude, (b) Mass, (c) Pressure, (d) Ascend Speed

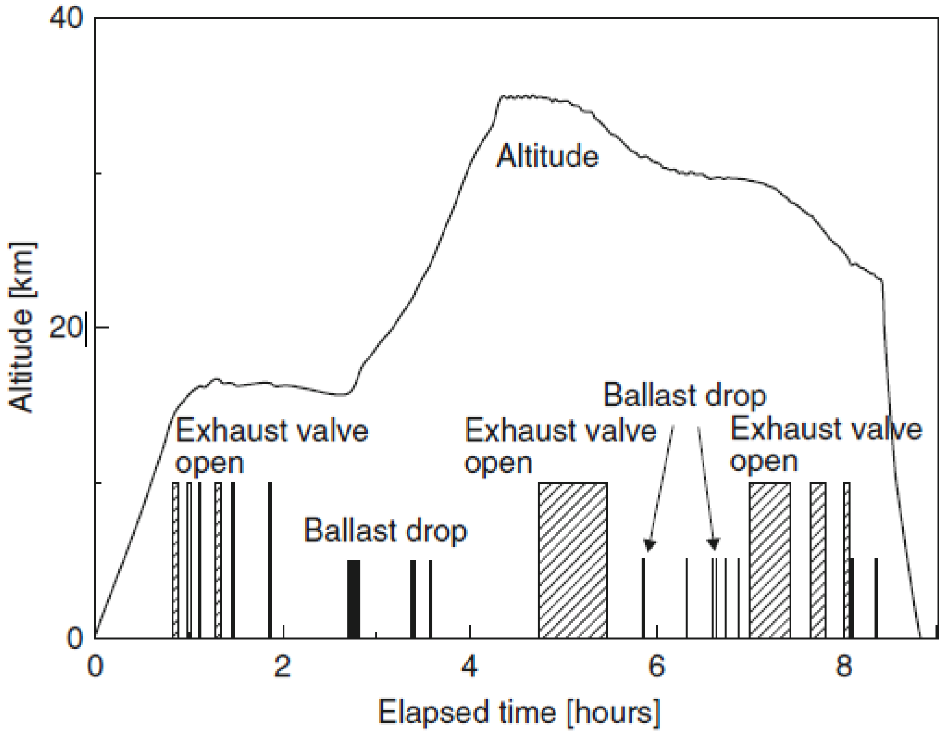

Figure 65: Venting and Ballasting Behavior Example [b.5]

A massive gas discharge then initiates its descend again. Even an OZP with a high enough over-pressure will start to descend after such a discharge. Although the aerobot in the example of Abe et al is descending, small amounts of ballast are dropped to slow down the descend. This has some effect but doesn't stop the descend initially. The user of BADS needs to be aware of this behavior when choosing the ballasting altitude for automatic ballasting, as mentioned in section 5.6. Dropping ballast at a very low altitude, or only dropping a limited amount of ballast, shall not give the aerobot enough time to recover to a positive velocity gradient.

6.3.6. Payload Parachute Descend

A small payload recovery module is integrated into BADS. When the program user wants to simulate an envelope failure a payload parachute descend will automatically be initiated. This module is currently only available for the OZP and ZP balloons as they are often selected for a high-altitude payload recovery mission. In the module envelope strain is not measured at this time, envelope failure will therefore be initiated once the maximum volume is reached for a zero-pressure balloon. The OZP failure mode will be initiated at the maximum balloon volume when a super-pressure of 2 times the design pressure is reached.

All buoyant gas mass will be lost when the balloon explodes or ruptures. This means that also the entire buoyant lift force is lost and the aerobot will start to free-fall! The vertical terminal velocity in free-fall, at a constant acceleration, is calculated from [a.7] and is rewritten for aerobot purposes;

$$V_z = \sqrt{\frac{2 \cdot m_{tot} \cdot g}{\rho_a \cdot C_{D_{parachute}} \cdot A_{xy_{parachute}}}}$$

Equation 129: Vertical Terminal Velocity during Parachute Descend

No extensive research has been done on parachute drag coefficients. Therefore the drag coefficient $C_{D_{parachute}}$ in BADS will be set to a general value of 1.75, which is based on NASA's literature [i.4]. Shape and size will influence the real value though.

Simulating a 'BADS parachute' in the program will be done by taking the top-half of the balloon at maximum volume as the reference area. Similarly the parachute mass is halve the balloon mass, as mentioned in section 5.6. In future, parachute specifics will be put into the program and better results will follow. Shape, size and mass of the parachute will influence the descend though.

The use of a parachute will definitely have a positive impact on the descend speed of the payload. It will slow down the descend through the drag of the parachute. Not using a parachute will be catastrophic for any payload dropping from high altitudes. Not using a big enough parachute however will be catastrophically too. Generally, a good payload descend speed is situated in the range of 3 to 4m/s [i.52].

The area effect is illustrated in Figure 66. One payload is dropped by means of a BADS parachute (a) and another payload is dropped with a parachute twice the size (b). The general BADS parachute has a high descend speed between 7 and 5.5m/s, too high for normal parachute criteria. Future improvements are therefore recommended. The parachute in Figure 66(b) has descend speeds between 5 and 3.9m/s and finally hits Earth with a speed of 3.9m/s. An acceptable speed.

It has to be mentioned that drop altitude will also play a role in the final descend speed at which the payload will hit the Earth. Drag increases when altitude drops and atmospheric density increases.

This influences the descend speed. The higher the drop altitude, the more time the parachute has had to slow down the payload to an acceptable level.

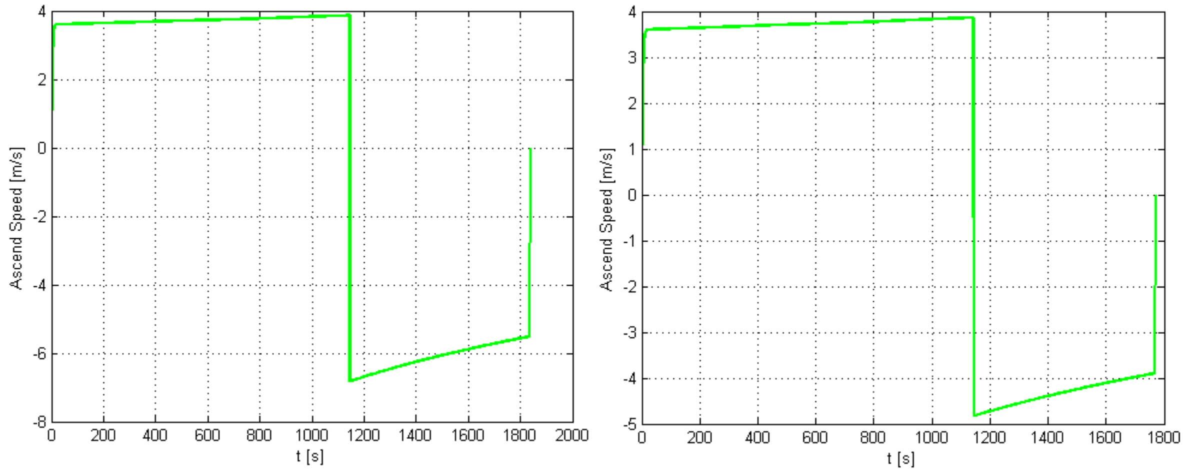

Figure 66: Parachute Descend; (a) Speed, (b) Speed with 2x Parachute Area

The parachute design can easily be improved by rewriting Equation 129 in function of the required parachute cross-sectional area;

$$A_{xy_{parachute}} = \frac{2 \cdot m_{tot} \cdot g}{\rho_a \cdot C_{D_{parachute}} \cdot V_z^2}$$

When a preferred descend speed is entered, the required parachute area can be found. In future a similar parachute can then be implemented in BADS, which would lower the descend speed to the preferred design value.

6.4. Flight Simulation Validation Process

The general flight behavior of a buoyant aerobot is quite difficult to simulate because of the huge amount of parameters that have to be taken into account. If every parameter is modelled such that it is based on all its variables, then and only then, the simulation might represent a realistic aerobot flight. The scientific community has the knowledge to model such a flight simulation tool but often holds onto this information. The amount of balloon ascend programs available to the public are therefore limited. Two balloon flight simulations modelled by NASA and the Wallops Flight Facility are of great importance to the scientific ballooning community, namely; SINBAD [a.36] and Balloon Ascent [a.22].

Scientists and engineers around the world have attempted to model a number of specific balloon ascend simulation tools that are similar to SINBAD or Balloon Ascent. Palumbo's [t.4] ACHAB program is one such example.

The mentioned simulation tools above will be used in the next subchapters to validate the BADS tool. Each program however makes use of its specific input parameters, and calculation methods. To effectively compare BADS with any of these programs an adjustment to the input module had to be carried out to ensure the data would be similar for all programs to make valid comparisons. Nevertheless some input parameters or environment parameters are not available. This will cause some inconsistencies in the output data.

6.4.1. SINBAD, Balloon Ascent, ACHAB

To explain both SINBAD and Balloon Ascent completely would be outside the scope of this thesis. Garde [a.38] made a good summary of, and comparison between, both programs. Further information about Balloon Ascent was found from Farley [a.22], while Raqué and Robbins [a.36] go into depth about SINBAD.

Both programs originate from within the ULDB program and are related to the NASA Wallops Flight Facility. SINBAD is not the first flight simulation program but is based on two predecessors; THERMTRAJ [a.37] and ALTIME. “THERMTRAJ is a Fortran computer program that was developed in the early eighties. It was used by NASA to compute the trajectory of high altitude scientific zero pressure balloons. In addition it was capable to compute balloon gas and film temperatures during flight. The program had the ability to account for ballasting, changes in cloud cover, variable atmospheric temperature profiles, and both unconditional and scheduled venting of the balloon gas [a.37].” “During the mid-eighties THERMTRAJ was modified and renamed to ALTIME . In 1989 Raqué merged ALTIME with a stress index program. The combined program was called SINBAD [a.36].”

“Balloon Ascent has been developed by NASA employee, Rodger Farley. Balloon Ascent, unlike other flight simulation codes, does not rely on SINBAD to simulate a balloon flight. Farley independently developed this software from first principles. Balloon Ascent uses similar input parameters to SINBAD, but provides different simulations [a.38].” Some of the more prominent changes and features compared to SINBAD are; a Super-pressure/Zero-pressure distinction, wind direction/speed at altitude, planetary specificity, and the use of actual material properties. Especially the improvement of the up to date material properties has a big influence on the performance of the simulation according to Garde [a.38].

SINBAD and Balloon Ascent make use of a graphical user interface (GUI) which makes them very user friendly. The GUI makes use of comprehensive input and output screens both graphical and numerical. Further, clickable text or tabs create pop-up window that contain a low number of input parameters per topic. “Both programs neatly display general descriptions of inputs next to their text boxes. Upon completion of inputting parameters, simulation files may be saved for future use and a simulation can begin [a.38].” Layouts and esthetics however are not the main goal of these programs, the accuracy of the output data is.

While SINBAD definitely has the advantage of a development process of more than 20 years, Balloon Ascent has the advantage of using the latest available data and lessons learnt from the SINBAD development process. Garde summed up the advantages and disadvantage of both [a.38].

Next to these two professional programs of NASA another elaborate tool was found to evaluate BADS with. Analysis Code for High-Altitude Balloons (ACHAB) is a flight simulation software tool developed by Palumbo [t.4] to predict the flight trajectory and thermal behavior of high-altitude zero pressure balloons. Its equations seem to be based on those of Balloon Ascent. The program also makes use of a very effective variable drag coefficient which makes the results more realistic when compared to an actual balloon flight.

From the obtained information a list of features, improvements and tools available to SINBAD, Balloon Ascent and ACHAB was compiled. This list is compared to the capabilities of BADS in Table 36. Any discrepancies are due to a lack of information on the topic though.

Table 36: Program Capability Comparison; SINBAD, Balloon Ascent, BADS

Features	SINBAD	Balloon Ascent	ACHAB	BADS
Environment				
- Earth Atmospheric model	x	x	x	x
- Non-Earth Atmospheric models	x	x		x
- Wind Models		x	x	basic
- Launch Location/Date/Time		x	x	basic
- Day/Night Cycle		x	x	basic
Thermal Model				
- Cloud Modification	x	x		x
- Buoyant Gas Thermal Properties	x	x	x	x
- Convection	x	x	x	basic
- Envelope Optical Properties	x	x	x	x
- Solar Properties	x	x	x	x
Trajectory				
- Vertical Motion	x	x	x	x
- Horizontal Motion	?	x	x	x
- Variable Drag Coefficient			x	basic
- Powered Flight				basic
- Parachute Descend				x
Geometric Properties				
- Spherical Shape	x	x	x	x
- Natural Shape		x	x	
- Pumpkin Shape (Oblate)		x		x
- Airship Shape (Prolate)				x
- Volume Change	x	x	x	x
- Envelope Strain	x	x		
Envelope Material/Buoyant Gas				
- Multiple Materials	x	x	x	x
- Multiple Buoyant Gases	x	x	x	x
Balloon Systems				
- Zero-Pressure	x	x	x	x
- Super-Pressure	x	x		x
- OZP	x	x		x
- Automatic Venting	x	x	x	x
- Automatic Ballasting	x	x	x	x
- Manual Venting	x	x	x	
- Manual Ballasting	x	x	x	x
Software				
- Graphical User Interface	x	x		
- Graphical Output Data	x	x	x	x
- Text-file Output Data	x	x	x	x

6.4.2. Comparing Simulation Data; ACHAB Illustrative Example

The easiest way to validate the simulation program would be by comparing the simulation results to real life data. A meteorological balloon with an onboard computer can acquire the atmospheric and flight data. Test such as these were outside the scope of this thesis and therefore validation has to be done by means of acquiring the data from available aerobot missions.

The way in which flight data is presented will give a number of problems. First, not all balloon data might correspond with the input parameters of the simulation program. A workaround has to be made to get a similar balloon design and flight. Secondly, the weather during the day of flight can influence the data considerably. The data will then be out of order compared to the data of the simulated atmosphere model in BADS.

Palumbo [t.4] has done a very detailed comparison between SINBAD and ACHAB and some real balloon flights in Earth's atmosphere. The data obtained from his research will be compared to the BADS tool output data in section 6.4.3.

First BADS and ACHAB themselves will be compared to each other by an illustrative example from Palumbo. This will help identify the main inconsistencies between both tools before commencing the actual evaluations and validations through real mission data in the following section.

The exact input data used for the illustrative example can be found from Palumbo [t.4]. The ACHAB input parameters that were similar to those of BADS have been used as such, and are presented in Table 37 and Table 38.

Table 37: ACHAB Example Thermo Optical Data

Envelope Thermo-Optical Data		
$\alpha = 0.024$	$\alpha_{IR} = 0.1$	$c_e = 2092$ [J/kgK]
$\tau = 0.916$	$\tau_{IR} = 0.86$	

Table 38: ACHAB Example General Input Data

Mass Budget [kg]		Balloon & Flight Settings	
m_{gross}	4487	Volume	334705 [m^3]
$m_{envelope}$	1433	Altitude	~31000 [m]
m_{gas}	798.63	Free Lift Percentage	11 [%]
m_{tot}	5920	$C_{virtual}$	0.37 []
Ballasting Data		**Initial Settings**	
$t_1 = 5000$s	150 [kg]	x_0, y_0, z_0	0
$t_2 = 13000$s	350 [kg]	Vx_0, Vy_0, Vz_0	0
Ballast Rate	13.1 [kg/min]	Date of Launch	16-01-2006

The following adjustments had to be made to BADS to be able to compare both programs to some degree;

- Manual venting had to be added, as no such option was available in BADS. No valve specifics are being used. A general approach is used to simulate results similar to venting through valves. An automatic venting process is available in BADS, but only vents gas due to overpressure.
- A constant drag coefficient for BADS had to be assumed to resemble the variable drag coefficient in ACHAB as close as possible. C_D is therefore been set to 0.8 [a.22]. This resembles a rising spherical balloon with varying volume and shape the best as possible.

The graphical representation of the balloon's flight in Earth's atmosphere is represented in Figure 67, with the ACHAB data on the left and BADS simulation on the right, which will be the set-up of all following figures.

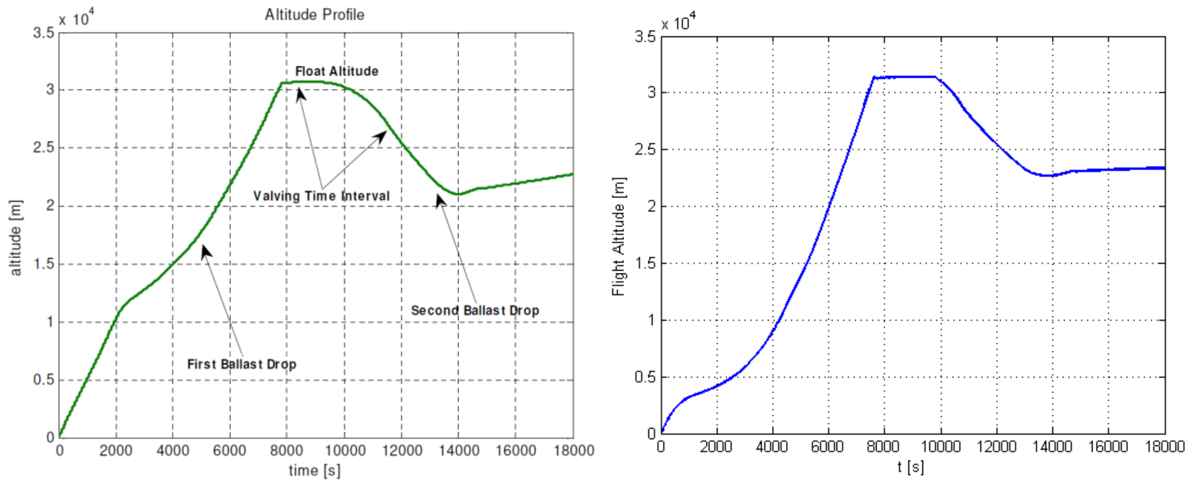

Figure 67: Illustrative Example; (a) ACHAB Altitude, (b) BADS Altitude

Altitude in ACHAB rises steadily, while altitude in BADS tends to be slowed down below 5000m. Initially thought to be caused by the high drag coefficient used, it turns out not to be the case, as other values were tested and the feature remained. Initial starting speeds however are influenced by the drag coefficient. A theory of what's causing this might be the impact of the high initial velocity on drag. A high initial velocity can cause a high counteracting drag value, limiting the lift force at launch. The effect still has to be investigated further before any changes to the program can be made though. Continuing this analysis with the following parameter; ascend velocity.

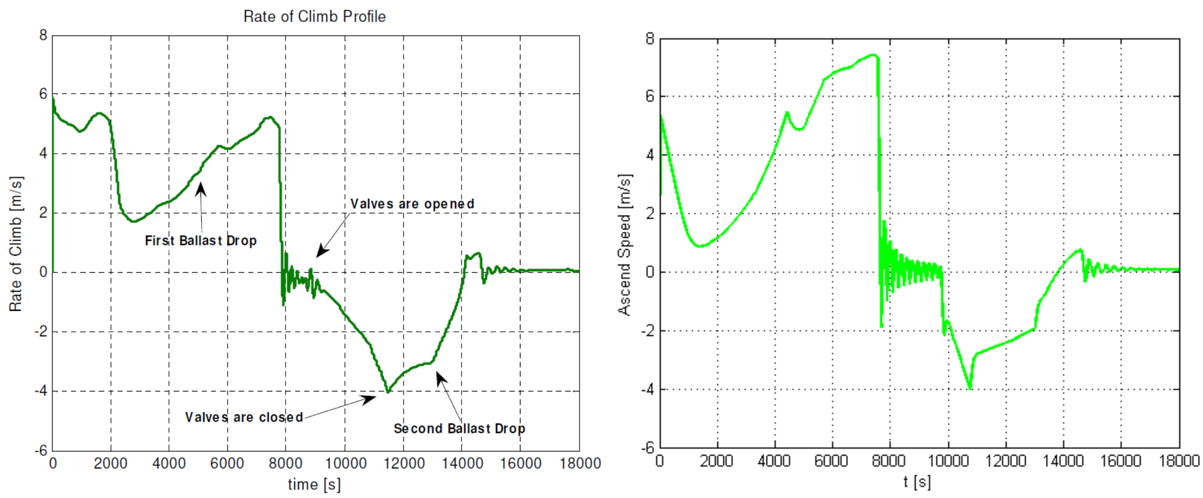

Figure 68: Illustrative Example; (a) ACHAB Ascend Speed, (b) BADS Ascend Speed

The ascend velocities, graphically represented in Figure 68, tend to be similar for both tools, with an exception of the first 2000 seconds. BADS's velocity drops towards 1m/s immediately after launch, where ACHAB's velocity remains around 5m/s before making the dive to 2m/s, 2000s later than BADS. It is also in this timeframe that the altitude shows the above mentioned irregularity.

Afterwards both simulated speeds increase to their maximum, where BADS again overshoots ACHAB's speed with 2m/s. Both simulations however reach their maximum altitude and maximum speed around the same time. Ascend speeds drop immediately to the bobbing velocity around zero, when the balloon stabilizes itself around the design altitude.

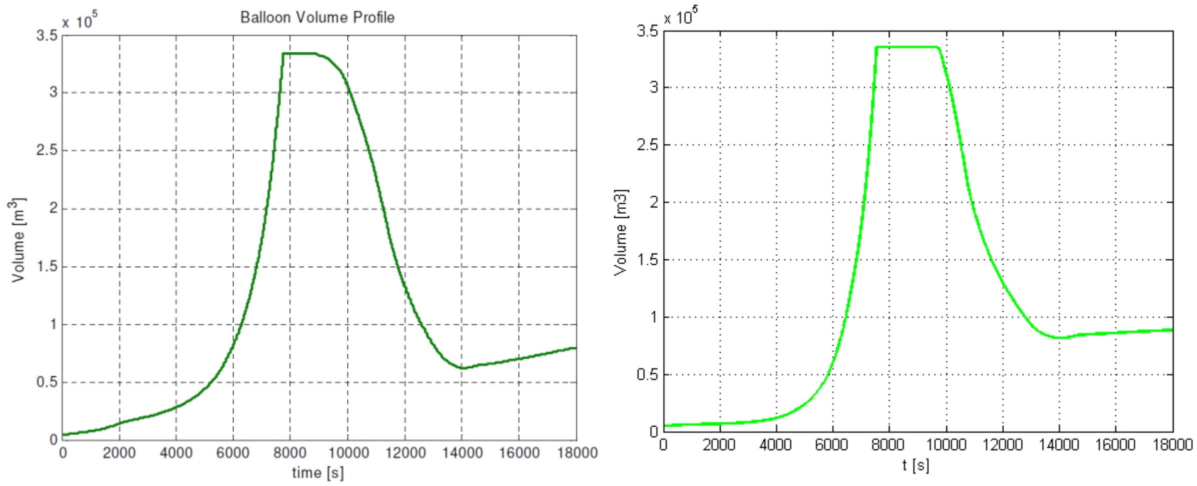

Figure 69: Illustrative Example; (a) ACHAB Volume, (b) BADS Volume

Similar to the timeframe of reaching maximum altitude and speed, also the maximum attainable balloon volume is reached. The effect of a slow launch in BADS is also visible here in the first 2000s where volume almost stays constant.

A small but visible effect on the balloon volume is the fact that the maximum volume is managed a while longer in BADS than in ACHAB. The reason for this is part of the venting adjustment that had to be made. As no vents are incorporated into the program, no dimensions or steady mass flow can be selected. The gas mass flow that is simulated in BADS linearly releases the gas over a similar timeframe than ACHAB, as seen in Figure 70. This causes over-pressure in the balloon which preserves the maximum volume of the balloon a while longer.

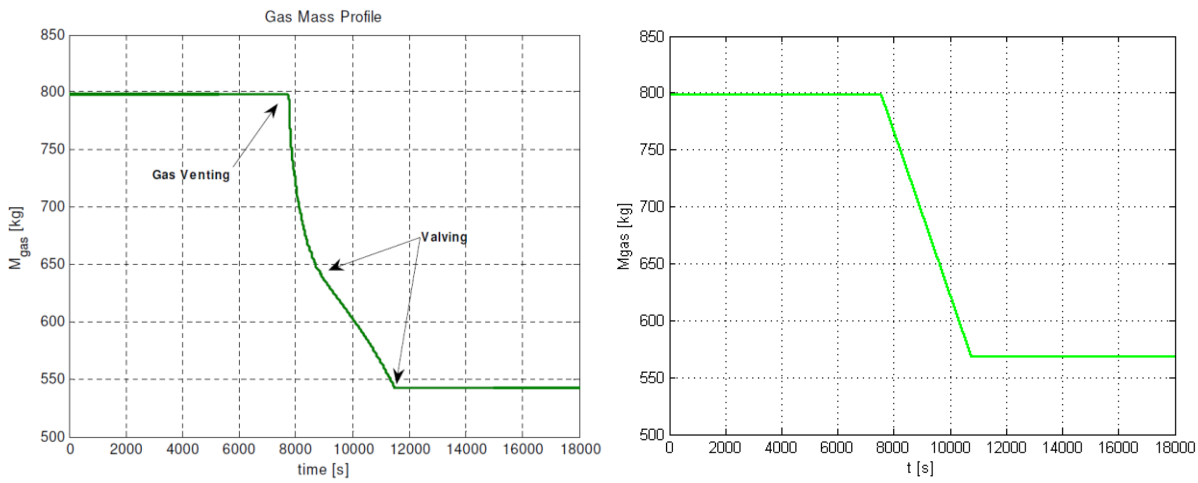

Figure 70: Illustrative Example; (a) ACHAB Gas Mass, (b) BADS Gas Mass

Over-pressure makes for a more stable flight regime. When the over-pressure is lost, unstable behavior quickly returns. BADS is very sensitive to losses in gas mass, especially on zero-pressure balloons. This is visible in the ascend speed, when ACHAB gently decelerates the balloon during venting, BADS will descend suddenly when the build-up over-pressure is lost.
Once the minimum speed is reached at -4m/s all gas valves in ACHAB close. This is also the reason why less gas is released in BADS than in ACHAB. -4m/s is reached here sooner so less gas is released. If no such boundary condition is used BADS will continue to dump gas mass, but will reach a much lower speed value due to venting.

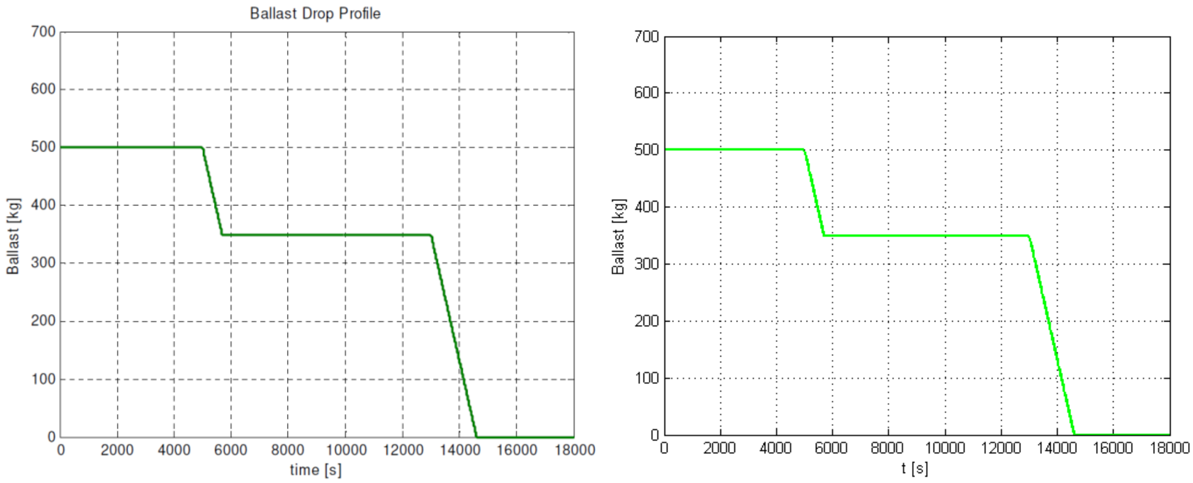

Figure 71: Illustrative Example; (a) ACHAB Ballast, (b) BADS Ballast

Both simulations increase their speed towards positive values next. BADS does this more aggressively than ACHAB but that difference is cancelled out as BADS returns to a slower approach afterwards.
Ballast drops throughout the simulation are exactly the same for both tools. The response of BADS to changes is more instant, aggressive, a bit unstable even, while ACHAB lacks the instability and reacts more gradually on changes. On average however BADS always reaches the same altitude, ascend speed or any other parameter after it stabilizes from any sudden change.
The reason for the fragile stability in BADS might originate in the thermal model. Here the main dissimilarity between ACHAB and BADS can be found. Though we can’t disregard the possible effect the different atmosphere models and mathematical methods used in both tools have on the results, thermal modelling is known for its instable and difficult simulation behavior.
It has to be said however that BADS’s thermal model has its influence on the simulation and its results. Smaller time steps were required to preserve stability each time the thermal model was included in the simulations. More specific, the use of the thermal model forced the programmer to run each simulation with a time step of 1s. Time steps either smaller or larger where not appropriate.
Figure 72 shows the temperatures of the envelope or film, the buoyant gas, and of the atmosphere for BADS. The first difference originates in the atmospheric model, as BADS starts with a 10 degree higher day temperature compared to ACHAB. Further, atmospheric differences are not comparable due to a lack in information from Palumbo [t.4] on this subject. It has to be assumed that there are additional differences though.

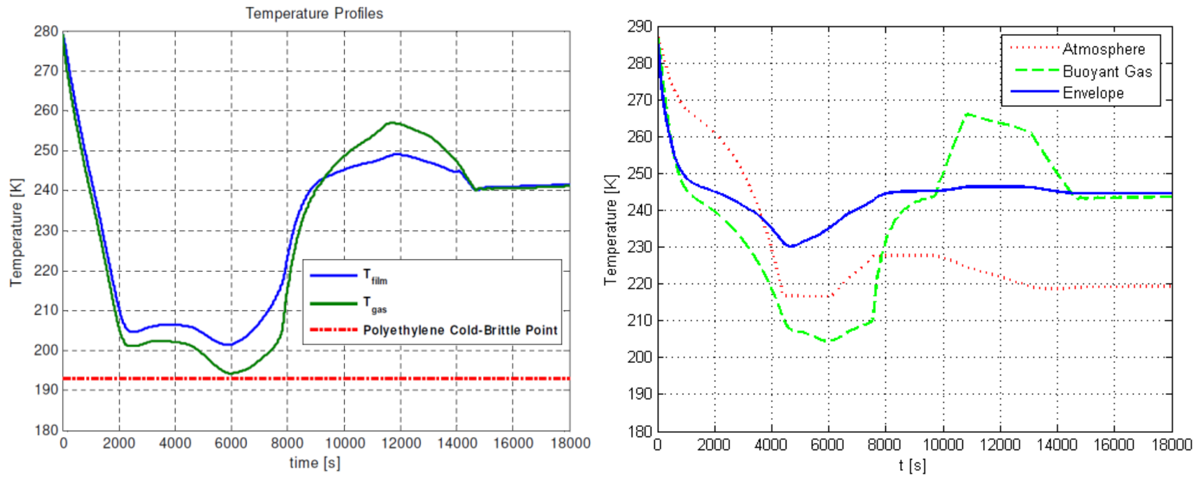

Figure 72: Illustrative Example; (a) ACHAB Temperatures, (b) BADS Temperatures

The initial temperature behavior is similar in both tools. Gas and envelope temperature drop simultaneous towards their minimum. Halfway the drop however, BADS's envelope temperature stabilizes to a higher value than that in ACHAB, indicating a higher intake of solar heat, while the temperature of the buoyant gas continues to drop due to volume expansion. Again both BADS temperatures drop at a lower slope than temperatures in ACHAB. The temperature drop in BADS takes about twice the time, similar to the behavior of ascend speed and altitude.

Again it has to be said that when all sudden changes such as mass and gas drops are done, the results of both tools stabilize themselves around similar values.

Both ACHAB and BADS have their similarities. The ACHAB tool is however a much more stable tool than BADS. Nevertheless, the end results of BADS can be used as an initial, rough estimation of a buoyant balloon flight. Chapter 7 will further explore what effect a modification of the temperature model and the atmosphere model will have on the results.

All variations between the programs are limited to the flight simulation and do not affect the initial aerobot design. Only the amount, or lack of, input parameters has an effect on the design. A thorough improvement of BADS should therefore focus on the dynamical model, the atmospheric model and the thermal model.

Now that the biggest problems and inconsistencies in BADS have been identified, the validation process of the BADS tool can continue, bearing in mind the limitations of the program.

6.4.3. Comparing Simulation Data; HASI 2003

The high altitude balloon, actually flown, compared to SINBAD and BADS is the HASI (Huygens Atmospheric Structure Instrument) 2003. It was a high altitude balloon mission which had to simulate the Huygens probe mission on Titan in the terrestrial atmosphere. The data available from HASI through Palumbo was limited. Weather and atmospheric conditions were not available, nor was the ballast history, total mass and envelope mass. The envelope had the same characteristics however as the one used before, according to Palumbo. From the balloon volume and the design altitude, the total mass was therefore calculated to be 1340.1kg. Using Equation 109 and the available free lift percentage the gas mass was calculated. From the mass breakdown it was then possible to calculate the envelope mass.

Table 39: ACHAB HASI 2003 General Input Data

Mass Budget [kg]		Balloon & Flight Settings	
$m_{payload}$	607.5	Volume	98862 [m^3]
$m_{envelope}$	528.61	Altitude	~32000 [m]
m_{gas}	203.99	Free Lift Percentage	12 [%]
m_{tot}	1340.1	$C_{virtual}$	0.37 []
Ballasting Data		**Initial Settings**	
/		x_0, y_0, z_0	0
		Vx_0, Vy_0, Vz_0	0
		Date of Launch	07-06-2003

For the comparison between BADS and the obtained results of ACHAB, HASI and SINBAD, a constant drag coefficient was used; C_D = 0.45. This coefficient is also used by SINBAD. The variable drag coefficient integrated in BADS, and based on the Reynolds number, wasn't able to represent similar values to those of ACHAB. The drag coefficient modelled in BADS tends to underestimate the actual drag value. During ascend, high velocities are achieved and high Reynolds numbers follow from it, generally lowering the drag coefficient, consequently resulting in an underestimated drag coefficient. A better model which would take into account the shape and size is recommended for future work. The HASI 2003 flight results can be found in Figure 73 and Figure 74, together with ACHAB, SINBAD and BADS results.

As only a graphical comparison of altitude and ascend speed was available from Palumbo [t.4] it is difficult to explain each small inconsistency in the graph. The lack of data on temperatures, buoyant gas loss, drag coefficient and atmosphere conditions, which all influence the balloon flight tremendously, also limits the assessment of the data above. However, with the variations between BADS and ACHAB defined in section 6.4.2, a general analysis can be made between ACHAB, SINBAD and BADS results.

The initial speed of BADS is similar to that of SINBAD, while those of ACHAB and HASI start somewhat lower. BADS immediately returns to its well-known descend towards lower values, seen in section 6.4.2. Which is suspected to be a result of a combined drag and thermal problem. As mentioned before, the high initial speed is immediately counteracted by the drag force. Additionally the thermal drop in gas temperature, due to volume expansion, contributes to the drop in lift force.

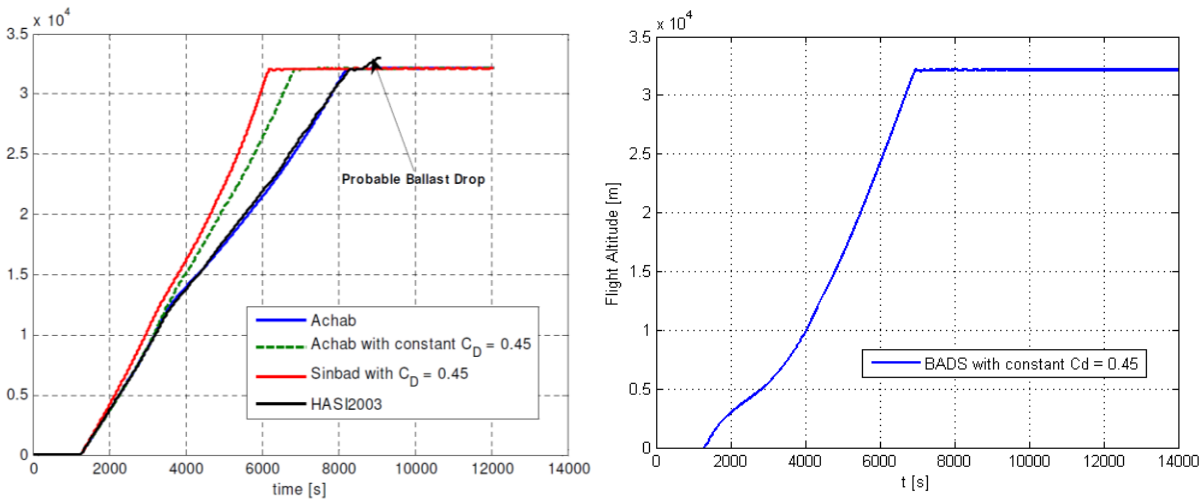

Figure 73: (a) Altitude [t.4], (b) BADS Altitude Simulation

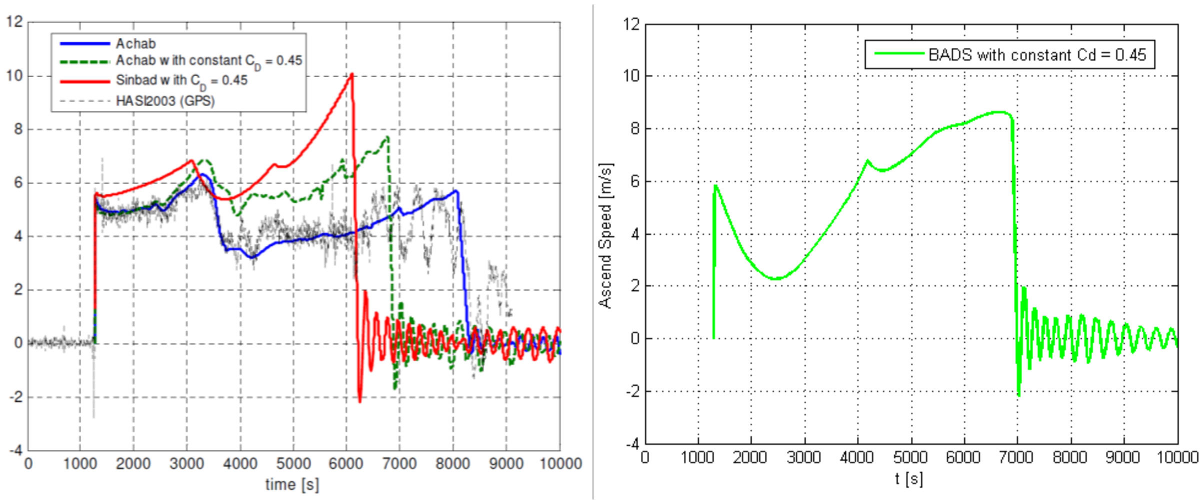

Figure 74: (a) Ascend Speed [t.4], (b) BADS Ascend Speed Simulation

Due to the underestimation of the velocity early-on, BADS will start to return velocity values that overestimate the real values for the remainder of the rise. This makes up time for the slow launch and eventually the aerobot arrives at the design altitude in a similar time to ACHAB with constant C_D. "Comparisons between ACHAB and SINBAD using the same set of input parameters show that SINBAD typically tends to estimate an overall rate of climb greater than ACHAB leading to an early arrival at the float altitude. Typical ascend speed differences between the two tools are of the order of 1 m/s . Conversely, comparison between ACHAB and actual flight data show that this tool is in good agreement with experimental data with a mean error on the rate of climb of about 0.1 m/s [t.4]." A similar study between BADS, ACHAB and SINBAD from the HASI study, results in;

Table 40: Ascend Speed Comparison on HASI

	$V_{initial}$ (t=1300)	V_z (t=2500)	V_z (t=4000)	V_z (t=6000)	V_z (t=8000)	Average
BADS	5.85m/s	2.30m/s	6.00m/s	8.25m/s	0.00m/s	
ACHAB C_D=0.45	~5.40m/s	~5.10m/s	~5.00m/s	~6.20m/s	-0.90m/s	
Difference	0.45m/s	-2.80m/s	1.00m/s	2.05m/s	0.9 m/s	1.44m/s
BADS	5.85m/s	2.30m/s	6.00m/s	8.25m/s	0.00m/s	
SINBAD	~5.70m/s	~6.00m/s	~5.70m/s	~9.80m/s	~0.00m/s	
Difference	0.15m/s	-3.70m/s	0.30m/s	-1.55m/s	0.00m/s	1.14 m/s
ACHAB C_D=0.45	~5.40m/s	~5.10m/s	~5.00m/s	~6.20m/s	-0.90m/s	
SINBAD	~5.70m/s	~6.00m/s	~5.70m/s	~9.80m/s	~0.00m/s	
Difference	-0.30m/s	-0.90m/s	-0.70m/s	-3.60m/s	-0.90m/s	1.28 m/s

From Table 40 it can be stated that the statement of Palumbo about ACHAB and SINBAD is quite correct, with an average difference of 1.28m/s. The difference between ACHAB and BADS varies with time, but it can generally be stated that the biggest differences occur at 2000s and 6000s, which is just after launch and just before float. On average BADS and ACHAB differ about 1.44m/s which isn't too bad if one considers the difference between ACHAB and SINBAD to be 1-1.28m/s. The difference between BADS and SINBAD is even lower. This would indicate that BADS's accuracy and performance currently stands closer to that of SINBAD than that of ACHAB.

Detailed BADS results are not of equal accuracy as the real HASI flight, or any of the simulated results from ACHAB. On average though, the simulated aerobot reaches its design altitude in a timeframe better than SINBAD and almost equal to ACHAB with constant drag coefficient.

6.4.4. BADS Validation Conclusions

The BADS tool is intended to design buoyant aerobots and to explore the behavior of the designed aerobots in different atmospheres. The goal to design buoyant aerobots, and more specifically define their mass breakdown and volume for a specific flight altitude, has been achieved. From section 6.2 it can be concluded that the design is mostly dependent on the atmospheric influences, which can only be improved with a better atmospheric model or day to day measurements. Other design improvements can be achieved by adding some extra design parameters such as; safety factors or construction factors, better and more extensive material properties, etc.
The second goal of BADS, exploring the buoyant behavior, and more specifically simulating the flight path of a buoyant aerobot, has been partially achieved. The general behavior of a buoyant aerobot, discussed in section 6.3, has shown the possibilities of BADS in this field. Section 6.4.2 and 6.4.3 however, have shown the limitations of the program. The program has need of further research and improvement to achieve the goal of a worthy buoyant aerobot simulation package.
A varying drag coefficient, an improved mathematical coding, more comprehensive atmospheric and thermal models, etc. would definitely improve the results. The obtained results however can't be discarded as they are promising enough at this stage of program development. The current accuracy of BADS can be compared to that of SINBAD in its early years. Which on itself is an achievement, but also reveals the work that still has to be done.

7. BADS Sensitivity Study

This chapter will explore the effects of small changes in fixed parameters and models used in BADS. The assumptions made throughout the program will be investigated, in section 7.1, by exploring the effect a change in parameter has on the results. This chapter will also address some inconsistencies, in section 7.2, that were created in BADS by assuming conditions that differ from reality.

7.1. Assumptions Analysis

A number of assumptions on parameter value and relations have been made throughout this thesis. Values have been assumed constant due to a lack of data on a specific parameter. Further some relations have been simplified in the program, affecting validity in the process. The main parameters that were assumed constant are;

- Gravitational Acceleration g
- Virtual Mass Coefficient $C_{virtual}$
- Shape Factor F_{bs}
- Permeability Factor λ
- Ground Temperature T_{ground}

The sensitivity analysis of BADS shall focus on the flight path of the aerobot through means of the altitude. The parameter will be compared throughout each modification of the above mentioned constants. Each constant will be subjected to highs and lows to get a widespread data analysis. The sensitivity study however shall limit the numerical analysis of the variance percentages to regions near the design altitude.

The aerobot example design on which the sensitivity study will be based on throughout the analysis shall have the following conditions;

Table 41: Sensitivity Design Example

Design Input Parameters		Flight Input Parameters	
Planet	Earth	Initial Position	(0, 0, 0)
Flight Altitude	5000m	Initial Flight Speed	(0, 0, 0)
Total Mass	500kg	Initial Wind Speed	(0, 0, 0)
Shape	Sphere	Drag Coefficient C_D	0.55
Fineness Ratio	1	Permeability	No
Free Lift %	2	Ballast Drops	No
Balloon Type	SP	Temperature Model	Yes
Super-Pressure	100Pa	Coating	Nr. 1
Buoyant Gas	Helium		
Envelope Density	$20g/m^2$	Time Step	1s

Coating Nr. 1 is the brilliant aluminum paint from the coating database, shown in appendix D. Further the standard design example will not include permeability. There is however one exception when the sensitivity analysis of the permeability factor will take place. The sensitivity design example will include the use of a thermal model throughout the sensitivity analysis, as two constant parameters discussed in this chapter are related to this module.

7.1.1. Gravitational Acceleration Sensitivity Analysis

The gravitational acceleration changes with geometric altitude, through Equation 15. During the BADS simulation process however this parameter has been set constant. Through Equation 15 the ground value was calculated for Earth, Mars, Venus and Titan and presented in Table 13. The atmospheric models of Mars and Venus are only modelled up to 100km into the atmosphere. Therefore gravity at 100km altitude will be selected as the worst case scenario for the gravitational acceleration, while the gravity at 0km will be the design case against which all other cases will be compared to. The following values represent the intermediate and maximum values for the gravity sensitivity analysis.

Earth's Geometric Altitude	**0km**	**20km**	**40km**	**60km**	**80km**	**100km**
Gravitational Acceleration [m/s^2]	9.80	9.74	9.68	9.61	9.56	9.498

While simulating the aerobot, of the design example in Table 41, through each gravitational modification above, the following results were obtained near the design altitude;

Table 42: Sensitivity Results on Gravitational Acceleration

	t=2706s		t=4963s	
Gravity [m/s^2]	**Altitude [m]**	**Variance% [%]**	**Altitude [m]**	**Variance% [%]**
9.80	5000.592	0	5000	0
9.74	5002.681	0.042	4999.828	0.003
9.68	5004.571	0.079	4999.653	0.007
9.61	5006.545	0.119	4999.446	0.011
9.56	5007.812	0.144	4999.3	0.014
9.498	5009.23	0.173	4999.123	0.017

The case at t=2706s, in Table 42, is the first time the aerobot reaches its design altitude. The aerobot is on its way to overshoot the altitude because of balloon bobbing. The variance percentage in altitude for all gravitational modifications stays below 0.2%. On a 5000m rise this means a 10m difference. Case 2, is at t=4963s when the aerobot is stabilized around its design altitude. The variance percentage here stays below 0.02%. On a flight of 5000m this gives a difference of less than 1m. With these results from the sensitivity analysis it's obvious that the use of a constant gravitational acceleration has no significant effect on the accuracy of BADS.

7.1.2. Virtual Mass Coefficient Sensitivity Analysis

For the virtual mass coefficient a constant value of 0.37 is currently programmed into BADS. To investigate the impact of the parameter on the program, the following values are being compared to the currently programmed value of 0.37;

Virtual Mass Coefficient []	0.20	0.30	0.37	0.5	0.6	0.7	0.8	0.9	1

While simulating the aerobot through each modification in virtual mass coefficient, the following results, listed in Table 43, were obtained near the design altitude;

Table 43: Sensitivity Results on Virtual Mass Coefficient

	t=2706s		t=4963s	
Virtual Mass Coefficient []	**Altitude [m]**	**Variance% [%]**	**Altitude [m]**	**Variance% [%]**
0.2	5000.118	0.009	4998.763	0.025
0.3	5000.415	0.003	5001.497	0.030
0.37	5000.592	0	5000	0
0.5	5000.899	0.006	4999.357	0.013
0.6	5001.083	0.010	5001.957	0.039
0.7	5001.248	0.013	4999.726	0.005
0.8	5001.363	0.015	4997.744	0.045
0.9	5001.442	0.017	5000.095	0.002
1	5001.507	0.018	5002.582	0.052

The virtual mass coefficient has no significant effect on the flight altitude of the aerobot. This is illustrated by the very low variance percentages in Table 43. On a flight trajectory of 5000m the maximum difference in altitude is only about 2.5m. The parameter's small influence on the BADS simulation results demonstrates that a constant value can be maintained during simulation.
The discrepancy will increase with higher coefficient values however, and for other balloon shapes than those in BADS this could have a bigger effect than the one demonstrated above. Further research should be done on this subject if other balloon shapes and sizes are considered.

7.1.3. Shape Factor Sensitivity Analysis

The current shape factor in BADS, which has the standard value of a sphere, is 0.5. To investigate the impact of this parameter the following values are being compared to the current one;

Shape Factor []	0.20	0.30	0.4	0.5	0.6	0.7	0.8	0.9	1

While simulating the aerobot through each modification in shape factor, the following results were obtained near the design altitude;

Table 44: Sensitivity Results on Shape Factor

	t=2706s		t=4963s	
Shape Factor []	**Altitude [m]**	**Variance% [%]**	**Altitude [m]**	**Variance% [%]**
0.2	0	100	0	100
0.3	0	100	0	100
0.4	0	100	0	100
0.5	5000.592	0	5000	0
0.6	5002.055	0.029	5000.654	0.013
0.7	5002.322	0.034	5000.951	0.019
0.8	5001.656	0.021	5000.714	0.014
0.9	4998.509	0.042	4999.325	0.013
1	4999.42	0.023	4999.697	0.006

Table 44 shows a huge discrepancy in simulation results for shape factors below 0.5, while trajectory with larger shape factors tends to have no inconsistencies. The lower value shape factors influence the flight trajectory in such a way that the aerobot is only able to lift-off a few meters before dropping back to Earth. This is illustrated in Figure 75, Figure 76 and Figure 77 for shape factors of 0.2, 0.3 and 0.4 respectively.

The shape factor is a parameter used in the heat loads of Equation 57 and Equation 58. It is connected to the emissivity of both gas and envelope and to the absorptance of reflected planetary surface heat through albedo. This relation to absorptance and emissivity can be a reason why the lower value shape factors influence the flight so much; In all cases gas temperatures are higher than the envelope temperature. The actual trajectory of a spherical balloon is shown in Figure 78. Its temperature profile shows the exact opposite of the aforementioned observation. How shape factors influence the buoyant aerobot's flight trajectory should therefore be researched further.

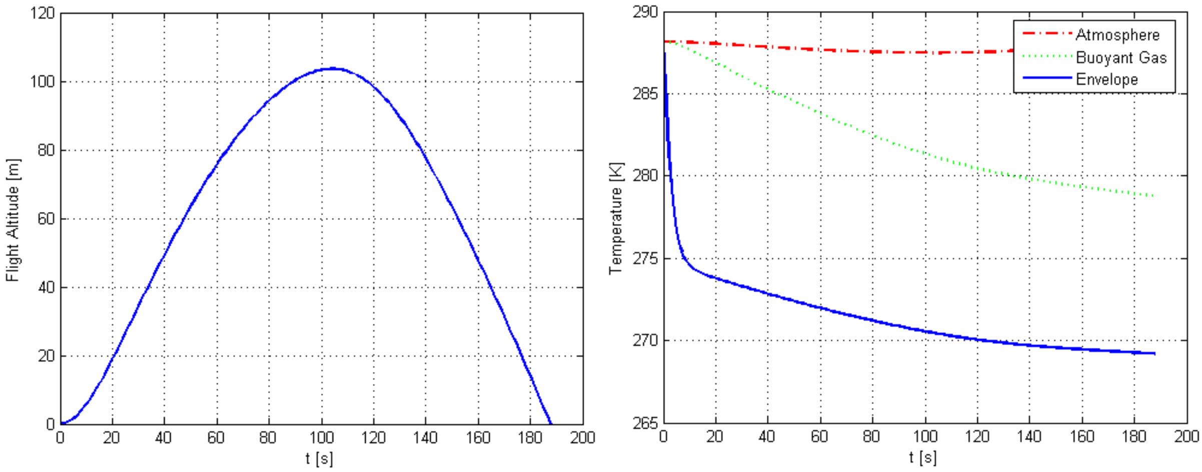

Figure 75: Shape Factor of 0.2; (a) Altitude, (b) Temperature

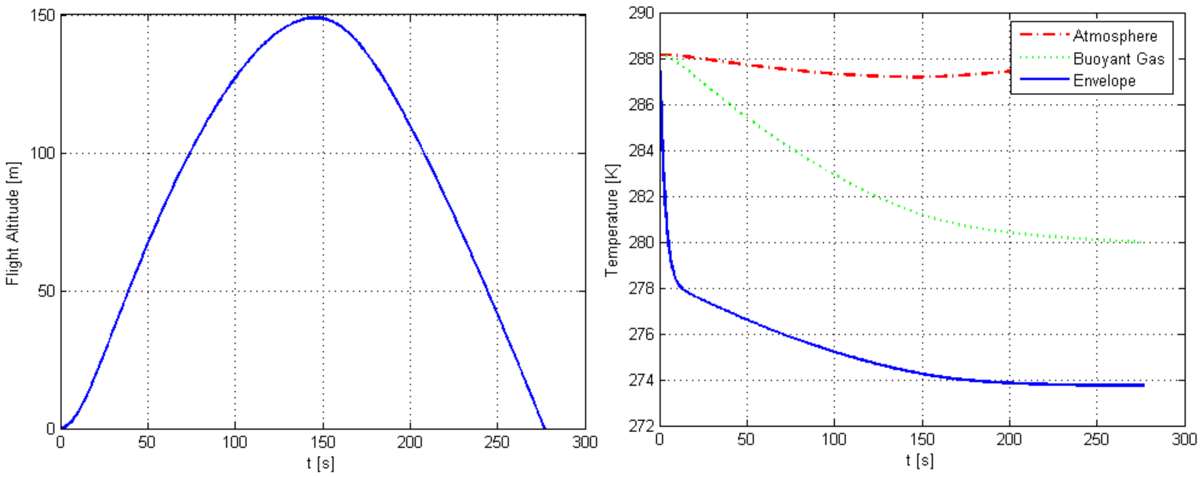

Figure 76: Shape Factor of 0.3; (a) Altitude, (b) Temperature

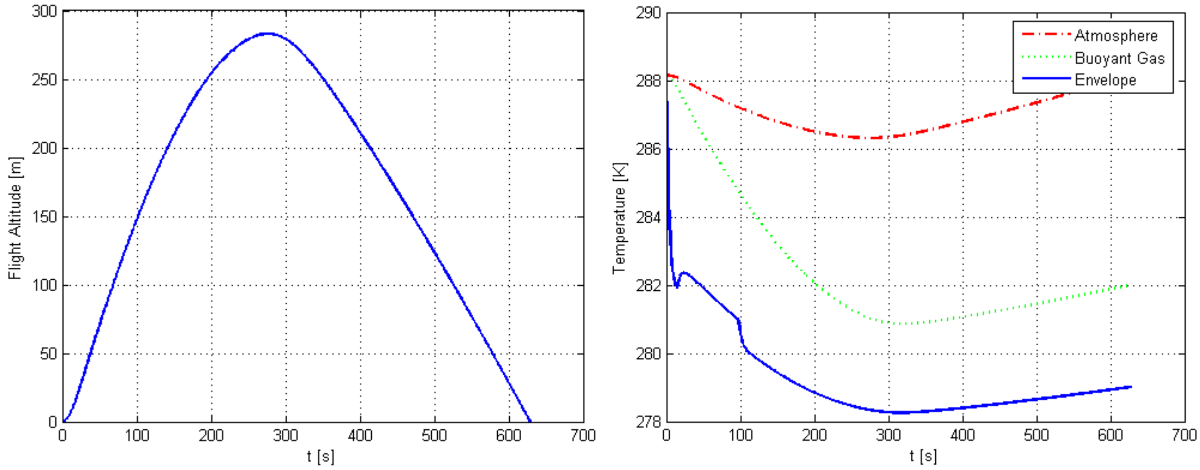

Figure 77: Shape Factor of 0.4; (a) Altitude, (b) Temperature

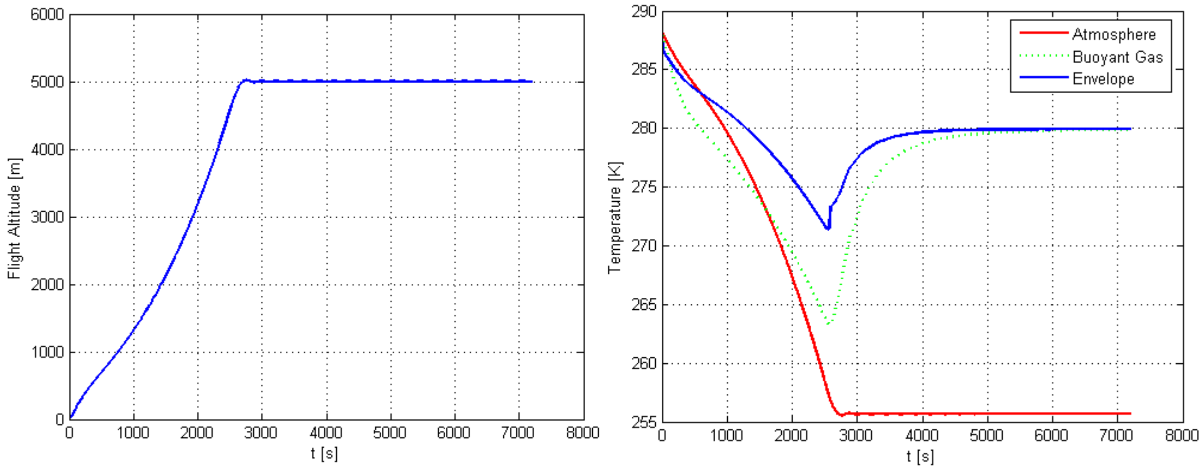

Figure 78: Shape Factor of 0.5; (a) Altitude, (b) Temperature

7.1.4. Ground Temperature Sensitivity Analysis

The ground temperature in the heat load equations is currently set equal to the atmosphere's temperature at ground. The observed ground temperature by the aerobot changes with altitude though. To investigate the impact, a few high and lows will be subjected to this parameter;

Ground Temperature [K]	263	273	278	288.15	293	298	303	308	313

While simulating the aerobot through each modification in ground temperature, sensitivity results were obtained near the design altitude. These are shown in Table 45. At first glance the results are similar to those of the shape factor. The first two cases, which demonstrate subzero temperatures, are not able to keep the aerobot afloat for long. This is illustrated in Figure 79 and Figure 80. An observation, similar to the one seen for low shape factors, can be made about the gas and envelope temperatures. Both are opposite to standard values during climb of an aerobot. This tends to influence the buoyancy.

The third case for a ground temperature of 278, illustrated in Figure 78, has a 69.64% variance with the aerobot example at time t=2706s. The aerobot has a very slow climb rate but continues to climb, up to the design altitude, although at a much slower pace. That's why the third case has almost no variance percentage at time t=4963 when the balloon is stabilized around its design altitude. The reason however for its slow ascend could be traced back to its gas and envelope temperatures which are affected by the cold ground temperature.

Table 45: Sensitivity Results on Ground Temperature

	t=2706s		t=4963s	
Ground Temperature [K]	Altitude [m]	Variance% [%]	Altitude [m]	Variance% [%]
263	0	100	0	100
273	0	100	0	100
278	1518.237	69.64	4997.649	0.047
288.15	5000.592	0	5000	0
293	5006.674	0.122	5001.185	0.024
298	5000.757	0.003	5000.169	0.003
303	4995.729	0.097	4998.718	0.026
308	5003.873	0.066	5001.309	0.026
313	4996.608	0.080	4998.761	0.025

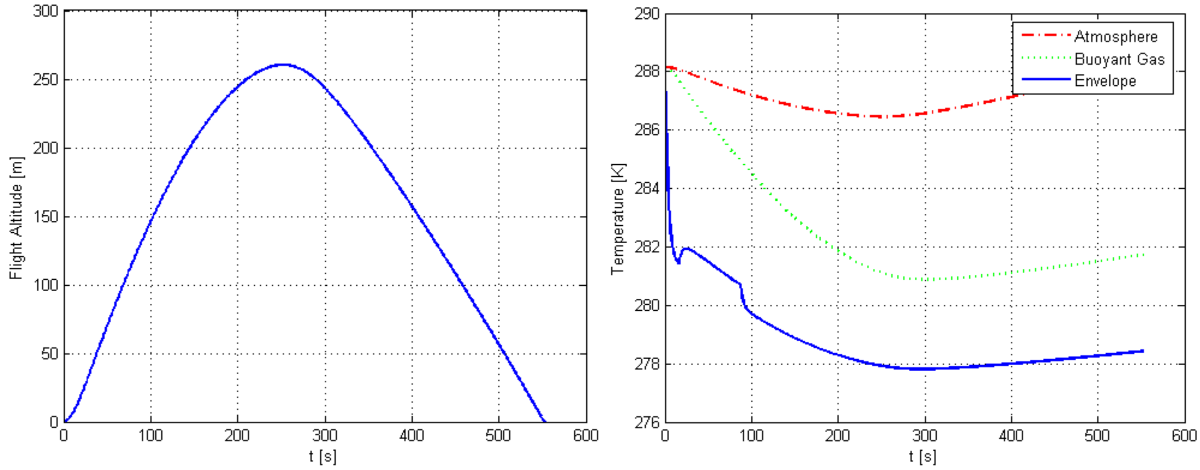

Figure 79: Ground Temperature of 263K; (a) Altitude, (b) Temperature

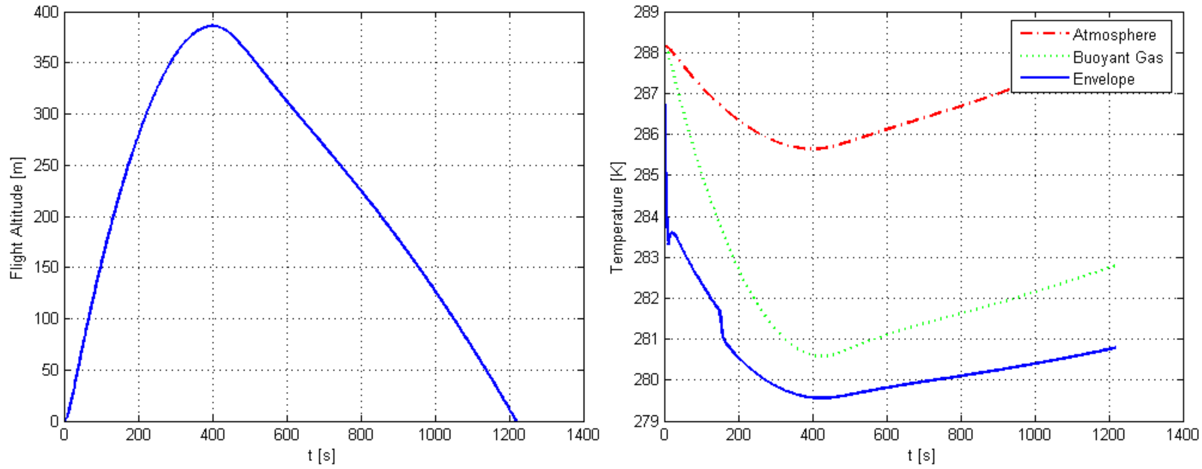

Figure 80: Ground Temperature of 273K; (a) Altitude, (b) Temperature

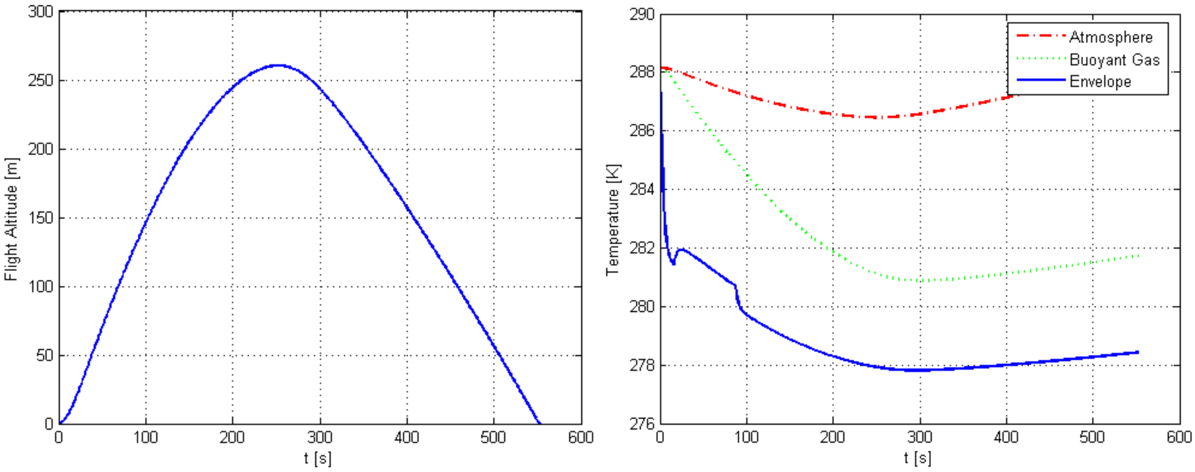

Figure 79: Ground Temperature of 263K; (a) Altitude, (b) Temperature

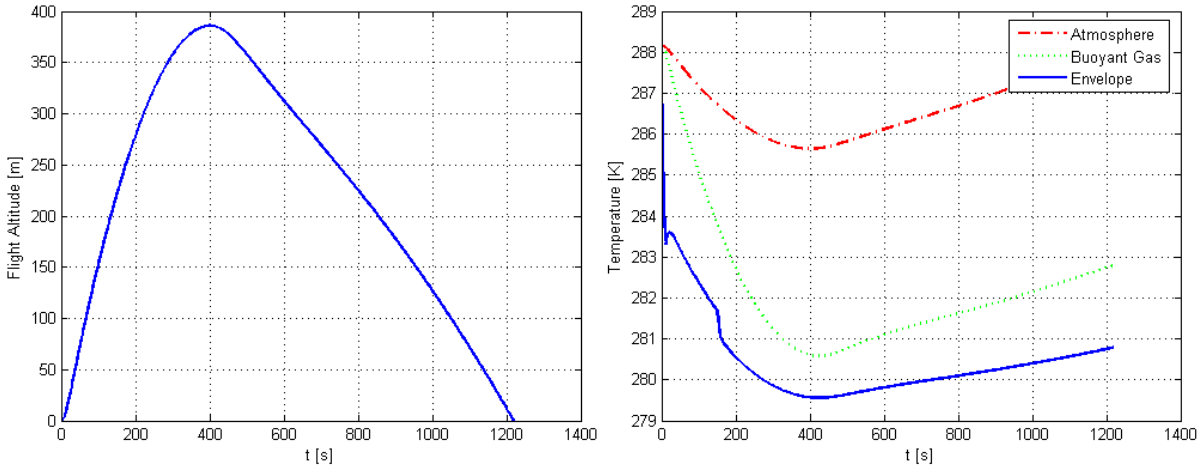

Figure 80: Ground Temperature of 273K; (a) Altitude, (b) Temperature

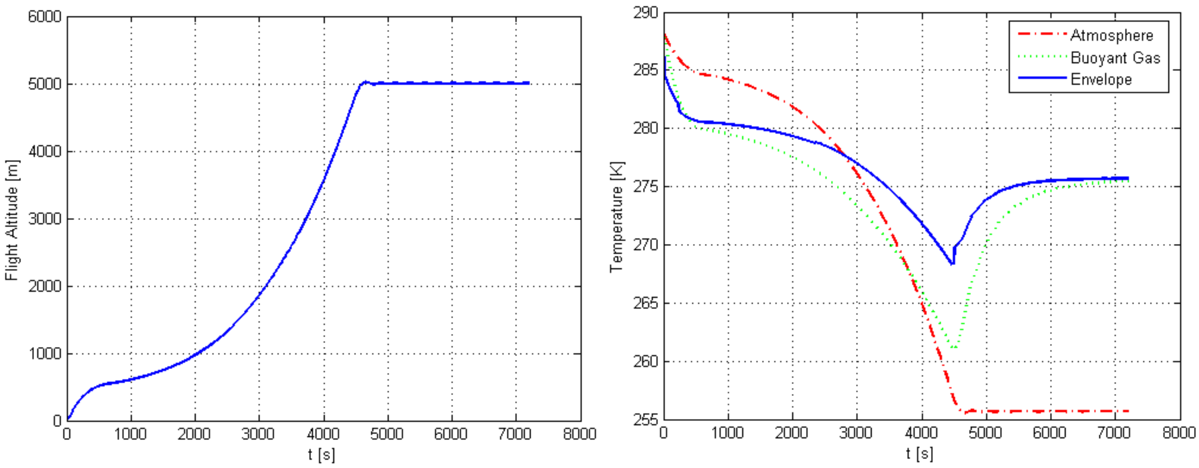

Figure 81: Ground Temperature of 278K; (a) Altitude, (b) Temperature

When ground temperature rises almost no effect is noticeable between the example and the modifications. Further research on ground temperature and its effect on BADS's thermal model, plus the effect on the aerobot's behavior, should be conducted in the future though.

7.1.5. Permeability Sensitivity Analysis

The effect of permeability on BADS's results will be investigated through modifying the current constant coefficient into a few highs and lows. These are the following

Permeability	2E-22	1E-21	1E-20	1E-19	2E-19	3E-19	1E-18	1E-17	2E-16

While simulating the aerobot through each modification in permeability coefficient, the following results were obtained near the design altitude;

Table 46: Sensitivity Results on Permeability

	t=2706s		t=4963s	
Permeability [m^2]	**Altitude [m]**	**Variance% [%]**	**Altitude [m]**	**Variance% [%]**
2E-22	5000.592	0	5000	0
1E-21	5000.592	0	5000.002	0
1E-20	5000.592	0	5000.024	0
1E-19	5000.594	0	5000.235	0.05
2E-19	5000.592	0	5000	0
3E-19	5000.599	0	5000.704	0.14
1E-18	5000.615	0	5002.333	0.047
1E-17	5000.826	0.005	5021.584	0.432
2E-16	5004.889	0.005	5142.188	2.844

In the first part of the flight no inconsistency can be found worth mentioning. This is simply because BADS only initiates the permeability effect when pressure builds up inside the balloon. For the super-pressure example in this sensitivity study this occurs when design altitude is reached. Permeability is also an effect that will only contribute to change over long periods of time, high pressures and permeable fabrics. Only a very large permeability factor will influence the flight trajectory in short term though. This can be seen in the last two modified cases of Table 46, where a high permeability coefficient results in a higher flight altitude of 21.5m and 142m respectively.
The current permeability factor will require no need in change for the moment though, as for medium flight durations no effect is visible. Long duration missions however will require further research in the area of permeability for multiple gases and envelope fabrics.

7.2. Differences with Reality

BADS has two main inconsistencies, excluding the assumptions discussed above, that make results differ from reality. These are;

- The standard atmosphere profiles,
- The balloon drag assumption

The standard atmosphere profiles make use of year-long averaged data sets of temperature, pressure and density. They exclude the air moisture and don't take into account day to day changes, such as a hot or a cold day. Section 6.2 has shown that atmosphere conditions have a big influence on the initial aerobot design. During flight this atmosphere influence will definitely have an effect on the flight trajectory. Section 7.2.1 shall explore this effect.

In section 4.2.2 the assumption was made that the balloon is the only component on an aerobot that would create drag. Any other components were neglected. Section 7.2.2 shall explore this assumption briefly and also its effect on the results.

7.2.1. Atmosphere Sensitivity Analysis

The atmosphere model of Earth implemented in BADS exists out of listed data on temperature, pressure and density. To modify this model for hot and cold days, or add moisture to the air is not without difficulty. A general approach will therefore be used to simulate the effect of an atmospheric model with humidity.

Relative humidity is the ratio of the partial pressure of water vapor in an air-water mixture to the saturated vapor pressure of water at a prescribed temperature. The relative humidity of air depends on temperature and the pressure of the system of interest. To simulate this effect use is made of the Dry Adiabatic Lapse Rate (DALR) and the Saturated Adiabatic Lapse Rate (SALR). The DALR has a value of 9.8 °C/km, while the SALR has a value of about 5 °C/km [i.53].

"The reason for the difference between the dry and moist adiabatic lapse rate values is that latent heat is released when water condenses, thus decreasing the rate of temperature drop as altitude increases [i.53]." By introducing these lapse rate into the temperature profile of BADS the effect of a dry and a saturated atmosphere can be explored.

Table 47: Sensitivity Results on Saturated and Dry Air

t=2590s			
Dry Air		Saturated Air	
Altitude [m]	Variance% [%]	Altitude [m]	Variance% [%]
4508.801	9.83	5000.609	0

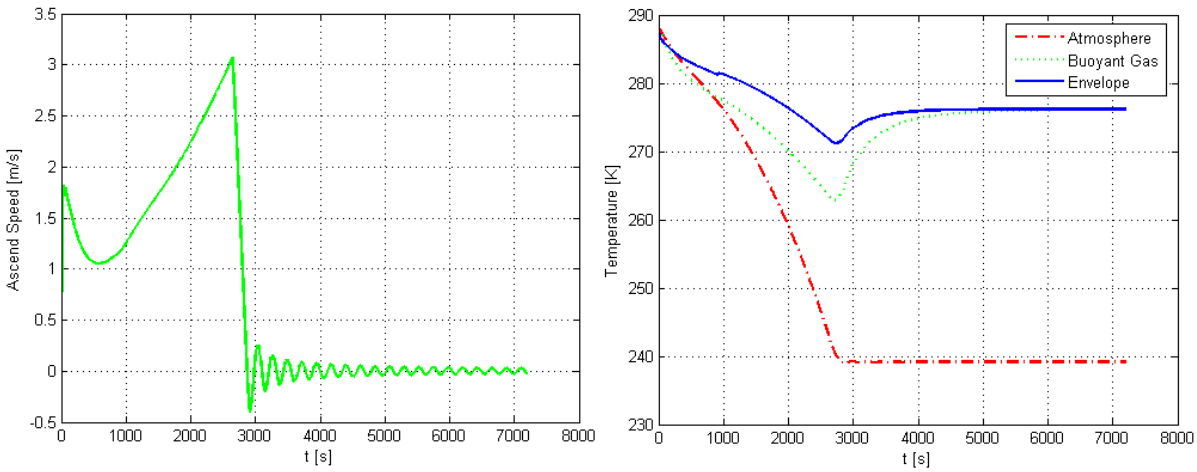

Figure 82: Aerobot in Dry Air; (a) Ascend Speed, (b) Temperature

From a simulated aerobot flight with both lapse rates, it was observed that the aerobot in a moist atmosphere reaches its design altitude faster than the one in a dry atmosphere. A variance percentage of 9.83% in altitude exists when the aerobot in dry air is compared to the aerobot in saturated air. The difference in ascend speed and temperature profile are illustrated in Figure 82 and Figure 83.

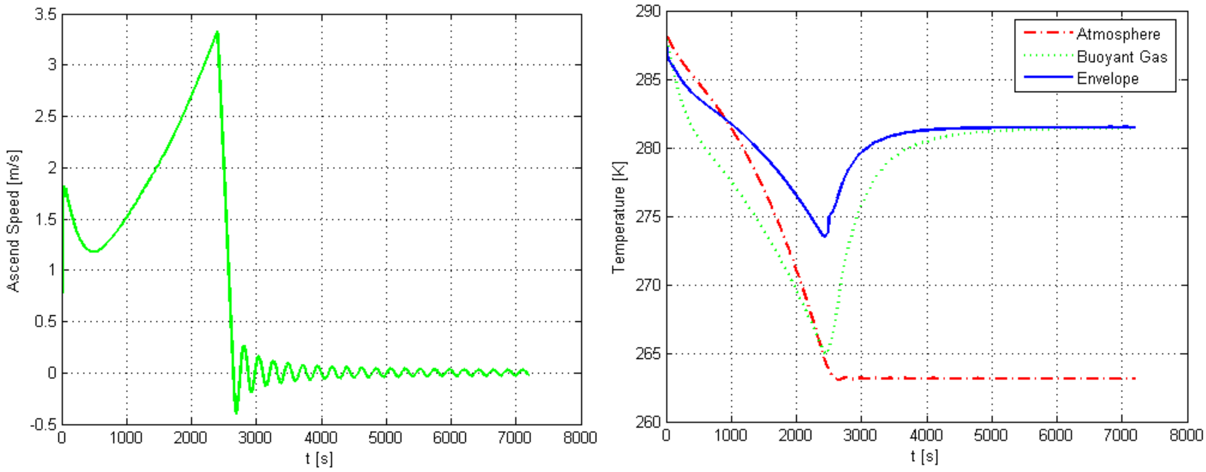

Figure 83: Aerobot in Saturated Air; (a) Ascend Speed, (b) Temperature

The effect of the slower rise in an atmosphere with a DALR is explained through the lower temperature of the atmosphere, which influences the aerobot's gas and envelope temperatures slightly. In an atmosphere with a DALR, the gas and envelope temperatures are affected such that they are lower than when the aerobot would fly in an atmosphere with a SALR. It can be concluded that, moist air gives warmer air and therefore generates a higher ascend speed.

7.2.2. Aerobot Component Drag Analysis

Based on the aerobot example of Table 41, the maximum balloon diameter is close to 10m. For a sensitivity analysis the following drag areas will be added to the simulation to explore the effect of small aerobot components creating drag;

Added Drag Area [m^2]	0	1	1.5	2	3	4	5
Drag Coefficient []	1.05	1.05	1.05	1.05	1.05	1.05	1.05

The drag coefficient of the added drag area, is considered to be that of a box, illustrating a small to medium container. Simulating the aerobot through each modification in drag, gave the results of Table 48, near the design altitude.

The results show a significant altitude loss over time, due to the extra drag surfaces. It must be mentioned however that the extra drag area is simulated such that the surface is actually making the balloon larger or such that the payload is far below the balloon and inducing the extra drag. In reality however the payload could be just below the balloon, making it 'invisible' compared to the balloon surface area. The highest inconsistencies occur during flight though, and not during float.
Nevertheless a substantial difference has been noted, and future work on BADS should consider including the drag areas of payload and connections in the aerodynamic module, to improve results on that end.

Table 48: Sensitivity Result on Added Component Drag Area

	t=2706s		t=4963s	
Added Drag Area [m^2]	**Altitude [m]**	**Variance% [%]**	**Altitude [m]**	**Variance% [%]**
0	5000.592	0	5000	0
1	4981.092	0.390	4999.035	0.019
1.5	4969.047	0.631	4998.673	0.026
2	4955.578	0.900	4998.442	0.031
3	4924.658	1.518	4998.444	0.031
4	4888.882	2.234	4999.023	0.019
5	4848.751	3.036	4999.959	0.001

8. BADS Potential in Projects and Applications

The validation process of the BADS tool has specified its strengths and limitations. With these in mind BADS can show its potential in current and future projects and applications. The potential of the design and flight parameters in BADS, indicating the amount of options and possibilities in BADS, is discussed in section 8.1. BADS can also be of great use in scientific planetary ballooning, due to the amount of atmospheric models. As an example, BADS analyzes the impact of each planetary atmosphere on a general aerobot model in section 8.2.

Further BADS can be used as a helpful tool in student design projects, which will be discussed in section 8.3. These can include meteorological studies with payload recoveries and university aerobot competitions.

8.1. The Potential of BADS's Design and Flight Parameters

As discussed in section 5.2.2 a large amount of input parameters is available to the user. This is also one of the main strong points of BADS as each alteration in design input shall create a new aerobot model, and each modification in flight input parameter might change the aerobot flight path. Which parameter will influence the aerobot design and which one will influence the flight of the aerobot, is indicated in Table 49.

Table 49: Design Parameters vs Flight Parameters

Design Parameters	**Impact on Design via;**
Design Flight Altitude	Design Volume
Total Mass	Design Volume
Atmosphere Selection	m_{gas}, Design Volume
Shape and Fineness Ratio	Cross-Sectional Areas
Free Lift Percentage	m_{gas}
Balloon Pressure Type	m_{gas}
Maximum Super-Pressure	m_{gas}
Buoyant Gas Selection	m_{gas}
Envelope Selection	$m_{envelope}$
Flight Parameters	**Impact on Flight via;**
Initial Position	Trajectory
Initial Flight Speed	Trajectory
Initial Wind Speed	Trajectory
Powered Flight	Trajectory, Aerodynamics
Balloon Pressure Type	Buoyancy
Maximum Super-Pressure	Buoyancy
Drag Coefficient C_D	Trajectory, Aerodynamics
Parachute	Trajectory
Free Lift Percentage	Buoyancy
Permeability	Mission Life, m_{gas}
Ballast Drops	$m_{payload}$, Aerodynamics
Buoyant Gas Selection	Buoyancy
Temperature Model	Temperatures
Coating Selection	Gas, Envelope Temperature

This division does not represent every option in BADS, but includes the main ones. Also keep in mind that flight parameters don't affect the initial design much, but initial design parameters do influence flight. Each parameter in the table can be varied to investigate the effect on either design or flight. Which makes BADS a very versatile resource in aerobot design and flight simulation.

To give an impression of what a change in parameters can do to the design and flight, an exemplary aerobot analysis is presented. In Table 50 six different aerobot designs are compared against an initial design, design 1. Each design has one input parameter changed to analyze what impact that parameter has on aerobot design 1.

A change in altitude in design 2, gives a large shift in envelope mass as a much larger volume is required to stay afloat at that altitude. This also means a drop in available payload space. A double amount of total mass in design 3 almost linearly increases every other mass and volume in the design. A change in shape in design 4 has a small impact on the envelope mass, as the surface area of an oblate spheroid is larger than that of a sphere with an equal volume. When free lift is increased in design 5 an obvious increase in gas mass occurs at the expends of payload mass. In design 6 the buoyant gas is changed into hydrogen. This halves the gas mass and increases the payload mass. Design 7 changes the type of envelope by changing the envelope areal density. This only impacts the envelope mass at the expends of payload mass.

From Table 50 the program user is able to get an understanding on how input parameters influence the design and to what extent.

Table 50: Input Parameter's Influence on Initial Aerobot Design

Design Input Parameters							
Parameter	**Design 1**	**Design 2**	**Design 3**	**Design 4**	**Design 5**	**Design 6**	**Design 7**
Planet	Earth	Earth	Earth	Earth	Earth	Earth	Earth
Flight Altitude	5000m	30000m	5000m	5000m	5000m	5000m	5000m
Total Mass	500kg	500kg	1000kg	500kg	500kg	500kg	500kg
Shape	Sphere	Sphere	Sphere	Oblate	Sphere	Sphere	Sphere
Fineness Ratio	1	1	1	5	1	1	1
Free Lift %	10	10	10	10	15	10	10
Balloon Type	ZP	ZP	ZP	ZP	ZP	ZP	ZP
Super-Pressure	0Pa	0Pa	0Pa	0Pa	0Pa	0Pa	0Pa
Buoyant Gas	Helium	Helium	Helium	Helium	Helium	Hydrogen	Helium
Envelope Density	20g/m^2	20g/m^2	20g/m^2	20g/m^2	20g/m^2	20g/m^2	50g/m^2
Influenced Initial Aerobot Designs							
	Design 1	**Design 2**	**Design 3**	**Design 4**	**Design 5**	**Design 6**	**Design 7**
m_{tot} [kg]	500	500	1000	500	500	500	500
m_{pay} [kg]	417.57	338.35	838.23	413.1	414.70	454.52	406.37
$m_{envelope}$ [kg]	7.47	86.69	11.86	11.94	7.47	7.47	18.68
m_{gas} [kg]	74.95	74.95	149.91	74.95	77.83	38	74.95
Volume [m^3]	678.95	2.683E4	1.358E3	678.95	678.95	678.95	678.95

A similar analysis as the one above, will now be made with respect to the flight parameters. This analysis is based on design 1 in Table 50, and will be compared to 6 new designs in Table 51. There are however some exceptions and variations included in the design, whenever the balloon shape, or pressure type is considered. Both can affect the flight of the aerobot which will also be illustrated. This analysis is done to show the effect of a change in input parameters on flight results, but not to quantify the alteration or discuss the effects in great detail though.

Table 51: Input Parameter's Influence on Flight Simulation

Design Input Parameters							
Parameter	**Design 1**	**Design 2**	**Design 3**	**Design 4**	**Design 5**	**Design 6**	**Design 7**
Planet	Earth	Earth	Earth	Earth	Earth	Earth	Earth
Flight Altitude	5000m	5000m	5000m	5000m	5000m	5000m	5000m
Total Mass	500kg	500kg	500kg	500kg	500kg	500kg	500kg
Shape	Sphere	Sphere	Sphere	Sphere	Oblate	Sphere	Sphere
Fineness Ratio	1	1	1	1	5	1	1
Free Lift %	10	10	10	10	10	10	10
Balloon Type	ZP	ZP	ZP	ZP	ZP	SP	SP
Super-Pressure	0Pa	0Pa	0Pa	0Pa	0Pa	500Pa	500Pa
Buoyant Gas	Helium	Helium	Helium	Helium	Helium	Helium	Helium
Envelope Density	20g/m^2	20g/m^2	20g/m^2	20g/m^2	20g/m^2	20g/m^2	20g/m^2
Flight Input Parameters							
Initial Position	(0, 0, 0)	(0, 0, 0)	(0, 0, 0)	(0, 0, 0)	(0, 0, 0)	(0, 0, 0)	(0, 0, 0)
Initial Flight Speed	(0, 0, 0)	(0, 0, 0)	(0, 0, 0)	(0, 0, 0)	(0, 0, 0)	(0, 0, 0)	(0, 0, 0)
Initial Wind Speed	(0, 0, 0)	(0, 0, 0)	(0, 0, 0)	(0, 0, 0)	(0, 0, 0)	(0, 0, 0)	(0, 0, 0)
Drag Coefficient C_D	0.55	Variable	0.55	0.55	0.55	0.55	0.55
Permeability	No	No	No	No	No	No	Yes
Ballast Drops	No	No	No	No	No	No	No
Temperature Model	No	No	Yes	Yes	No	No	No
Coatings	Nr. 1	Nr. 1	Nr. 1	Nr. 70	Nr. 1	Nr. 1	Nr. 1

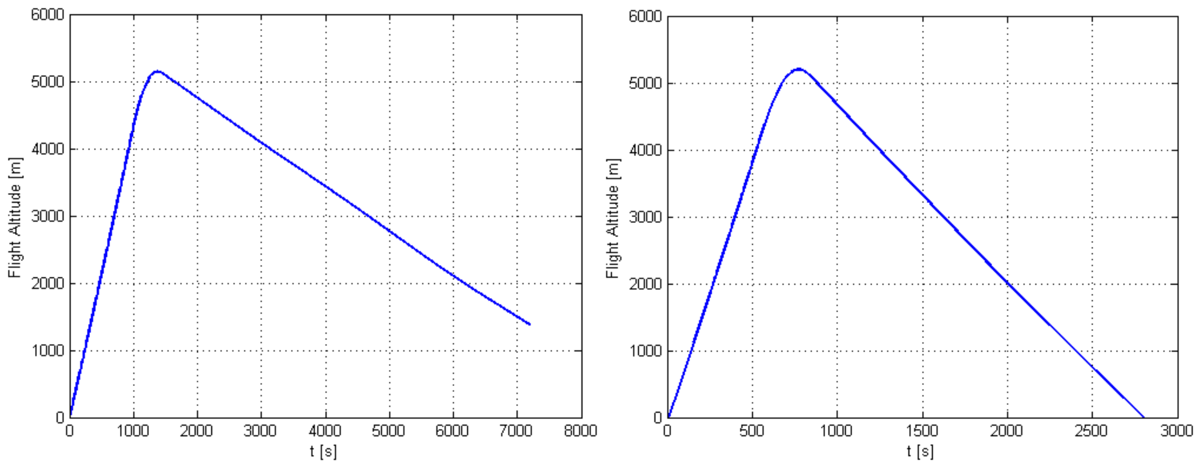

Figure 84: Altitude; (a) Design 1, (b) Design 2

Design 1 and 2 in Table 51 have a different drag coefficient. Design 2 makes use of the programmed variable drag coefficient from Equation 126. The effect this has on the simulated trajectory is illustrated in Figure 84 and Figure 85 through altitude and ascend speed. Design 2, with the variable drag coefficient reaches its design altitude after 800s, while design 1 succeeds in this after 1300s. This indicates that the variable drag coefficient generally produces lower values than the constant value of 0.55 from design 1. The lower drag coefficient results in a maximum ascend speed of 8m/s for design 2, while design 1 its maximum velocity is 4.5m/s. This difference is illustrated in Figure 85.

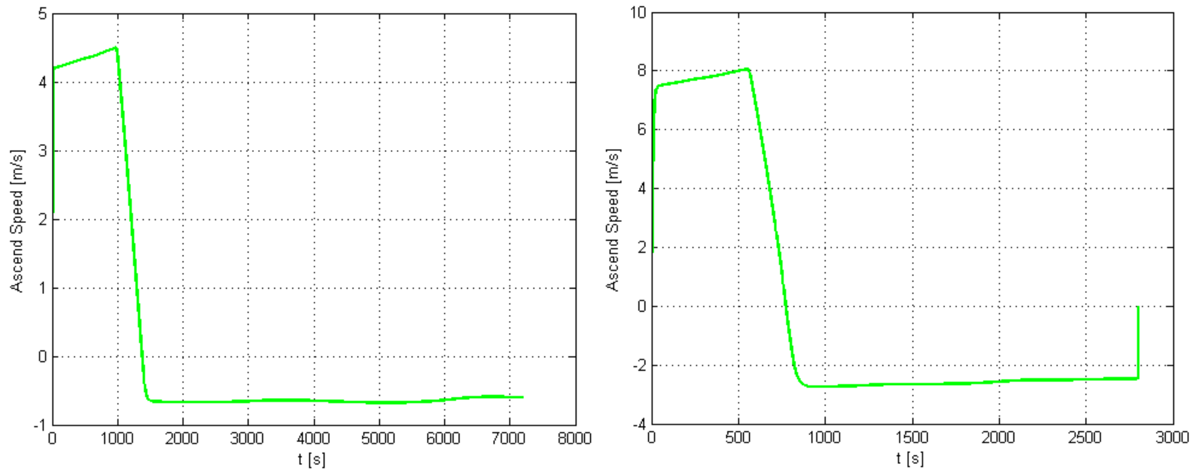

Figure 85: Ascend Speed; (a) Design 1, (b) Design 2

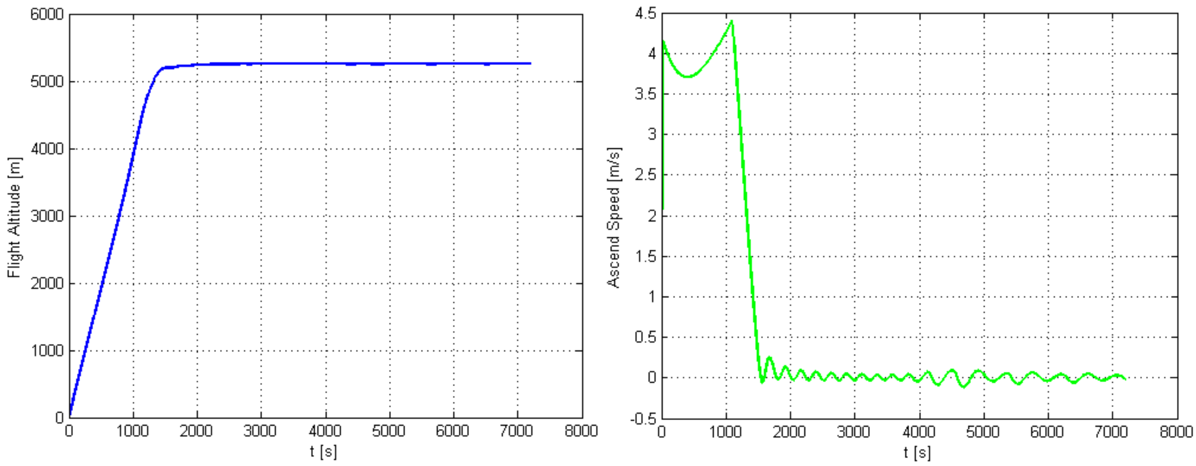

Figure 86: Design 3; (a) Altitude, (b) Ascend Speed

The modification to design 1 in design 3 is the addition of a thermal model. The effect of a thermal model to a zero-pressure balloon is quite large. When a zero-pressure balloon's gas, atmosphere and envelope temperatures are set equal, shown in Figure 87(a), the balloon will never stabilize around its design altitude. The aerobot will overshoot its design altitude, release gas and never recover altitude stability. When a thermal model is included, the gas and envelope temperatures will drop during ascend and rise during float, illustrated in Figure 87(b). This has a stabilizing effect on the aerobot's flight path and ascend speed, shown in Figure 86.

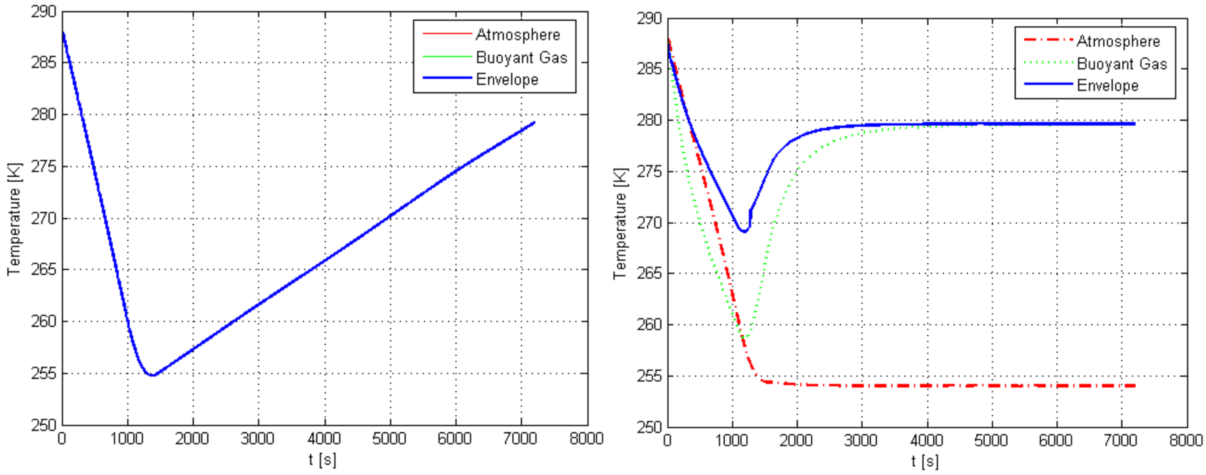

Figure 87: Temperature; (a) Design 1, (b) Design 3

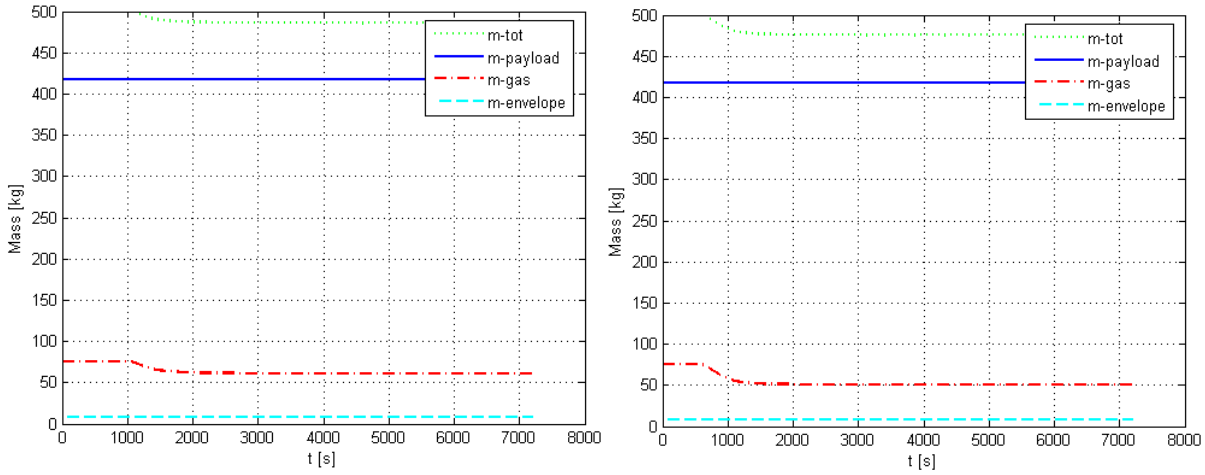

Figure 88: Mass; (a) Design 3, (b) Design 4

The modification to design 4, is the addition of a thermal model with a different envelope coating. Designs 1-3 and 5-7 use a brilliant aluminum paint as coating, while design 4 uses Tedlar Black Plastic. Brilliant aluminum paint has an effective absorptance of 0.3 and an infrared emissivity of 0.31, according to appendix D. The Tedlar black plastic has a much higher effective absorptance of 0.94 and a higher infrared emissivity factor of 0.9.

The effect these thermo-optical parameters have on the rise and float of the aerobot is illustrated in Figure 89. During aerobot rise both gas and envelope temperatures are not immediately dropping like they did in Figure 87(b) for design 3. Due to the larger absorptance the black balloon catches a lot of heat of the sun, allowing the gas and envelope temperatures actually to counteract the temperature drop due to volume expansion and velocity forced convection.

During float the temperature rises even further, up to its maximum, as illustrated in Figure 89. Due to the higher temperature a higher altitude and higher ascend speeds are achieved. The higher gas and envelope temperatures will increase buoyancy but also expand the gas further. This leads to more gas discharge compared to design 3, which is illustrated in Figure 88. Normally the gas loss will cost the aerobot buoyancy, but this is now compensated by the higher gas temperature.

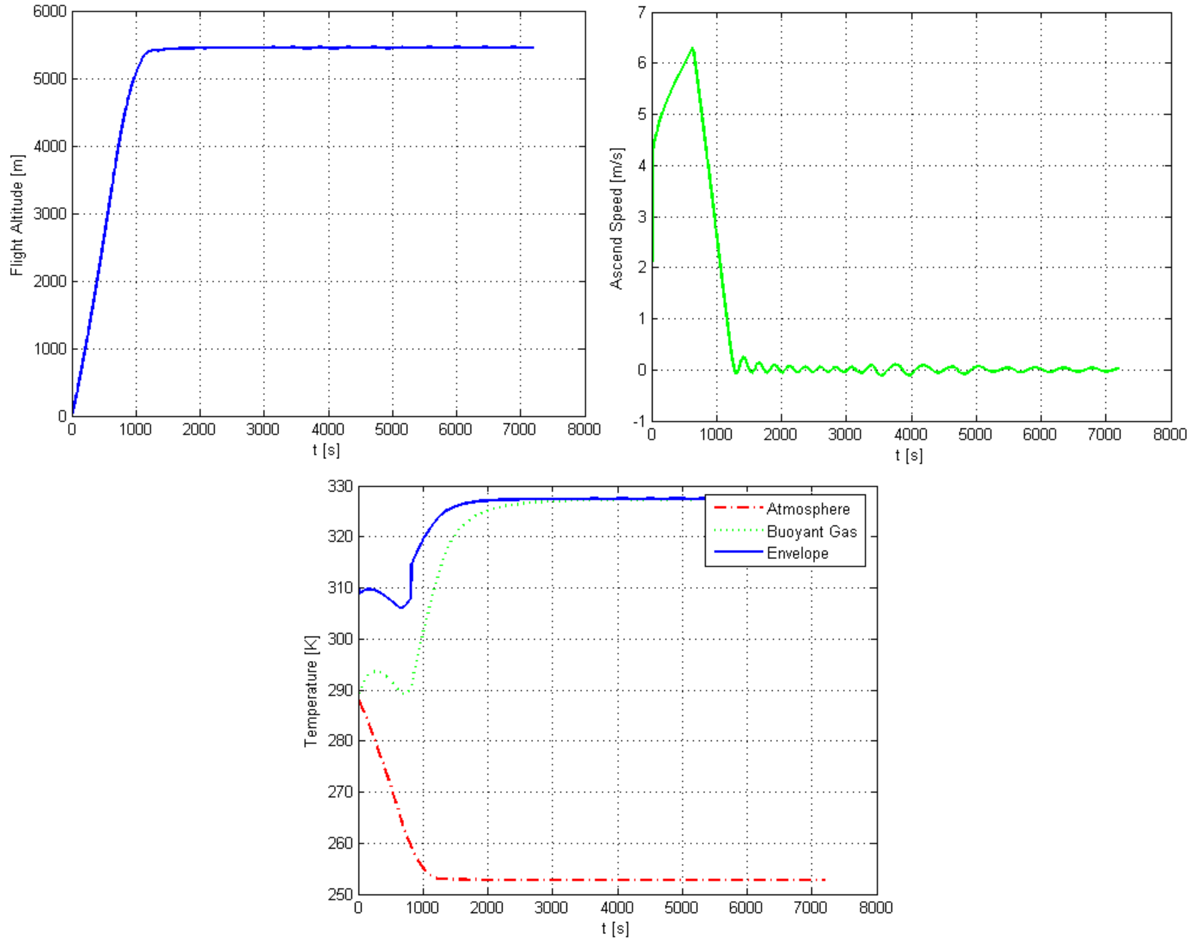

Figure 89: Design 4; (a) Altitude, (b) Ascend Speed, (c) Temperature

Design 5 has an oblate spheroid balloon shape, which has a higher cross-sectional area in the xy-plane, compared to the spherical balloon of design 1. This results in a higher drag force being exerted on the aerobot, which lowers the ascend velocity. The aerobot will therefore need more time to climb to its design altitude, as illustrated in Figure 90.

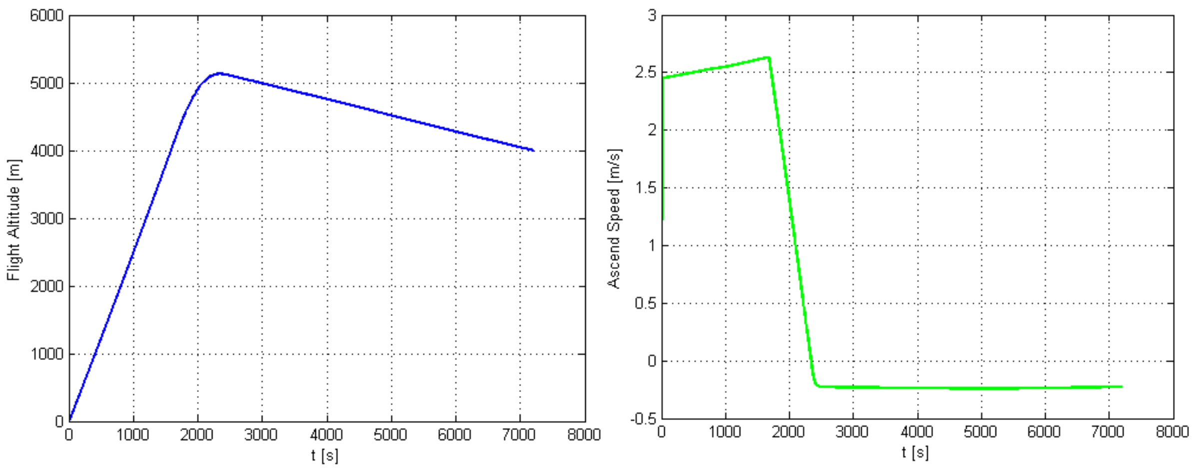

Figure 90: Design 5; (a) Altitude, (b) Ascend Speed

Design 6 and 7 will both be modified into a super-pressure balloon with a super-pressure of 500Pa. Design 7 will also include the effect of permeability. The super-pressure balloon in design 6 will not expel any gas mass when the design altitude is reached, but instead will build-up pressure. The zero-pressure balloon from design 1 shall discharge gas mass to maintain its zero-pressure level. This is illustrated in Figure 91.

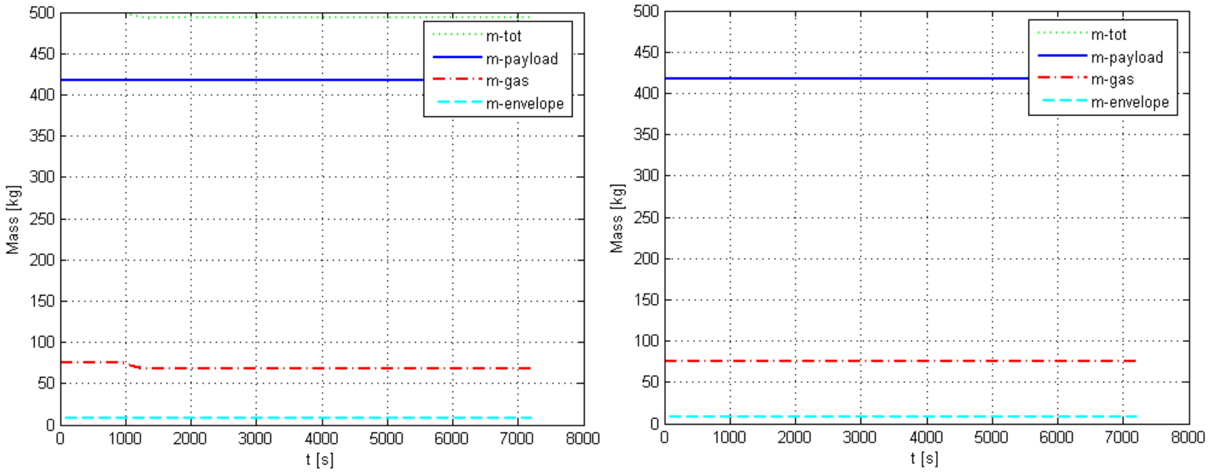

Figure 91: Mass; (a) Design 1, (b) Design 6

The flight path of the aerobot in design 6 during climb is exactly the same as that in design 1, illustrated in Figure 92, Figure 84 and Figure 85. This is due to the fact that the super-pressure acts like a zero-pressure until the maximum balloon volume is reached. Afterwards the zero-pressure balloon of design 1 descends to Earth, while the super-pressure of design 6 stabilizes itself around its design altitude.

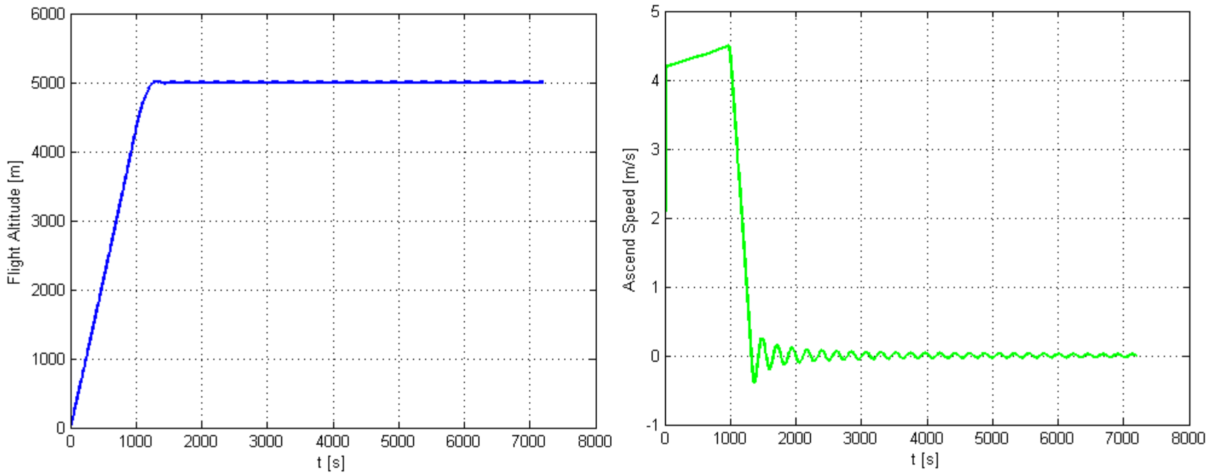

Figure 92: Design 6; (a) Altitude, (b) Ascend Speed

Design 6 and 7 will build-up a super-pressure during float. Due to the addition of extra gas mass, to comply with the 10% free lift, both balloons will attain higher pressures than the preferred design level of 500Pa, illustrated in Figure 93. These higher pressures can eventually result in an envelope rupture, as mentioned in section 6.3.1.

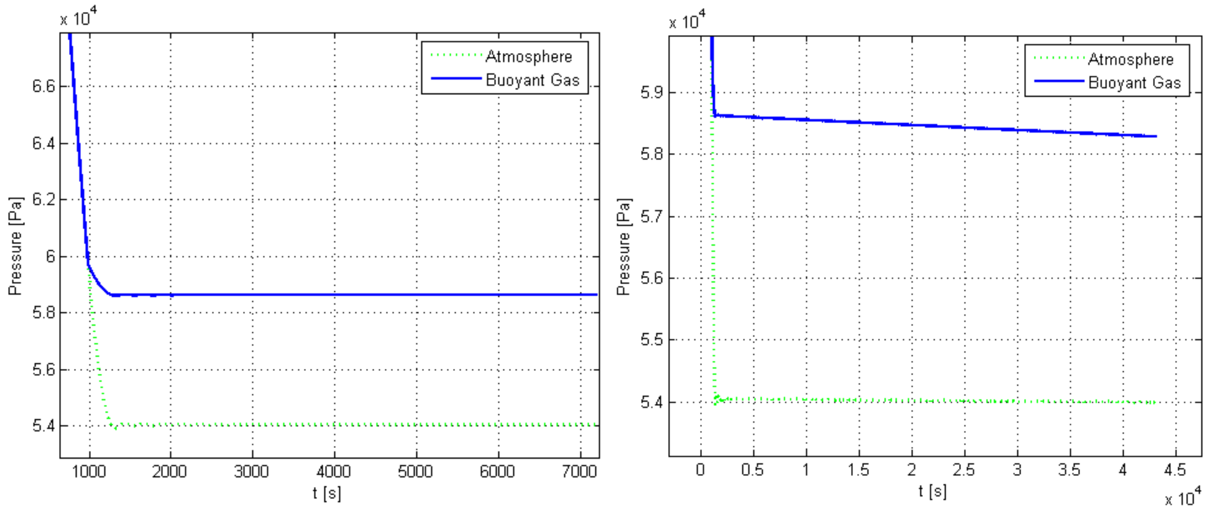

Figure 93: Pressure; (a) Design 6, (b) Design 7

A pressure difference will also actively press gas mass through a balloon envelope. The permeability effect grows with increasing pressure. To illustrate the effect, design 7 included permeability in its flight simulation. Permeability is a slow process if a good impermeable envelope fabric is selected. Design 7 has been flown in a simulated 12hrs flight. The permeability effect after 12hrs results in a loss of about 400g of helium, illustrated in Figure 94. Due to this loss, permeability also affect the gas pressure inside the balloon. A drop in gas pressure over time can be noticed in Figure 93(b).

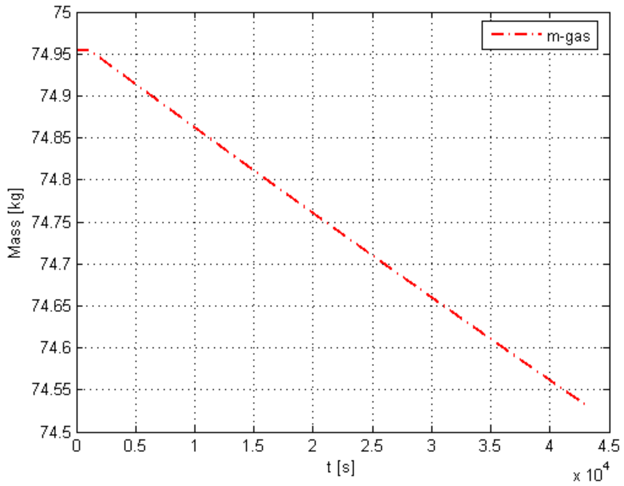

Figure 94: Design 7; Loss of Gas Mass due to Permeability

The above design and flight analysis on the modification of input parameters gives only a minor impression of what BADS is capable of. The results however show that it presents a lot of possibilities and has great potential in buoyant aerobot design and flight simulation.

8.2. Scientific Planetary Ballooning

Section 8.1 illustrated the strength of the amount of input parameters. One of the other main strengths of BADS is the amount of planetary vertical atmosphere models that are incorporated into the program. This makes the program an interesting candidate to be used as a simulation tool for planetary scientific ballooning.

Any scientific balloon and payload can be flown here on Earth. To distinguish if that same system is capable of flying on a different planet a simulation tool is required with a good atmospheric model of the planet in question. BADS can be used for this purpose if the target planet is Mars, Venus or Titan. The tool is able to simulate ZP, SP and OZP balloons and with the right input parameters and the thermal model activated even a Montgolfier balloon can be simulated.

These different types of aerobots combined with the number of planetary environments give some insight into the effect the environment has on design and flight. To illustrate the usefulness of the program in an aerobot comparison, a super-pressure aerobot is flown for all 4 planetary atmospheres. The following configuration holds for the aerobot;

Table 52: Planetary Mission Example Design Parameters

Design Parameter	Value
Design Flight Altitude	5000m
Total Mass	500kg
Shape	Sphere
Fineness Ratio	1
Balloon Pressure Type	OZP
Maximum Super-Pressure	100Pa
Buoyant Gas Selection	Helium
Envelope Areal Density	$20g/m^2$
Flight Parameters	**Value**
Initial Position	(0, 0, 0)
Initial Flight Speed	(0, 0, 0)
Initial Wind Speed	(0, 0, 0)
Powered Flight	No
Drag Coefficient C_D	0.55
Parachute	No
Free Lift Percentage	10%
Permeability	No
Ballast Drops	No
Temperature Model	No
Coating Selection	Brilliant Aluminum Paint

The initial aerobot design calculated from the planetary mission example design parameters in Table 52, is illustrated in Table 53 for Earth, Mars, Venus and Titan. The mass distribution of the aerobot per planet never remains the same. The key factor in this mass breakdown is the balloon envelope mass, which is related to the balloon volume. Planets with a high density atmosphere, like Venus and Titan, require less balloon volume to stay afloat. Consequently, the envelope mass will be low, and more space becomes available for payload.

Table 53: Planetary Aerobot Design Comparison

	Earth		Mars		Venus		Titan	
		[% m_{tot}]		[% m_{tot}]		[% m_{tot}]		[% m_{tot}]
m_{tot} [kg]	500	100%	500	100%	500	100%	500	100%
m_{pay} [kg]	417.57	83.5%	328.68	65.7%	449.98	89.9%	421.81	84.3%
$m_{envelope}$ [kg]	7.74	1.5%	120.99	24.2%	0.45	0.1%	2.27	0.4%
m_{gas} [kg]	74.95	15%	50.32	10%	49.57	9.9%	75.91	15.2%
Volume [m^3]	678.95	/	$4.42E^4$	/	9.99	/	114.03	/

The Martian aerobot clearly requires the largest balloon volume, due to the very low atmospheric density, to stay afloat. The Venusian aerobot needs the smallest balloon volume, due to the planet's high atmospheric density. The largest amount of payload can be flown on Venus, followed by Titan, Earth and finally Mars. The planetary atmosphere affects both the aerobot design and the flight data. Figure 95 to Figure 100 illustrate the flight data of Earth's aerobot concept of Table 52, together with the flight data of the modified planetary concepts of Table 53, through time.

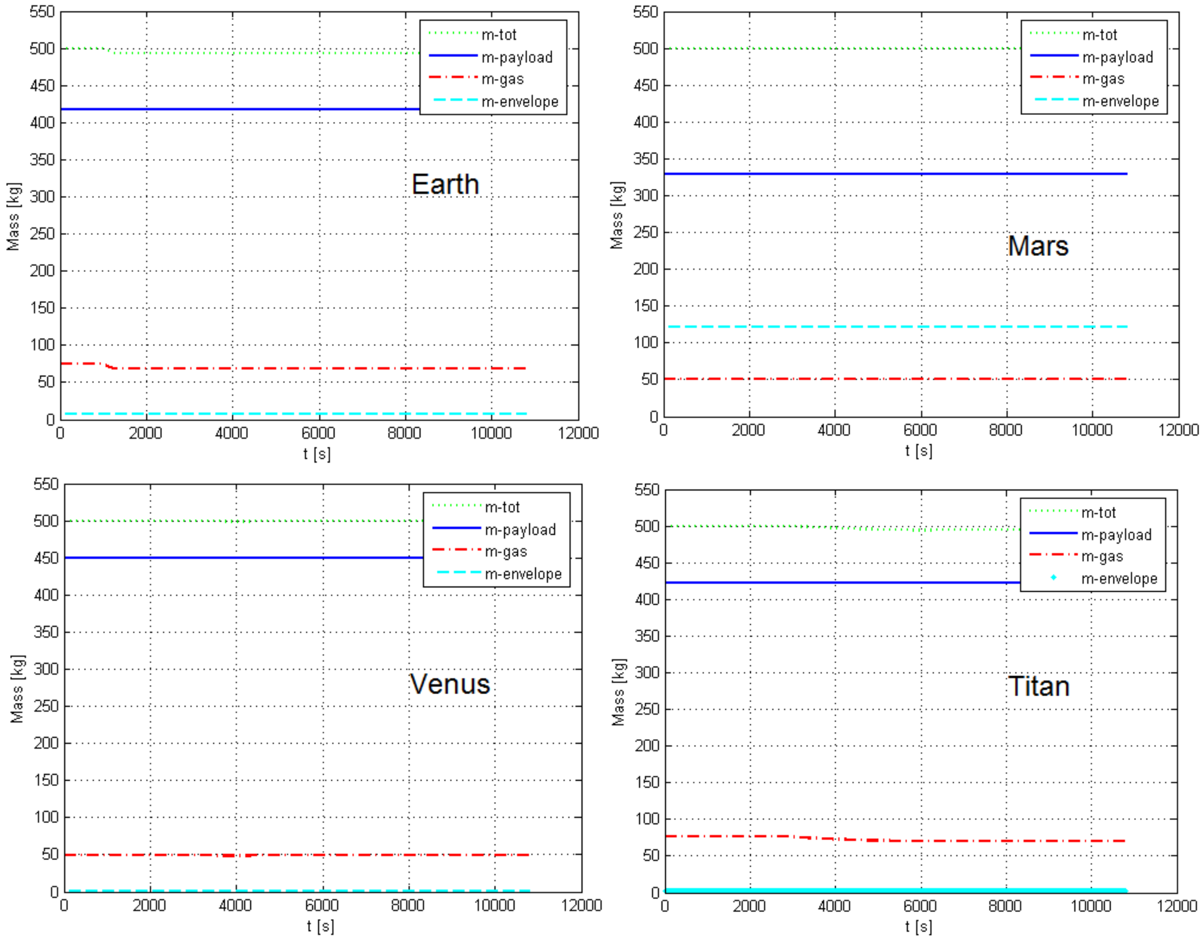

Figure 95: Mass Budget; (a) Earth, (b) Mars, (c) Venus, (d) Titan

Figure 95 shows the mass distribution of the four planetary aerobots. Over time not much variation exists, with the exception in gas mass. The gas mass vents when the OZP overshoots its design altitude and/or the pressure in the aerobot rises above the maximum valve pressure of 100Pa. The

Martian and Venusian aerobots never vent gas because the gas pressure stays below the valve's design pressure, which is illustrated in Figure 97.

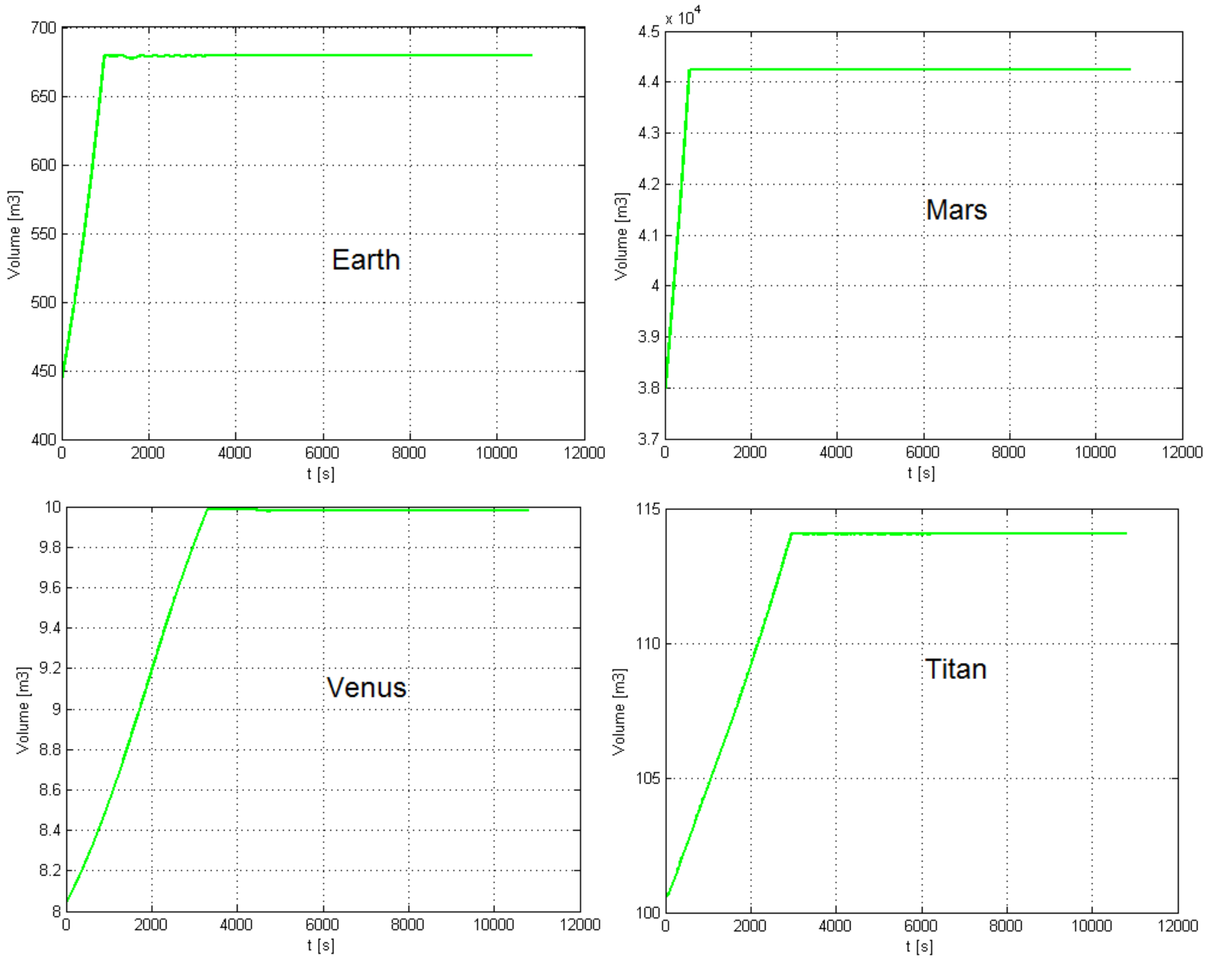

Figure 96: Balloon Volume; (a) Earth, (b) Mars, (c) Venus, (d) Titan

The difference in mass distribution of each planetary aerobot is not only illustrated through Figure 95, but also through the cause of the difference, namely the balloon volume in Figure 96. All volumes grow from launch to the design altitude, where they reach their maximum design volume. As mentioned before an aerobot on Mars will require the largest balloon volume, due to the low atmospheric density.

The reason for the constant volume over time, once the aerobots reached their design altitude, is the gas super-pressure in the balloon. The super-pressure will give the aerobot a stable flight altitude, and will make sure that the size and shape of the aerobot is maintained. If the super-pressure becomes higher than the valve pressure of the OZP, gas mass is vented. This is illustrated in Figure 95 for the aerobots of Earth and Titan. Both aerobots attain a positive pressure difference near their design altitude. Due to momentum however they overshoot their altitude, immediately building-up an over-pressure above the intended 100Pa, illustrated in Figure 97.

When the aerobots overshoot their design altitude they discharge gas to slow down ascend speed, until they stabilize around an altitude. Due to the fact they have overshot their design altitude and still have a pressure difference beyond zero, they don't stabilize around the desired altitude but around the altitude where the they stopped ascending as illustrated in Figure 98 and Figure 99.

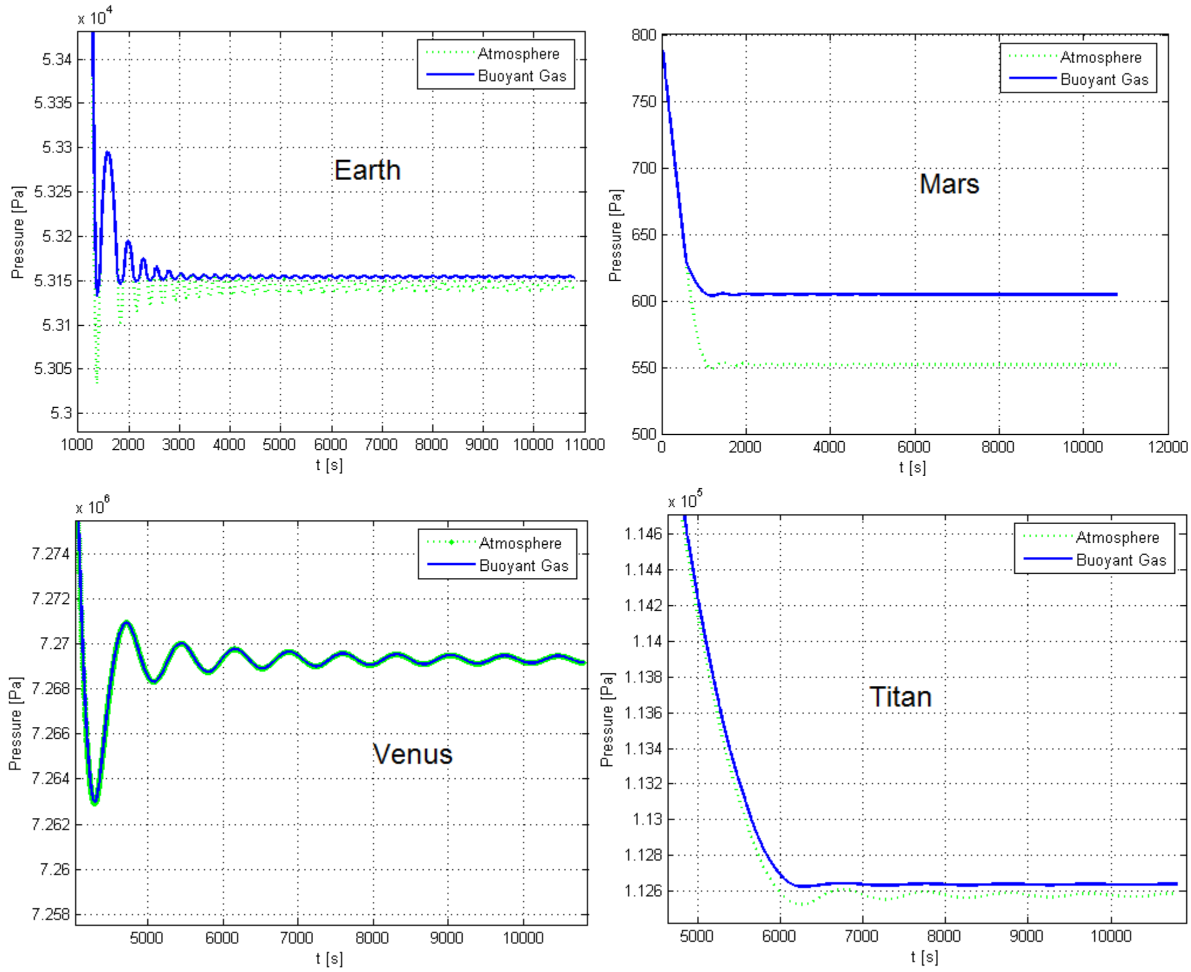

Figure 97: Balloon Pressure; (a) Earth, (b) Mars, (c) Venus, (d) Titan

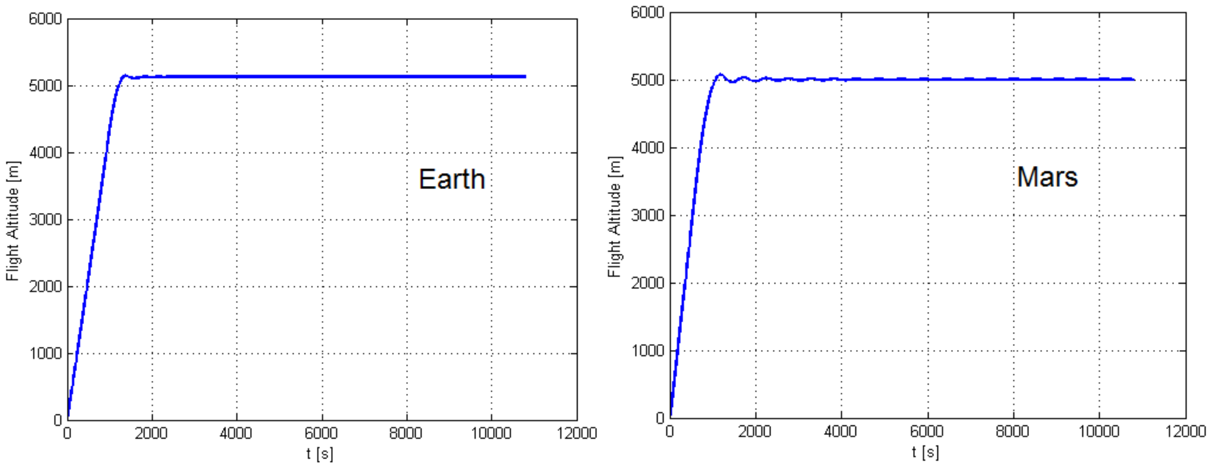

Figure 98: Flight Altitude; (a) Earth, (b) Mars

The flight path of each aerobot, in Figure 98 and Figure 99, is mainly dominated by the ascend speed, which is influenced by the atmosphere conditions, gravity and drag. The denser atmospheres of Titan and Venus tend to have slow ascend velocities compared to those of Earth and Mars, which is illustrated in Figure 100.

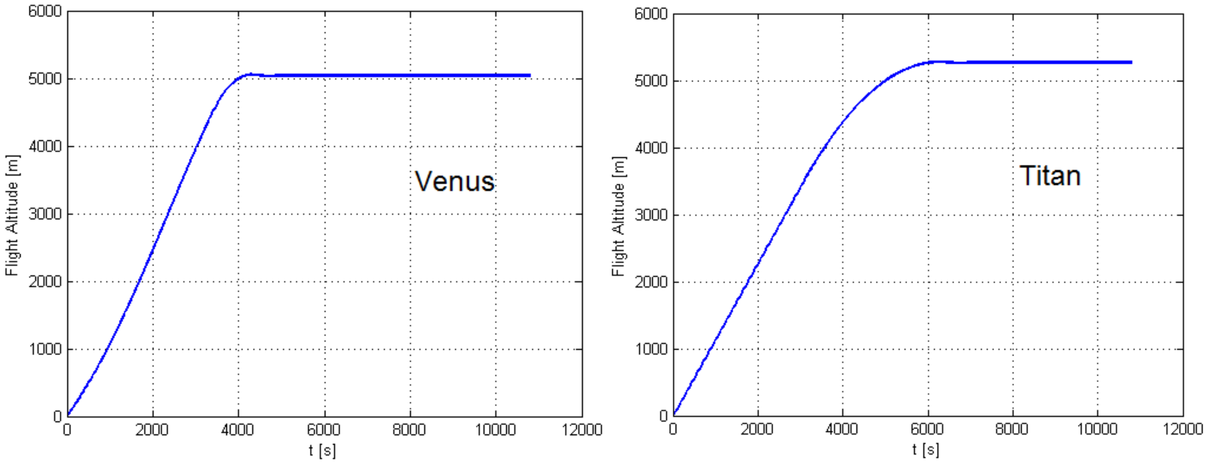

Figure 99: Flight Altitude; (a) Venus, (b) Titan

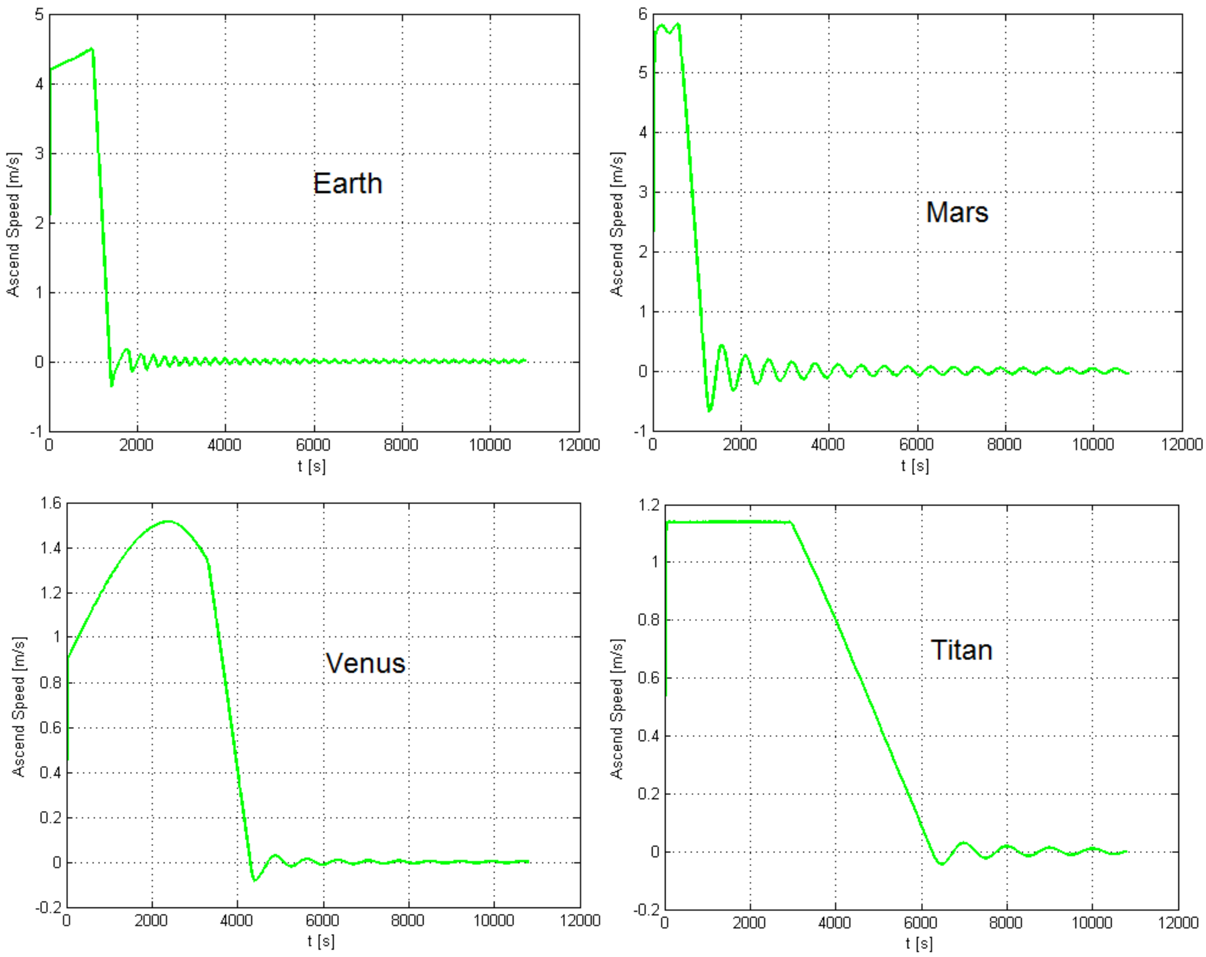

Figure 100: Aerobot Ascend Speed; (a) Earth, (b) Mars, (c) Venus, (d) Titan

8.3. Student Aerobot Design Projects

A lot of high schools and universities have been using scientific balloons for student projects. They send up an un-propelled meteorological balloon with a small payload which they try to recover later on. The payload mostly exist out of a camera, GPS, temperature and pressure sensors; much like the AAB's system in section 3.1.8. The capabilities of BADS in such project are discussed in section 8.3.1.

Other student projects are robotic championships in which propelled robots have to complete a course as efficient and fast as possible. Aerobots take a small role in today's competitions, and a purely buoyant aerobot competition is not yet heard of. It might however be the start of a pioneering way to test new balloon fabrics, aerobot payload technology, etc. and gain the interest of a bigger community.

For both projects there is an opportunity for the implementation of BADS during design and flight. These projects might also be beneficial to BADS itself as the knowledge and data gained from them can be used to improve the accuracy of the simulation tool.

8.3.1. Meteorological Balloon with Payload Recovery

A meteorological balloon is a zero-pressure balloon which rises into the atmosphere until the envelope fabric fails and where the payload is recovered by a slow parachute descend. These high-school projects give students the chance to learn basic aerodynamics, physics of buoyant gases and some trajectory planning, but mainly knowledge about the composition of Earth's atmosphere is gathered and some nice footage of Earth's atmosphere is made.

For this type of mission BADS can be used to help with the initial mass budget of the aerobot, shape selection and size. Once the initial design is chosen BADS can simulate the flight to estimate the time of arrival at the design altitude or the time of envelope failure. When envelope failure is taken into account, BADS is able to simulate the parachuted descend of the payload. This can only be so if the user selects the parachute set-up in the input parameters. Envelope strain is not measured at this time in BADS. Therefore envelope failure will be initiated once the maximum volume is reached for a ZP balloon or a maximum pressure level is reached for the OZP, as discussed in section 6.3.6.

Figure 101 shows a simulated zero-pressure balloon flight with payload recovery. The balloon explodes when it reaches maximum volume. At the same moment the aerobot will lose all its gas mass and halve its envelope mass. This event will start an immediate descend, although much slower than when no parachute would have been onboard.

Figure 101(d) illustrates the flight path of the aerobot in a non-uniform wind profile. When a good wind model is incorporated into BADS, it is possible to estimate the position of the payload drop site. Payload recovery will be easier this way. Currently the user of BADS is only able to enter a uniform wind profile at the start of the simulation though. The example below has been programmed with a non-uniform wind profile to better illustrate the change in aerobot position and the possibilities of BADS in payload recovery. Future work however will include a better wind profile for each of the atmospheric models.

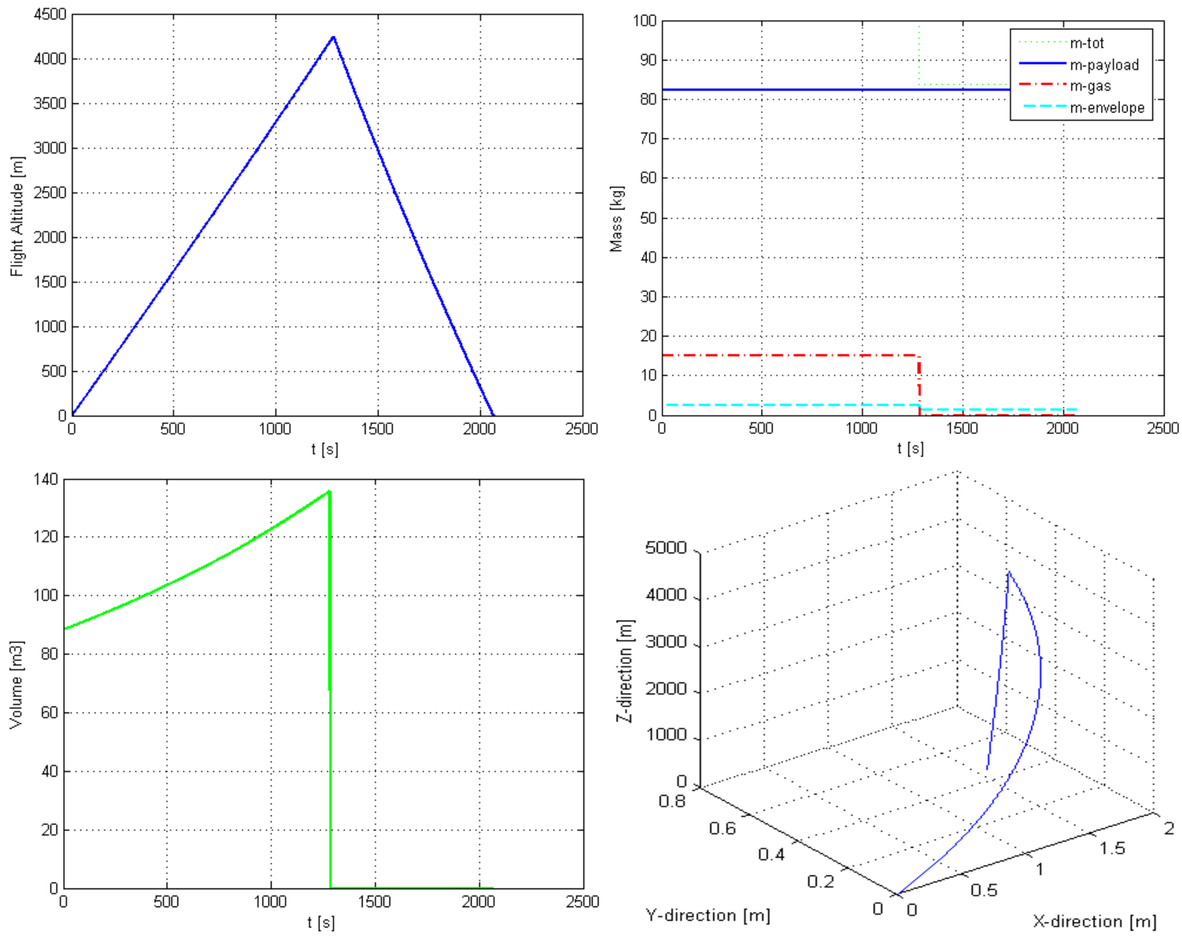

Figure 101: Parachute Descend; (a) Altitude, (b) Mass, (c) Speed, (d) 3D Trajectory

In addition to student projects, as discussed above, a similar project under supervision by professor Menenti at the Delft University of Technology, called the Delft2Mars Balloon [t.6], could have been a good test formula for BADS.

Part of the project included the design of a Martian balloon and its deployment on Mars. BADS could have been useful during the project in two main sections of the project, namely;

- The design of the balloon and the mass breakdown
- Balloon deployment from atmosphere or ground

The BADS initial aerobot design could have been useful during the calculations of the project's own design calculations either as a reference tool to their computations or as a design tool. Next, the extensive atmospheric database in BADS could have been used to simulate the Martian atmosphere for the Delft2Mars balloon.

Throughout the thesis it's been made clear that BADS is able to simulate a balloon launch from the planet's surface. BADS is however also able to simulate aerobot deployment from high altitudes if necessary. This is done through modifying the initial position coordinates and the initial velocities as such that they represent an atmosphere entry. This is illustrated in Figure 102 for a super-pressure aerobot entering the Earth's atmosphere at 30km. Dropping initially at speeds around 90m/s the aerobot quickly decelerates to drop speeds near 60m/s, 40m/s, 20m/s and finally 0m/s, to stabilize around its design altitude of 5000m.

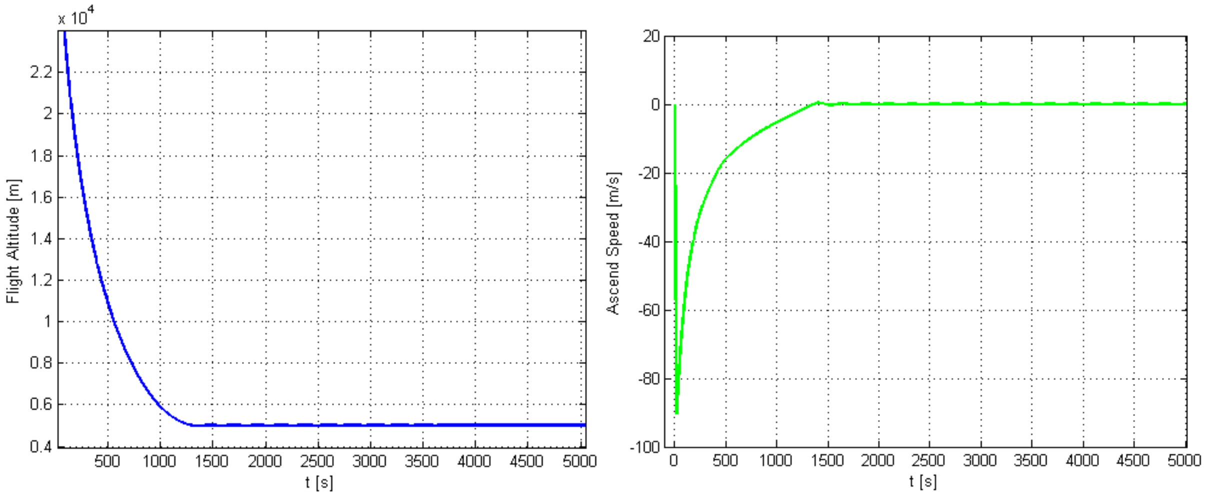

Figure 102: Aerobot Atmosphere Entry and Deployment

For projects such as Delft2Mars, who can be situated in-between student meteorological projects and scientific planetary ballooning missions, BADS could definitely be valuable. Such projects could also be beneficial to BADS itself, as they can be used as reference or improvements to BADS.

8.3.2. Buoyant Aerobot Competition

Many technological and scientific competitions between university, college, or high-school teams exist across the world. Some famous international competitions are;

- World Solar Challenge (WSC) [i.13]: Solar Powered Cars
- Frisian Solar Challenge (FSC) [i.15]; Solar Powered Boats
- International Submarine Races (ISR) [i.14]; Human Powered Submarines

These competitions have multiple beneficial qualities for both the students, the universities and the industry often sponsoring these events. Firstly the students get hand-on experience of the topics they are studying at university. Secondly the universities and the industry can use these competitions as technology demonstrators and promotion opportunities. The WSC, FSC and ISR competitions have proven these features many times.

A competition which is more on topic with the thesis subject is the International Aerial Robotics Competition (IARC). “The International Aerial Robotics Competition is the longest running collegiate aerial robotics challenge in the world. Entering its third decade of advancing the state of the art in autonomous aerial robotic behavior, the competition continues to tackle challenges that are currently impossible for any flying robots owned by government or industry [i.12].”

Figure 103 gives a detailed representation of the different aerial robot types with which most participating teams enter the competition. The IARC contestants mainly use light helicopters, quadrocopters and so on. Buoyant aerobots however are missing, leaving a vacuum for a Buoyant Aerobot Competition.

Before the idea of a unique Buoyant Aerobot Competition can take shape a lot of planning has to be done. Guidelines have to be made, mission statements formed, requirements stated. This is outside the scope of this thesis, but an exemplary study of buoyant aerobot mission statements, requirements and architecture, general and technical guidelines for a buoyant aerobot competition can be viewed in Appendix E and F respectively.

Figure 103: IARC Aerial Robots [i.12]

Teams joining the Buoyant Aerobot Competition would be encouraged to make use of BADS or any other simulation program to simulate their design and flight performance before actual flight. The available data in the program about buoyant gases, envelope fabrics, balloon shapes, balloon pressure types and atmosphere conditions will present them with an abundance of design options. Based on these results they can decide which type of buoyant aerobot they will fly. Further the program can be useful for initial calibrations of power usage, mass budget, etc.

BADS does not include a trajectory planning module yet. Precise GPS tracking and predetermined route planning is therefore not yet available. If this would be integrated into the tool in the future, it would be very beneficial to teams competing in a Buoyant Aerobot Competition.

9. Conclusions and Recommendations

This thesis has been an exploration on buoyant aerobots design and flight behavior on Earth and beyond. After an extensive literature research about the subject it was clear that the buoyant aerobot has a lot of potential for planetary exploration. The limited scientific and technological attention to these aerobots is actually surprising.

The available literature pushed me towards the interesting subject of aerobot flight simulation programs. Despite the fact that the buoyant technology isn't being used in today's space exploration there exists some history in balloon trajectory programs. Balloon trajectory simulation tools are the first step in the actual design of an aerobot testbed for planetary exploration. Also such programs benefits Earth's meteorological community and the space community. Reason enough to continue research on this subject. The outcome was the birth of BADS, a buoyant aerobot design and simulation tool for planetary balloon flights. The results of the program and the potential of it for future work will be described in this chapter.

9.1. Conclusions

As mentioned before a lot of research has been done to get an insight in the current aerobot technology and the available balloon simulation tools. The first is quite immense while the latter is limited at best. Nevertheless the scientific community has its experts and some of them were very happy to help out wherever possible.

The obtained knowledge has been used to write the buoyant aerobot design and simulation program, called BADS. While available equations of motion and existing thermal and aerodynamic models have been incorporated into the program, BADS did not just become a copy of the already existing simulation tools. BADS combines all the best features of the existing tools with as many input and output options and numerous databases available to the user. Among them are; 4 planetary atmospheric models, 4 different balloon shapes, 3 balloon pressure types, thermo-optical properties of 71 coatings, specifics of 15 envelope materials and many more.

The few things BADS lacks to compete with tools like SINBAD, AHAB and Balloon Ascent are; a good stable mathematical core code for the flight simulation, able to handle the amount of quickly varying parameters, a variable drag coefficient for different shapes and a stable thermal model with natural and forced convection for different shapes.

The use of the mathematical Euler method limits the accuracy for larger time steps, and even causes program crashes when too large time steps are used. At small time steps between 0.5 and 5s, BADS works quite well. The results present a good estimate on balloon flight and floating behavior. The accuracy of the bobbing effect was even a surprise to the programmer.

That said, the above only functions as long as no major thermal variations are being thrown in on the buoyant gas and envelope material. The program has three small thermal models incorporated and all of them are limited in use. The problem in all three models is the lack of knowledge on forced convection around arbitrary balloon shapes such as the pumpkin super-pressure balloon and the prolate shaped airship. Not enough data is available on these shapes and only equations and functions on spheres have been found.

Further, Euler can't handle the effect of temperatures changing too high and too fast. Other mathematical methods have been investigated during the development of the program, but were either not suitable for implementation into the code already written or were as unstable as Euler is. The writer acknowledges that his knowledge of the Matlab program was limited and programming is not his best skill. That said, Matlab might have the answer to the instability problem that BADS currently limits its effectiveness. Future work should definitely be placed in the hands of a skilled programmer.

The instability of the program however does not question the usefulness of the program, it only questions the accuracy but then again a simulation is always an estimation.
The atmospheric models incorporated into the program are the backbone of the planetary simulation model. This module alone is a helpful tool for meteorological or basic balloon flight studies. Further the geometric module in the program is a handy tool for calculating the balloon surface, volume and dimensions continuously during flight. Another main strength of BADS is the input section. Its huge amount of variable inputs has the ability to change a design or a flight totally. Demonstrating a high amount of design possibilities.

During validation the results of BADS were compared to results of ACHAB and HASI 2003. BADS initial ascend speed is similar to the results of both ACHAB and HASI. The launch of the aerobot at those speeds are no problem for a general simulation without thermal variations. Drag will lower the initial velocity soon after launch. With a thermal model included however, the aerobot is slowed down by the temperature drop plus the increase in drag force. Due to these features BADS tends to underestimate initial launch speeds too much. Afterwards, when temperature stabilizes and drag drops, the simulated aerobot starts to rise more stable but at an overestimated velocity to make up for the lost time during launch.
Comparing ACHAB, BADS and SINBAD led to the conclusion that at this stage BADS is closer to the program accuracy of SINBAD in its early days than it is to ACHAB. On average BADS and ACHAB differ about 1.44m/s in rate of climb, which isn't too bad considered that the difference between ACHAB and SINBAD is to be 1-1.28m/s. The difference between BADS and SINBAD lays around 1.14m/s.
The accuracy and performance of BADS are a work in progress. They could both be improved though, through the future work proposed in the recommendations.

9.2. Recommendations

NASA employees have been working on programs like SINBAD and Balloon Ascent for more than 3 decades. In that time they gathered the knowledge on the development of a balloon flight simulation program and combined it with in situ data and tests to improve the results.
BADS has been the work of 1 student attempting to program a buoyant aerobot simulation tool with a limited knowledge on Matlab coding, programming and aerobots during the last 2 years. A lot has been learned, processed and finished, but a lot has been left undone too.
BADS has a lot of small features integrated into the program, which are very interesting for a buoyant aerobot design and flight simulation. Without a good coding to ensure stability and accurate results however these features are useless. A lot of work still has to be done to make sure that BADS becomes the multifunctional, interplanetary, buoyant aerobot simulation tool that it should be.

9.2.1. Detailed Enhancements

To this day BADS is a very basic program. The amount of features in BADS resembles some of the better flight simulation programs, but the accuracy of the flight performance is unfortunately way lower than that of any professional program. Research on improvements should be initially in that area before any other problems are tackled. Attempting to increase accuracy will include sorting out the issue of stability. This will lead to investigating the use of a more stable mathematical method for the software programming.

When the mathematical instability is solved, detailed improvements can be made to the program. Enhancing the thermal modeling should be considered as one of the first. The thermal behavior of a balloon and its buoyant gas has a huge influence on the flight results. A new model should incorporate; multiple solar, planetary and atmospheric thermal parameters, envelope radiative properties and convection methods for multiple balloon shapes and sizes. These parameters can only improve the simulation results as long as the amount of parameters can be handled by the program's mathematical core code. In other words as long as simulation stability is ensured.

In Table 36 a number of features of ACHAB, SINBAD, Balloon Ascent and BADS were compared. The features such as; wind models, launch locations, date and time, day and night cycle, convection models, variable drag coefficients and powered flights were defined as 'basic'. These modules should be further investigated and improved so that BADS can make use of their full potential.

Next to the improvement of the current code, expansion of the program is recommended. Extra modules should include; actual wind models, GPS ground track, engine specifics, planetary coordinate systems. Another interesting feature to work on and expanding the program is the simultaneous run and/or storage of data of multiple simulations, making mission comparison more efficient.

9.2.2. Aerobot Testbed

While the initial thesis assignment was the design of an aerobot testbed, it shifted towards a design and simulation tool for buoyant aerobots. From the start however the idea of an aerobot testbed was never far away. An aerobot testbed would complete the BADS project as such a testbed could deliver the final validation of the program.

BADS can be used for the initial design of an aerobot testbed which can then in turn be used to validate simulated flight results. The joint venture of an aerobot testbed and an aerobot simulation program can only bring out the best of both projects.

The aerobot testbed would not only be validating flight results for BADS. The testbed would be the platform for testing different buoyant gases, new envelope materials, parachutes … Next to those, the propelled feature can be tested and used for further improvements. The testbed is also the best candidate to promote a buoyant aerobot competition between universities as mentioned before. This concept would lead to even more research, technology, and awareness of the potential of buoyant aerobots.

9.2.3. Graphical User Interface

Initially the aim of this thesis was to develop BADS towards a graphical user interface simulation program such as SINBAD or Balloon Ascent. As work progressed the code became quite big and stability issues became more important. Development towards a GUI was delayed because of it. At this time, coding of BADS spans about 1500 lines of code and contains 3000 extra lines with data in separate databases. A GUI specifically written for BADS would probably increase the amount of coding times two.

The Matlab GUI building tool also does not comply with the current coding of BADS. The program would have to be completely rewritten to incorporate input and output screens into the simulation code. One of the major improvements to BADS will therefore be the complete overhaul of the code to incorporate a GUI into the program which will make the program more user friendly.

```
Default settings;
  -Initial Distance;        [0 0 0]    [m]
  -Initial Speed;           [0 0 0]    [m/s]
  -Constant Wind Speed;     [0 0 0]    [m/s]
  -Propellor speed;         [0 0 0]    [m/s]
  -Design Altitude;         5000    [m]
  -Total Aerobot Mass;      10      [kg]
  -Balloon type;            "Zero-Pressure"
  -Parachute descend;       "No"
  -Balloon shape;           "Spherical"
  -Balloon Cd;              "Constant"
  -Balloon Cd;              "0.55"
  -Envelope;                "Urethane derivate"
  -Coating;                 "Brilliant Aluminum Paint"
  -Permeability;            "No"
  -Buoyant Gas;             "Helium"
  -Free Lift;               "10%"
  -Ballasting;              "No"
  -Planet;                  "Earth"
  -Day;                     "1"
  -Diurnal Cycle;           "No"
  -Clouds;                  "No"
  -Temperature Model;       "No"
  -Total Sim Time;          "2 hours"
  -Time Step;               "0.5 seconds"
```

```
INITIAL CONDITIONS
Give the initial distance vector as [x y z] in [m]                ;
Give the initial speed vector as [Vx Vy Vz] in [m/s]              ;
Give the wind speed vector as [Vwx Vwy Vwz] in [m/s]              ;

POWER
If it will be a powered flight press [1] else press [0]           ;

BASIC FLIGHT SET-UP
Give your design flight altitude in [m]                           ;
Give your maximum total Aerobot weight in [kg]                    ;

BALLOON SETTINGS
Give a balloon shape; 1)Sphere, 2)Oblate, 3)Prolate, 4)Airship;
Give constant or variable Cd; "1" Cd=constant, "2" Cd=variable;
Give the value for a constant Cd                                  ;
Choose a balloon type; 1)ZP, 2)SP, 3)OZP                          ;
Zero-Pressure or OZP parachute descend? Yes [1], No [0]           ;
Give the percentage of free lift (~10-15%)                        ;

BALLAST, GAS AND ENVELOPE SPECIFICS
Will permeability be an issue? 0 = NO; 1 = Yes                    ;
Give type of ballasting; None[0] Automatic[1] Manual[2]           ;
Choose a buoyant gas; 1)H2, 2)He, 3)CH4, 4)CO2, 5)NH3, 6)N2       ;
Press a number between 1-15 to select envelope material           ;
Press a number between 1-71 to select coating material            ;

TEMPERATURE MODELS
-Press 1 for Temperature Model of a Sphere (Abe et al)
-Press 2 for Temperature Model for Spheroids (Raithby & Hollands)
-Press 3 for Temperature Model for Spheroids (Yovanovich)
Choose your Temperature Model                                     ;

PLANETARY SETTINGS
Choose a planet; 1)Earth, 2)Mars, 3)Venus, 4)Titan                ;
Choose the start day of the mission                               ;
Press "1" for Diurnal Cycle or Enter if not!                      ;
Give cloud percentage between 0-1 as [CloudFraction Altitude];

TIME SETTINGS
Give total simulation time in [hrs]                               ;
Give the time step size Dt<=0.5s                                  ;
```

Figure 104: (a) BADS Default Settings, (b) BADS Data Input Screen

At this stage the data input screen is the Matlab command window. When the main program is run in Matlab, the first two things the user will see are the default settings and the question if he/she wants to modify these settings, as pictured in Figure 104. In the future a basic GUI console should appear when the program starts to run. In this console the user should be able to input all relevant data just by ticking boxes and adding additional numbers.

Figure 105 gives an example of a simply GUI start-up screen, under construction, on balloon specifics and atmospheric details. A graphical window is available for the illustration of the balloon when the input data is provided by the user. Next some selections can be made on planets, buoyant gases, envelope materials and atmospheric options just by clicking on them.

Similar GUI screens can be made for the output data. At this stage the numeric output data is saved into an Microsoft Excel file while the graphical output data appears on screen one by one. In the future graphical data might be combined into one data sheet with graphs such as the one in Figure 106. Zooming and editing options should allow the user to move freely through all of the graphs in detail.

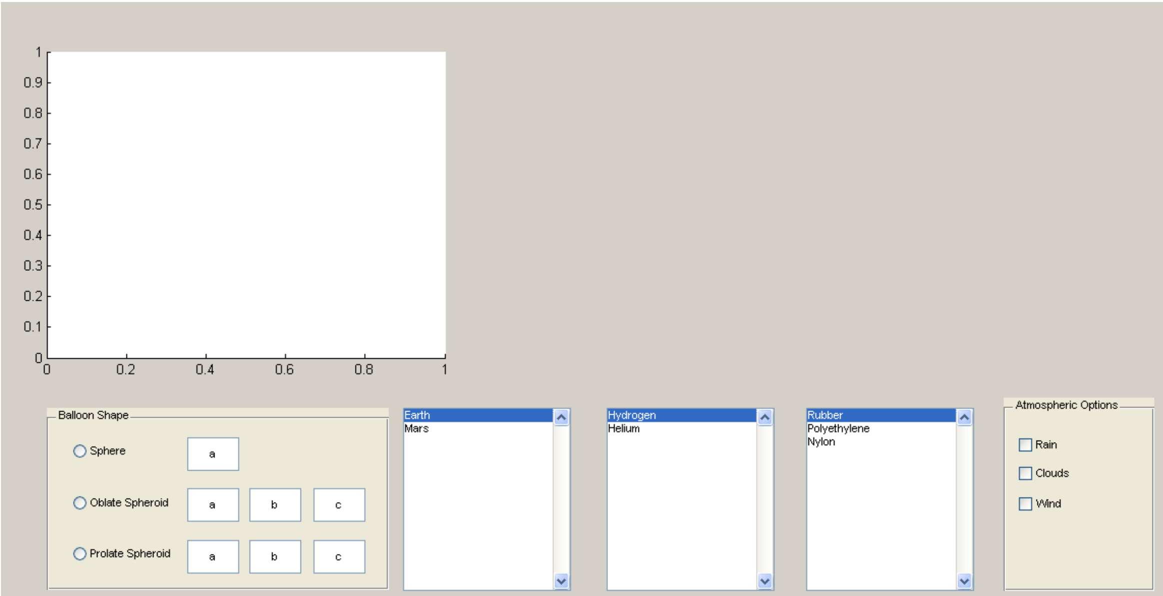

Figure 105: BADS GUI Example Under Construction

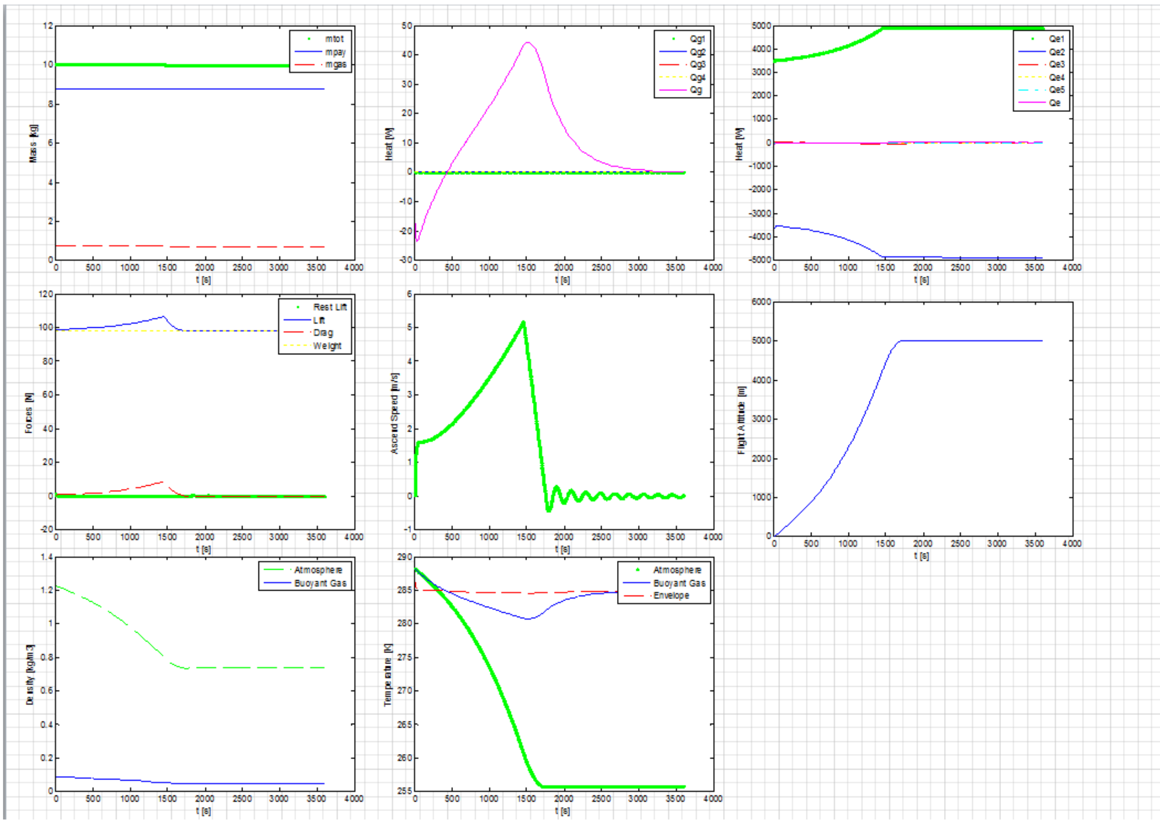

Figure 106: Example of a Graphical Output Summary

Literature

Webpages

[i.1] Earth fact sheet, http://nssdc.gsfc.nasa.gov/planetary/factsheet/earthfact.html
[i.2] Mars fact sheet, http://nssdc.gsfc.nasa.gov/planetary/factsheet/marsfact.html
[i.3] Venus fact sheet, http://nssdc.gsfc.nasa.gov/planetary/factsheet/venusfact.html
[i.4] Parachute Drag Coefficient, http://www.grc.nasa.gov/WWW/k-12/VirtualAero/BottleRocket/airplane/rktvrecv.html,
[i.5] Wikipedia, *Aerobot*, http://en.wikipedia.org/wiki/Aerobot
[i.6] Amateur balloon launch, http://icbnn.wordpress.com/
[i.7] Jet Propulsion Laboratory, *Prototype Aerobot Testbed*, http://www-robotics.jpl.nasa.gov/systems/system.cfm?System=7
[i.8] Archimedes, http://www.archimedes-ballon.de/index.php?id=EN
[i.9] NASA, 2010, http://nssdc.gsfc.nasa.gov/nmc/spacecraftDisplay.do?id=1984-128F
[i.10] 2004, http://www.mentallandscape.com/V_Vega.htm
[i.11] City Montessori School, Lucknow, India, http://schooramani.tripod.com/index.html
[i.12] International Aerial Robotics Competition, http://www.aerialroboticscompetition.org/
[i.13] World Solar Challenge, http://www.worldsolarchallenge.org/
[i.14] International Submarine Races, http://www.isrsubrace.org/
[i.15] Solar Boat Challenge, http://www.frisiansolarchallenge.nl
[i.16] *The Mars Climate Database*, http://www-mars.lmd.jussieu.fr/
[i.17] NASA's K12 Program, http://www-k12.atmos.washington.edu/k12/
[i.18] Mars Atmosphere vs Earth's Atmosphere, http://www.daviddarling.info/images/
[i.19] Wapedia, *Climate of Mars*, http://wapedia.mobi/en/Climate_of_Mars
[i.20] Wikipedia, *Mars*, http://en.wikipedia.org/wiki/Mars
[i.21] Data Mars, http://www.imagineeringezine.com/e-zine/mars-data.html
[i.22] Aerospaceweb, *Aerodynamics*, http://www.aerospaceweb.org/question/aerodynamics/q0015b.shtml
[i.23] Ellipsoids, Spheroids, http://elearning.algonquincollege.com/coursemat/viljoed/gis8746/concepts/geodesy/spheroid.htm
[i.24] http://hyperphysics.phy-astr.gsu.edu/hbase/ptens.html#lap2
[i.25] http://www.eoss.org/faq/zero_pressure.htm, 2003
[i.26] Czech Technical University in Prague, Faculty of Mechanical Engineering, *Drag Coefficients and Flow around Objects*, www.fsid.cvut.cz/~zitnyrud/MHMT5.ppt
[i.27] Drag Coefficient, http://en.wikipedia.org/wiki/Drag_coefficient
[i.28] Drag of a Sphere, http://www.aerospaceweb.org/question/aerodynamics/drag/drag-disk.jpg
[i.29] Viscosity, http://en.wikipedia.org/wiki/Viscosity
[i.30] Titan, http://www.esa.int/Our_Activities/Space_Science/Cassini-Huygens/Facts_about_Titan
[i.31] Earth's atmosphere model, http://www.grc.nasa.gov/WWW/K-12/airplane/atmosmet.html
[i.32] Mars' atmosphere model, http://www.grc.nasa.gov/WWW/K-12/airplane/atmosmrm.html
[i.33] ISA, http://www.engineeringtoolbox.com/international-standard-atmosphere-d_985.html
[i.34] Mars Climate Database, http://www-mars.lmd.jussieu.fr/
[i.35] Mars, http://atmos.pds.nasa.gov/data_and_services/atmospheres_data/Mars/Mars.html
[i.36] Martian Atmosphere, http://physics.uoregon.edu/~jimbrau/astr121/Notes/Chapter10.html
[i.37] Darcy's Law, http://en.wikipedia.org/wiki/Darcy's_law
[i.38] Titan, http://en.wikipedia.org/wiki/Titan_(moon)
[i.39] Stiff Equation, http://en.wikipedia.org/wiki/Stiff_equation
[i.40] Euler Method, http://en.wikipedia.org/wiki/Euler_method
[i.41] CNES balloons, http://www.cnes.fr/web/CNES-en/3641-stratospheric-balloons.php
[i.42] NASA WFF, http://www.nasa.gov/centers/wallops/home/
[i.43] JAXA ISAS, http://www.isas.jaxa.jp/e/enterp/ball/index.shtml
[i.44] University of Oregon, http://pages.uoregon.edu/jimbrau/astr121/Notes/Exam2rev.html

[i.45] Nature, http://www.nature.com/nature/journal/v438/n7069/fig_tab/nature04314_F2.html
[i.46] Titan's atmosphere, http://en.wikipedia.org/wiki/Atmosphere_of_Titan
[i.47] Planetary Surfaces, http://www.jpl.nasa.gov/infographics/infographic.view.php?id=10790
[i.48] Gravity, http://www.hsc.csu.edu.au/physics/options/geophysics/3076/phy.htm
[i.49] Ideal Gases, http://en.wikipedia.org/wiki/Ideal_gas
[i.50] Real Gases, http://en.wikipedia.org/wiki/Real_gas
[i.51] Ellipsoids, http://math.wikia.com/wiki/Ellipsoid
[i.52] Parachutes, http://www.totex.jp/sub3.html
[i.53] Lapse Rate, http://en.wikipedia.org/wiki/Lapse_rate

Books

[b.1] **National Research Council (U.S.), Committee on Planetary and Lunar Exploration, Space Study Board, Commission on Physical Sciences, Mathematics and Applications**, *Scientific rationale for mobility in planetary environments*, National Academy Press, Washington D.C., 1999
[b.2] **J.D. Anderson Jr.**, *Introduction to Flight*, 4th edition, McGraw-Hill, 2000
[b.3] **A.J. Ball, J.R.C. Garry, R.D. Lorenz, V.V. Kerzhanovich**, *Planetary Landers and Entry Probes*, Cambridge University Press, 2007
[b.4] **S. F. Hoerner**, *Fluid-Dynamic Drag, Practical Information on Aerodynamic Drag and Hydrodynamic Resistance*, 1965
[b.5] **T. Abe, T. Imamura, N. Izutsu, N. Yajima**, *Scientific Ballooning; Technology and Applications of Exploration Balloons Floating in the Stratosphere and the Atmospheres of Other Planets*, Springer, 2009
[b.6] **Archimedes**, H.T.L. (ed): *The Works of Archimedes*, Dover Publications, New York, 2002
[b.7] **W.M. Rohsenow**, **J.R. Hartnett**, **Y.I. Cho**, *Handbook of Heat Transfer*, 3rd edition, McGraw-Hill
[b.8] **David R. Lide, ed.**, *CRC Handbook of Chemistry and Physics*, Internet Version 2005, http://www.hbcpnetbase.com, CRC Press, Boca Raton, FL, 2005

Articles/Papers

[a.1] **K.T. Neck, J. Balaram & M.K. Heun, et al**, *Mars 2001 Aerobot / Balloon System Overview*, AIAA International Balloon Technology Conference, June 1997
[a.2] **J. L. Hall, V. V. Kerzhanovich, et al**, *An Aerobot for Global in Situ Exploration of Titan*, Jet Propulsion Laboratory, 2004
[a.3] **G.E. Dorrington**, *Development of an airship for tropical rain forest canopy exploration***,** The Aeronautical Journal, august 2005
[a.4] **H.S. Wright, J.S. Levine, et al,** *Measurements from an Aerial Vehicle: A New Tool for Planetary Exploration*, Jet Propulsion Laboratory, 2004
[a.5] **V.V. Kerzhanovich, J.A. Cutts**, *Balloons for planetary Exploration*, 2000
[a.6] **B. Grieger, H.S. Griebel, et al**, *Archimedes a balloon mission to Mars led by the German Mars Society*, 2006
[a.7] **R. Phoebus**, **C. Reilly**, *Differential Equations and the Parachute Problem*, May 10, 2004
[a.8] **V.M. Kovtunenko, R.Z. Sagdeev, V.L. Barsukov**, *Vega Project: Re-entry Vehicle of Vega Spacecraft*, 1986
[a.9] **B. Peeters, J.A. Mulder, et al,** 2008, *Exofly: A flapping winged Aerobot for autonomous flight in Mars atmopshere*
[a.10] **H.S. Griebel**, *High Altitude Sounding on Mars with an Inflatable Hypersonic Drag Body (Ballute)*, 2010
[a.11] **J. Nott**, *Ballutes: Launching Aerobots without Compromises*, 2006
[a.12] **J.L. Hall, J.A. Jones, et al**, *A gas management system for an ultra-long duration Titan blimp*, Elsevier Science Ltd on behalf of Cospar, 2008
[a.13] **M. van den Berg, P. Falkner, et al**, *ESA Venus Entry Probe Study*, 25th April 2005
[a.14] **S.M. Raqué, J.M. Simpson**, *Automated Pressure Control in Pressurized Balloon Systems*, Elsevier Science Ltd on behalf of Cospar, 1998
[a.15] **J. Nishimura**, *Scientific Ballooning in the 20th Century a Historical Perspective*, Elsevier Science Ltd on behalf of Cospar, 2002
[a.16] **L.G. Seely, M.S. Smith**, *A Realistic View of the Future of Scientific Ballooning*, Elsevier Science Ltd on behalf of Cospar, 2002
[a.17] **J.A Jones, J.J. Wu,** *Solar Montgolfiere Balloons for Mars*, Jet Propulsion Laboratory, 1999
[a.18] **J.A. Jones, J.A. Cutts, J.L. Hall, J.J. Wu, et al**, *Montgolfiere Balloon Missions for Mars and Titan*, Jet Propulsion Laboratory, 2005

[a.19] **H.C. Needleman**, *The NASA balloon program: Conventional and Long Duration*, Elsevier Science Ltd on behalf of Cospar, 1996

[a.20] **I.S. Smith Jr.**, *The NASA Balloon Program: looking to the future*, Elsevier Science Ltd on behalf of Cospar, 2003

[a.21] **H.M. Cathey Jr.**, *The NASA Super pressure balloon – A path to flight*, Elsevier Science Ltd on behalf of Cospar, 2009

[a.22] **R.E. Farley**, *BalloonAscent: 3-D Simulation Tool for the Ascend and Float of High-Altitude Balloons*, NASA/Goddard Space Flight Center, 2005

[a.23] **Schlatter**, *Atmospheric Composition and Vertical Structure*, NOAA Earth Systems Research Laboratory, 23rd July 2009

[a.24] **M. van den Berg, P Falkner**, *Study Overview of the Venus Entry Probe*, European Space Agency, 27th February 2007

[a.25] **G.A. Landis, A. Colozza, C.M. LaMarre**, *Atmospheric Flight on Venus: A Conceptual Design*, Journal of Spacecraft and Rockets Vol. 40, No. 5, September–October 2003

[a.26] **A. Colozza**, *Solid State Aircraft Phase I Project NAS5-98051, Final Report*, Northland Scientific and Ohio Aerospace Institute, November 30, 2002

[a.27] **V.S. Avduevsky et al**, *A Tentative Model of the Venus Atmosphere Based on the Measurements of Veneras 5 and 6*, USSR Academy of Sciences Moscow, 1970

[a.28] **R.V. Yelle, D.F. Strobell, E. Lellouch, D. Gautier**, *Engineering Models for Titan's Atmosphere*,

[a.29] **John H. Henninger**, *Solar Absorptance and Thermal Emittance of Some Common Spacecraft Thermal-Control Coatings*, NASA, April 1984

[a.30] **A.V. Hassani, K.G.T. Hollands**, *Conduction Shape Factor for a Region of Uniform Thickness Surrounding a Three-Dimensional Body of Arbitrary Shape*, 1990

[a.31] **A. Colozza**, *Initial Feasibility Assessment of a High Altitude Long Endurance Airship*, NASA, Glenn Research Center, December 2003

[a.32] **A. Colozza**, *Comparison of Mars Aircraft Propulsion Systems*, NASA, Glenn Research Center, May 2003

[a.33] **A. Colozza**, *Airships for Planetary Exploration*, NASA, Glenn Research Center, November 2004

[a.34] **G. Ahmadi**, *Hydrodynamic Forces*, Clarkson University

[a.35] **R. Shankar Subramanian**, *Drag on spherical particles and steady settling velocities*, Clarkson University

[a.36] **S.M. Raqué, E.J. Robbins**, *Recent Developments in the SINBAD Balloon Vertical Performance Model*, 32nd Aerospace Sciences Meeting & Exhibit, Reno, January 10-13, 1994

[a.37] **W.J. Horn**, **L.A. Carlson**, NASA, *Thermtraj; A Fortran Program to Compute the Trajectory and Gas Film Temperatures and Gas Film Temperatures of Zero Pressure Balloons*, February, 1983

[a.38] **G.J. Garde et al**, Wallops Flight Facility, *Comparison of Two Balloon Flight Simulation Programs*, Virginia, 26-28 September, 2005

[a.39] **IARC**, *Rules for the International Aerial Robotics Competition 6th Mission*, December 3, 2010

[a.40] **X. Deng**, **S. Pellegrino**, *Computation of Partially Inflated Shapes of Stratospheric Balloon Structures*, California Institute of Technology, Pasadena, 2008

[a.41] **A. Techet**, *Object Impact on the Free Surface and Added Mass Effect*, Massachusetts Institute of Technology, Fall 2005

Data Sheets

[d.1] **D.F. Strobell**, *HASI_Total_Atmos_Profile_v2.xls*, October 2010

[d.2] **Lamcotec; Laminating, Coating, Technologies Inc.**, *Lamcotec Laboratory Data*

Theses

[t.1] **Y. Li**, *Master Thesis; Information Gathering Strategies for a Combined Martian System of Aerobots and Rovers*, Cranfield University & Luleå University of Technology, Department of Space Science, Kiruna, 2007

[t.2] **J.A. DeMoss**, *Drag Measurements on an Ellipsoidal Body*, Virginia Polytechnic Institute and State University, August 21, 2007

[t.3] **L.L. Ha**, *Literature Study on Improvements of the Vega Balloon Aerobots for In-Situ Exploration of Venus*, Technical University Delft, 2012

[t.4] **Roberto Palumbo**, *A Simulation Model for Trajectory Forecast, Performance Analysis and Aerospace Mission Planning with High Altitude Zero Pressure Balloons*, University of Naples; Frederico II, Faculty of Engineering, November 2007

[t.5] **X. Deng**, *Clefted Equilibrium Shapes of Super-Pressure Balloon Structures*, California Institute of Technology, Pasadena, 2012

[t.6] **B. Ashari**, **S. Boer**, **B. van Bruchem et al**, *Delft2Mars Balloon*, Design Synthesis Exercise 2010, Delft, June 22, 2010

Useful Background Reading

[BR.1] **Richard L. Burden/J. Douglas Faires,** *Numerical Analysis,* Seventh Edition, Brooks/Cole, 2001

[BR.2] **Boyce/DiPrima,** *Elementary Differential Equations and Boundary Value Problems,* Seventh Edition, Wiley, 2001

[BR.3] **James Stewart,** *Calculus Early Transcendentals,* Fourth Edition, Brooks/Cole, 1999

[BR.4] **De Pater, Lissauer,** *Planetary Sciences,* Cambridge, 2001

[BR.5] **James R. Wertz, Wiley J. Larson,** *Space Mission Analysis and Design,* Third Edition, Kluwer Academic Publishers, 1999

[BR.6] **James R. Wertz et al,** *Mission Geometry; Orbit and Constellation Design and Management,* Kluwer Academic Publishers, 2001

[BR.7] **Peter Fortescue, John Stark,** *Spacecraft Systems Engineering,* Second Edition, Wiley, 2001

[BR.8] **John D. Anderson Jr.,** *Fundamentals of Aerodynamics,* Third Edition, McGraw Hill, 2001

[BR.9] **Michael J. Moran, Howard N. Shapiro,** *Fundamentals of Engineering Thermodynamics,* Third Edition, Wiley, 2002

[BR.10] **G.J.J. Ruijgrok,** *Elements of Airplane Performance,* Delft University Press, 1996

[BR.11] **Rien Elling et al,** *Rapportagetechniek,* 2de edition, Wolters Noordhoff, November 1999

[BR.12] **A.K. Noor, S.L. Venneri, NASA**, *Future Aeronautical and Space Systems*, Progress in Astronautics and Aeronautics, Volume 172, American Institute of Aeronautics and Astronautics Inc., 1997

[BR.13] **H. Ari-Matti**, In *Situ Observations of the Atmospheres of Terrestrial Planetary Bodies*, Finnish Meteorological Institute, 2005

[BR.14] **USAF Captain Eric R. Moomey**, *Technical Feasibility of Loitering Lighter-than-Air Near-Space Maneuvering Vehicles*, Air Force Institute of Technology, Department of the Air Force, Air University, Wright-Patterson Air Force Base, Ohio, March 2005

Appendices

Appendix A: U.S. Standard Atmosphere, 1976

Regions	Geometric Altitude [m]	Temperature [K]	Pressure [hPa]	Density [kg m^3]
Troposphere – Constant lapse rate 0.65Kkm^{-1} (cooling with altitude) from 0.0 to 11.0km.				
	0	288.150	1.01325 +03	1.2250 +00
	1,000	281.651	8.9876 +02	1.1117 +00
	2,000	275.154	7.9501 +02	1.0066 +00
	4,000	262.166	6.1660 +02	8.1935 -01
	6,000	249.187	4.7217 +02	6.6011 -01
	8,000	236.215	3.5651 +02	5.2579 -01
	10,000	223.252	2.6499 +02	4.1351 -01
Tropopause	11,000	216.774	2.2699 +02	3.6480 -01
Stratosphere – Isothermal (216.65K) from 11.1 to 20.0km, then warming with altitude. Lapse rate –1.0 K km^{-1} from 20 to 32 km, then -2.8 K km^{-1} from 32.0 to 47.4km.				
	15,000	216.650	1.2111 +02	1.9476 -01
	20,000	216.650	5.5293 +01	8.8910 -02
	25,000	221.552	2.5492 +01	4.0084 -02
	32,000	228.490	8.8906 +00	1.3555 -02
	37,000	242.050	4.3324 +00	6.2355 -03
Stratopause	47,400	270.650	1.1022 +00	1.4187 -03
Mesosphere – Isothermal (270.650K) from 47.4 to 51.0km, then cooling with altitude. Lapse rate 2.8 Kkm^{-1} from 51 to 71km, then 2.0 K km^{-1} from 71 to 86km.				
	15,000	216.650	1.2111 +02	1.9476 -01
	48,000	270.650	1.0229 +00	1.3167 -03
	51,000	270.650	7.0458 -01	9.0690 -04
	61,000	244.274	1.9157 -01	2.7321 -04
	71,000	216.846	4.4795 -02	7.1966 -04
Mesopause	86,000	186.87	3.7338 -03	6.958 -06
Thermosphere – Isothermal (186.87K) from 86 to 92km, then warming with altitude. Lapse rate decreases until it reaches -12Kkm^{-1} at 120 km, then increases toward zero. Temperature asymptotically approaches 1000K, and reaches that point at 815km altitude.				
	92,000	186.96	1.2887 -03	2.393 -06
	100,000	195.08	3.2011 -04	5.604 -07
	120,000	360.00	2.5382 -05	2.222 -08
	150,000	634.39	4.5422 -06	2.076 -09
	200,000	854.56	8.4736 -07	2.541 -10
	300,000	976.01	8.7704 -08	1.916 -11
	500,000	999.24	3.0236 -09	5.215 -13
	700,000	999.97	3.1908 -10	3.070 -14
	1,000,000	1000.00	7.5138 -11	3.561 -15

Appendix B: Mars

Figure 107: Planet Mars

Aerobots might be an interesting follow-up of planet rovers on the planets in the solar system. Only planets with atmospheres however are suitable candidates for these robots. That leaves Mars, Venus and the moon Titan. Each planet's atmosphere however is different than that of Earth, and therefore a thorough knowledge of these differences is required for any basic aerobot design. This chapter will go into detail about the Martian atmosphere and planetary details.

B.1. Mars Atmosphere

"Mars possesses a very thin atmosphere that consists mainly of carbon dioxide (~95%). The other major constituents are nitrogen (~2.7%) and argon (~1.6%), with oxygen and water vapor contributing trace amounts. The surface pressure is only 7 mbar, or less than 1% of Earth's current atmosphere. This tenuous body is the remnant of a much denser envelope that was gradually dispersed primarily through interactions with solar radiation and particles in the solar wind." [i.19]

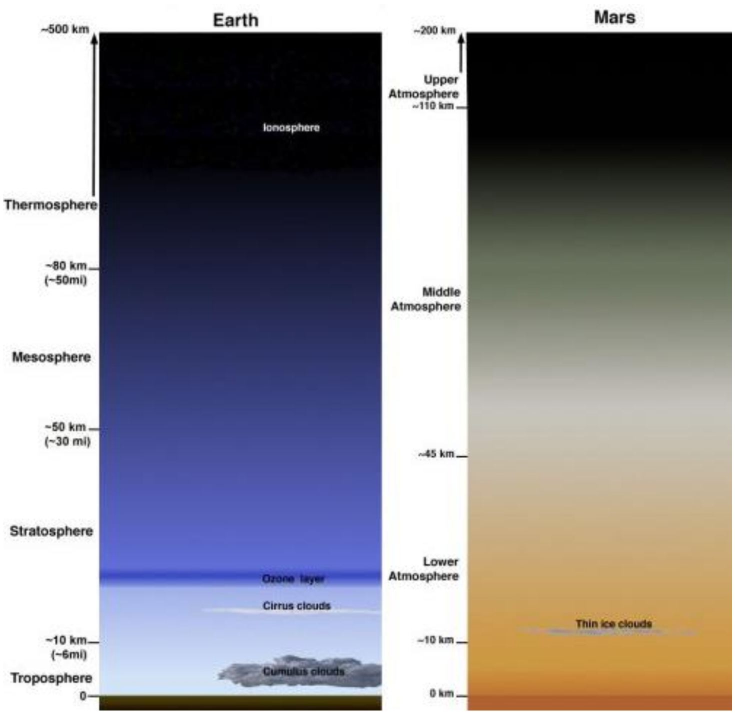

Figure 108: Earth's Atmosphere compared to Mars'

Figure 108 [i.18] shows a comparison between the size and build-up of Earth's atmosphere and Mars' atmosphere. "Mars lost its magnetosphere 4 billion years ago, so the solar wind interacts directly with the Martian ionosphere, keeping the atmosphere thinner than it would otherwise be by stripping away atoms from the outer layer. Both Mars Global Surveyor and Mars Express have detected these ionized atmospheric particles trailing off into space behind Mars. Compared to Earth, the atmosphere of Mars is quite thin. Atmospheric pressure on the surface ranges from a low 30 Pa on Olympus Mons to over 1155 Pa in the Hellas Planitia, with a mean pressure at the surface level of 600 Pa. The surface pressure of Mars is equal to the pressure found 35km above the Earth's surface. This is less than 1% of the Earth's surface pressure (101.3kPa). The scale height of the atmosphere is about 10.8 km, which is higher than Earth's (6 km) because Mars' surface gravity is only about 38% of Earth's, an effect offset by both the lower temperature and 50% higher average molar weight of Mars' atmosphere." [i.20]. Gravity and pressure play an important role in designing an aerodynamically shaped aerobot and the propulsion system.

B.2. Mars Climate and weather

This section summarizes the differences on Mars compared to Earth on; temperature, solar flux, dust storms, wind patterns and the seasons. For further detailed in situ information on these subjects the reader could consult [i.34] and [i.35].

B.2.1. Temperature

"Of all the planets in the Solar System, Mars' seasons are the most Earth-like, due to the similar tilts of the two planets' rotational axes. However, the lengths of the Martian seasons are about twice those of Earth's, as Mars' greater distance from the Sun leads to the Martian year being about two Earth years long. Martian surface temperatures vary from lows of about -87 °C during the polar winters to highs of up to 20 °C in summers. The wide range in temperatures is due to the thin atmosphere which cannot store much solar heat, the low atmospheric pressure, and the low thermal inertia of Martian soil." [i.20]

"Differing values have been reported for the average temperature on Mars, with a common value being -55 °C. Surface temperatures have been estimated from the Viking Orbiter Infrared Thermal Mapper data; this gives extremes from 27 °C to -143 °C at the winter polar caps. Actual temperature measurements from the Viking landers range from -17.2 °C to -107 °C. In southern spring and summer, variance is dominated by dust storms, which increase the value of the night low temperature and decrease the daytime peak temperature, resulting in a small 20°C decrease in average surface temperature, and a moderate 30°C increase in upper atmosphere temperature." [i.19]

B.2.2. Solar Flux

"The planet is about 1.52 times as far from the sun as Earth, resulting in just 43 percent of the amount of sunlight [i.20]." This distance is an important factor to take into account for any electrical system based on solar power. Using Equation 130 the solar flux at Mars can be calculated.

$$I_{Mars} = I_{Earth} \cdot \left(\frac{r_{sun-earth}}{r_{sun-mars}} \right)^2$$

Equation 130: Solar Flux

Using a constant solar flux at Earth of $1370 W/m^2$ and distances of 1 astronomical unit (AU) and 1.5AU for the radiuses between sun and Earth and sun and Mars respectively; the value for the solar flux at Mars becomes: $608.9 W/m^2$.

Table 54: Mars Season Data

Month	Ls Range [°]		Sol Range		Duration [sols]	Specifics
1	0	30	0.0	61.2	61.2	Northern hemisphere spring equinox at Ls=0
2	30	60	61.2	126.6	65.4	
3	60	90	126.6	193.3	66.7	Aphelion at Ls=71
4	90	120	193.3	257.8	64.5	Northern hemisphere summer solstice at Ls=90
5	120	150	257.8	317.5	59.7	
6	150	180	317.5	371.9	54.4	
7	180	210	371.9	421.6	49.7	Northern hemisphere Autumn equinox at Ls=180 Dust storm season begins
8	210	240	421.6	468.5	46.9	Dust Storm Season
9	240	270	468.5	514.6	46.1	Perihelion at Ls251 Dust storm season
10	270	300	514.6	562.0	47.4	Northern hemisphere winter solstice at Ls=270 Dust storm season
11	300	330	562.0	612.9	50.9	Dust storm season
12	330	360	612.9	668.6	55.7	Dust storm season ends

B.2.3. Seasons of Mars

“If Mars had an Earth-like orbit, its seasons would be similar to Earth's because its axial tilt is similar to Earth's. However, the comparatively large eccentricity of the Martian orbit, as represented in Figure 109 [i.16], has a significant effect. Mars is near perihelion when it is summer in the southern hemisphere and winter in the north, and near aphelion when it is winter in the southern hemisphere and summer in the north. As a result, the seasons in the southern hemisphere are more extreme and the seasons in the northern are milder than would otherwise be the case. The summer temperatures in the south can reach up to 30 °C warmer than the equivalent summer temperatures in the north.” [i.20]

“A Martian year is 668.6 sols, or Martian solar day, long and a sol is 88775.245 seconds long. Martian months are defined as spanning 30 degrees in solar longitude. Due to the eccentricity of Mars' orbit, Martian months differ in time from 46 to 67 sols long [i.16]”. The effects of each season and the length of them are represented in detail in Table 54, where Ls is the solar longitude in Figure 109 [i.16].

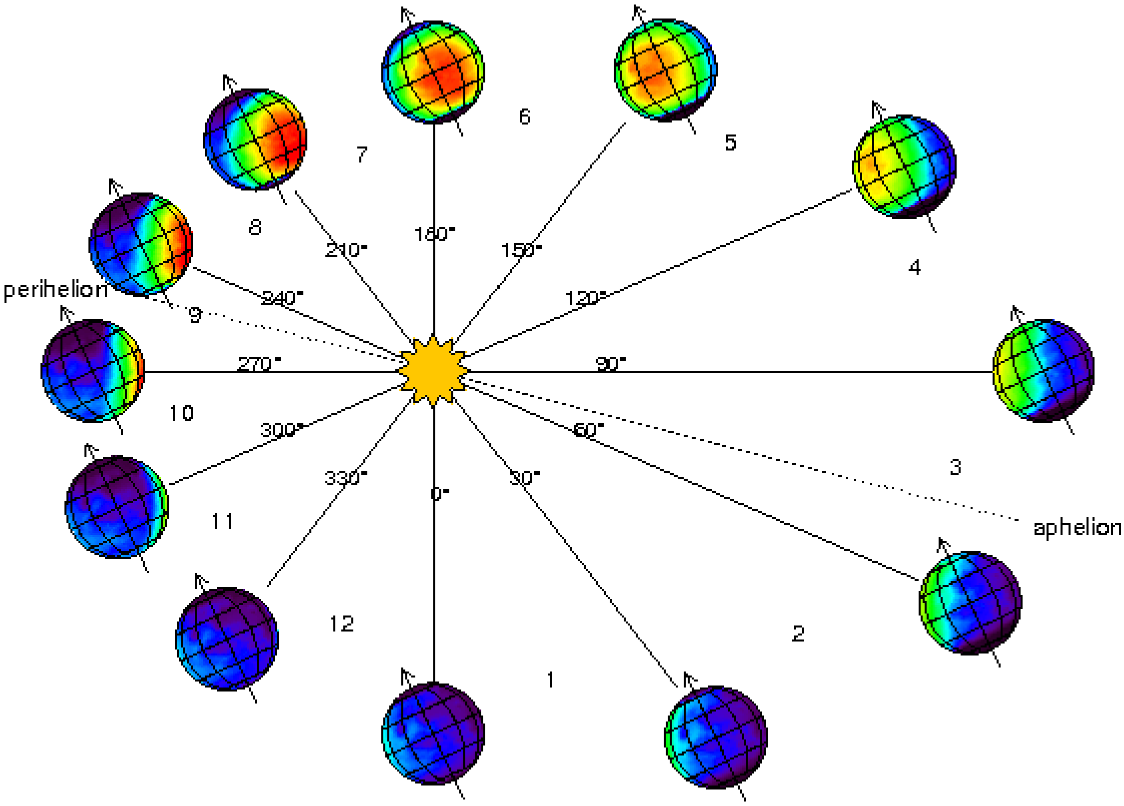

Figure 109: Mars orbit around the Sun

B.2.3.1. Dust

From Table 54 some distinctive weather phenomena can be found, one of them are the dust-storms on Mars. “Mars has the largest dust storms in our Solar System. These can vary from a storm over a small area, to gigantic storms that cover the entire planet. They tend to occur when Mars is closest to the Sun, and have been shown to increase the global temperature [i.20].” During these dust storms, the maximum daytime temperature decreases and the minimum, night time temperature increases: the effect is very similar to that of clouds on Earth. [i.17]

“Atmospheric dust causes daily pressure variations proportional to the dust amount; the magnitude of the daily variation can increase rapidly, but decreases slowly as the dust falls out of the atmosphere if it’s a deep, great dust storm. ‘Great’ dust storms, such as the 1977 A and 1977 B storm, produced a large increase in the daily variation which slowly decreased over tens of sols. The global oscillations observed produce daily pressure variations, which increase and decrease over a few sols, and are indicated by the label ‘Transient Normal Modes’. They seem to reoccur at the same time each year due to the atmospheric temperature causing the resonance to drift through the diurnal period at the same time of year. Finally, the frontal activity is indicated by marked increases in this variability indicator, but the sol to sol values change significantly as the storms pass by [i.17].” A view of a global storm is shown in Figure 110.

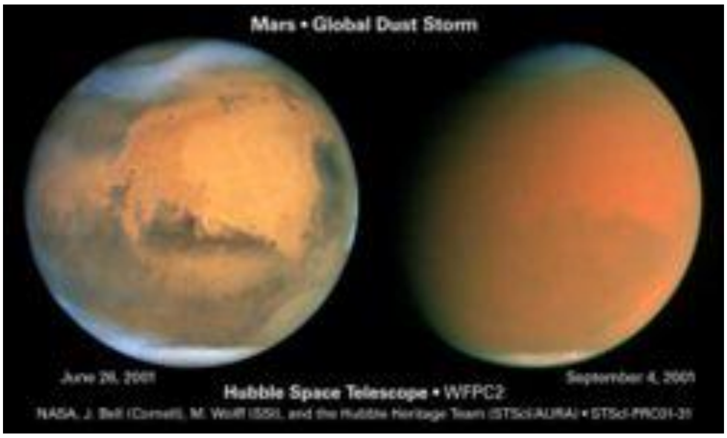

Figure 110: Global Dust Storm on Mars

B.2.3.2. Winds

"The surface of Mars has a very low thermal inertia, which means it heats quickly when the sun shines on it. Typical daily temperature swings, away from the Polar Regions, are around 100 K. On Earth, winds often develop in areas where thermal inertia changes suddenly, such as from sea to land. There are no seas on Mars, but there are areas where the thermal inertia of the soil changes, leading to morning and evening winds akin to the sea breezes on Earth." [i.19] Mars is dryer and colder than Earth, and in consequence dust raised by these winds tends to remain in the atmosphere longer than on Earth as there is no precipitation to wash it out, with some exception to CO^2 snowfall once and a while [i.19]. Winds at Mars during summer were light at both Viking sites, ranging from 0m/s to 10m/s [i.17]. They do depend on landing locations as it is clear that winds are different in strength at mountains and valleys or craters. During fall and winter, as the fronts become stronger, the winds increase. "At Viking 2's landing site they reached 23 m/s [i.17]. An important thing to remember is that the force of the wind is lower on Mars by about a factor of 10, compared to Earth due to its lower density.

B.3. Aerodynamic differences on Mars

The difference in gravitational force and atmospheric density has a great influence on basic aerodynamic forces. Considering a helicopter-type based aerobot, which need at least one blade turning to have thrust and lift at the same time.

The lift-equation in Equation 131 shows the relation between atmospheric density, speed and reference area. The reference area for a helicopter is actually the circle that the rotating blade makes when delivering the thrust, as shown in Figure 112, while that for a plane is the wing surface [i.22]. The reference area for a spherical balloon is quite similar to the one of a helicopter. The cross-sectional area of a balloon is also a circle. For spheroids the reference area is an ellipse.

$$L = 0.5 \cdot \rho \cdot C_L \cdot V^2 \cdot A$$

Equation 131: Lift - Equation

While the gravitational parameter on Mars is only a third of what it is on Earth and is an advantage for any aerobot, the density is 61.5 times smaller than on Earth and is a big disadvantage. These values are general values for simplicity. Actual values vary with altitude.

$$\rho_E = 1.23\,\text{kg/m}^3 \qquad \rho_M = 0.02\ \text{kg/m}^3 \qquad [\text{i.21}]$$
$$g_E = 9.81\ \text{m/s}^2 \qquad g_M = 3.74\ \text{m/s}^2 \qquad [\text{i.20}]$$

When taking the lift-equation into account for both planets, each with their individual gravitational parameters and atmospheric densities, but with the same aerobot parameters, like: lift coefficient, fly speed, mass; the following equations hold:

$$L_E = W_E = g_E \cdot m = 0.5 \cdot \rho_E \cdot C_L \cdot V^2 \cdot A_E$$

$$L_M = W_M = g_M \cdot m = 0.5 \cdot \rho_M \cdot C_L \cdot V^2 \cdot A_M$$

When the two equations are divided by each other, the correlation between the required reference area on Earth and that on Mars can be found. Parameters like speed, lift coefficient and mass can be cancelled out as these are the same for both Earth and Mars. Equation 132 shows a relation where only gravity and atmospheric density contribute to the difference in reference area:

$$A_M = A_E \cdot \frac{\rho_E}{\rho_M} \cdot \frac{g_m}{g_E}$$

Equation 132: Reference Area

The relation between the two reference areas in numerical values is found by using the gravitational parameters and the atmospheric density of both planets:

$$A_M = 23.446 \cdot A_E$$

Equation 133: Mars-Earth Area relation

As the reference area for a spherical balloon is a circle, this equation can be rewritten as Equation 134 with D being the diameter of the circle or rotor blade:

$$A = \pi \cdot d^2$$

Equation 134: Circle Area

A Martian aerobot then requires a rotor blade the size of:

$$d_M = 4.84 \cdot d_E$$

Equation 135: Mars-Earth Rotor Blade Diameter relation

This is a large factor especially considering that this increase in rotor blade size influences power, mass and many other subsystems. One solution to avoid larger engines might be the increase in a number of small rotor blades instead of one large one. This however will not reduce power, and might only have a slight benefit in weight.

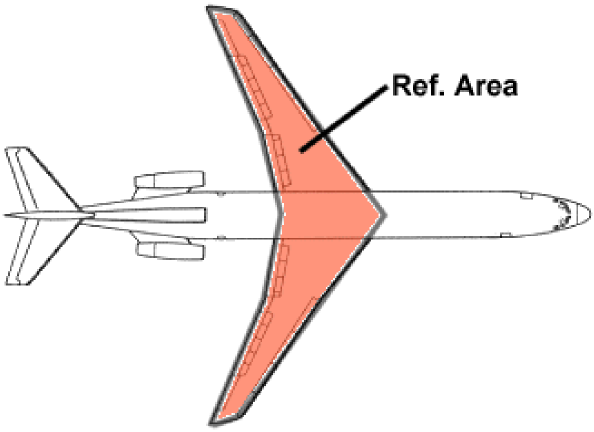

Figure 111: Reference Area of a Plane

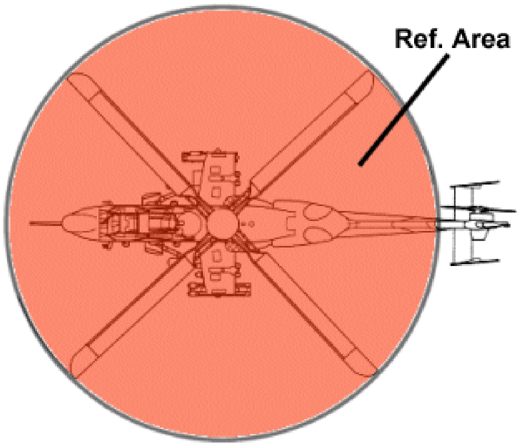

Figure 112: Reference Area of Helicopter

Appendix C: Free Convection Nusselt Number Correlation Constants

Geometry and geometric parameters				Nu_{COND}	G	n	$\bar{C}_l$, Pr = 0.71	6.0	100	2000	m	Data
Sphere												
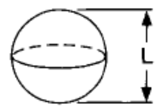	$Nu = \bar{h}L/k$, $Ra = \frac{g\beta\Delta T L^3}{\nu\alpha}$, $A_s = \pi L^2$			2.00	0.878	1.0	0.104	0.111	0.098	0.086	15	See Table 4.3*b*.
Prolate spheroid		C/L	f_1									
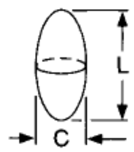	$Nu = \bar{h}L/k$	0.1	1.578	8.43	1.012	1.07	0.103	0.112	0.091	0.066	10	NA
		0.2	1.598	5.35	1.005	1.07	0.103	0.112	0.091	0.069	10	NA
	$Ra = \frac{g\beta\Delta T L^3}{\nu\alpha}$	0.4	1.665	3.51	0.980	1.07	0.103	0.111	0.093	0.076	10	NA
		0.5	1.709	3.08	0.964	1.07	0.103	0.111	0.094	0.078	10	See Table 4.3*b*.
	$A_s = \pi L c f_1/2$	0.6	1.759	2.76	0.948	1.07	0.103	0.111	0.095	0.080	10	NA
		0.8	1.873	2.31	0.913	1.07	0.104	0.111	0.097	0.083	10	NA
		1.0	2.000	See sphere								
Oblate spheroid		C/D	f_1									
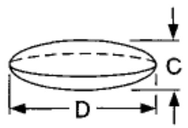	$Nu = \bar{h}D/k$	0.1	1.030	2.63	0.713	1.04	0.094	0.097	0.094	0.090	10	See Table 4.3*b*.
		0.2	1.094	2.62	0.745	1.07	0.100	0.103	0.098	0.092	10	NA
	$Ra = \frac{g\beta\Delta T D^3}{\nu\alpha}$	0.4	1.274	2.48	0.845	1.07	0.103	0.108	0.100	0.092	10	NA
		0.5	1.380	2.40	0.866	1.07	0.104	0.109	0.101	0.091	10	See Table 4.3*b*.
	$A_s = \pi D^2 f_1/2$	0.6	1.494	2.31	0.877	1.07	0.104	0.110	0.100	0.090	10	NA
		0.8	1.739	2.15	0.884	1.07	0.104	0.110	0.099	0.088	10	NA
		1.0	2.000	See sphere								
Short vertical circular cylinder—square ends		L/D										
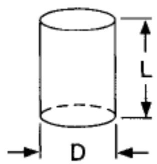	$Nu = \bar{h}D/k$	0.0		2.55	0.670	1.07	0.070	0.070	0.073	0.075	10	NA
		0.1		2.44	0.730	1.06	0.076	0.077	0.076	0.073	15	See Table 4.3*b*.
	$Ra = \frac{g\beta\Delta T D^3}{\nu\alpha}$	0.5		1.93	0.792	1.07	0.087	0.091	0.082	0.069	10	NA
		1.0		1.59	0.839	1.11	0.092	0.098	0.085	0.068	10	See Table 4.3*b*.
		2.0		1.26	0.733	1.07	0.096	1.04	0.087	0.066	10	NA
	$A_s = \frac{\pi D^2}{2}\left(1 + \frac{2L}{D}\right)$	4.0		0.99	0.657	1.07	0.099	1.08	0.089	0.065	10	NA

Shape	Reference	Ra range	Pr	E_{RMS} (%)	E_{MAX} (%)
Sphere	38, 39	10^1–10^8	0.71	0.7	4.1
	242	10^9–10^{12}	~6	10.7	18.5
	301	10^8–10^{10}	2000	5.2	9.5
	280	10^7–10^{11}	2000	9.7	18.9
Prolate spheroid					
$C/L = 0.52$	124, 126, 127	10^1–10^8	0.71	1.8	4.7
	229	10^3–10^7	0.71	6.0	9.3
Oblate spheroid					
$C/L = 0.5$	124, 126, 127	10^1–10^7	0.71	3.3	6.4
$C/L = 0.1$	229	10^3–10^6	0.71	7.2	11.9
	124, 126, 127	10^1–10^8	0.71	3.3	7.4
Short vertical cylinder					
$L/D = 0.1$	124, 126, 127	10^1–10^8	0.71	3.1	10.2
$LD = 1.0$	255	10^1–10^7	0.71	1.4	5.1
		10^4–10^5	0.71	5.0	5.9
Short horizontal cylinder					
$L/D = 0.1$	124, 126, 127	10–10^7	0.71	1.3	3.0
$L/D = 1.0$	124, 126, 127	10–10^7	0.71	1.0	2.9
$0.069 \le L/D \le 0.155$	301	10^2–10^5	0.71	~3.0	~10.0
Short inclined cylinder					
$L/D = 1.0, \theta = 45°$	124, 126, 127	10–10^7	0.71	2.4	9.9
Vertical cylinder with spherical end caps					
$L/D = 2.0$	124, 126, 127	1–10^7	0.71	2.0	4.9
Horizontal cylinder with spherical end caps					
$L/D = 2.0$	124, 126, 127	1–10^7	0.71		
Bisphere					
	124, 126, 127	1–10^7	0.71	1.9	5.6
	280	10^8–10^9	2000	?	32%
Short vertical square cylinder					
$L/D = 0.1$	124, 126, 127	10–10^8	0.71	2.7	4.9
Cube—corner up					
	38, 39	1–10^7	0.71	1.5	4.3
	262	10^5–10^7	0.71	0.9	1.8
	262	10^5–10^7	6.0	2.9	5.6
	280	10^8–10^{11}	2000		
Cube—edge up	38, 39	1–10^7	0.71	2.1	7.3
	262	10^3–10^6	0.71	1.9	3.2
	262	10^5–10^7	~60	2.5	3.7
	280	10^8–10^{10}	2000	7.9	19
Cube—face up	38, 39	10^2–10^7	0.71	0.9	2.6
	262	10^3–10^6	0.71	0.9	1.5
	262	10^5–10^7	6.0	5.3	9.7
	286	10^6–10^{10}	2000	7.8	15.1
	280	10^6–10^9	2000	8.4	14.2
Short square cylinder—edge up					
$L/D = 0.1$	124, 126, 127	10^2–10^7	0.71	1.7	4.2
$L/D = 1.0$	see Cube—edge up				
Short square cylinder—face up					
$L/D = 0.1$	124, 126, 127	10–10^8	0.71	1.6	3.7
$L/D = 1.0$	see Cube—face up				
Horizontal cones					
$3.5 < \phi < 11.5$	212	10^5–10^6	0.71	3.1	10.6
	280	10^6–10^{11}	2000	10.1	33.9
L corner	234	10^6–10^9	6.0	4.2	
V corner	234	10^6–10^9	6.0	3.4	4.0

NA, none available.

Appendix D: Thermo-Optical Coating Data

CONDUCTIVE PAINTS			
Coating	BADS Nr.	α_e	ε_{IR}
Brilliant Aluminum Paint	1	0.30	0.31
Epoxy Aluminum Paint	2	0.77	0.81
Finch Aluminum Paint 643-1-1	3	0.22	0.23
Leafing Aluminum in Epon 828	4	0.37	0.36
Leafing Aluminum (80-U)	5	0.29	0.32
NRL Leafing Aluminum Paint	6	0.24	0.24
Silicone Aluminum Paint	7	0.28	0.29
Silicone Aluminum Paint	8	0.29	0.30
Dupont Silver Paint 4817	9	0.43	0.49
Chromeric Silver Paint 586	10	0.30	0.30
GSFC Yellow NS-43-G	11	0.38	0.90
GSFC Green NS-53-B	12	0.52	0.87
GSFC Green NS-43-E	13	0.57	0.89
GSFC White NS-43-C	14	0.20	0.92
GSFC Green NS-55-F	15	0.57	0.91
GSFC Green NS-79	16	0.57	0.91
WHITE COATINGS			
Barium Sulphate with Polyvinyl Alcohol	17	0.06	0.88
Biphenyl-White Solid	18	0.23	0.86
Catalac White Paint	19	0.24	0.90
Dupont Lucite Acrylic Lacquer	20	0.35	0.90
Dow Coming White Paint DC-O07	21	0.19	0.88
GSFC White Paint NS43-C	22	0.20	0.92
GSFC White Paint NS44-B	23	0.34	0.91
GSFC White Paint MS-74	24	0.17	0.92
GSFC White Paint NS-37	25	0.36	0.91
Hughson White Paint A-276	26	0.26	0.88
Hughson White Paint A-276 + 1036 ESH UV	27	0.44	0.88
Hughson White Paint V-200	28	0.26	0.89
Hughson white Paint Z-202	29	0.25	0.87
Hughson White Paint Z-202 + lO00 ESH UV	30	0.40	0.87
Hughson White Paint Z-255	31	0.25	0.89
Mautz White House Paint	32	0.30	0.90
3M-401 White Paint	33	0.25	0.91
Magnesium Oxide White Paint	34	0.09	0.90
Magnesium Oxide Aluminium Oxide Paint	35	0.09	0.92
Opal Glass	36	0.28	0.87
OSO-H _Vhite Paint 63W	37	0.27	0.83
P764-I A White Paint	38	0.23	0.92
Potassium Fluorotitanate White Paint	39	0.15	0.88
Sherwin Williams White Paint (A8Wl l)	40	0.28	0.87
Sherwin Williams White Paint (F8W2030)	41	0.39	0.82

Sherwin Williams F8W2030 with Polasol V6V241	42	0.20	0.87
Sperex White Paint	43	0.17	0.85
Tedlar White Plastic	44	0.39	0.87
Titanium Oxide White Paint with Methyl Silicone	45	0.20	0.90
Titanium Oxide White Paint with Potassium Silicate	46	0.17	0.92
Zerlauts S-l 3G White Paint	47	0.20	0.90
Zerlauts Z-93 White Paint	48	0.17	0.92
Zinc Orthotitanate with Potassium Silicate	49	0.13	0.92
Zinc Oxide with Sodium Silicate	50	0.15	0.92
Zirconium Oxide with 650 Glass Resin	51	0.23	0.88
BLACK COATINGS			
Anodize Alack	52	0.88	0.88
Carbon Black Paint NS-7	53	0.96	0.88
Catalac Black Paint	54	0.96	0.88
Chemglaze Black Paint Z306	55	0.96	0.91
Delrin Black Plastic	56	0.96	0.87
Ebanol C Black	57	0.97	0.73
Ebanol C Black-384 ESH* UV	58	0.97	0.75
GSFC Black Silicate MS-94	59	0.96	0.89
GSFC Black Paint 313-1	60	0.96	0.86
Hughson Black Paint H322	61	0.96	0.86
Hughson Black Paint L-300	62	0.95	0.84
Martin Black Paint N-150-1	63	0.94	0.94
Martin Black Velvet Paint	64	0.91	0.94
3M Black Velvet Paint	65	0.97	0.91
Paladin Black Lacquer	66	0.95	0.75
Parsons Black Paint	67	0.98	0.91
Polyethylene Black Plastic	68	0.93	0.92
Pyramil Black on Beryllium Copper	69	0.92	0.72
Tedlar Black Plastic	70	0.94	0.90
Velestat Black Plastic	71	0.96	0.85

Appendix E: Aerobot Engineering Example

Originally, as a thesis assignment, a mission statement was written for the design of an aerobot testbed. This statement is now used to select mission elements as an example and as a starting point for the aerobot design and simulation program that was developed in chapter 5. From the mission concept, architecture and some preliminary aerobot requirements, a system engineering model will follow for a standard aerobot.

E.1. Mission Statement

“Flying above obstructions and carried by the winds, an aerobot could inspect large regions of a planet in great detail for relatively low cost. To achieve successful exploration, the aerobot has to explore a large area on ground. It shall be highly maneuverable to allow pointing the instruments in the right direction.”

E.2. Mission Architecture

From the mission statement two main mission elements can be found: High maneuverability (1) for instrument pointing and inspection of large areas (2), signifying a good endurance. Some related mission objectives can be deduced from and added to the mission statement. Use of buoyant gases (3), excluding high mass helicopters and such, the stable flight path control (2), use of COTS systems for operation to lower costs (4), and the use of extra payload depending on the detailed mission concepts (5). Figure 113 shows the basic mission and aerobot elements which are all explained in detail below.

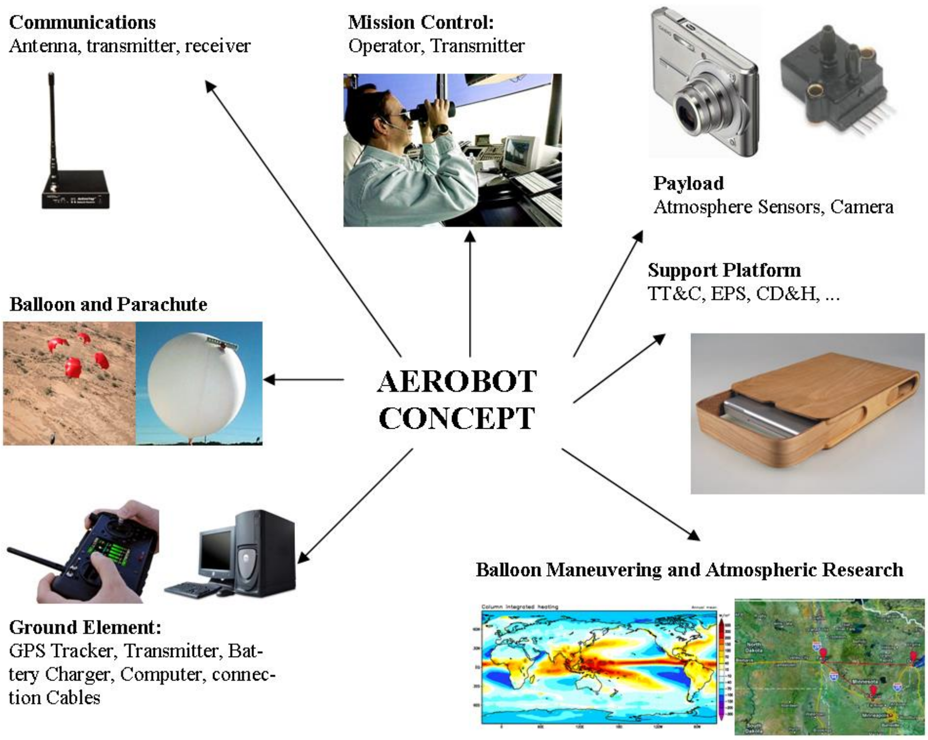

Figure 113: Aerobot Architecture

Flying and Maneuvering

One of the most basic operations of the aerobot will be flying and maneuvering. The aerobot will fly to a certain altitude and maneuver across or around objects. Hovering in the air is also one of the capabilities an aerobot should have for good instrument pointing accuracy.

Control and Operations

From a ground station, which is basically a transmitter with receiver, the entire mission will be controlled. The aerobot will be flown by a controller handling the transmitter. The controller should be capable of flying the aerobot to a predefined position or let the aerobot fly through an automated pathway to that position. If automated, the controller should still be in control when the program fails. Among its operations the aerobot should also fly payload into the air and send data back and forth to the controller.

Communications

To control the aerobot over a certain distance the controller should communicate with the aerobot. An antenna, receiver and transmitter should be onboard of the aerobot and at the ground station.

Balloon System

The balloon will deliver the lift to fly the aerobot. The balloon system also deals with recovering the payload.

Support Platform

To support the payload the aerobot will require a support platform with basic systems like: power, Telemetry, Tracking and Command (TT&C) and Command and Data Handling (C&DH). For controllability the platform will also have some kind of propulsion system installed.

Payload

The payload should minimal consist out of a camera and some sensors. The camera can be used for scientific purposes but also as a visual aid for the controller to fly the aerobot. The sensors may include atmospheric sensors like temperature, pressure and wind sensors. The payload should be able to send its data down to the ground station.

E.3. System Requirements

From the mission statement above it is clear that the design of an aerobot can include commercial off the shelf components to keep production costs as low as possible. Further the aerobot should consist out of a balloon or a derivative of it controlled by a propulsion system to be highly maneuverable.

E.3.1. Mission Elements

Redefining the mission architecture into mission elements shown in Figure 114, four major elements can be set: the aerobot [A] as key-element, the aerobot's mission control [B], the mission area [D] and the mission itself [C]. These elements can be defined into detail a few levels down until all components on system level are listed. The aerobot's main elements that were defined in chapter 4

are: the balloon [A1], the payload [A2] and the gondola [A3] or support systems. The gas in the envelope and the connections between the gondola and the balloon are left out of the main components in Figure 114 but have been put on a sublevel for simplifying requirements later-on. The Mission Control element can be subdivided into the ground station [B1] and the controller [B2].
Two standard mission topics came to mind after the aerobot research of chapter 0: An aerobot competition [C1] between university teams and a planetary mission [C2]. The planetary mission is set on hold at this point and will not be further discussed, but will always be considered the end goal when designing aerobots. Technology demonstration for such a planetary mission on the other hand can be reached by means of a competition and will therefore be further discussed.
Depending on the mission topic there will be a mission area where the aerobot has to work in. For an aerobot contest two areas come to mind, namely: a gym [D1] and outdoors [D2].
All the mission elements and their sublevel systems will need a number of design requirements, which will be set in the following subchapters.

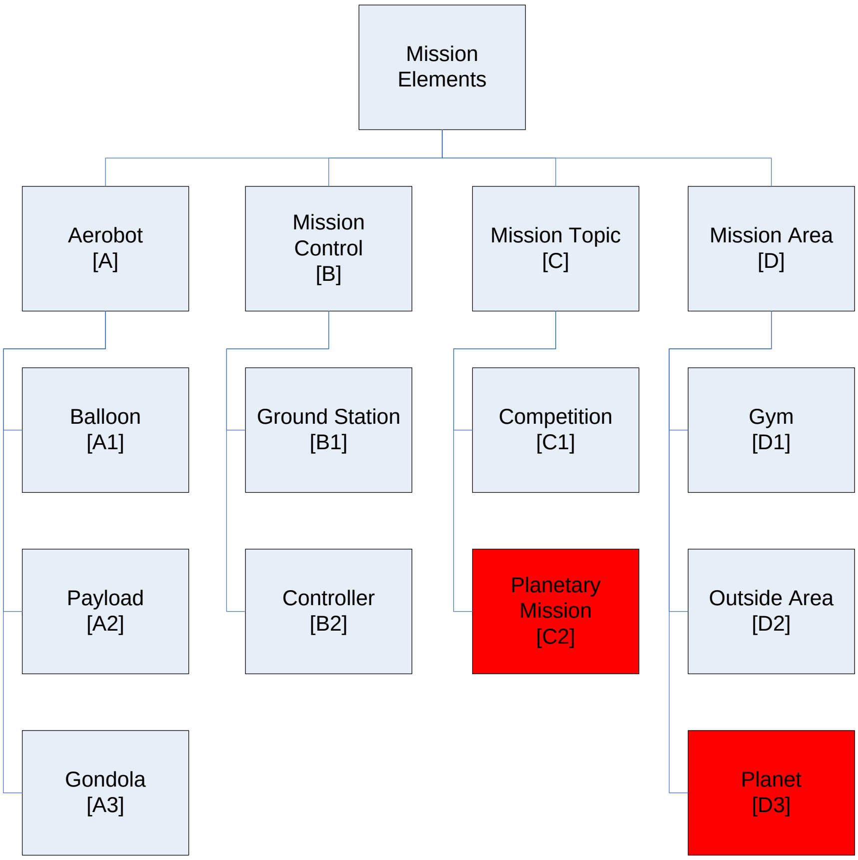

Figure 114: Aerobot Mission Elements

Table 55: Aerobot System Requirements to be Verified

Requirement	**Details**
A2.2a	Camera Resolution at 150m: 300x300
A2.3c	Drone size <10x10x10cm
A3.3.1c	Data rate >= 100Kbps
A3.4.2a	Store 100Mb

E.3.2. Aerobot System Requirements

The aerobot is the main component of the four mission elements, this is shown in the number of sublevels and number of components the aerobot is divided in. All systems are bound to a number of requirements which each receive a number. The requirements of the systems follow from existing aerobots, research, limitations and preliminary design data. Other requirements however still have to be recalculated in detail in the upcoming design process and will be verified afterwards. These requirements are listed in Table 55.

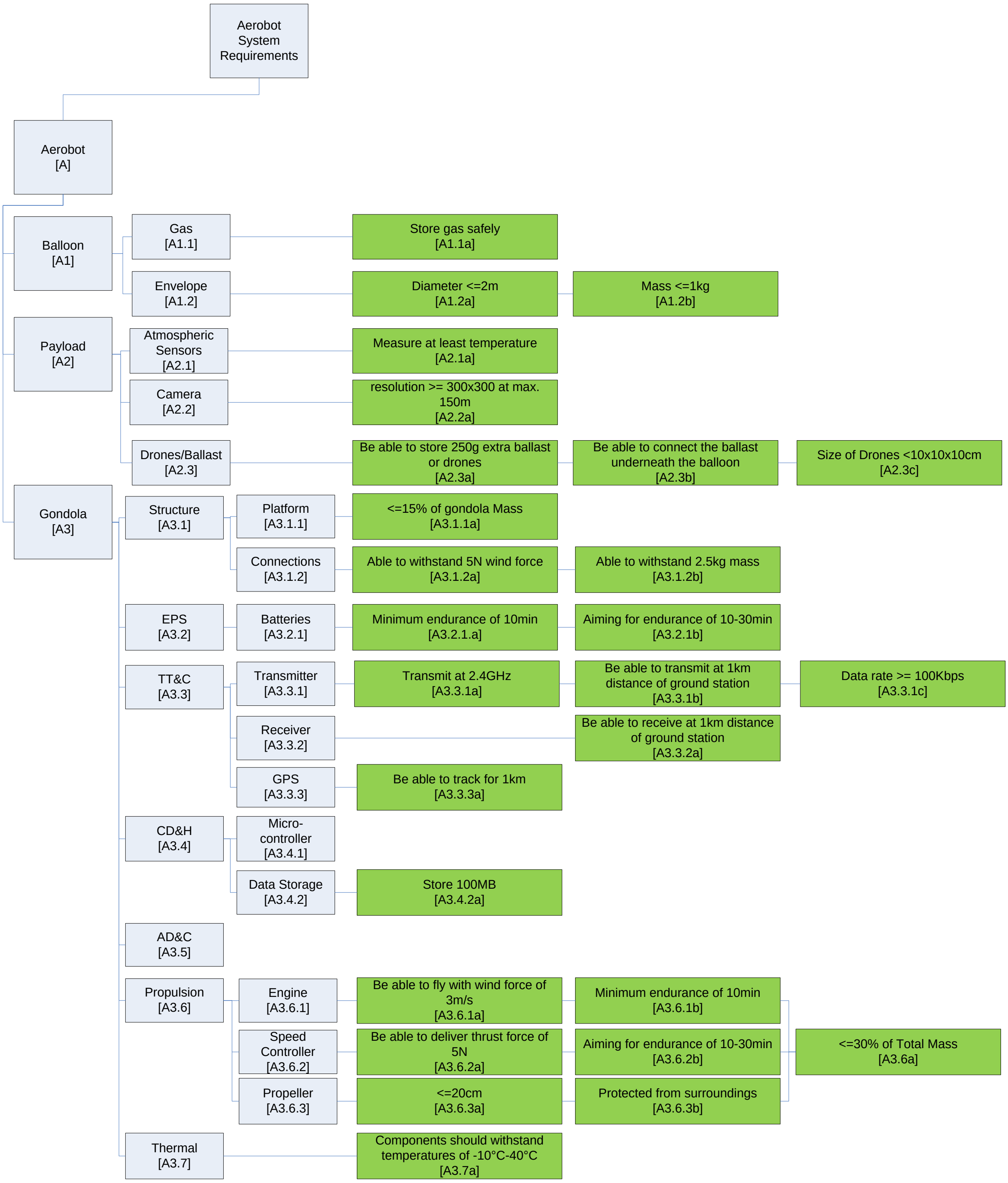

Figure 115: Aerobot System Requirements

E.3.3. Mission Control Requirements

Requirements from the aerobot are sometimes related to the requirements of another mission element and vice-versa. This is the case with the transmitter and receiver of the ground station that should transmit and receive at the same frequency as the one onboard the aerobot. Further any person should be able to steer the aerobot on a predetermined path, from which follows that a straightforward control board should be present.

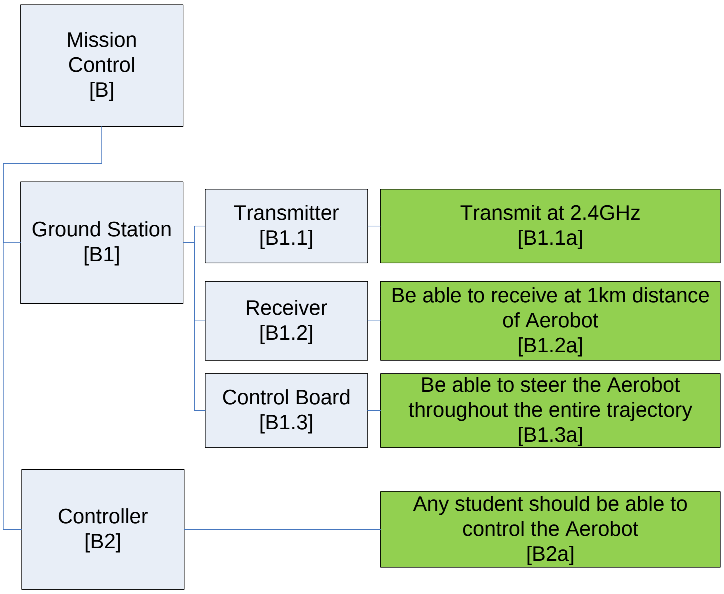

Figure 116: Mission Control Requirements

E.3.4. Mission Area Requirements

Mission area requirements are very straightforward as it only requires a sizeable gym and a place outside the same building were an aerobot competition can be held.

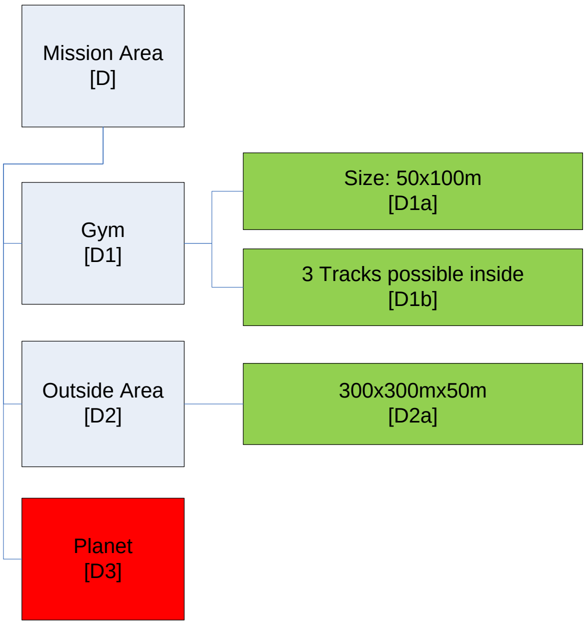

Figure 117: Mission Area Requirements

E.3.5. Mission Requirements

The mission selected was an Aerobot Technology Demonstration by means of an aerobot competition. Due to the fact that buoyant gases can be used as lift and always keeping in mind that someday aerobots can be used for planetary missions, where buoyant gases will be delivering the lift of the vehicle, this will be the group of aerobots that will be focused on.

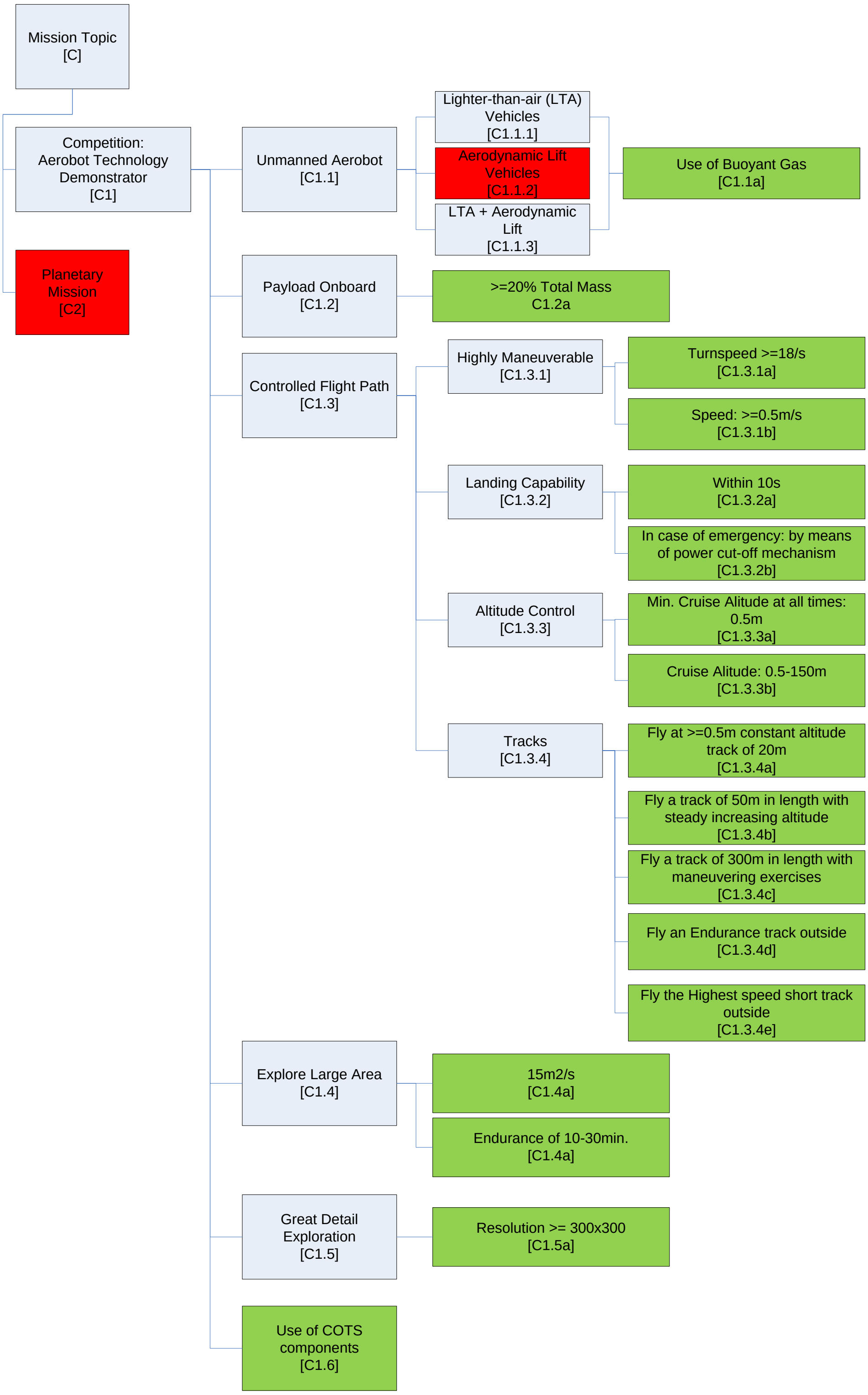

Figure 118: Mission Requirements

The red square [C1.1.2] in Figure 118 is therefore the type of aerobots that will not be allowed in the designing process. Some requirements again follow from or are the same for other mission elements and systems, as it is for the resolution [C1.5a]. A few mission requirements will be refined later on due to incomplete data, but are set at the current values as approximation. These requirements are:

Table 56: Mission Requirements to be Verified

Requirement	Detail
C1.3.1a	Turn speed 18^{o}/s
C1.4a	Explore area of $15m^2$/min
C1.5a	Resolution: >=300x300

Next to the general requirements that hold for all categories of an aerobot design some competition requirements are based on two separate missions of the aerobot: The indoor maneuverability tracks and the outdoor endurance races. Some requirements hold for both missions as it might be the same aerobot that will fly both inside and outside. Indoor and outdoor requirements are set below.

E.3.6. Indoor Capabilities Requirements

An aerobot competition indoor can be held in a standard 100x50m gym. Aerobots should be capable of flying the following tracks:

- Fly at a 0.5m or higher constant altitude over a distance of 20m.
- Fly a track of 50m with steady increase in altitude: Figure 120.
- Fly a track of about 300m long while doing maneuvering exercises: Figure 121.

When payload is involved an aerobot should be able to pick-up the payload and drop it at the requested position, represented in Figure 119. The payload will have a maximum mass of 250g. An extra experiment can be done to find out which balloon has the largest lift capability.

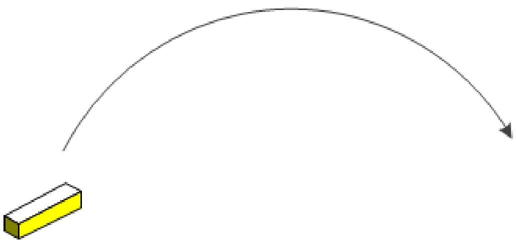

Figure 119: Pick-Up and Drop-Off

Figure 120: Steady Rise

E.3.7. Outdoor Capabilities

For an outdoor competition tracks can be made for:

- Highest speed
- Endurance race

Such tracks can be simple straight lines in a field, or a closed track as represented in Figure 121. Outdoor competition has one extra difficulty, the presence of wind. Therefore the competition can be set up to find out the aerobot's controllability at low level wind levels of less than 3m/s.

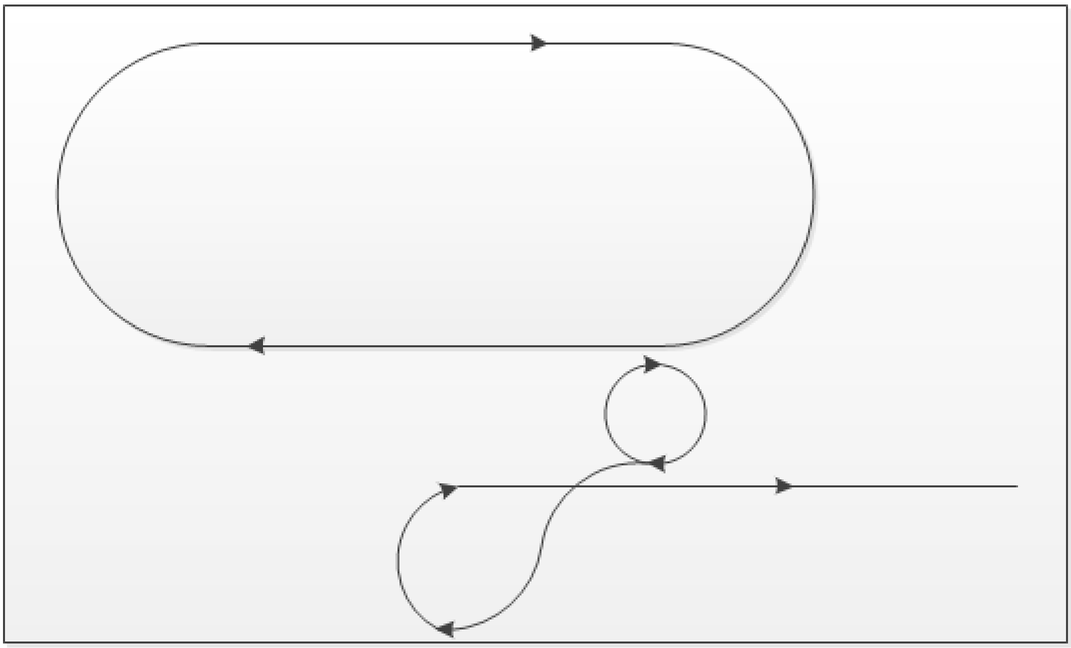

Figure 121: Maneuvering Track and Endurance Track

Appendix F: Aerobot Competitions

Universities and colleges around the world are encouraging and motivating their students by introducing small competition projects into the study to delve into broad technology areas of various engineering disciplines. For the industry such competitions are good technology demonstrators and promotion opportunities, while the students get hand-on experience with designing and building. Competitions like the World Solar Challenge (WSC) [i.13], the International Submarine Races (ISR) [i.14] and the Frisian Solar Challenge (FSC) [i.15] are famous examples of such competitions. Aerobot competitions are therefore a possible solution, to increase awareness of the advantages aerobots have in future space or Earth missions and with that increase technology development in this area.

F.1. Competition Guidelines Set-Up

When an aerobot competition will be set up one needs a set of rules and regulations to start with. Though the concept of aerobot competitions isn't used very much two examples were found of such competitions, namely: the Biology, Electronics, Aesthetics, and Mechanics (BEAM) robot games [i.11] in Lucknow India and the International Aerial Robotics Competition (IARC) [i.12] from the Association for Unmanned Vehicle Systems International (AUVSI) in the United States. The latter makes use of all kinds of Aerial Vehicles except the buoyant aerobot. The BEAM competition was a similar competition as the IARC making use of different kind of robots, but included some ground robots and an aerobot competition too.

When comparing the set of guidelines of the WSC, ISR, FSC, IARC [a.39] and BEAM, some similarities can be found. Therefore rules and regulations for the aerobot competition can be based on the guidelines of the five above mentioned competitions.

F.1.1. General Guidelines

A number of general guidelines are so common that they are widely used in many competitions. Figure 122 shows a set of these guidelines that were found in all mentioned competition examples. In all competitions a lot of administrative actions have to be fulfilled. It starts with an entry form to subscribe to the competition, up to medical forms and financial issues like insurance and fees. A lot of attention is being paid to safety. The organization hosting the competition can't afford any accidents or medical issues, so medical safety of all contestants and technical safety of all vehicles is watched carefully. Compliance checks of all vehicles follow from those safety regulations. Each vehicle will be tested and inspected before the contestants are allowed in the race. No-one can rule out all dangers, therefore a liability form will be presented in most competitions and only when signed by all team-members a team will be allowed to the race.

Next to the administration and safety issues general information like time schedules, logistics and the lay-out of the race track or competition building are shown in the general guidelines. For each competition there have to be prizes at the end, which are handed out by the judges who make sure that everything went according to the rules and regulations. Within one competition different categories might be present which are explained and bounded by certain criteria. Not depending on the vehicle category, or even on the kind of competition there are some general awards that can be hand out afterwards for: maneuverability, best team-spirit, overall performance, best design, most innovative, safest design, highest speed.

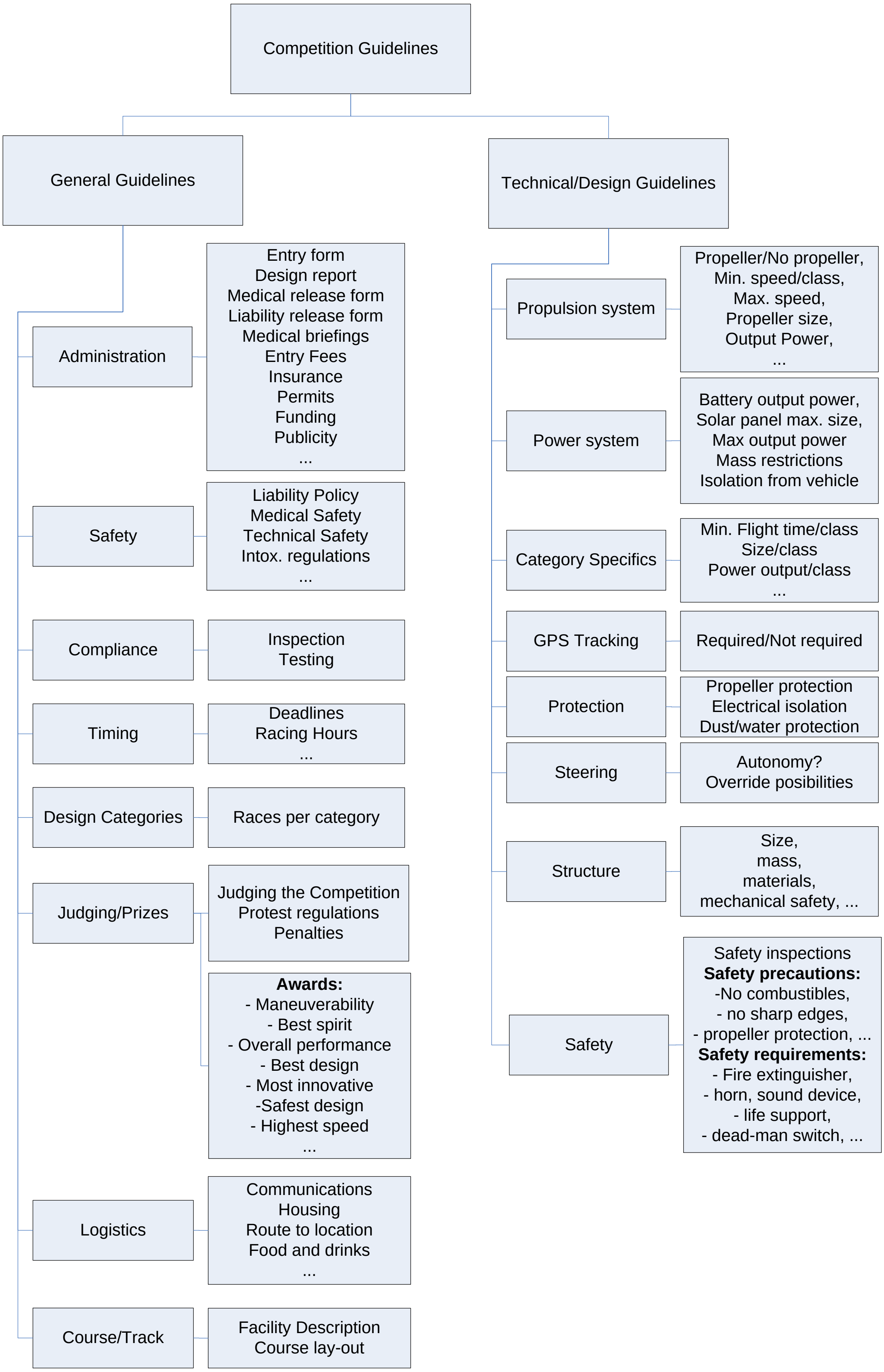

Figure 122: Competition Guidelines

F.1.2. Technical Guidelines

Technical guidelines are more vehicle dependent than general guidelines. There are some however that hold for ISR, WSC, BEAM, IARC and FSC and are therefore interesting for an aerobot design too, shown in Figure 122.

While there are general guidelines for safety, there are also some technical guidelines on safety. First an aerobot can be inspected before use. Next to that some safety precautions can be made and some safety requirements can be executed. Propeller protection when used in a propulsion system avoids bystanders to be injured when in proximity of the aerobot. Electrical engines prevent the use of combustibles and avoid combustibles fires. To improve safety however some active measures can be taken, like the installment of a fire extinguisher. On the vehicle a sound or light device can be mounted so that it is visible and hearable when it is approaching. For the controller a dead-man switch might be installed to, for example, cut all power.

An interesting choice to make is the autonomy level of an aerobot. One can choose to make it an aerobot category in the competition, where autonomous aerobots will not compete against non-autonomous. GPS tracking of an aerobot will be a requirement for long-distance flights, but will be an open option for indoor flights. It can be used for autonomous aerobots when positioning is required on a simulated flight path.

The most documented guidelines are those of the propulsion systems and power systems during competitions. The criteria on these two systems determine the category in which aerobots or any other vehicle will compete against each-other. Maximum and minimum levels for speed, power, propeller size, solar panel size are minimum requirements. Category selection can also be based on mass and size solely, but to keep it fair some similarities should be present in the power and propulsion systems.

Basic protection, which is part of the safety guidelines, is recommended for water and dust, and any moving parts. Further all components should have structural integrity to handle the forces on the aerobot.

While the above technical guidelines aren’t very detailed, as they are coming from systems including solar cars, solar boats and submarines, the guidelines can be used and further refined for aerobots.

F.2. Example of Technical Guidelines for Aerobots

From the contest examples one set of guidelines might be completely useful for an aerobot, competition namely the guidelines of the BEAM competition. The BEAM competition was set up for a number of aerial vehicles, like the IARC competition, but included a specific buoyant aerobot category. The guidelines of this robot category are shown below in Figure 123.

The set-up of the system engineering shown in this figure and the corresponding design guidelines can be used as a guideline for an aerobot competition and aerobot design in co-operation with the more general guidelines of Figure 122.

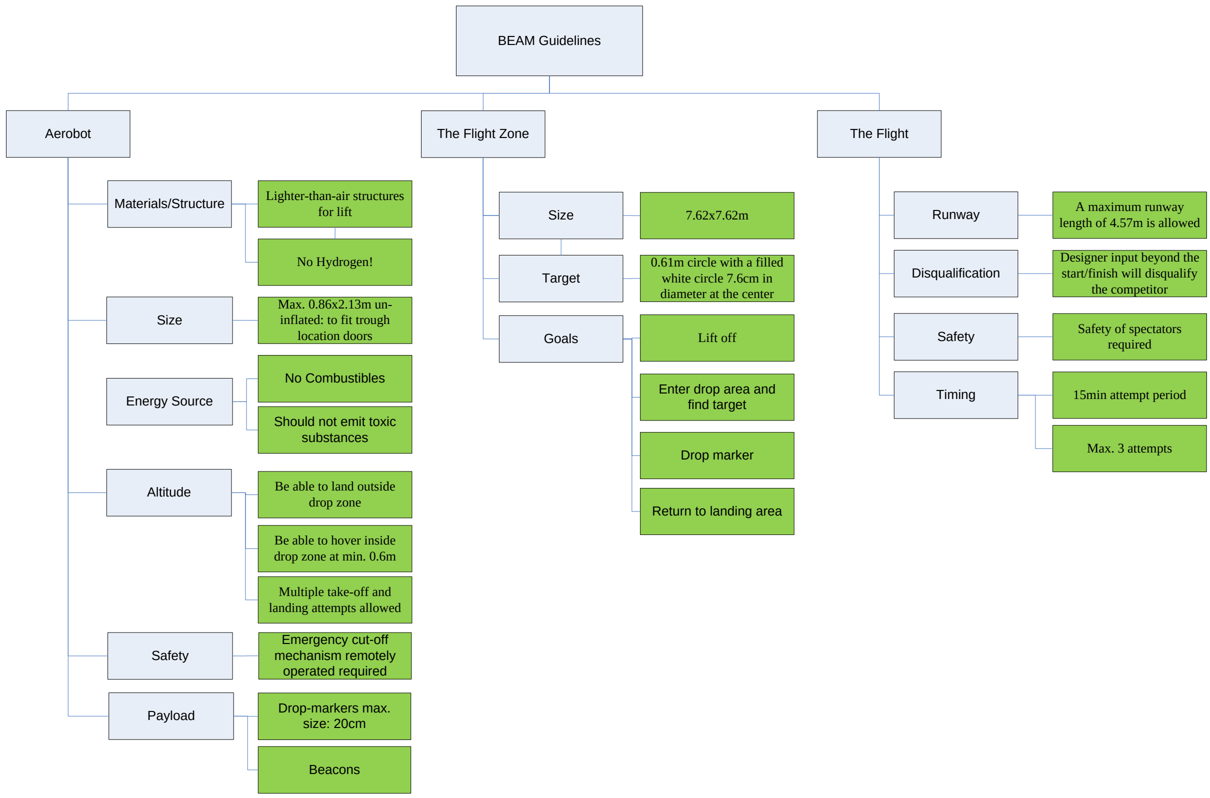

Figure 123: BEAM System Engineering